



**HAL**  
open science

# Can the respiratory rhythm be a global signal promoting long-range communication in the brain?

Maxime Juventin

► **To cite this version:**

Maxime Juventin. Can the respiratory rhythm be a global signal promoting long-range communication in the brain?. Neuroscience. Université de Lyon, 2021. English. NNT : 2021LYSE1334 . tel-03789626

**HAL Id: tel-03789626**

**<https://theses.hal.science/tel-03789626>**

Submitted on 27 Sep 2022

**HAL** is a multi-disciplinary open access archive for the deposit and dissemination of scientific research documents, whether they are published or not. The documents may come from teaching and research institutions in France or abroad, or from public or private research centers.

L'archive ouverte pluridisciplinaire **HAL**, est destinée au dépôt et à la diffusion de documents scientifiques de niveau recherche, publiés ou non, émanant des établissements d'enseignement et de recherche français ou étrangers, des laboratoires publics ou privés.



N°d'ordre NNT : 2021LYSE1334

## **THESE de DOCTORAT DE L'UNIVERSITE DE LYON**

opérée au sein de  
**l'Université Claude Bernard Lyon 1**

**Ecole Doctorale N° 476**  
**Neurosciences et Cognition**

**Spécialité de doctorat** : Neurosciences

Soutenue publiquement le 14/12/2021, par :  
**Maxime Juventin**

---

# **Can the respiratory rhythm be a global signal promoting long-range communication in the brain?**

---

Devant le jury composé de :

Nowak, Lionel (**Rapporteur**)  
Zugaro, Mickael (**Rapporteur**)  
Chavane, Frédéric (**Examineur**)  
Julliard, Karyn (**Examinatrice**)  
Buonviso, Nathalie (**Directrice**)  
Amat, Corine (**co-Directrice**)  
Crochet, Sylvain (**Invité**)



## **Université Claude Bernard – LYON 1**

Président de l'Université	M. Frédéric FLEURY
Président du Conseil Académique	M. Hamda BEN HADID
Vice-Président du Conseil d'Administration	M. Didier REVEL
Vice-Président du Conseil des Etudes et de la Vie Universitaire	Mme Céline BROCHIER
Vice-Président de la Commission de Recherche	M. Petru MIRONESCU
Directeur Général des Services	M. Pierre ROLLAND

### **COMPOSANTES SANTE**

Département de Formation et Centre de Recherche en Biologie Humaine	Directrice : Mme Anne-Marie SCHOTT
Faculté d'Odontologie	Doyenne : Mme Dominique SEUX
Faculté de Médecine et Maïeutique Lyon Sud - Charles Mérieux	Doyenne : Mme Carole BURILLON
Faculté de Médecine Lyon-Est	Doyen : M. Gilles RODE
Institut des Sciences et Techniques de la Réadaptation (ISTR)	Directeur : M. Xavier PERROT
Institut des Sciences Pharmaceutiques et Biologiques (ISBP)	Directrice : Mme Christine VINCIGUERRA

### **COMPOSANTES & DEPARTEMENTS DE SCIENCES & TECHNOLOGIE**

Département Génie Electrique et des Procédés (GEP)	Directrice : Mme Rosaria FERRIGNO
Département Informatique	Directeur : M. Behzad SHARIAT
Département Mécanique	Directeur M. Marc BUFFAT
Ecole Supérieure de Chimie, Physique, Electronique (CPE Lyon)	Directeur : Gérard PIGNAULT
Institut de Science Financière et d'Assurances (ISFA)	Directeur : M. Nicolas LEBOISNE
Institut National du Professorat et de l'Éducation	Directeur : M. Pierre CHAREYRON
Institut Universitaire de Technologie de Lyon 1	Directeur : M. Christophe VITON
Observatoire de Lyon	Directrice : Mme Isabelle DANIEL
Polytechnique Lyon	Directeur : Emmanuel PERRIN
UFR Biosciences	Administratrice provisoire : Mme Kathrin GIESELER
UFR des Sciences et Techniques des Activités Physiques et Sportives (STAPS)	Directeur : M. Yannick VANPOULLE
UFR Faculté des Sciences	Directeur : M. Bruno ANDRIOLETTI

Mon travail de thèse a été effectué au sein du Centre de Recherche en Neurosciences de Lyon (CRNL) dans l'équipe Olfaction : du codage à la mémoire (CMO) dirigée par Nathalie Buonviso et Emmanuelle Courtiol (CNRS UMR 5292, Inserm UMRS 1028, Université Claude Bernard Lyon1, Université Jean Monnet Saint-Etienne). Ma thèse a été encadré par Nathalie Buonviso et Corine Amat. Cette a été financée par une bourse ministérielle attribuée en 2018 par l'École Normal Supérieure de Lyon. Pendant ses trois années de thèse, j'ai également eu l'occasion d'être moniteur en neurosciences à de l'université Claude Bernard Lyon 1.

## REMERCIEMENTS

- C'est une bonne situation ça thésard ?

- Vous savez, moi je ne crois pas qu'il y ait de bonne ou de mauvaise situation. Moi, si je devais résumer ma thèse aujourd'hui avec vous, je dirais que c'est d'abord des rencontres. Des gens qui m'ont tendu la main et que je voudrais maintenant remercier.

Pour commencer, je me dois de remercier Nathalie et Corine qui m'ont permis de découvrir les neurosciences au fil des stages et de cette thèse. Elles ont su me faire adorer les postes d'électrophysio malgré toutes les galères qui y sont généralement associées. « Si n'importe qui dans la rue peut le faire, ce n'est pas drôle » dixit Nath. Vous avez su me transmettre votre savoir-faire du moins je l'espère ☺. Je me rappelle le début du stage de M2, Corine tu as passé des heures et des heures avec moi pour me former à l'intra. Et quand ça ne mordait pas et que je commençais à décourager, tu prenais les manettes puis quelques minutes plus tard tu attrapais une cellule. Ça me remotivait énormément, je me disais : « Ah mais c'est possible en fait, allez j'y retourne ». Vous m'avez aussi inculqué cette passion pour le signal brut, parce que premièrement c'est beau et deuxièmement parce qu'avoir le nez de les tracés bruts évite beaucoup d'écueil d'analyse. Et enfin merci pour les échanges scientifiques passionnant qu'on a pu avoir. Cerise sur le gâteau, vous êtes de belles personnes et j'ai pris plaisir à papoter avec vous deux.

Merci Garcia de m'avoir enseigné les voies impénétrables du Code mais aussi de m'avoir endurci avec toutes les vacheries que tu m'aies dites. Tu as néanmoins pris la peine de me vanner avec classe, une classe à l'américaine je dirais. Enfin, j'me comprends.

Merci Nico pour tes petits coups de pouce qui m'ont permis d'avancer les analyses à grand pas.

Et dans la même lignée, merci à Marc et Bel qui m'ont aidé à mettre en place et réparer mes postes

Merci aux anciens jeunes du labo Bab alias Usain Bolt, Marine dite la farceuse, Anne et sa mémoire, Lucile-post-it-en-folie et aux nouveaux jeunes (Julio, Val, Jayjay) pour avoir mis une ambiance dans le bureau.

Merci Emma de m'avoir initié aux IPA et à la vie New-Yorkaise. Et par la même occasion, merci Don de m'avoir accueilli dans ton labo, ça restera pour moi une très belle expérience.

Merci aux autres membres de CMO, Nadine, Philou, Damien, Alex, Jane, Karyn et Brigitte pour votre accueil chaleureux.

Merci aux membres de mon CSID, Paul Salin et Valérie Ego-Stengel pour m'avoir écouté et conseillé aux fils de nos réunions. Et merci aux membres du jury, Karyn Julliard, Lionel Nowak, Mikael zugaro, Sylvain Crochet et Frédéric Chavane pour avoir pris le temps d'évaluer mon travail.

Merci aux infos Hervé, Thibault, PierreM pour m'avoir dépanné quand je faisais dans c\*\*neries avec les ordi/clusters et pour m'avoir aidé/conseillé dans mes bricolages, disons originaux pour être gentils.

Merci à mes parents, ma famille et mes amis de m'avoir soutenu et écouté quand je vous racontais à quoi consistait mon travail.

And last but not least, merci Malo de m'avoir accompagné et supporté tout au long de cette thèse, surtout sur la fin.

# Can the respiratory rhythm be a global signal promoting long-range communication in the brain?

## ABSTRACT

The brain is a place of intense rhythmic activity, each brain area can express one or more rhythms. A central question in neuroscience is to understand how these rhythmic activities can coordinate across very distant brain areas to enable functions as complex as environmental perception, adapted motor responses or memory formation. One possibility is that the system uses a common temporal reference, a kind of central clock, from which the different neural networks involved in a function could coordinate. Today, the existence and nature of this clock are still debated. We hypothesize that the respiratory rhythm could be one of these central clocks, constituting a reference signal for the coordination of different brain areas. As a central clock, breathing has major advantages: reliability (it is a vital function), flexibility (it adapts to the needs of the organism), low cost (it is a rhythm which is not created specifically for this function). In the olfactory system, the link between respiratory rhythm and neuronal activity is undeniable. Respiration drives slow oscillations at the respiratory frequency, bursts of fast oscillations (gamma and beta) and the discharge of neurons. Recent literature, in which my team participates, has shown that this respiratory influence of neuronal activity is not restricted to the olfactory system, but on the contrary extends to the entire brain (neocortex, amygdala, hippocampus, thalamus). In most of the non-olfactory areas recorded, the respiratory rhythm also modulates the discharge of neurons and fast oscillations. The slow oscillations related to breathing therefore seem to affect the overall dynamics of the brain.

My PhD project is composed of two parts. First, in order to confirm an influence of the respiratory rhythm on neurons, I made intracellular recordings in four non-olfactory areas in anesthetized rats. The targeted structures were the median prefrontal cortex, the primary somatosensory cortex, the primary visual cortex and finally the hippocampus. I was able to observe respiration modulation in most of these neurons. The quantification of these data shows that the events of respiratory modulation are short but observed in a significant number of neurons. These data also provide evidence that the respiratory modulation of various brain areas is not solely due to volume conduction

In a second step, in order to study the coordination of brain areas by the respiratory rhythm, I analyzed recordings of multisite local field potentials (LFP) in the conscious rat. The recordings contain seven brain areas (olfactory bulb, anterior piriform cortex, primary visual cortex, median prefrontal cortex, primary somatosensory cortex, CA1, dentate gyrus) and respiration. I was able to observe slow oscillations related to respiration in all brain states. But it is during calm awakening that respiratory modulation is greatest and appears in all recorded areas. In parallel, these slow oscillations are coupled with several types of fast oscillations. Finally, I wanted to know if, during the quiet waking state, where LFP of a large brain network are synchronized with respiration, unit activities can also synchronize with the respiratory signal. To do this, I developed an electrophysiological recording setup in head-fixed conscious rats allowing the recording of numerous neurons in pairs of brain areas with "silicon probes". The setup is now functional, and I was able to register 6 animals. These last data will not be fully processed when I am defending my thesis. I will present preliminary results which already allow us to show that respiration can synchronize the unit activities of many cells in even spatially distant regions of the brain.

All of these studies allow me to conclude that breathing is one of the central clocks of the nervous system.

## KEY WORDS

Respiratory rhythm – Brain rhythm – Long-range communication – Central clock - Synchronization

# Le rythme respiratoire peut-il constituer un signal global favorisant la communication cérébrale ?

## RESUME

Le cerveau est le siège d'une activité rythmique intense, chaque aire cérébrale exprimant un ou plusieurs rythmes. Une question centrale en neurosciences est de comprendre comment ces activités rythmiques peuvent se coordonner à travers des zones très distantes du cerveau pour résoudre des fonctions aussi complexes que la perception de l'environnement, des réponses motrices adaptées ou la formation de mémoires. Une possibilité est que le système utilise une référence temporelle commune, sorte d'horloge centrale, à partir de laquelle les différents réseaux neuronaux impliqués dans une fonction pourraient se coordonner. Aujourd'hui, l'existence et la nature de cette horloge sont encore débattues. Nous faisons l'hypothèse que le rythme respiratoire pourrait être l'une de ces horloges centrales, constituant un signal de référence pour la coordination des différentes aires cérébrales. Comme horloge centrale, la respiration présente des avantages majeurs : fiabilité (car c'est une fonction vitale), flexibilité (car elle s'adapte aux besoins de l'organisme), faible coût (car c'est un rythme qui n'est pas créé spécifiquement pour cette fonction). Dans le système olfactif, le lien entre rythme respiratoire et l'activité neuronale est indéniable. La respiration entraîne des oscillations lentes à la fréquence respiratoire, des bursts de d'oscillations rapides (gamma et beta) et la décharge des neurones. La littérature récente, à laquelle mon équipe participe, a montré que cette influence respiratoire de l'activité neuronale n'est pas restreinte au système olfactif, mais bien au contraire s'étend au cerveau entier (néocortex, amygdale, hippocampe, thalamus). Dans la plupart des aires non-olfactives enregistrées le rythme respiratoire module également la décharge des neurones et les oscillations rapides. Les oscillations lentes liées à la respiration semblent donc bien affecter la dynamique globale du cerveau.

Mon projet de thèse est composé de deux parties. Dans un premier temps, de manière à confirmer une influence du rythme respiratoire sur les neurones, j'ai réalisé des enregistrements intracellulaires dans quatre aires non-olfactives chez des rats anesthésiés. Les structures ciblées étaient le cortex préfrontal médian, le cortex somesthésique primaire, le cortex visuel primaire et enfin l'hippocampe. J'ai effectivement pu observer une modulation respiration dans la plupart de ces neurones. La quantification de ces données montre que les événements de modulation respiratoire sont courts mais observés dans un nombre conséquent de neurones. Ces données apportent aussi la preuve que la modulation respiratoire des diverses aires cérébrales n'est pas uniquement due à de la conduction volumique.

Dans un second temps, de manière à étudier la coordination d'aires cérébrales par le rythme respiratoire, j'ai analysé des enregistrements de potentiels de champ locaux (LFP) multisites chez le rat vigile. Les enregistrements contiennent sept aires cérébrales (bulbe olfactif, cortex piriforme antérieur, cortex visuel primaire, cortex préfrontal médian, cortex somesthésique primaire, CA1, gyrus denté) et la respiration. J'ai pu observer des oscillations lentes liées à respiration dans tous les états cérébraux. Mais c'est pendant l'éveil calme que la modulation respiratoire est la plus importante et apparaît dans toutes les aires enregistrées. En parallèle, ces oscillations lentes sont couplées avec plusieurs types d'oscillations rapides. Enfin, j'ai voulu savoir si, lors de l'état d'éveil calme, où les LFP d'un large réseau cérébral sont synchronisés à la respiration, les activités unitaires pouvaient aussi se synchroniser par rapport au signal respiratoire. Pour cela, j'ai mis en place un poste d'enregistrement électrophysiologique chez le rat vigile contraint permettant d'enregistrer de nombreux neurones dans des paires de structures cérébrales avec des « silicon probes ». Le poste est aujourd'hui fonctionnel et j'ai pu enregistrer 6 animaux. Ces dernières données ne seront pas entièrement traitées au moment où je soutiendrai ma thèse. Je présenterai des résultats préliminaires qui nous permettent d'ores et déjà de montrer que la respiration peut synchroniser les activités unitaires de nombreuses cellules dans des régions cérébrales même spatialement éloignées.

L'ensemble de ces études me permet de conclure que la respiration constitue l'une des horloges centrales du système nerveux.

#### MOTS CLES

Rythme respiratoire – Rythmes cérébraux – Communication longue distance – Horloge centrale -Synchronisation

# Table of contents

<b>Abbreviation</b>	<b>11</b>
<b>1 - Introduction</b>	<b>12</b>
<b>1.1 - Brain rhythms</b>	<b>13</b>
1.1.1 – What is the brain electrical activity?	15
1.1.2 – Spatiotemporal dynamics of the resting brain	20
1.1.3 – Neuronal communication through oscillations	26
1.1.3.1 What is a cell assembly?	26
1.1.3.2 How does a cell assembly work?	27
1.1.3.3 Gamma oscillations as time unit for information exchange	27
1.1.3.4 Long-range communication	29
1.1.4 – Concrete examples of long-range communication supported by slow rhythms	30
1.1.4.1 – Sleep slow waves (0.1-4.5Hz), a NREM coordinator	30
1.1.4.2 - Theta rhythm (4-8Hz), a REM and active wake coordinator	31
<b>1.2. – Respiratory &amp; brain rhythms: how the couple has been seen so far?</b>	<b>32</b>
1.2.1 – Respiratory rhythm generation	33
1.2.2 – Respiratory rhythm interaction with brain and body	34
1.2.3 – Respiratory rhythm shapes neuronal activity in the olfactory system	35
<b>1.3 The new face of Respiration-related oscillations</b>	<b>40</b>
1.3.1 What is the extent of respiratory modulation in the non-olfactory brain?	40
1.3.2 The possible routing of Respiration-related oscillations across the brain	47
1.3.3 And so what? What functions support this respiratory modulation?	49
1.3.4 Respiratory modulation across species?	50
<b>2. Questions and objectives.</b>	<b>52</b>
<b>2.1 Context</b>	<b>53</b>
<b>2.2 Are non-olfactory neurons really affected by respiratory modulation?</b>	<b>53</b>
<b>2.3 May the respiratory rhythm bind distant brain areas?</b>	<b>53</b>
<b>2.4 May the respiratory rhythm shapes assemblies?</b>	<b>54</b>
<b>3. Results</b>	<b>55</b>
<b>3.1. Respiratory modulation of intracellular activity in non-olfactory neurons</b>	<b>56</b>
3.1.1 Context and summary	56
3.1.2 Results	56
<b>3.2. Role of the respiratory rhythm in supporting the long-range communication in the brain</b>	<b>70</b>
3.2.1 Context	70
3.2.2. Methods	70
3.2.3. Results	73
3.2.4. Conclusion and perspectives	84
<b>3.3. May respiratory rhythm shape neural assemblies?</b>	<b>86</b>
3.3.1. Context	86
3.3.2. Methods	87
3.3.3. Results	92
3.2.4. Conclusion and perspectives	102
<b>4. Discussion</b>	<b>104</b>
<b>4.1. Respiratory modulation and respiration monitoring</b>	<b>105</b>
<b>4.2. Respiratory drive: One respiratory phase to bind them all (the brain areas)?</b>	<b>106</b>
<b>4.3. Does an interaction between slow rhythms exists?</b>	<b>108</b>

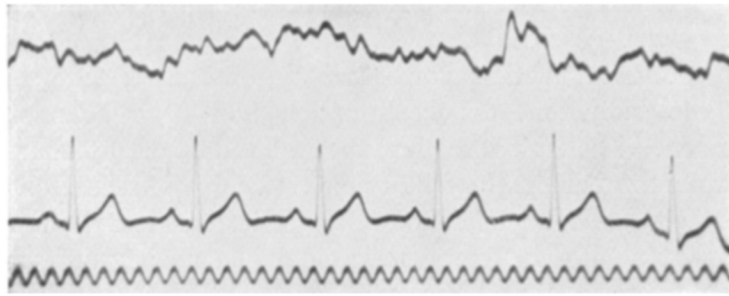
4.4. Origin and propagation of respiratory modulation?	110
4.5. General conclusion	113
<b>5. Bibliography</b>	<b>114</b>
<b>6. Annexes</b>	<b>132</b>
6.1 Co-author published article	133
6.2 Posters	149

## Abbreviation

AHP = after hyperpolarization  
AP = action potential  
eAP = extracellularly recorded action potential  
AMPA = alpha-amino-3-hydroxy-5-methylisoxazol-4 propionic acid  
AON = anterior olfactory nucleus  
aPCX = anterior piriform cortex  
CA1 = cornu Ammonis 1  
CSD = current source density  
DG = dentate gyrus  
eAP = extracellular action potential  
ECoG = electrocorticogram  
EEG = electroencephalogram  
iEEG = intracerebral electroencephalogram  
EPSP = excitatory post-synaptic potential  
EPSC = excitatory post-synaptic current  
EEG = electroencephalography  
GABA= gamma-amino-butyric acid  
HRV = heart rate variability  
IPSP = inhibitory post-synaptic potential  
IPSC = inhibitory post-synaptic current  
 $I_T$  = calcic current deactivated by hyperpolarization and triggered by depolarization  
 $I_H$  = sodium-potassic current triggered by hyperpolarization  
LEC = lateral entorhinal cortex  
LFP = local field potential  
LOT = lateral olfactory tract  
M/T cells = mitral/tufted cells  
MEA = multi-electrode array  
mPFC = medial prefrontal cortex  
NMDA = N-Méthyl-D-Aspartique Acid  
NREM = non rapid eye movement  
OB = olfactory bulb  
OE = olfactory epithelium  
OSN = olfactory sensory neuron  
OT = olfactory tract  
PV = parvalbumin  
pPCX = posterior piriform cortex  
REM = rapid eye movement  
RRo = respiration-related oscillations  
RSA = respiratory sinus arrhythmia  
S1= primary somatosensory cortex  
V1= primary visual cortex

## **1 - Introduction**

## 1.1 - Brain rhythms



Abb, 12. Klaus im 16. Lebensjahre. Doppelspulengalvanometer. Kondensation. Nadel-  
elektroden subcutan an Stirn und Hinterhaupt. Widerstand = 700 Ohm. Elektrokardio-  
gramm mittels Bleifolienelektroden von beiden Armen. Oben die von der Kopfhaut  
abgeleitete Kurve, in der Mitte das Elektrokardiogramm, unten die Zeit in  $\frac{1}{10}$  Sekunden.

*Figure 1 : Early human brain activity recording using a galvanometer. Top: electroencephalogram of a 16 years-old. Mid: electrocardiogram. Bottom: time in 1/10 second. Extracted from Berger, 1929.*

The notion that the brain has an electrical activity is quite old, now. Richard Caton, in 1875, placed a galvanometer onto anaesthetized rabbit and monkey brains, and showed the existence of weak currents. After these findings and for more than four decades, electrophysiologists were confronted to technical issues. Yet, in 1929 Hans Berger, 1929 finally managed recording human electroencephalogram. He was the first to show the brain activity is rhythmical (see *Figure 1*). He initiated the study of brain rhythms, as a way to understand the functioning of the brain. This rhythmical activity has been scattered in frequency bands (see *Figure 2*). Consequently, a sinusoidal signal is fully described with its amplitude, phase and frequency (see *Figure 3*). Such a decomposition implicitly supposes different mechanisms and functions for each frequency band.

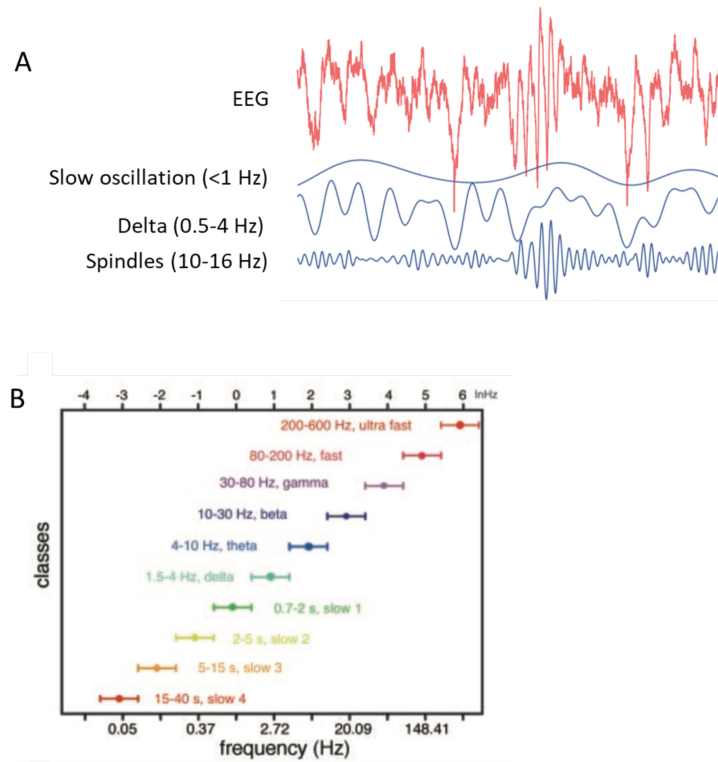


Figure 2 : Decomposition of brain activity in frequency band. A. Example of raw EEG signal decomposed in filtered signal from top to bottom in slow oscillation band (<1Hz), delta band (0.5-4 Hz) and spindles band (10-16 Hz). Extracted from Adamantidis et al., 2019 B. Classical frequency band classification. Extracted from Buzsáki and Draguhn, 2004.

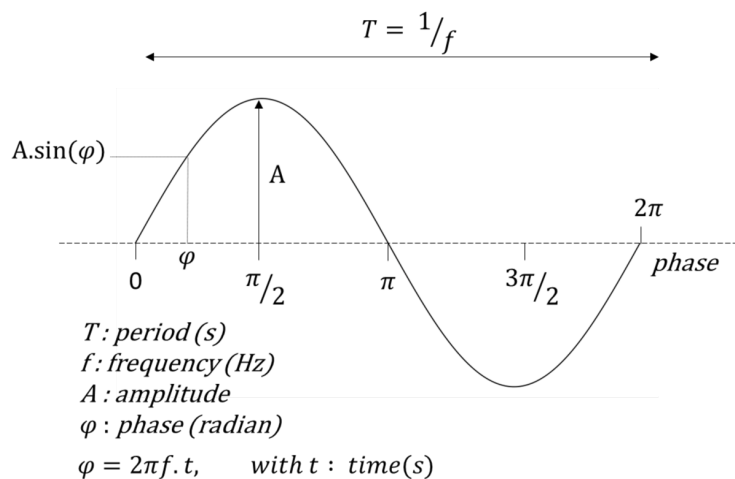


Figure 3 : Sinusoidal signals description. A sinusoidal signal is fully described with its amplitude and frequency. Advancement of the signal is described by the phase.

In this chapter, I firstly aim to clarify how transmembrane mechanisms generate recordable extracellular potentials. Then I will describe the diversities of brain rhythms and how these rhythms are distributed in brain areas and brain states. The last section will answer: which functions do these rhythms support? This section will be a cornerstone for my thesis, as I will argue in favor to the theory of the long-range communication through nested oscillations (Bonfond et al., 2017). In that direction, I will highlight a hierarchy between rhythms according to their frequencies. This hierarchy subdivides slow (<10 Hz) and fast rhythms. The formers are currently thought to dynamically and transiently connect widespread brain areas, hence shaping functional networks amongst a distributed system. The latter enables efficient and precise information exchange (Fries, 2015, 2005). After presenting theory of communication, I will illustrate the theory with two rhythms closely related to my work, Sleep slow waves and theta rhythm.

### **1.1.1 – What is the brain electrical activity?**

Electrophysiology aims at studying the brain electrical activity. To achieve this goal, scientists have developed various methods measuring different physical quantities, namely electrical and magnetic fields, magnetic resonance, and photon. Methods can be direct, where recorded variations reflect directly neuronal electrical activity, or indirect, where recorded signal correspond to delayed consequences of the electrical activity, most frequently a regenerative metabolism. In my thesis, I will focus on direct methods, *i.e.*, what I used, namely unitary intracellular and extracellular recordings, and electrical field recordings. The nature of the intracellular signal is not ambiguous, as it corresponds to the pure signal of one single cells, there are no confounding effects. Intracellular signal consists in membrane potential variations, which subthreshold component corresponds to oscillatory activity and supraliminal component give rise to action potentials (AP) (see *Figure 4* top B). Hence, intracellular signals present a continuous and a discrete component. This activity has direct repercussion on the extracellular electrical field, in which one can observe continuous oscillations (see *Figure 4* bottom B and C) and discrete extracellularly recorded action potentials (eAP). Nonetheless, extracellular signal is complicated as it corresponds to the summed activity of a population of unknown size and unknown composition (pyramidales, interneurons, glia). For example, eAP from different cells can be confounded. Fortunately, with development of dense electrodes and associated analyses, extracellular discrimination of neurons was improved (see *Figure 5*). The aim of this paragraph is to explain what an electrical field signal is.

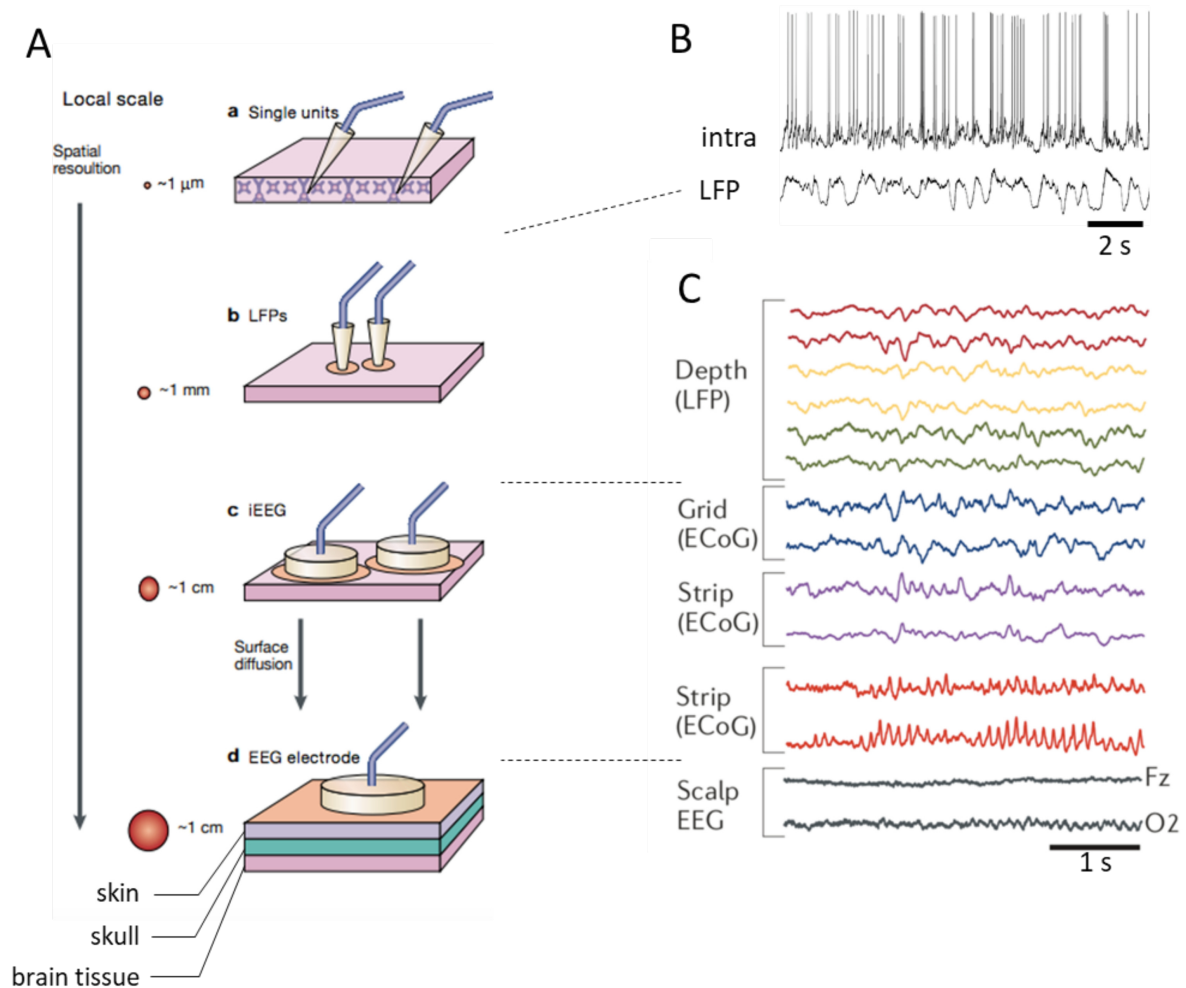


Figure 4 : Electrical activity aspect depends on electrodes types. A. Representation of different recording methods. a. Glass pipettes enable recording of intracellular activity (shown in top B) or extracellular single cell activity. b. Metal wires or silicon probes are inserted within brain tissue. Activity of a local population are monitored in the LFP (shown bottom B and C). c. intracranial EEG electrodes on the top of the cortex, just below meninges. Electrical fields recorded (shown in C) corresponds a medium size population. d. EEG electrodes are placed on the scalp. Neurons electrical fields are recorded throughout skull and skin. Signal represents summed activity of a large population. Extracted from Varela et al., 2001. B. Intracellular (top) and LFP (bottom) co-recordings in the medial PFC of urethane anesthetized rats. Note, the great similarity between signal. Scale bar = 2 s. Extracted from personal data. C. Simultaneous recordings from three depth electrodes (hippocampus and amygdala), from one grid and two strip electrode array placed on temporal lobe and scalp EEG. Temporal resolution and amplitude decrease from top to down. Scale bar = 1s. Extracted from Buzsáki et al., 2012.

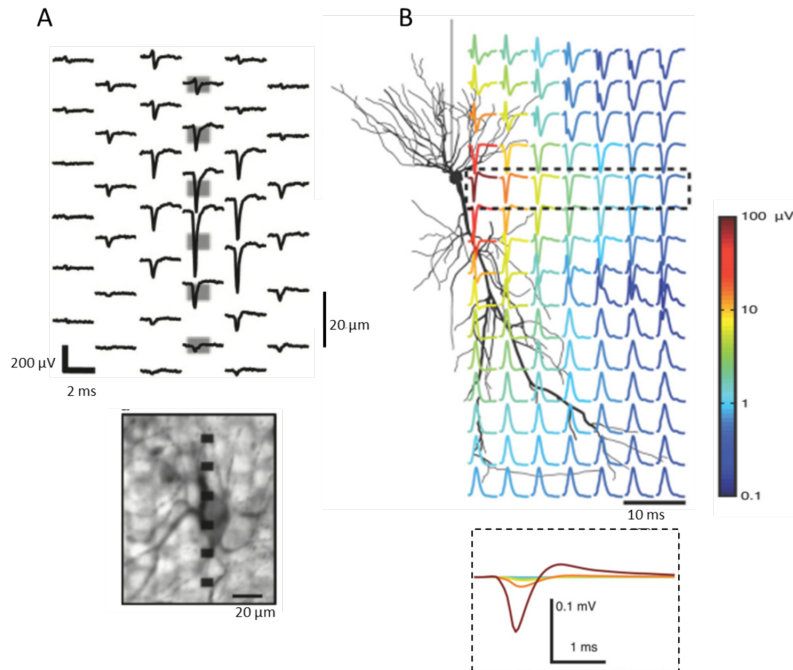


Figure 5 : Rapid decay of eAP in LFP signal. A. In vitro recording of extracellular AP. Inset shows micrographs of the recorded neuron and the electrode array. 80 μm away from the neuron, eAP becomes imperceptible in LFP. Spatial scale bar = 20 μm. Amplitude scale bar = 200 μV. Time scale bar = 2 ms. Extracted from Bakkum et al., 2013. B. eAP waveform with normalized amplitude modelling for a hippocampal pyramidal neuron. Inset represents same eAP with respect to their amplitudes. Amplitude decrease is extremely fast. Extracted from Schomburg et al., 2012.

Ion channels are the elementary unit of current generation in living organisms. Biological currents consist in ion displacements across cell membrane (through ion channel). These flows are made possible because living cells actively maintain unequal concentration of ions on both sides of cell membrane. But how, elementary micro-currents can lead to extracellularly recordable brain electrical activity? A convincing illustration can be found in electric eel's physiology. These animals possess an organ in which cells are optimally arranged for currents summation. As a result they can produce tremendous extracellular currents about 400-500 V (Hagiwara et al., 1965). To come back to neurons, György Buzsáki and colleagues in 2012 wrote an excellent review which detailed a lot of parameters explaining the generation of extracellular fields in the brain. In any given point of the brain space, we can measure an extracellular electrical field, named Local Field Potential (LFP), which corresponds to the superimposition of all transmembrane currents generated by the surrounding cells. The contribution of each cell to this field is a complex function comprising variables such as distance to recording sites, cell type, size and morphology, transmembrane currents features, cell synchronization, cells arrangement, etc.

The very basic law that allows extracellular field generation is the spatiotemporal summation, *i.e.*, in every point of the extracellular medium, currents from surrounding cells are cumulating. However, current amplitude decreases proportionally to the inverse of the distance ( $1/r$ ) from the source, in a theoretical non-resistive medium. Hence, the resulting activity of the field will reflect the activity of the closest (spatial component) and most synchronized (temporal component) cells. With this approximation, we have the intuition that extracellular field will vary with the size of the electrode (see Figure 4 A). Consequently, nomenclature of signals is defined by the volume of brain that is recorded, which itself depends on the electrodes features. When electrodes are on the scalp, signal is called electroencephalogram (EEG), when electrodes are placed directly at the cortical surface, signal is called electrocorticogram (ECoG), when electrodes are in the depth of the brain, signal is called intracranial EEG (iEEG) or LFP (see Figure 4). Electrode size,

and thus recording field, reduces from EEG to LFP. A large electrode (*e.g.*, EEG) will smooth the activity of a large population and the resulting activity will represent the majority of the cells, yet information from some cells (less active and less synchronized) will be imperceptible. On the contrary, micro-electrodes (*e.g.*, silicon probes, glass pipette) monitor more local activity which grants access to more precise information, nevertheless the sampled volume is small (see *Figure 4*).

### Participating currents

As mentioned above, the temporal coordination of cellular currents will greatly influence the resulting extracellular current amplitude. Consequently, the duration of whole cell transmembrane currents is a major factor, since brief currents will be harder to coordinate compared to slower ones. I will present only cellular events relevant for my thesis, for more detail see Buzsáki et al., 2012.

- *Synaptic currents (=inputs)*. Neurotransmitter inputs induce ion channels opening, generating inhibitory or excitatory currents. These currents are slow enough to be easily summed, and their preponderance made them the principal component of the extracellular field. Hence, it is commonly admitted that extracellular fields reflect local synaptic inputs, and theory of long-range communication are based on that principle. AMPA and NMDA receptors mediate strong currents, as Na<sup>+</sup> and respectively Ca<sup>2+</sup> equilibrium are far from resting membrane potential. On the contrary, GABA<sub>A</sub> receptors generate weak currents when cells are at rest. However, when cells are depolarized, membrane potential moves away from Cl<sup>-</sup> equilibrium, then GABA<sub>A</sub> currents contribution to LFP becomes consequent (Bazélot et al., 2010; Glickfeld et al., 2009; Trevelyan, 2009). Finally, Ca<sup>2+</sup> dendritic spikes are ample (60mV) and long-lasting (10-100ms) calcic currents (Kamondi et al., 1998; Wong et al., 1979) which are supposed to strongly participate to extracellular field.

- *Action potentials (=outputs)*. Na<sup>+</sup> AP are very ample (~100mV) but extremely short in duration (~2ms). Temporal summation of AP requires extremely precise synchronization, since time window is very short. Additionally, spatial summation imposes synchronized neurons to be close, since eAP amplitude rapidly decreases (within 50-100μm) in the extracellular field medium (see *Figure 5*). As a result, the strong constraint on time and space gives rise to a low rate of summation. As a consequence, extracellular amplitude of AP decreases rapidly. Interestingly, highly synchronized firing appears to affect the extracellular field, and particularly high frequency (>100Hz) (Buzsáki et al., 2012; Buzsáki and Wang, 2012). Indeed, Manning et al. in 2009 observed on implanted human a positive correlation between spiking rate and broadband (2-150Hz) power increase. Complementarily, Zanos et al. in 2011 showed AP contaminate high frequency domain (0-150Hz) of extracellular field, even if AP were cautiously removed. On the contrary, after hyperpolarization (AHP) displays an amplitude and a kinetic similar to synaptic currents. Consequently, neural events involving high firing synchronization such as sharp-waves and ripples (SPW) (Ylinen et al., 1995) or cortical DOWN states (Buzsaki et al., 1988; Sanchez-Vives and McCormick, 2000) result in remarkable LFP event due to the extracellular summation of AHP.

- *The brain electrical field, a neuronal privilege?* Astrocytes, although they are not excitable cells, show intracellular Ca<sup>2+</sup> concentration variations, which are correlated with inward current in proximal neurons (Parri et al., 2001). This calcium waves propagate in the glial syncytia. Hence, glia is not a passive actor in brain electrical activity. Later, astrocytes have been shown to regulates UP/DOWN cortical state (Fellin et al., 2009; Poskanzer and Yuste, 2011). Interestingly, stimulation of one single astrocyte, induces a calcium increase in the whole astrocyte network, which results in a global neuronal UP state (Poskanzer and Yuste, 2011). This synchronization of close neurons probably strongly contributes to LFP. Lastly, glia is thought to generate infra-slow oscillations and (<0.1Hz) of extracellular field (Hughes et al., 2011; Vanhatalo et al., 2004) and BOLD signal (He et al., 2008).

Extracellular field corresponds to the summed currents from neighboring cells. This summation is favored when currents are concentrated in space and time.

#### Spatial concentration:

The strength of extracellular field depends on the one hand on transmembrane currents (listed above), and on the other hand on its propagation in the extracellular medium. Morphology of cells generating the current is an important parameter for dipole formation. Large and asymmetric cells, like pyramidal cells population (see *Figure 5*), offer a great distance between dendrites and soma. Consequently, when a pyramidal cell receives excitatory inputs, an inward current is generated at the dendrite. Local circuit theory principle imposes an outward current at the soma. The simultaneous dendritic charge inflow and somatic charge outflow generates a dipole. Strength of the dipole is correlated with distance between the sink (here the dendrite) and the source (here the soma). Hence, morphology and quantity of pyramidal cells made them strong contributors to extracellular field. Conversely, symmetric neurons *i.e.* neurons with spatially homogeneous dendrites arborescence (ex: thalamocortical cells) should only generate monopole, and thus poorly participate to LFP. However, dendrites are rarely all and simultaneously stimulated. Consequently, stimulation of one of the dendrites generates a small dipole. Finally, cellular morphology must be appreciated more globally, as the electrical field represents a population. Thus, spatial arrangement of the contributing cells, *i.e.* the cytoarchitecture, is an important feature. Aligned dipole, *i.e.* layered structures like in the cortex, olfactory bulb or the rodent hippocampus, facilitate the spatial summation. Conversely, in the human hippocampus, dipoles are alternated, which configuration two-by-two suppresses extracellular current propagation. Finally, cell proximity, *i.e.* cell density increases LFP amplitude, which explain mice present larger LFP than rats (Buzsáki et al., 2012).

#### Temporal concentration

In a given cytoarchitecture, the more synchronized the cells, the stronger the resulting extracellular field. Yet, electric field power scales in  $1/frequency$ . A possible explanation can be found in network synchronization. Indeed, a slow oscillation imposes a long period, this period represents a long-time window during which more inputs and from more neurons (even distant neuron) can be integrated. For the same reason, fast oscillations rather integrate more local activity. Because of that, slower oscillation tends display a stronger LFP, than faster ones.

#### Paradox of non-sinusoidal oscillations

At the very beginning of this section, I explained that brain rhythms are decomposed in sinusoidal oscillations. This modeling is convenient as it is, in first approach, a good estimation, and it opens a plenty of simple mathematical tools to study oscillations. However, when looking in more details, most neuronal oscillations are not symmetrical, thus sinusoidal models cannot perfectly fit this activity (example for gamma oscillation of membrane potential in Fourcaud-Trocmé et al., 2018)). Cole and Voytek in 2017 proposed an excellent review about the future direction for neuronal oscillations analyses, in other words analysis closer to the real signal. Indeed, they show that Fourier, Morelet wavelet and Hilbert transform-based analyses are biased for signals with non-homogeneous phase, *i.e.* non-sinusoidal signals. Especially, cross-frequency analysis could be biased but only few authors did take it into account in their interpretations. Noteworthy, the respiration-related oscillations which are the heart of my thesis are particularly asymmetric oscillations. Unfortunately, this review is frustrating as it highlights very few tools for proper non-sinusoidal oscillations analysis. Amongst these tools, non-sinusoidal spectral analyses are already available (see review for more details). Later, these same authors developed a cycle-by-cycle oscillations detection which respects the non-sinusoidal nature of the signal (Cole and Voytek, 2019). In my opinion, the era of Fourier-based analysis has brought plenty of knowledge about neuronal communication, but now it is time to turn into to the era of non-sinusoidal signal analysis.

### 1.1.2 – Spatiotemporal dynamics of the resting brain

The aim of this paragraph is to depict what the oscillatory brain activity looks like in time and in the different brain areas. Over time, repeated pattern occurs in brain oscillatory activity. Noteworthy, these patterns are correlated with vigilance states, namely non-rapid eye movement (NREM but also called slow wave sleep: SWS) and rapid eye movement (REM) sleeps, quiet and active wakefulness (Moser et al., 2009). However, if we go down to the LFP activity of brain areas, we observe different oscillatory patterns across brain areas during a same brain state. In order to describe the oscillatory map of the brain I had two options. First, describe oscillations state by state, but as different brain states can share similar frequency oscillations, it would be redundant. The second option, which I chose, was to describe the different frequency bands and then associate them to each brain state. To offer the reader a better representation of brain oscillations across the different brain states, I drew oscillatory brain map for each state (*Figure 6**Figure 7**Figure 8*). Please, note that I do not pretend to give an exhaustive view of what happens during each brain state, as it is beyond the scope of my thesis. However, I would like to give a comprehensive view how brain areas, that I was interested in during my PhD, oscillate across brain states. To be noted, I will focus on rodents' brain since most of the studies around my thesis project arise from these models.

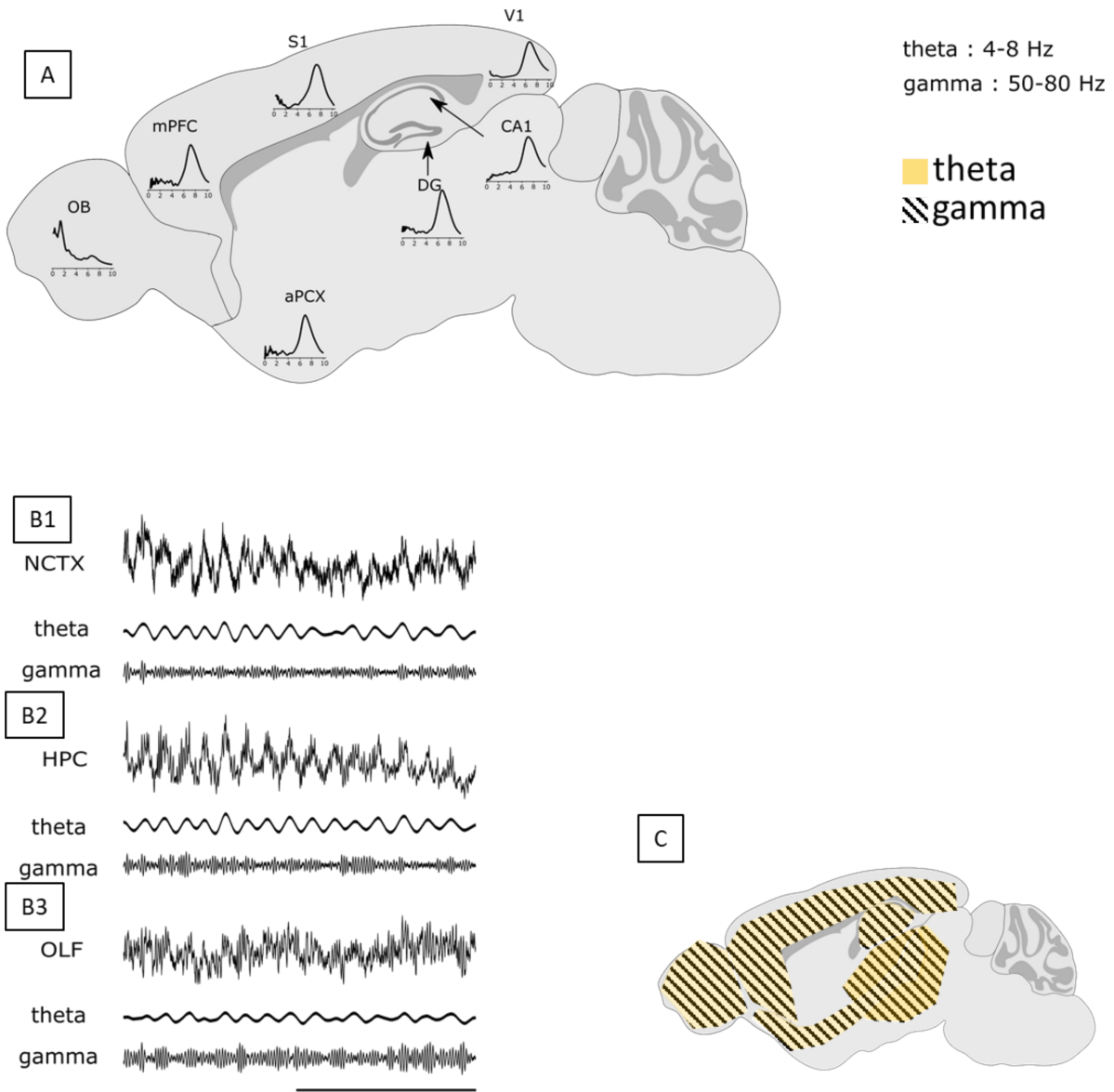


Figure 6 : REM oscillatory brain map. A. Power spectrum (0-10 Hz) of seven structures during NREM sleep. All spectra exhibit high power in a 6-8 Hz narrow band. Note: OB still maintains a respiration-related oscillation (2 Hz). B. Illustrative simultaneous raw signals and filtered signals in typical REM sleep frequency: theta (4-8 Hz) and gamma (50-80 Hz). Scale bar 1 s. B1 shows a neocortical signal (S1), B2 shows a hippocampal signal (CA1) and B3 shows an olfactory signal (aPCX). These traces highlight the domination of theta and gamma oscillations. D. Map distribution of REM rhythm. Theta (yellow) and gamma (black stripes) are observed in everywhere. OB: Olfactory bulb, mPFC: medial prefrontal cortex, S1: primary somatosensory (barrel field) cortex, aPCX : anterior piriform cortex, DG: dentate gyrus, CA1: Cornu Amonnis 1, V1: primary visual cortex.. Extracted from personal data. Brain image was taken from <https://scidraw.io>.

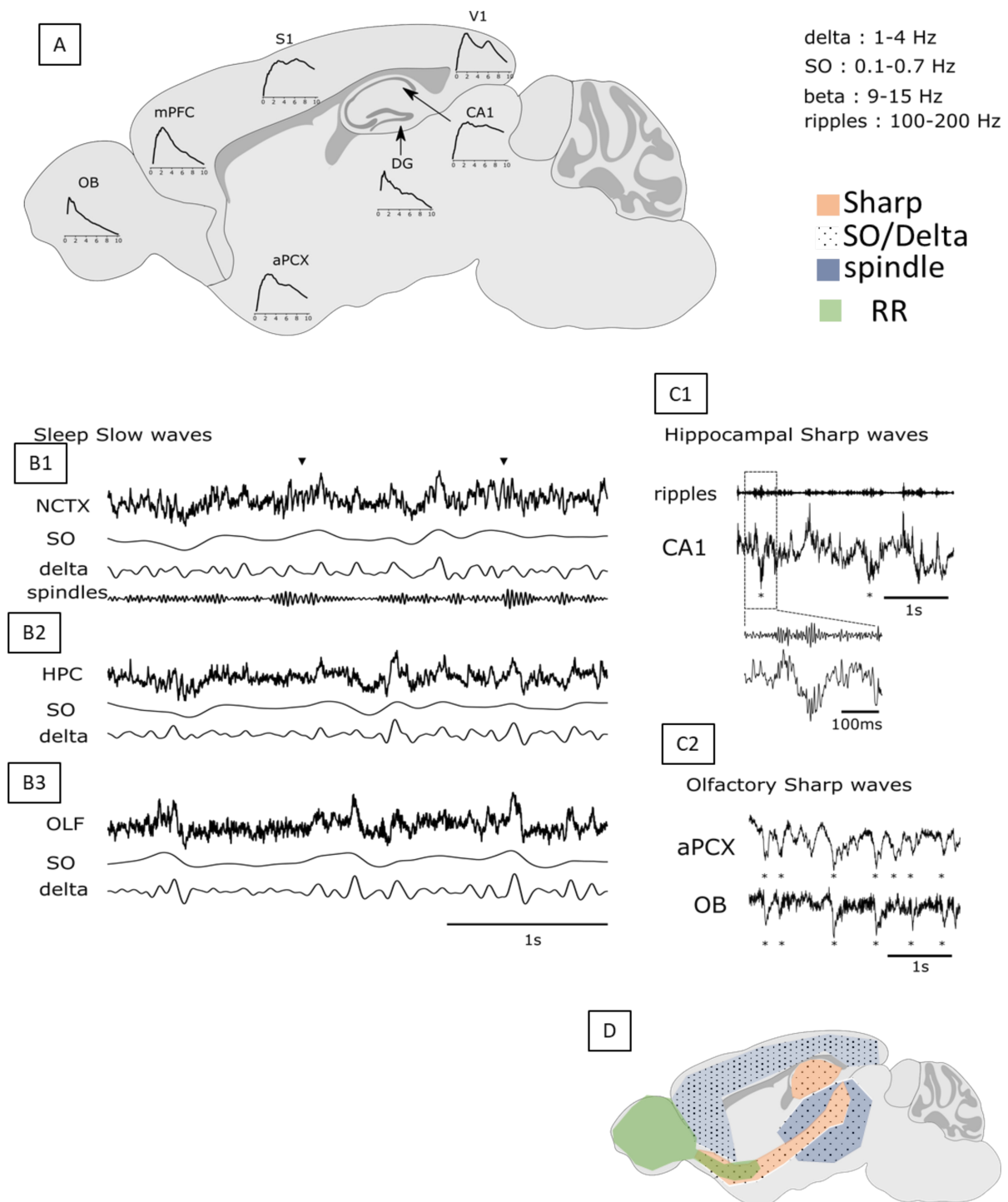


Figure 7 : NREM oscillatory brain map. A. Power spectrum (0-10 Hz) of seven structures during NREM sleep. All spectra exhibit high power in a 0-4 Hz broadband. B. Illustrative simultaneous raw signals and filtered signals in typical NREM sleep frequency: slow oscillation (0.1-0.7 Hz), delta (1-4 Hz), spindles (9-15 Hz). Scale bar 1 s. B1 shows a neocortical signal (S1), B2 shows a hippocampal signal (CA1) and B3 shows an olfactory signal (aPCX). These traces highlight the domination of low frequencies oscillations during NREM. Black triangles highlight sleep spindles. C. Illustration of sharp waves. C1. In the hippocampus sharp waves and ripples (100-200 Hz filter) can be observed. These events are coordinated with the sleep slow oscillation. C2. Olfactory system also exhibits sharp waves, which also are coordinated with neocortical sleep slow oscillation. However, they are not correlated to hippocampal sharp waves. Asterix highlight sharp waves events. D. Map distribution of NREM rhythm. Slow oscillation and delta (black spots) are observed in olfactory structures, hippocampus, neocortex and thalamus. Sharp waves (orange) are present in hippocampus and olfactory structure. Spindles (blue) are confined to thalamo-cortical circuit. Respiration-related oscillation (green) can be observed in olfactory structures. OB: Olfactory bulb, mPFC: medial prefrontal cortex, S1: primary somatosensory (barrel field) cortex, aPCX: anterior

piriform cortex, DG: dentate gyrus, CA1: Cornu Amomnis 1, V1: primary visual cortex. RR: respiration-related oscillations. Extracted from personal data. Brain image was taken from <https://scidraw.io>.

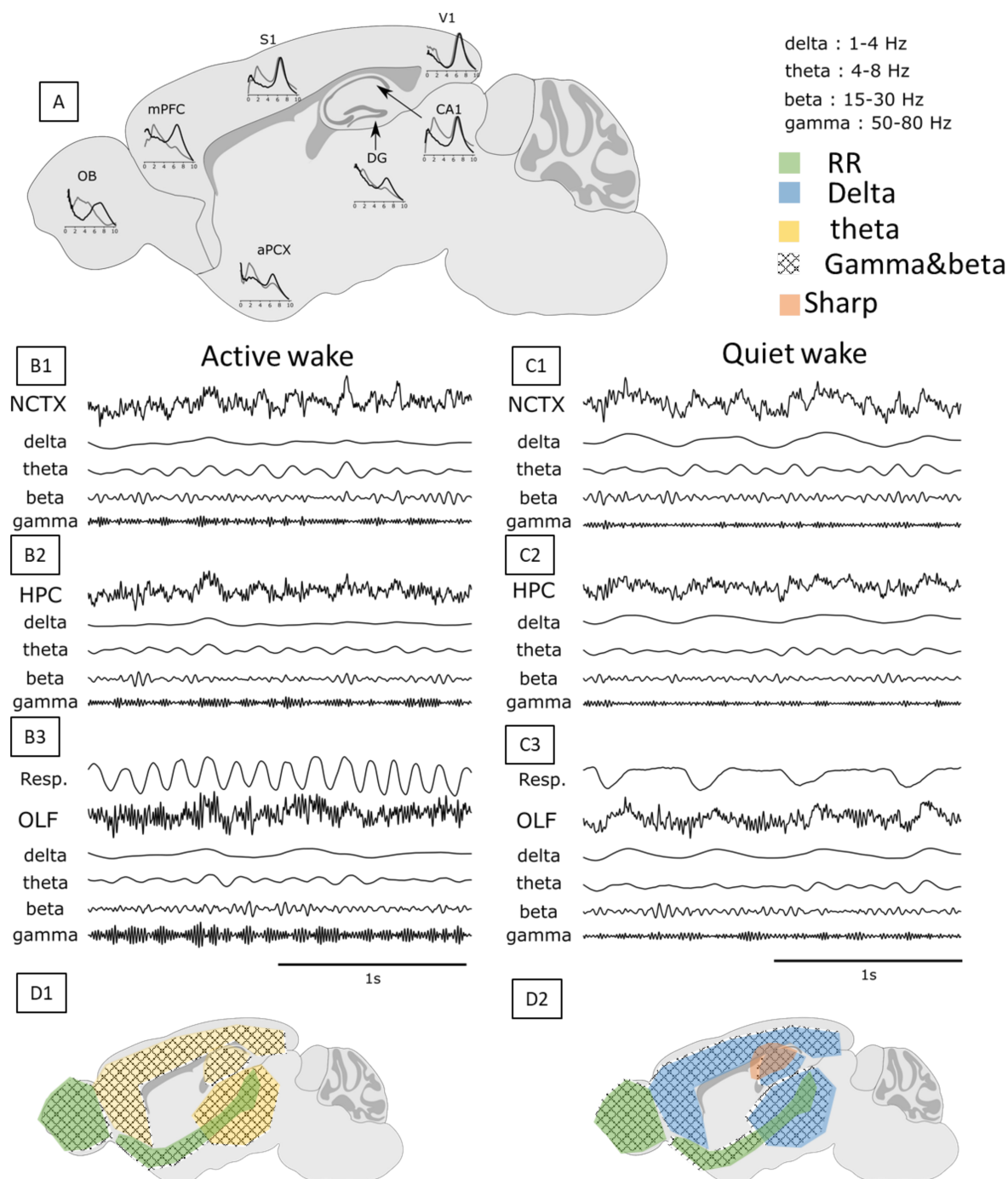


Figure 8 : Wakefulness oscillatory brain map. A. Power spectrum (0-10 Hz) of seven structures during active (black) and quiet (grey) wakefulness. In all structures, quiet and active power spectrum express similar frequencies. However, quiet wake exhibits stronger power in delta band (1-4 Hz). Note: high frequency power spectrum is not shown, but they should display high power in fast oscillations (beta and gamma). B. Illustrative simultaneous raw signals and filtered signals in typical active wakefulness frequency: delta (1-4 Hz), theta (4-8 Hz), beta (15-30 Hz) and gamma (50-80 Hz). Scale bar 1 s. B1 shows a neocortical signal (S1), B2 shows a hippocampal signal (CA1) and B3 shows an olfactory signal (aPCX) and respiratory signal (Resp.). Inspiration is down. These traces highlight the domination of theta and fast oscillations. C. Illustrative simultaneous raw signals and filtered signals in typical quiet wakefulness frequency: delta (1-4 Hz), theta (4-8 Hz), beta (15-30 Hz) and gamma (50-80 Hz). Scale bar 1 s. C1 shows a neocortical signal (S1), C2 shows a hippocampal signal (CA1) and C3 shows an olfactory signal (aPCX) and respiratory signal (Resp.). Inspiration is down. These traces highlight the domination of a delta oscillation probably linked to respiration. Fast oscillations are still present. D. Map distribution of

wakefulness rhythms. D1. During active wake, theta rhythm (yellow) is observed in all structures. In olfactory structures, theta rhythm (7Hz) can be confounded with sniffing entrained oscillation (6-10 Hz). Fast oscillations (black squaring) are observed everywhere. D2. During quiet wake, hippocampus can produce sharp waves (orange), delta oscillations (blue), potentially linked to respiration, are observed in neocortices, thalamus and hippocampus. Olfactory structures display respiration-related oscillations (green). Fast oscillations (black squaring) are observed everywhere. OB: Olfactory bulb, mPFC: medial prefrontal cortex, S1: primary somatosensory (barrel field) cortex, aPCX: anterior piriform cortex, DG: dentate gyrus, CA1: Cornus Amonnis 1, V1: primary visual cortex. RR = respiration-related oscillations. Extracted from personal data. Brain image was taken from <https://scidraw.io>.

### Behavior and oscillations define brain states, or vice versa

Over the course of the day, an animal will alternate between aroused and sleeping states. In parallel, brain oscillatory pattern will simultaneously alternate. Indeed, a faithful relation has been established between each brain state and oscillatory patterns (Gervasoni et al., 2004). NREM sleep is characterized by low external stimuli sensitivity and is associated with cortical slow oscillations (slow oscillations (<1 Hz), delta oscillations (1-4 Hz) and spindles (10-15 Hz) (Achermann and Borbély, 1997; Destexhe et al., 1999; Steriade, 1993). The other sleep state is REM sleep. It represents 20% of sleeping time and is associated to dreaming, even if dreaming has also been observed during NREM sleep (Siclari et al., 2018). REM sleep oscillatory pattern is associated with cortical high frequency oscillations (theta (4-8 Hz), beta (15-30 Hz), gamma (30-150 Hz)) similar to wakefulness (Destexhe et al., 1999; Steriade, 1993), and with a prominent theta oscillation in the hippocampus (Vanderwolf, 1969; Winson, 1974). Wakefulness corresponds to the conscious state and is composed of active wake, during which the animal explores, moves and quiet wake, where the animal does not move or makes stereotyped movement (eating, grooming) (Gervasoni et al., 2004). Active wake is associated with cortical fast oscillations (theta, beta and gamma) (Destexhe et al., 1999; Steriade, 1993) and an hippocampal theta (Winson, 1974). On the contrary, quiet wake encompasses slower oscillations (delta, theta) (Gervasoni et al., 2004). To reinforce the idea that brain states and behavioral states are tightly linked, Damien Gervasoni and colleagues in 2004 were able to precisely predict behavioral state through the analysis of several brain areas LFPs. Importantly, the analysis of brain state using LFP activities leads to spatial and temporal refinement of brain state transition. Indeed, EEG-mediated scoring gives access to a spatially smoothed brain state scoring. Studies using both EEG and LFP revealed local aspect of sleep (Siclari and Tononi, 2017). For example, sleep slow waves were considered as highly synchronized oscillation over the whole cortex, however DOWN states display spatial heterogeneity (Siclari and Tononi, 2017). Additionally, anesthetized and natural brain states were accurately identified thanks to olfactory bulb high frequency oscillations (gamma and beta) and hippocampal theta (Bagur et al., 2018). Local activity of these two particular areas fully replaced traditional EEG/EMG scoring.

### Brain oscillations: What? Where? How? Which functions?

Here, I will give a short overview of the principal brain oscillations, depicting i) what the oscillation looks like, ii) where and when the rhythm is observed, iii) how it is generated, and iv) which function the rhythm could support. The next paragraph (1.1.3 – Neuronal communication 1.1.4 – Concrete examples of long-range communication supported by slow rhythms) will go into details for the function of inter-areas coordination, the heart of my thesis topic.

- *Infra-slow oscillations (<0.1Hz)*. Infra-slow oscillations are periodical modulation of faster events like firing or alpha/sigma oscillations (Hughes et al., 2011). One can observe them in neocortices, hippocampus, basal ganglia, brainstem nuclei, and above all in the thalamus (Hughes et al., 2011). They are thought to be generated by an glia-neuron interaction (Hughes et al., 2011). Infra-slow oscillations functions are not well documented, nonetheless they divide NREM sleep into fragile (susceptibility to wake up) and continuous (sleep through) mode, and are linked with heartbeat variability (Lecci et al., 2017).

- *Sleep slow waves* are composed of slow oscillations (0.1-1Hz) and delta oscillations (1-4Hz) (see *Figure 7 B1, 2, and 3*)

*Slow oscillations (0.1-1Hz)*. The slow oscillation is an asymmetric oscillation, composed of a short DOWN state and a longer UP state. UP/DOWN states reflect membrane potential polarization of cortical neurons (Steriade et al., 1993a). DOWN state corresponds to a hyperpolarization of neocortical neurons, inducing a local discharge silencing. UP state contains neuronal activity including firing and oscillatory coupling. Indeed the slow oscillation phase-locks delta oscillations, spindles and also gamma oscillations during the UP state (Steriade, 2006). This oscillation is observed in neocortices and in the thalamus (Steriade et al., 1993a). The slow oscillation is generated by pacemaker cells in cortical layer V (Sanchez-Vives and McCormick, 2000). UP state initiations and terminations are modulated by astrocytes (Fellin et al., 2009; Poskanzer and Yuste, 2011). The slow oscillation is thought to mediate synaptic homeostasis and plasticity (Neske, 2016; Tononi and Cirelli, 2014). Furthermore, the slow oscillation allows information exchange in thalamo-cortical (Crunelli and Hughes, 2010) and cortico-hippocampal (Sirota et al., 2003) networks during NREM sleep. This information transfer between neocortices, hippocampus and thalamus supports memory consolidation (Rasch and Born, 2013). This function will be detailed in the next paragraph. Of note, two other slow oscillations exist in the NREM sleeping brain, one in the hippocampus (Wolansky et al., 2006) and the other in the olfactory system (Fontanini et al., 2003; Jessberger et al., 2016). Additionally, neocortical and hippocampal slow oscillations are coordinated. Otherwise, hippocampal slow oscillation is poorly studied. Finally, during NREM sleep, olfactory structures (olfactory bulb and piriform cortex) display a hybrid oscillatory pattern switching between a slow oscillation related to respiratory rhythm (Fontanini and Bower, 2006), and a neocortical-like slow oscillation (Jessberger et al., 2016; Onisawa et al., 2017).

*Delta oscillations (1-4Hz)*. Delta oscillations are broadband slow oscillations (1-4 Hz) occurring during deep NREM stages and quiet wake. Delta oscillations can be phase-locked to the neocortical slow (Steriade, 2006). As with the slow oscillation, delta oscillations are present in thalamus and neocortices. Two generators are proposed for delta, a cortical layer V pacemaker (Lörincz et al., 2015) and a thalamic generator (based on  $I_T$  and  $I_H$  currents) (Steriade et al., 1993b). The thalamic generator is supposed to drive delta oscillations (Gent et al., 2018). Delta oscillations share the same functions the neocortical slow oscillations, yet they are less studied.

- *Sleep spindles (10-15Hz)*. Sleep spindles are transient 10-15Hz oscillatory events with a duration between 6 et 15 cycles (Lüthi, 2014) (see *Figure 7 B1*). Spindles can phase-lock the slow oscillation (Steriade, 2006) and the infra-slow oscillation (Lecci et al., 2017). They are observed in the thalamocortical network (Lüthi, 2014). Generation of these oscillations results in the interaction between thalamic reticular nucleus and thalamocortical cells (Lüthi, 2014). Sleep spindles are associated with a decreased sensibility of sensory neocortices, neuronal plasticity, neuronal development, and memory (Lüthi, 2014; Rasch and Born, 2013).

- *Sharp waves and ripples*. Sharp waves and ripples are hippocampal events composed of a sharp wave (large LFP deflection) followed by ripples oscillations (150-250Hz) (Csicsvari et al., 2000; Ylinen et al., 1995) (see *Figure 7 C1*). These events can be coupled to the neocortical slow oscillation (Battaglia, 2004; Clemens et al., 2007; Isomura et al., 2006; Mölle et al., 2006). Sharp waves and ripples are observed in CA1, during NREM and quiet wake (Girardeau and Zugaro, 2011; Roumis and Frank, 2015). They are the consequence of CA3 burst inputs, causing a strong sink (sharp wave) in CA1 apical dendrite layer (*stratum radiatum*), whereas interneuron stimulation in soma layer (*stratum pyramidale*) induces high frequency oscillations (ripples) (Csicsvari et al., 2000; Girardeau and Zugaro, 2011). Hence, sharp waves and ripples waveforms depend on CA1 depth. Sharp waves and ripples are involved in plasticity and memory consolidation through sleep reactivation of awake experience (Girardeau and Zugaro, 2011; Rasch and

Born, 2013). Sharp-waves are also observed in olfactory structures (see *Figure 7 C2*) (Manabe et al., 2011; Onisawa et al., 2017), however these events are restricted to olfactory structures and are uncorrelated with hippocampal sharp-waves.

- *Theta (4-8Hz)*. Theta rhythm are 4-8Hz (see *Figure 6 B1, 2, and 3; Figure 8 B1, 2, and 3*) oscillations typically referenced as the hippocampal rhythm, nonetheless it is also observed in olfactory structures, neocortices and limbic structures, hypothalamus (Kahana et al., 2001; A. B. L. Tort et al., 2018). This rhythm appears during REM sleep and wakefulness. Hippocampal theta pacemakers have been identified in the medial septum (Colgin, 2013), however for the other regions no generators are known (Kahana et al., 2001). Volume conduction from hippocampus to the rest of the brain is envisaged (Colgin, 2013). During REM sleep, theta rhythm allows neuronal reactivation and synaptic plasticity, yet evidence of memory consolidation induced by REM theta are weak (Rasch and Born, 2013). Furthermore, neocortices, limbic areas and hippocampus coordination is impaired during REM sleep (reduced coherence in theta and gamma range) and these areas are thought to process local information (Rasch and Born, 2013). During wakefulness, theta rhythm is involved in information multiplexing, navigation through theta phase precession, inter-areas coordination (Colgin, 2013). Interestingly theta frequency matches with some sensory sampling frequencies like rodent sniffing (Macrides et al., 1982) and whisking (Berg and Kleinfeld, 2003), human eye-saccades (Bonfond et al., 2017).

- *Gamma (30-150Hz)*. Gamma oscillations cover a huge frequency band (30-150Hz) (see *Figure 6 B1, 2, and 3; Figure 8 B1, 2, and 3*) These oscillations are observed in every brain areas (Buzsáki and Wang, 2012), and during every brain state, although prominent during REM and wakefulness. Several models are proposed for gamma oscillation generation, and all models are based on a pyramidal neuron perisomatic inhibition mediated by local interneurons via GABA<sub>A</sub> receptors (Buzsáki and Wang, 2012). Hence, they are local oscillations. Gamma oscillations are proposed to favor information transfer between neural assemblies (detailed in 1.1.3 – Neuronal communication).

### **1.1.3 – Neuronal communication through oscillations**

This paragraph aims to explain the current theory of information exchange between distant neurons, namely cross-frequency coupling. It will anchor low frequency rhythms as brain orchestrators and bring them to of outstanding interest. Furthermore, it will justify the upcoming track for respiratory-related oscillation all over the brain.

#### **1.1.3.1 What is a cell assembly?**

Brain is organized as a distributed system with several scales of distribution; indeed, the brain contains specialized structures (*e.g.*, cortex, thalamus, hippocampus), structures are subdivided in specialized areas (visual or somatosensory cortices, thalamic nuclei), areas may themselves be subdivided in specialized layers (thalamic reception function of neocortical layer IV), even single neurons can be specialized (hippocampal place cells, anterior thalamic head-direction cells). However, adapted behavioral responses required a correct integration of input information and a coordinated output. Hebbian theories (Hebb, 1949) proposed cell assemblies, *i.e.* local interconnected neurons which fire in close timing relation, as the cognitive elementary unit. Nonetheless, the terms local and related information may be blurred as brain displays several scales of specialization. In any case, come two problems: 1) how cell assemblies are shaped and dynamically reshaped? 2) How distant assemblies, therefore supposed to underlie different information, are bound and coordinated?

### 1.1.3.2 How does a cell assembly work?

In theory, neuronal information transfer would require neuronal transduction from one input AP toward an output AP. However, this 1:1 ratio is never observed neither *in vitro* nor *in vivo*, in other words, a single EPSP cannot trigger an AP. Neurons are rather modeled as coincidence detectors (Abeles, 1982; König et al., 1996), that is, an AP is emitted when multiple EPSP are embedded in a precise time window. As an illustration, if a neuron receives randomized inputs from several other neurons, the output function of the neuron of interest will reveal input coincidences. The time window for coincidence detection mostly depends on post-synaptic current channels (AMPA, NMDA, GABA<sub>A</sub>) time constant (König et al., 1996) and quantities (Daoudal, 2003). Coincidence time window for cortical neurons is in magnitude order of few milliseconds (König et al., 1996). Well synchronized excitatory inputs result in a short and large EPSP, which triggers AP with more efficiency compared to long-lasting depolarization (Azouz and Gray, 2000). Consistently with Hebbian learning, *i.e.* reinforcement of synapses that elicit AP, cell assembly formation is a robust means for synaptic plasticity (Fell and Axmacher, 2011). As a consequence, repeated formations of one cell assembly are facilitated over time. Spike timing-dependent plasticity reinforces the most synchronized assemblies. Therefore, coincidence detection mode is a fundamental cornerstone for cell assembly existence, as it justifies the need for temporal synchronization. However, brain does not process random information, thus there must be a mechanism that schedules these “coincidences”.

### 1.1.3.3 Gamma oscillations as time unit for information exchange

Gamma oscillations as a means for cell assembly shaping.

As explained previously (1.1.1 – What is the brain electrical activity?) LFP mainly represents synaptic currents, then LFP oscillations reflect excitability fluctuations of the underlying neuronal population (Buzsáki et al., 2012). Thus, LFP oscillations design time windows suited for information transfer (high excitability) and on the contrary time windows during which communication is impaired (low excitability). In the point of view of a neuron, speaking time is discontinuous and imposed by the LFP fluctuations. Hence, cell assemblies are preferentially put together during LFP peak, which corresponds to moment with the higher firing rate of neurons (see *Figure 9 B*, blue curve inset). Such LFP phase-locking of firing has been observed in different frequency band, *e.g.* sleep slow oscillation (Steriade et al., 1993a), theta (Fox et al., 1986; O’Keefe and Recce, 1993), gamma (Csicsvari et al., 2003; Eeckman and Freeman, 1990; Jacobs et al., 2007; Womelsdorf et al., 2007). Amongst all mentioned rhythms, gamma is the only one with compatible features to shape cell assembly. First, based on the principle of coincidence detector, timing of an assembly is fundamental, and has been estimated to be below 15ms (König et al., 1996). Secondly, in the case of hippocampal-mediated navigation, firing of place cells supports spatial information, and animal position can be predicted by the sequence of firing of individual cells (O’Keefe and Recce, 1993). Further experiments showed the prediction is more accurate if we consider firing of assemblies rather than individual cells (Harris et al., 2003). This suggests cell assembly firing supports a more reliable information than isolated spikes. Then, on the same data, authors defined cell assembly of variable duration for their predictions. Optimal predictions of animal position were obtained with cell assemblies of 10-30ms. This functional time windows is consistent with previous model estimation (König et al., 1996). The only LFP rhythm with compatible time windows is gamma (frequency :30-150Hz, period 33.3ms – 6.6 ms)

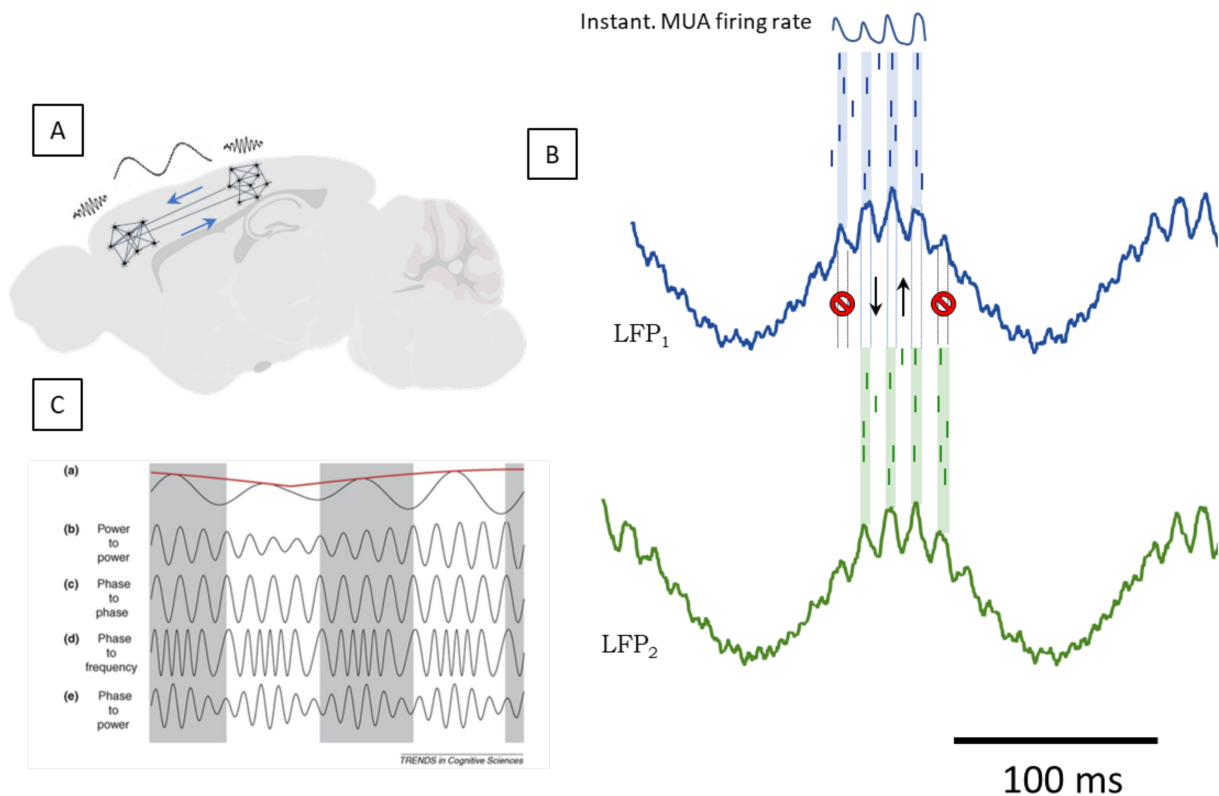


Figure 9 : Schematic representation of long-range communication through cross-frequency coupling. A. Long-range communication rely on dense local connection and rare projections, allowing an efficient communication with a wiring economy. Brain image was taken from <https://scidraw.io> B. Artificial signal illustrating information exchange through cross-frequency coupling (theta: 7Hz, gamma: 80Hz) between two brain areas. Blue rectangles show cell assemblies time windows allocated gamma oscillations (see cell assembly formation). Top blue curve represents the instantaneous firing rate of the population. Most AP are restricted to gamma peaks. Low frequency rhythm, here theta, aligned some gamma cycles, allowing information transfer between distant brain areas (blue arrows). Precise low frequency coordination is required otherwise, gamma misalignment renders communication not possible (red prohibition signage). Scale bar: 100 ms. Simulated signals.C. Different possibilities of cross-frequency coupling. (a) Slow rhythm (blue) and its envelope (red). (b) Envelope of the fast rhythm is modulated by the slow envelope. (c) Phases of the two rhythm are synchronized here with a (5:1 ratio). (d) frequency of the fast rhythm is modulated by slow rhythm phase. (e) Envelope of the fast rhythm is modulated by the phase of the slow rhythm. This case is also called phase-amplitude coupling (PAC). Extracted from Jensen and Colgin, 2007.

#### Gamma synchrony establish communication channel between cell assemblies.

So far, I explained how gamma oscillation form unit of information, *i.e.*, a cell assembly. However, information processing will require coordination of a myriad of assemblies, especially in system where information is processed in parallel. First evidence of fast rhythm being involved in neural communication come from olfactory system. From a 64 channels matrix placed on the olfactory bulb, Walter Freeman observed gamma synchronization pattern that varied according to the meaning of the odor (Freeman and Schneider, 1982). This suggests that at the level of the structure, information is carried by gamma synchronization. Underlying idea is that a multitude of cell assemblies are shaped all across the olfactory bulb, but the information is supported by the way (synchronization pattern) assemblies are coordinated in time. The idea has been extensively developed in the visual cortex. Distant columns in the visual cortex respond to different stimulus (Van Essen et al., 1992). Singer's group showed preferred stimulus elicits a gamma paced response in LFP and firing in a column (Gray and Singer, 1989). Furthermore, during stimulus presentation distant columns can synchronize their firing response in gamma range (Gray et al., 1989). These gamma synchronizations are transient (100-900 ms in cats : Gray et al., 1992 and 100-300 ms in macaques Kreiter

and Singer, 1992). To summarize, gamma oscillations shape cell assemblies and gamma synchronization in space ensure binding of these assemblies. Gamma synchronization allows establishing functional network. Later in 2005 and 2015, Pascal Fries synthesized and proposed to export these findings from olfactory and visual system to the whole brain through to the theory of “communication through coherence”.

### **1.1.3.4 Long-range communication**

As tackled previously, information processing requires coordination at each step of the system. An assembly corresponds to coordinated neurons. Two areas synchronized on gamma rhythm correspond to coordinated assemblies. However, gamma oscillations are locally generated (Buzsáki and Wang, 2012; Cardin et al., 2009). Therefore, it involves the synchronization of two (at least) distant and independent gamma oscillators. It is highlighting a contradiction, how a rhythm can be local and distant at the same time? If fast rhythms cannot support all facets of long-range communication, we should have a look on slower ones. Slow rhythms (<10Hz) are characterized by oscillations of long periods allowing the integration of lot of inputs. As a consequence amplitude of slow rhythm are usually larger than faster ones (Buzsáki et al., 2012). Additionally to the greater number of inputs, slow rhythms allow the integration of inputs from a large volume, thus from distant neurons (Buzsáki et al., 2012; von Stein and Sarnthein, 2000). Slow rhythms (<10Hz) are observed over long distance (Buzsáki et al., 2012). Therefore, the same oscillator could synchronize distant neurons. However, time windows proposed by slow rhythms are not compatible with formation of assemblies. To summarize, on the one hand fast rhythm locally set up cell assemblies and on the other hand, slow rhythms can bind distant areas. These two families of rhythms have then complementary features. Consequently, long-range communication could be achieved by coupling slow and fast rhythms. This idea is supported by the observation of hierarchy between rhythms (Lakatos et al., 2005). Indeed, as presented above, the slower the rhythm the larger. Therefore, a slower rhythm can constrain a faster one, which is called cross-frequency coupling. Cross-frequency coupling can display different appearances (see *Figure 9 C*). The most studied and most intuitive is the phase-amplitude coupling. It means the phase of the slow rhythm constrains the power of the fast rhythm. In other term, slow rhythms control fast rhythms dynamics, and this over distance. Furthermore, based on anatomy and modeling, neuronal networks exhibit dense local connection and few long-range projections (see *Figure 9 A*). This organization favors efficient local processing and then transmission of treated information with low cost wiring (Buzsáki et al., 2004). This wiring hierarchy is echoing oscillatory hierarchy, indeed cross-frequency coupling involves a global (slow) rhythm which constrains the activity (phase and/or amplitude) of a local (faster) rhythm (Bonfond et al., 2017; Canolty and Knight, 2010; Jensen and Colgin, 2007). Therefore, slow rhythms are thought to be a major actor in the selection of communicating areas. Although focused on alpha in the visual system, Bonfond and colleagues in 2017 advanced several predictions for a slow rhythm to be a good brain coordinator. They suggest that “interareal synchrony control the transfer of information carried by gamma oscillations”, meaning there are two levels of synchrony, slow rhythms synchrony binds two areas, but information transfer is mediated by gamma oscillations synchrony (see *Figure 9 B*). Additionally, “to communicate between two specific pools of neurons, alpha oscillation must be modulated locally on a fine spatial scale”. In other words, the slow rhythm must pop up simultaneously in concerned areas. To conclude, cross-frequency coupling cumulate spatial precision of the slow rhythm with the temporal precision of the fast ones. This low/high frequency coupling, imputed to inter-areal communication, has been observed with all low frequency rhythms, namely theta (Canolty et al., 2006; Chrobak and Buzsáki, 1998; Colgin et al., 2009), alpha (Cohen et al., 2008; Palva et al., 2005), delta (Lakatos et al., 2005), and sleep slow oscillations (Hasenstaub et al., 2005; Isomura et al., 2006; Steriade et al., 1993b)

### **1.1.4 – Concrete examples of long-range communication supported by slow rhythms**

My PhD topic hinge in two actors, on the one hand brain rhythms and on the other hand respiratory rhythm. Now, that foundations are laid on “what is the electrical activity?”, “how oscillations are distributed in brain space and time?” and “how oscillations mediate long-range communication?”, we can go closer to the other actor of my PhD: respiratory rhythm. However, before directly demonstrate respiratory rhythm can be one of the coordinator rhythms of the brain, I will present some of its competitors. I chose to present long-range communication properties of theta rhythm and sleep slow waves, as they are prominent rhythms in rodent brain

#### **1.1.4.1 – Sleep slow waves (0.1-4.5Hz), a NREM coordinator**

Quick reminder from 1.1.2 – Spatiotemporal dynamics of the resting brain :

Sleep slow waves contains actually two rhythms, the slow oscillation (0.1-1 Hz) and delta rhythm (1-4 Hz). They occur during NREM sleep. First identified in thalamo-cortical circuit, equivalent oscillations were observed in the hippocampus and olfactory structures.

Communication between brain structures

During NREM, three brain structures seem interconnected: thalamus, neocortex and hippocampus. This triade is important for memory consolidation (Möller and Born, 2011; Rasch and Born, 2013). NREM sleep hallmarks of neocortices are sleep slow waves, thalamic hallmarks are sleep spindles and hippocampal hallmarks are sharp-waves and ripples. Oscillatory dynamics of these three structures have been shown not to be independent. Indeed ripples and spindles phase-lock the slow oscillation in rodent (Isomura et al., 2006; Latchoumane et al., 2017; Möller et al., 2006; Siapas and Wilson, 1998; Sirota et al., 2003; Steriade et al., 1993b) and in human (Clemens et al., 2011, 2007; Helfrich et al., 2019; Staresina et al., 2015). Also ripples are phase-locked to spindles (Siapas and Wilson, 1998; Sirota et al., 2003). Additionally, cerebellar activity is coupled to slow oscillation and spindles (Xu et al., 2021). Therefore, the sleep slow oscillation mediates a dynamic binding between thalamus, neocortex, hippocampus and cerebellum. As the coordination of these areas is closely related with memory consolidation (Hahn et al., 2020; Helfrich et al., 2018; Latchoumane et al., 2017; Möller et al., 2009; Muehlroth et al., 2019; Xu et al., 2021), one can suggest the coupling supports information exchange. However, this long-range communication does not suit for basal ganglia, since the different nuclei fire independently from sleep slow oscillation (Mizrahi-Kliger et al., 2018).

Communication between cortical areas

During NREM sleep, neocortical slow waves have long been thought to be homogenous, resulting in a hyper-synchronous neocortex. This would mean that in the neocortex all neurons talk to all neurons at the same time. However, fine-tuned sleep analysis revealed NREM sleep oscillations display spatial heterogeneity (Cox et al., 2014; Fernandez et al., 2017; Massimini et al., 2004; Nir et al., 2011; Siclari and Tononi, 2017; Vyazovskiy et al., 2011). As a reminder, 3<sup>rd</sup> prediction of Mathilde Bonnefond (Bonnefond et al., 2017), proposed that a good coordinator rhythm must display spatial dynamics. Hence, sleep slow waves locality may serve to shape neocortical subnetworks (Cox et al., 2014; Fernandez et al., 2017).

Olfactory slow oscillation.

As discussed earlier, olfactory structures present hybrid NREM oscillations alternating between respiratory rhythm and a slow oscillation close the one from neocortex. Piriform cortex also display sharp waves which are correlated with olfactory areas (olfactory bulb (Manabe et al., 2011) and olfactory tubercle (Narikiyo et al., 2014)) but also with neocortical slow oscillation (Onisawa et al., 2017). These sharp waves are not related to hippocampal sharp waves and ripples (Manabe et al., 2011). Then, an olfactory slow oscillation mediates olfactory information transfer, but that slow oscillation is also linked

to neocortical slow oscillation, which probably enable olfactory-neocortex communication.

#### ***1.1.4.2 - Theta rhythm (4-8Hz), a REM and active wake coordinator***

Quick reminder from 1.1.2 – Spatiotemporal dynamics of the resting brain :

Theta is a 4-8 Hz oscillation. Theta is the hallmark of active wake and REM sleep oscillatory activity of the hippocampus. Furthermore, it often modulates gamma amplitude (Canolty et al., 2006; Winson, 1974). To be noticed, theta-gamma coupling is higher during REM sleep compared to wake (Scheffzük et al., 2011)

##### REM sleep coordinator

During REM sleep, neocortices (infra- and pre-limbic, cingulate cortices), hippocampus (dorsal and ventral) and amygdala display coherent theta oscillations (Popa et al., 2010; Totty et al., 2017; Vijayan et al., 2017). Contrarily to sleep slow waves in NREM sleep, REM theta synchronization is very constant, hence the resulting network shows very little dynamic. Nonetheless, this theta-shaped network supports emotion and fear memory consolidation (Popa et al., 2010; Totty et al., 2017; Vijayan et al., 2017).

##### Active wake coordinator

Active wake is a period of extreme sensitivity to the environment, where all senses are in alert. The brain has to handle with olfactory, visual, auditory, sensory, proprioceptive information. In addition, environments or behaviors constantly evolve, and consequently, activity of brain areas must adapt to these changes. For the brain, it means relevant areas (sensory and associative) must be put forth as quick as the context imposes it. So, there must be as many active wake networks as there are different contexts existing. To illustrate my purpose with a very naïve example: for an instant the brain will be in an environment where vision and audition are important, but a short moment after, olfaction becomes the only important sense, and so on. So, each context requires different weighting of the senses and the internal information (memory, physiological needs). Furthermore, theta is a predominant rhythm of the awake brain oscillatory activity. So, the question is: can theta rhythm mediate long-range communication during active wake. In addition, theta rhythm is observed to synchronized various brain areas, e.g. the anterior thalamus and the hippocampus (Albo et al., 2003), neocortices (primary and secondary motor, somatosensory, posterior associative, secondary visual, entorhinal and retrosplenial) and the hippocampus (Mizuseki et al., 2009; Schomburg et al., 2014; Sirota et al., 2008), the striatum and the neocortex (von Nicolai et al., 2014). Some cognitive function appears correlated with binding of brain areas by theta rhythm. I chose to illustrate it with the example of spatial navigation in a T or Y maze. This task involves the rodent to decision making, memory and spatial navigation. Animals are motivated by a reward placed in one of the two arms. Usually, animal have to learn a rule to predict where will be the reward. During the task prefrontal cortex (Benchenane et al., 2010; Ito et al., 2018, 2015), striatum (DeCoteau et al., 2007; Tort et al., 2008), reuniens thalamic nucleus (Ito et al., 2018, 2015) are synchronized to hippocampal theta (Benchenane et al., 2010; DeCoteau et al., 2007; Ito et al., 2018, 2015; Tort et al., 2008). Prefrontal is thought to participate in the decision making, the striatum and the hippocampus couple to support spatial navigation, and the hippocampus to provide learning and recall of the task. Hence, each area has a specialized function, but theta rhythm coordinates the good couples at the good time, allowing the completion of the task. To conclude, active wake is a very dynamic state during which the brain has to adapt to what is going on. So, there should be plenty of different networks. Current research highlights mainly theta rhythm as the active wake coordinator. However, with such variability during this state, it would be surprising if theta rhythm were the only master clock.

## 1.2. – Respiratory & brain rhythms: how the couple has been seen so far?

First things first, I need to clarify the different term associated to respiration. Four terms may be confusing for uninitiated, namely respiration, breathing, respiratory rhythm and ventilation. **Breathing** and **respiration** are synonyms. They correspond to all the steps allowing consumption of O<sub>2</sub> and reject of CO<sub>2</sub> for an organism. For mammals, it includes airflow generation, alveolar gas exchange, blood flow generation, tissular gas exchange, cellular and mitochondrial metabolism. **Ventilation** is the mechanism enabling the air renewable through inflation and deflation of the lungs. **Respiratory rhythm** describes the temporal dynamic of this airflow. Amongst its principal parameters, one can quote frequency, inspiration duration or inspiration-expiration ratio (see *Figure 10 A*). Complementarily, information given by the amplitude of the signal allows to access respiratory volume (see *Figure 10 A*). Nevertheless, in the forthcoming literature breathing and respiration are often assimilated to respiratory rhythm. To be noted, **sniffing** is used to depict high frequency respiratory rhythm. The exploration of an olfactory environment elicits sniffing, referred as **active exploration** (see *Figure 10 B – exploration*).

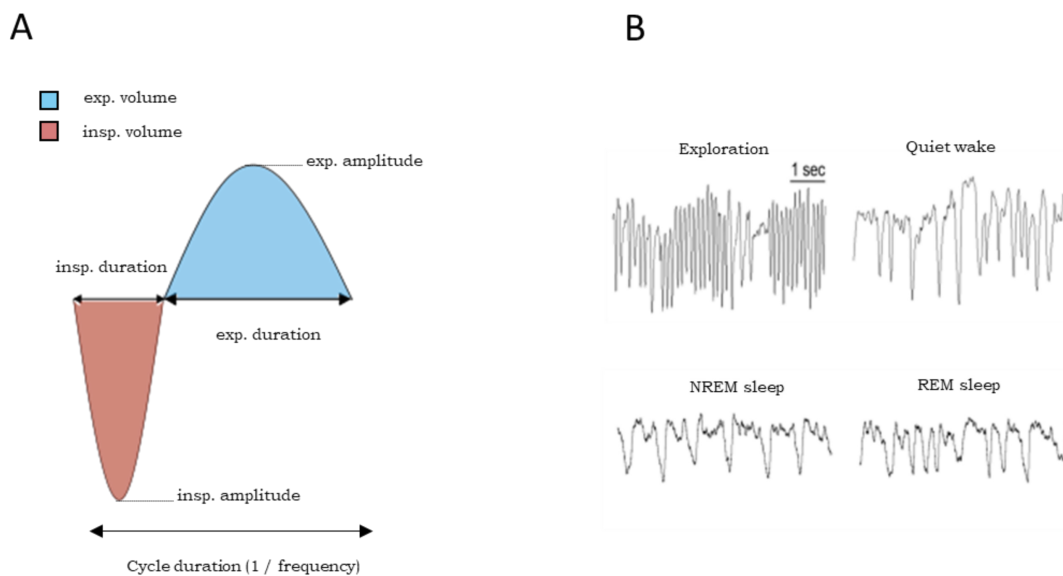


*Figure 10 : Respiration covers a wide range of frequencies and patterns. A. Presentation of the usual parameters to characterize a respiratory cycle. Simulated signal B. Respiratory pattern varied across vigilance state. Here are presented respiratory signal during exploration (upper left), quiet wake (upper right), REM sleep (lower left) and NREM sleep (lower right). Extracted from Girin et al., 2021.*

As mentioned previously, respiration (and heartbeat) involves chest movements. These movements mechanically spread in the body, and the brain is not preserved from them. For this reason, respiration-related events in electrophysiology have long been thought to be annoying artefact. Nevertheless, two research fields did not ignore respiration, on the one hand research on the physiology of respiration, and on the other hand research on olfactory system. In this section, I will first explain how respiratory rhythm is generated, then I will review respiratory feedback onto psychology, and finally I will present how respiratory rhythm completely shapes neuronal activity in the olfactory system. Most important, this section aims at providing clues suggesting respiratory rhythm has a brain-wide role, which justifies the urge for tracking respiratory modulation in the whole brain (see 1.3 The new face of Respiration-related oscillations).

### 1.2.1 – Respiratory rhythm generation

Del Negro and colleagues in 2018 offered an excellent review about the current view of mammals' respiratory rhythm generation. Respiratory cycle contains up to three phases: inspiration, post-inspiration and active expiration. At rest, inspiration is assumed by the contraction of the diaphragm. Lung volume expansion is enabled by the particular form of the diaphragm and its adherence to the lungs. Because of the expansion, air is sucked into the lungs. Lungs elasticity and diaphragm relaxation produce passive expiration. Post-inspiration corresponds to maintained contraction of diaphragm, which delays lung deflation (see *Figure 11*) Gas exchange time is therefore increased. Active expiration is mediated by expiratory muscles, which fasten and amplify diaphragm lift. Post-inspiration and active expiration are observed occasionally, these phases are considered conditional. On the contrary, all respiratory cycles present an inspiration, consequently this phase is inexorable. (see inset *Figure 11*). For the following section, I will focus on inspiration and active expiration. Each phase is handled by different brainstem nuclei: inspiration is constantly generated by pacemaker neurons in preBötzinger complex, while active expiration is conditionally generated by pacemaker neurons in the parafacial nucleus (also called retrotrapezoidal nucleus). Firing of these pacemakers activate inspiratory, respectively expiratory, motor nuclei. Respiratory nuclei receive a bunch of chemo- and mechano-feedbacks from the body, which allowed to adapt respiration to physiological needs (see *Figure 11* However, I will not detail these, as it is beyond the scope of my thesis. Interestingly, preBötzinger complex and parafacial nuclei have broad projections toward non-motor structures. Noteworthy, preBötzinger projects to locus coeruleus, which noradrenergic projections invade the entire brain (Jones and Moore, 1977). Parafacial nucleus project on pedunculopontine, which cholinergic projections also invade brain. One can suppose, respiratory rhythm modulates neuromodulator levels of the brain. Hence, there are few synapses between respiratory nuclei and the rest of the brain. Whether a global respiratory modulation of the brain transits through these projections remained an unanswered question.

Now that the very basis of respiration definitions and generation are laid, I will present the first evidence showing that respiratory rhythm impacts high order brain structures functioning.

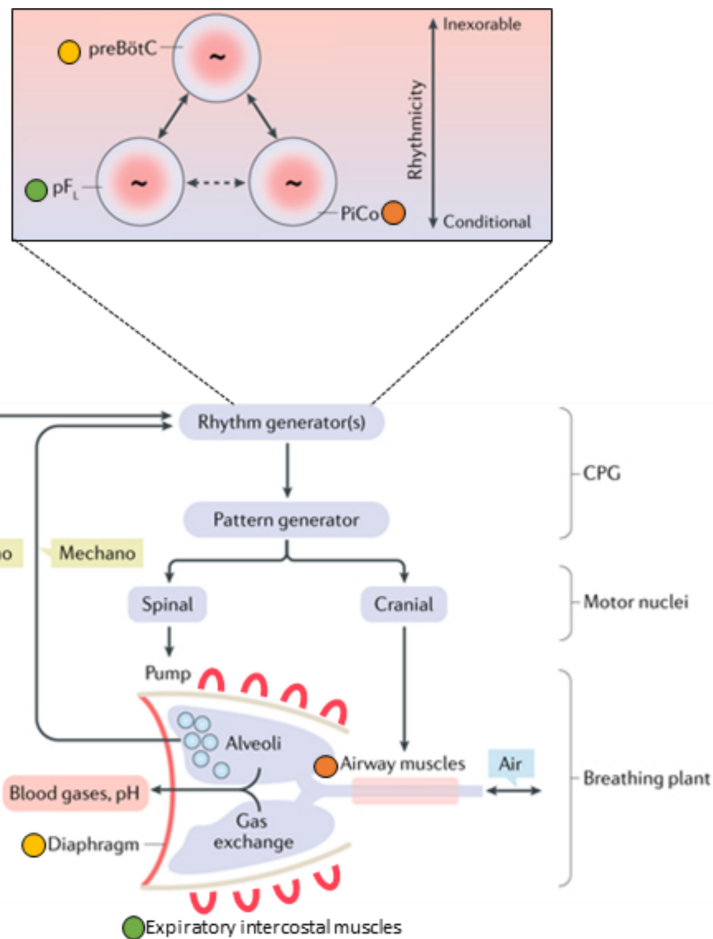


Figure 11 : Schematic organization of the generation of respiration. Temporal dynamic of respiratory pattern is determined by the discharge frequency of rhythm generator neurons. Amplitude features of respiratory pattern depend on the strength of inputs onto pattern generator neurons. Diaphragm contraction is involved at each inspiration. Forced expiration recruits expiratory muscle like external intercostal muscle. Contraction of airway muscle increases resistance, which lengthen gaz exchange time. Inset: Details of respiratory rhythm generators. Only the inspiratory (generator in the preBötz) rhythm generator is inexorable, forced expiration (generator in the pFL) and post-inspiration (generator in the PiCO) are conditional. Green, orange and yellow dot associate rhythm generator (presented in the inset), which principal effectors. preBötz: preBötzingner complex, pFL: parafacial nucleus, PiCO: post-inspiration complex. Adapted from Del Negro et al., 2018.

### 1.2.2 – Respiratory rhythm interaction with brain and body

While the rest of the thesis focus on rodents, the following paragraph concerns mainly human studies.

Respiratory signal can flexibly explore various frequency and flow rate. Variation range depends on the size of the studied animal. Looking at rest frequencies, humans breathe at 0.2-0.4 Hz (Krieger et al., 1990), rats at 1-4 Hz (Girin et al., 2021, and see Figure 10), and mice at 3-5 Hz (Wesson et al., 2008). The breathed air volume depends on both the frequency, *i.e.* the duration of a cycle, and the flow rate, *i.e.* the volume per second that is displaced. The relation is not linear, as  $Volume = flow\ rate / frequency$ . For example, for the higher respiratory frequency, so called sniffing, cycle duration is so short that even high flow rate does not allow stirring a big volume.

In addition to set air volume consumption, the way we breathe (slow vs fast) influences cardiovascular variable such as heart rate variability (HRV), respiratory sinus arrhythmia (RSA). The HRV measures the instantaneous heart rate variability. Across a respiratory cycle, heart rate varies. The RSA measures heart rate difference between inspiration and expiration. HRV and RSA increase are associated to peaceful feelings (Zaccaro et al., 2018). Slow breathing tends to increase both HRV and RSA (Zaccaro et al., 2018). Besides

physiological changes, respiratory regime has been highlighted to affect human's mood. Indeed, deep (large amplitude) and slow respiration is associated to peaceful state, whereas fast respiration is associated to stress (Brown and Gerbarg, 2009; Carnevali et al., 2013; Homma and Masaoka, 2008; Pappenheimer, 1977; Suess et al., 1980). Furthermore, respiration is intimately linked with emotion (Homma and Masaoka, 2008). In particular, Philippot and colleagues in 2002 led a two-step study. First, they evoked emotion on subjects and monitored associated respiratory patterns. Consistently with Boiten et al., 1994, they observe a different respiratory pattern for each emotion. Secondly, they discretely imposed respiratory pattern to subjects. Interestingly they showed that respiratory pattern triggers the associated emotion. Mood and cardiovascular results indicates that slow breathing promotes parasympathetic tone (calm behaviors), whereas fast breathing promotes sympathetic tone (aroused and stressed behaviors) (Brown and Gerbarg, 2009; Noble and Hochman, 2019; Zaccaro et al., 2018). Notably, Noble and Hochman in 2019 proposed to consider basal respiratory frequency as a stress indicator, since respiratory frequency reflects parasympathetic/sympathetic balance. A recent meta-analysis of slow breathing techniques (Zaccaro et al., 2018) highlighted seven (out of eleven) studies that shows slow breathing has positive effect on psychology or behavior (Edmonds et al., 2009; Gross et al., 2016; Gruzelier et al., 2014; Lehrer et al., 2003; Lin et al., 2014; Park and Park, 2012; Van Diest et al., 2014). However to contrast this view, four similar studies did not found clear effect (Kharya et al., 2014; Sakakibara et al., 2013; Siepmann et al., 2008; Stark et al., 2000). Physiological benefits (heart-respiration synchronization) and relaxation induced by slow breathing are used in association with regular treatment for asthma (Lehrer et al., 2004), epilepsy (Yuen and Sander, 2010), depression (Janakiramaiah et al., 2000; Karavidas et al., 2007), post-traumatic stress disorders (Brown and Gerbarg, 2009; Descilo et al., 2010; Gerbarg and Brown, 2005; Sageman, 2004; Zucker et al., 2009). All together, these results demonstrate an undeniable link between respiratory rhythm and human psychology. Therefore, one can imagine that brain activity is influenced by respiratory rhythm.

### **1.2.3 – Respiratory rhythm shapes neuronal activity in the olfactory system**

Based on tracing and electrophysiology, olfactory system has been well delimited (Igarashi et al., 2012; Price, 1985; Sosulski et al., 2011). A simplified view of the olfactory system organization is proposed *Figure 12*. In brief, odorants are perceived by OSN in the olfactory epithelium (OE), which neurons projects onto olfactory bulb (OB). Olfactory bulb is the first olfactory relay. Principal neurons of the OB are mitral and tufted (M/T) cells. They receive information from OSN, and their axons converge to form the lateral olfactory tract (LOT), which ends in the olfactory cortex. Olfactory cortex is a huge paleocortex (3 layers instead of 6), divided into cortical amygdala (anterior/posterolateral cortical amygdaloid cortex (ACO/PLCO)), anterior olfactory nucleus (AON), olfactory tubercule (OT), lateral entorhinal cortex (LEC), and anterior and posterior piriform cortex (aPCX and pPCX) (Igarashi et al., 2012; Price, 1985; Sosulski et al., 2011). Olfactory cortex projects then to the hippocampus, the thalamus and hypothalamus, the prefrontal cortex and amygdala (Price, 1985). Amongst prefrontal cortices, orbitofrontal, prelimbic and agranular insular cortices are particularly targeted by olfactory inputs (Clugnet and Price, 1987; Datiche and Cattarelli, 1996; Moberly et al., 2018).

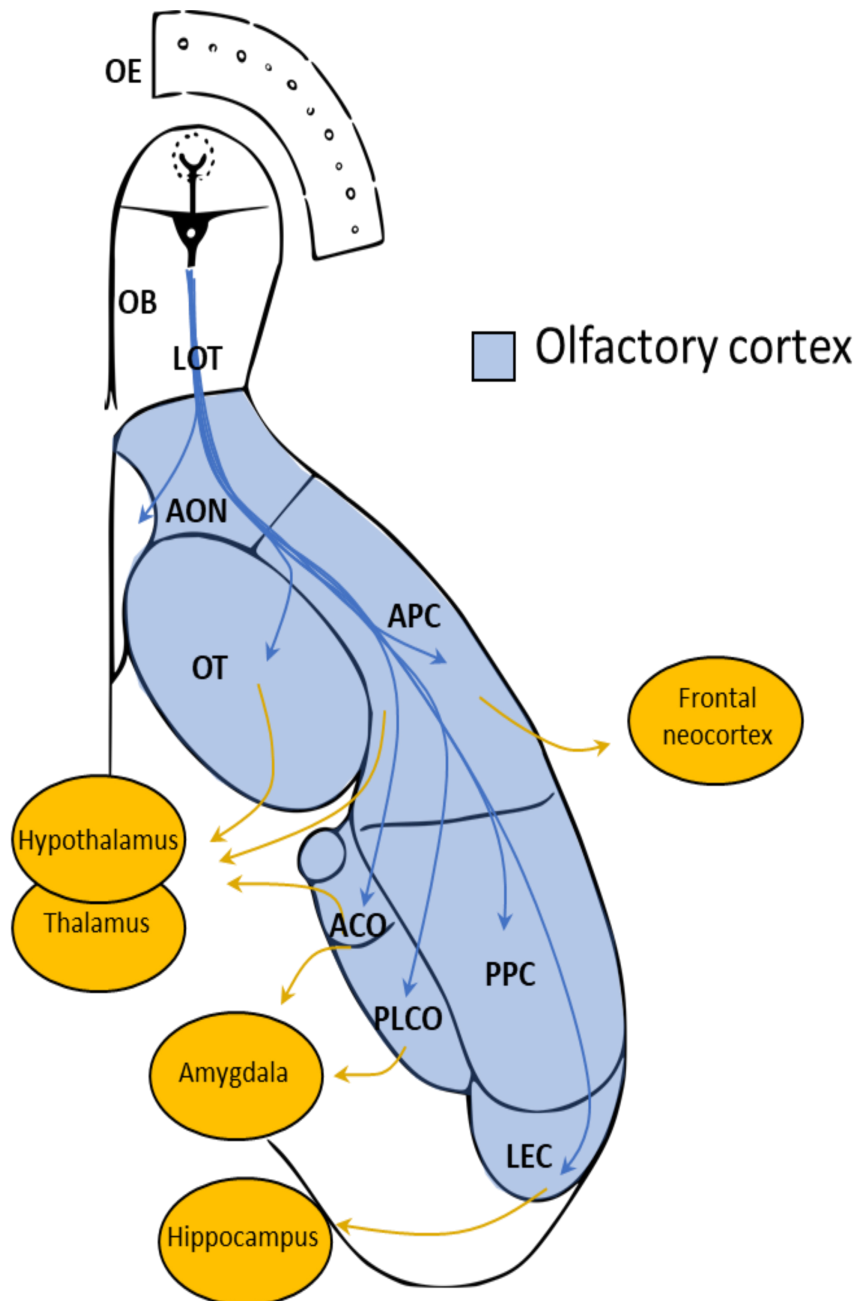


Figure 12 : Representation of the olfactory system and its main areas of projection. Olfactory system is composed of the olfactory epithelium, the olfactory bulb and the olfactory cortex (blue area). Yellow areas are beyond olfactory system but receive direct projection from the olfactory cortex. AON: anterior olfactory nucleus, ACO: anterior cortical amygdaloid nucleus, APC: anterior piriform cortex, OB: olfactory bulb, OT: olfactory tubercle, LENT: lateral entorhinal cortex, LOT: lateral olfactory tract, PLCO: posterolateral cortical amygdaloid nucleus, TT: tenia tecta. Adapted from Igarashi et al., 2012

One could ask what the link between olfaction and respiration is but it would be a very naïve question. Olfaction and respiration are intimately associated, since ventilation vehicles the air, which may contain odors. Air flows in and out the nose at a rhythm imposed by respiration. In the following paragraphs, I will describe neuronal activity in the olfactory system, not with regard to odor processing but rather with regard to respiratory modulation. Indeed, I aim at highlighting that the activity of each level of the olfactory system is shaped by respiratory rhythm.

### Olfactory epithelium.

During odor presentation, electro-olfactogram (olfactory epithelium LFP) of freely breathing rat shows oscillatory responses synchronized to respiration (Chaput, 2000). Oscillations peak at the end of the inspiration and are minimal during the expiration. Odorant molecules are adsorbed on olfactory sensory neurons (OSN) during inspiration, while expiration expulses them out. Interestingly, on the raw traces presented by the authors, one can observe the same respiratory EOG oscillation before odor stimulation, (see arrow in *Figure 13*). Even if oscillation amplitude is very low compared to odor presentation, it remains existing. It is echoing previous findings from Lord Adrian (Adrian, 1942). Indeed, he observed that even odor-free air was able to pace olfactory bulb LFP activity. He therefore suggested that the epithelium is not only chemo-sensitive but also mechanosensitive. In 2007, Grosmaître and colleagues showed in vitro that OSN effectively display a dual chemo and mechano-sensitivity. Hence, whether the air contains odors or not, downstream olfactory structures receive recurrent respiration-related inputs. Yet, odorants increase intensity of these inputs (Chaput, 2000).

### Olfactory bulb.

Lord Adrian was the first to describe LFP oscillations in the olfactory bulb with anesthetized preparation (Adrian, 1950, 1942). Anesthetized rabbit respiratory rhythm is about 1 Hz, and although this frequency is below audible range, he was able to hear each inspiration when a wire was inserted into the olfactory bulb. This first observation shows respiratory rhythm modulates amplitude of higher frequency rhythm. In addition, when air puff or odors are delivered, respiratory “music” get even more out from the noise, suggesting an amplification of the coupling phenomenon. Finer analysis showed gamma bursts are concentrated just after the inspiration. In parallel, one can observe a slow oscillation at respiratory frequency that peaks during inspiration and drops during expiration (see *Figure 13 A and B*). From the low frequency waveform and the presence of high frequency burst at inspiration, he supposed olfactory bulb receives lot of inputs at each inspiration. For the rest of the thesis, this wave will be referred to as respiration-related oscillation (RRO). To be noted, one cannot define this oscillation by its frequency since respiration of an animal offers a broad range of frequencies and respiratory range varies between species. Later, Walter Freeman made similar observation in awake rabbit preparation, namely respiration-related oscillations coupled with gamma bursts inspiration-locked (see *Figure 13 B*) (Freeman, 1978; Freeman and Schneider, 1982). Complementarily to LFP, membrane potential oscillations of mitral cells also display respiration-related oscillations during odor and also in air free condition (Briffaud et al., 2012; Cang and Isaacson, 2003; Charpak et al., 2001; Margrie and Schaefer, 2003). Recently these observations have been confirmed in awake mice (Ackels et al., 2020). While respiratory influence on the olfactory system is obvious, only few authors studied olfactory oscillations with regard to respiration. Amongst these rare pearls, Buonviso’s lab put one more step closer to respiration. First, they fine-time analyzed fast oscillations distribution over respiratory cycle in the olfactory bulb under anesthesia. Gamma bursts phase-lock inspiration to expiration transition, while beta bursts phase-lock late expiration (see *Figure 13 C*) (Buonviso et al., 2003). In addition to segregation of high frequency oscillations over the respiratory cycle, two firing populations of M/T cells emerge. One fires preferentially close to inspiration/expiration transition, and the other prefers late expiration (Briffaud et al., 2012; Cenier et al., 2009). Gamma and beta bursts delimit two parallel networks in the olfactory bulb (Cenier et al., 2009; Fourcaud-Trocmé et al., 2014). It was proposed that gamma burst mediates feedforward information transfer (from the bulb to the cortex) while beta burst supports feedback (from the cortex to the bulb) (Buonviso et al., 2006).

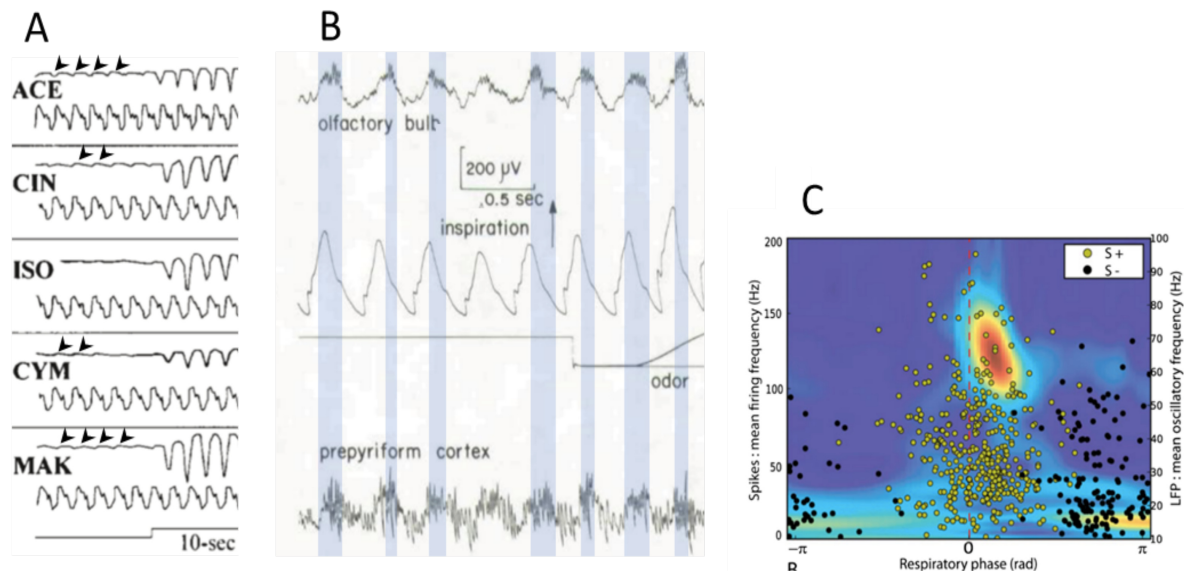


Figure 13 : Neural activity in the olfactory system is shaped by respiratory rhythm. A. Electroolfactogram from anesthetized rat. Odor presentation induces huge RRo, however before odor delivery baseline can also display small RRo (arrowhead) Adapted from Chaput, 2000. B. Olfactory bulb and cortex from freely moving rabbit exhibit clear RRo. Furthermore, gamma bursts (blue square) rhythmically appear just after the inspiration. Adapted from Freeman and Schneider, 1982. C. Synthesis of olfactory bulb LFP and unitary activity during anesthesia and odor. A gamma burst phase-lock the early inspiration, while a beta burst covers the expiration. Each dot represents the preferred phase (x-axis) and discharge frequency (y-axis) of the respiratory modulated firing pattern. Preferred phases of firing are correlated with gamma/beta phase of occurrence. Extracted from Cenier et al., 2009.

#### Olfactory cortex.

Activity of the olfactory cortex with regard to respiration has also been studied, yet in a lesser extent. Amongst olfactory cortical areas, piriform cortex has been the main focus. The fact that piriform cortex is huge contributes to that. Piriform (also called prepyriform in former literature) cortex displays respiration-paced oscillations in anesthetized and awake preparation (Freeman, 1959), even without odor. As in the olfactory bulb, a coupling between respiration-related oscillations and gamma oscillations is observed. Gamma bursts still occur just after inspiration. Simultaneous LFP recording of olfactory bulb and cortex shows activity of these structures are synchronized by respiration (Freeman and Schneider, 1982). Additionally, membrane potential of piriform cortex cells can display RRo during deep anesthesia (Fontanini et al., 2003; Fontanini and Bower, 2005), while membrane potential oscillations desynchronized from respiration during light anesthesia. Piriform cortex appears to be able to connect and disconnect from respiration. Furthermore, gamma bursts from the bulb and the piriform cortex are highly coherent during inspiration, while this coherence drops during expiration (see Figure 13 B) (Bressler, 1987). The question of cortical firing has been poorly tackled, and only with anesthetized preparation. In addition, during odor presentation, cortical cells can present a respiratory drive (Bouret and Sara, 2002; Litaudon et al., 2003; Wilson, 1998). Even under anesthesia still 48.5% of piriform cortex cells present a spontaneous firing activity, which is driven by respiration in most cases (71.7%) (Litaudon et al., 2003). Compared to the olfactory bulb, a large population of cells do not respond to odor presentation. In addition, piriform cortex displays an anteroposterior heterogeneity, the more posterior, the less responsive (Litaudon et al., 2003). A similar anterior to posterior decrease is observed for the percentage of respiratory entrained spontaneous activity (Litaudon et al., 2003). Then, it seems that respiratory influence decreases with distant to the nose. Does it mean spreading of respiratory modulation in olfactory system is only mediated by nasal pathway?

### Origin and extent of respiratory modulation in the olfactory system.

Pinching nostril of awake restrained rabbits forces them to breathe through the mouth. As a result, respiration-related oscillations and gamma burst inspiration-locked disappeared simultaneously in olfactory bulb and cortex (Freeman, 1975; Freeman and Schneider, 1982). Additionally, tracheotomized and double cannulated rat preparation allows to uncouple nasal airflow and lung respiration. Consequently, different air frequencies and flowrates can be imposed in the nose, independently from lung respiration. First use of this technique showed M/T cells firing acquired synchronization to nasal respiration during odor presentation (Sobel and Tank, 1993). A deeper look showed olfactory bulb LFP oscillations strictly follows imposed nasal rhythm in the physiological range (1-10Hz) (Courtiol et al., 2011b). Very interestingly, changing flowrate at a given frequency, significantly influences the beta/gamma power balance, while keeping phase-locking to respiration. Low flowrates increase beta power and reduce gamma power. Conjointly, principal cells firing shows a strong phase-locking with beta and not with gamma. Conversely, high flowrate reverse the balance, *i.e.* gamma power increases, beta power decreases and spikes phase-lock gamma rather than beta (Courtiol et al., 2011a). Taken together these elements suggest that nasal airflow pattern fully conditions oscillatory dynamic of the olfactory bulb, and then potentially the olfactory system. Nonetheless, this scheme must be refined, since respiratory modulation of firing pattern persisted under tracheotomy for 31% of bulbar cells in the awake rat (Ravel et al., 1987; Ravel and Pager, 1990). Therefore, a central and a peripheral (nasal pathway) respiratory modulation coexists, yet in the olfactory system, nasal pathway dominates. As respiratory modulation decreases with distance to nose, as illustrated in the piriform cortex, one can wonder i) if respiratory modulation persists outside of olfactory system ii) if the central/nasal balance of the respiratory modulation varies with distance to the nose. Since olfactory cortex projections are broad, one can envisage activity of non-olfactory structures is modulated by respiration. Based on olfactory projections and to what happened in the olfactory system, brain areas “beyond the primary olfactory cortex” (Clugnet and Price, 1987; Datiche and Cattarelli, 1996; Price, 1985) *i.e.* prefrontal cortex, hippocampus, thalamus, hypothalamus and amygdala, may presumably present respiratory modulation.

## 1.3 The new face of Respiration-related oscillations

### 1.3.1 What is the extent of respiratory modulation in the non-olfactory brain?

#### Pioneer but forgotten work

Early studies found respiration-correlated firing in cat's thalamus, subthalamus (Vibert et al., 1979), central amygdala nuclei (Zhang et al., 1986), periaqueductal grey matter (Ni et al., 1990) and anterior cingulate cortex (Frysinger and Harper, 1986). Respiration-related firing is observed during all states (REM, NREM, waking), while prominent during wakefulness. Similar observations have also been made in hippocampus and amygdala (Frysinger and Harper, 1990, 1989) of epileptic humans. However, this movement ran out of steam. It was maybe too early for brain-wide respiratory modulation literature to emerge.

#### Fontanini's hypothesis

After 10 silent years, in 2006 Fontanini's lab pushed back respiratory modulation on stage. They studied rats OB and piriform cortex activity in relation to respiration across different ketamine/xylazine states of anesthesia. They showed that olfactory bulb LFP, piriform cortex LFP and piriform membrane potential oscillations were coherent with respiration during deep anesthesia, while piriform cortex was desynchronized from respiration during light anesthesia (Fontanini et al., 2003; Fontanini and Bower, 2005). Causality has been assessed since tracheotomy completely suppressed respiration-related oscillations in olfactory bulb and piriform cortex. From these data, they drew a comparison between the olfactory bulb/ piriform cortex couple and the thalamus/neocortex couple (Fontanini and Bower, 2006). Indeed, both couples share the property of being synchronized by a slow oscillation, which provide information exchange. Since the olfactory slow oscillation is related to respiration, they wonder if such relation could also affect the neocortical sleep slow oscillation. To support their theory, authors brought phylogenetic and anatomic arguments. Olfaction is the older sensory system, consequently the neocortex develop latter. Therefore, the neocortex appeared and evolved around a preexisting and dominant olfactory system. One can then assume neocortical functioning still presents traces of the former olfactory influence. In addition, frontal cortex seem important for generation of neocortical slow oscillation and for its antero-posterior propagation (Massimini et al., 2004). Interestingly, tracing studies showed the olfactory cortex project to prefrontal cortex (Clugnet and Price, 1987; Datiche and Cattarelli, 1996; Price, 1985). Consequently, respiration-paced inputs could reach prefrontal cortex and could potentially propagate to the rest of the brain, like neocortical sleep SO. So, Fontanini and Bower hypothesize activity of the whole neocortex could be influenced by respiration (Fontanini and Bower, 2006). Similar reasoning can be made for amygdala and hippocampus since they also receive inputs from olfactory cortex (Price, 1985). The review points out the nasal pathway as the main driver for respiratory modulation propagation throughout the brain. They called the ensemble of areas entrained by the respiratory rhythm the "sniffing brain". However, at the time of the review the extent of the "sniffing brain" was only based on guessing (see *Figure 14 A*). This work represents a major hypothesis in the field which inspired a lot of forthcoming studies.

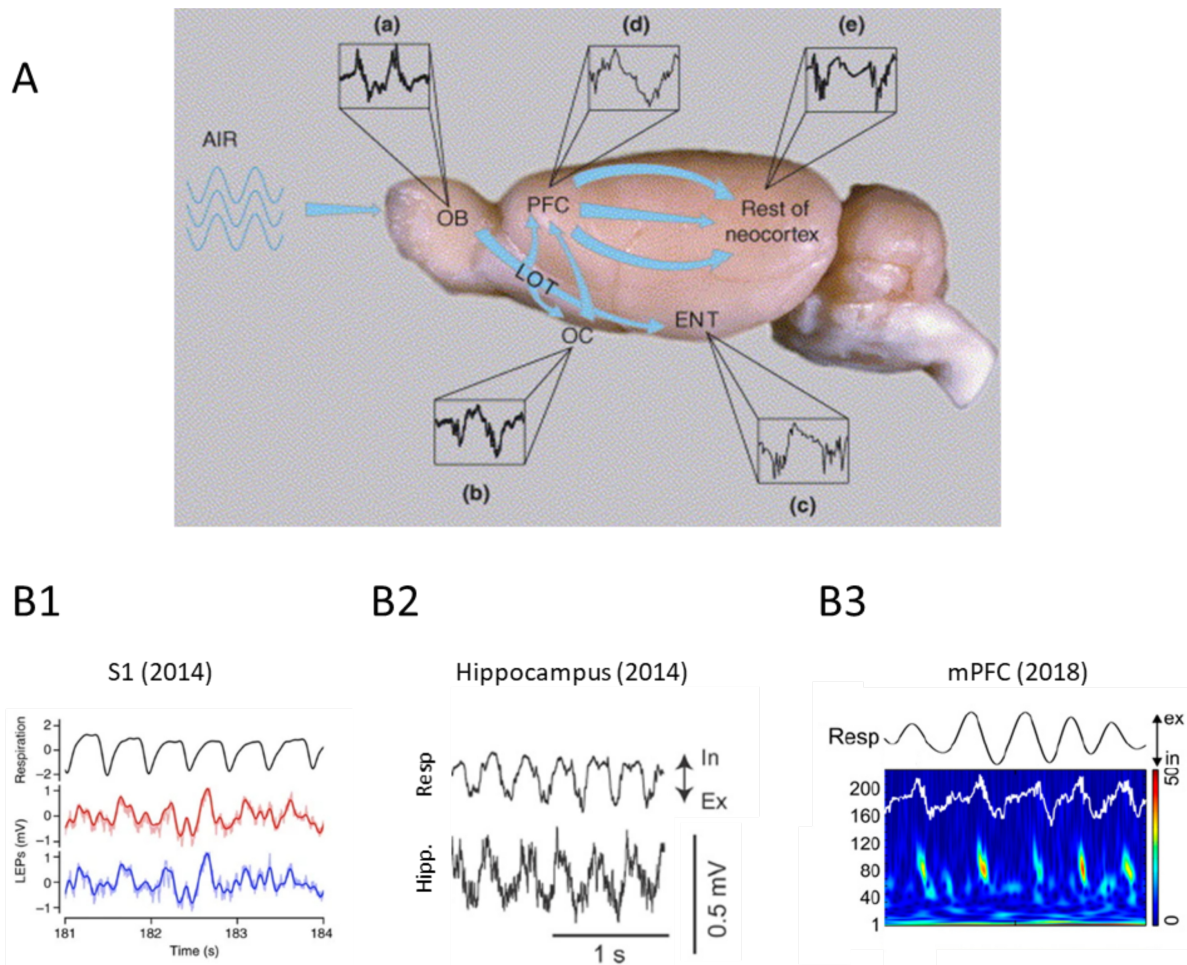


Figure 14 : First evidence of the extent of respiratory modulation outside of the olfactory system. A. Fontanini proposed the hypothesis that respiratory modulation benefit from olfactory projections to invade the rest of brain (Extracted from (Fontanini and Bower, 2006). B. First observation of RRo in LFP signal of awake mice barrel cortex (B1, extracted from Ito et al., 2014), anesthetized mice hippocampus (B2, extracted from Yanovsky et al., 2014), awake mice medial prefrontal cortex (B3, extracted from (Zhong et al., 2017).

### Masterclock hypothesis

Few years later, in 2014, Kleinfeld and Deschênes presented a review of their recent work which emphasizes the role of respiratory rhythm in orofacial behaviors coordination (Kleinfeld et al., 2014). Breathing and whisking frequency can evolve independently, however during exploratory behavior they synchronize (Cao et al., 2012; Deschênes et al., 2012; Welker, 1964). Anatomical and electrophysiological approaches showed that preBötzing complex projects to medullar whisking premotor area (Moore et al., 2013). Therefore, during sniffing the whisking pattern is driven by inspiratory inputs. PreBötzing complex also projects toward chewing and licking premotor areas. Since, these behaviors are coordinated with respiration as well, Kleinfeld and Deschênes proposed that respiratory rhythm could act as a masterclock which allows to coherently bind orofacial behaviors (Kleinfeld et al., 2014). Such binding allows synchronizing olfactory (sniffing), somatosensory (whisking) and gustative (licking) sampling, as a result each respiratory cycle provides a complete snapshot of the environment. If sensory samplings are bound by respiratory rhythm, it could be consistent that multisensory integration are also modulated by respiration. Contrarily to Fontanini's view, respiratory modulation, here, spreads from respiratory centers and not from the nose. Yet, these two pathways are far from antagonist but rather complementary (detailed in 1.3.2 The possible routing of Respiration-related oscillations across the brain). In a lesser

theoretical view, we should at least expect respiratory modulation in barrel cortex, as whisker movements themselves can synchronize to respiratory rhythm.

#### Rediscovery of respiratory modulation in non-olfactory brain

To summarize, rodent prefrontal cortex, barrel cortex, and hippocampus legitimate target for the expression of respiratory modulation. Consequently, these areas were the first to be investigated. Since Fontanini's (Fontanini and Bower, 2006) and Masterclock's (Kleinfeld et al., 2014) hypotheses, the hippocampus was the first non-olfactory structure where respiratory modulation was (re)observed (Tsanov et al., 2014), closely followed by the barrel cortex (see *Figure 14 B1*) (Ito et al., 2014). Prefrontal cortex evidence emerged few years later (see *Figure 14 B3*) (Biskamp et al., 2017; Zhong et al., 2017).

*Hippocampus.* Consistently with Frysinger and colleagues findings in humans (Frysinger and Harper, 1989), firing of medial septum neurons and CA1 place cells have been observed to phase-lock respiration during slow breathing and sniffing in freely moving rats (Tsanov et al., 2014). Additionally, LFP slow oscillations in CA1 displayed RRo during sniffing episodes. Shortly after, two contradictory articles tackle the relation between respiration and hippocampal LFP oscillations (Viccko et al., 2014; Yanovsky et al., 2014). Although their titles (Viccko: Lack of respiratory coupling with neocortical and hippocampal slow oscillations, Yanovsky: Slow oscillations in the mouse hippocampus entrained by nasal respiration) oppose them, their contents are complementary. These studies worked on sleeping states (NREM and REM) and sleep-like states associated to anesthesia. Deactivated state (deep anesthesia) corresponds to LFP activity consisting in low frequency oscillations. On the contrary activated state (light anesthesia) is associated to higher frequency LFP oscillations. Urethane induces particular cyclic variation of LFP and respiratory activities, which shows similarity with natural sleep cycles (Pagliardini et al., 2013). Urethane-activated state is considered as a REM-like state, while urethane-deactivated state to NREM-like state. On the one hand, Viccko and colleagues focused on deep anesthesia (deactivated state) and NREM. They studied LFP oscillations close to sleeping and anesthetized respiration frequency (about 1 Hz), namely the neocortical (Steriade et al., 1993a) and the hippocampal (Wolansky et al., 2006) slow oscillation. None of them were not related with respiration. Albeit it occupies a discrete place in the article, authors showed significant neocortical and hippocampal coherence to respiration during activated state (light anesthesia), see figure 6A and table 8 in (Viccko et al., 2014). On the other hand, Yanovsky and colleagues studied only hippocampal activity during urethane activated state (Yanovsky et al., 2014). They observed a coexistence of theta and respiration-related oscillations (RRo) (see *Figure 14 B2*) in hippocampal activated LFP. In complement, they made two other important observations which keep away the criticism of a possible volume conduction contaminating the LFP signal i) gamma oscillation and AP phase-lock respiration, ii) one DG cell presented membrane potential RRo. In 2016, two simultaneous studies from Tort's lab closed the debate by confirming the hippocampal LFP effectively displays RRo in awake (Chi et al., 2016) and anesthetized mice (Lockmann et al., 2016). Lockman's study explicitly aimed to clarify contradictory findings from Viccko (Viccko et al., 2014) and Yanovsky (Yanovsky et al., 2014). Authors reproduced Viccko setup. The study did not provide any new findings compared to Yanovsky and Viccko, but it reproduced the two results. Namely RRo are observed in activated hippocampus, whereas it is not the case in deactivated state. Additionally, Lockman insisted on the fact that the hippocampus can develop three type of low frequency oscillations, namely theta, RRo and hippocampal slow oscillation. Interestingly, occurrence of these rhythms is sequential since hippocampal slow oscillation is present during deactivated state, theta during activated state and RRo during transition. However, these rhythms are not strictly exclusive, as during transition, RRo oscillations can coexist with theta or neocortex-related slow oscillation. Importantly the study proposed three reasons to explain why Viccko and colleagues may have miss RRo: i) hippocampal RRo present a laminar pattern, so it is possible to miss RRo if electrode is not in the good layer, ii) animal models (mice vs. rats) may present difference,

iii) Vickzo focused on deactivated state during which hippocampal slow oscillation is predominant. The second study I mentioned extended Yanovsky's findings to awake mice (Chi et al., 2016). RRo were preferentially observed in DG rather than in CA1 during awake immobility, walking and running. Respiration-related firing was only observed in DG. Interestingly these DG cells could synchronize to respiratory rhythm only, to theta only or to both. Consistently with findings in anesthetized mice, although RRo and theta have different temporal dynamics, they still can overlap. So far, all studies showed that low frequency oscillations in the hippocampus are not affected by respiratory modulation during deactivate state and NREM. However, hippocampal activity is not limited to low frequency oscillations. Besides, in 2017 sharp waves and ripples (high frequency events) have been shown to preferentially occur at inspirations during NREM sleep(Liu et al., 2017). Result has been reproduced in another lab (Karalis and Sirota, 2018). To conclude, these pioneer results on hippocampus showed respiratory modulation during awake and sleeping activities. To be noted according to Fontanini, modulation was only expected during deactivated state and NREM sleep. However, it is during activated state that hippocampus developed clear RRo which couples which local gamma oscillations and extracellular action potentials. While, during deactivated state and NREM sleep, respiratory modulation is less obvious since hippocampal low frequency oscillations are not coherent with respiration. However, sharp waves and ripples, hallmarks of NREM and memory consolidation, display a phase preference for inspiration.

*Somatosensory cortex.* The first cortical respiratory modulation was observed in the mice barrel cortex (see *Figure 14 B1*)(Ito et al., 2014). Delta band oscillations in the barrel cortex from quietly awake mice were coherent with respiratory rhythm. Furthermore, local signals such as extracellular action potentials and gamma oscillations were also correlated with respiration. A recent study refined the anatomy of rodent somatosensory cortex by highlighting the existence of nostril somatosensory area between barrels (Maier et al., 2020). This area displays stronger RRo and spike phase-locking to respiration compared to barrels.

*Medial prefrontal cortex.* Two studies from independent labs were published the same month and both showed respiratory modulation in the mPFC, more precisely in the prelimbic cortex (Biskamp et al., 2017; Zhong et al., 2017). Tort's lab (him, again) provided a nice study which tackled the question of theta and RRo coupling with high frequency in associative cortices and hippocampus (Zhong et al., 2017). Assuming RRo and theta both enable long-range communication, the aim of the article was to quantify how these rhythms "share the work", since both rhythm can occur in the same structures (Lockmann et al., 2016; Yanovsky et al., 2014). They performed phase-amplitude coupling computation in the olfactory, prelimbic and parietal cortices, and CA1 in freely moving mice. They were able to discriminate three gamma subbands: low gamma (40-80 Hz), mid gamma (80-120) and high gamma (120-160 Hz). Interestingly, mid gamma exclusively coupled with respiratory rhythm and low/high gamma exclusively coupled with theta. Selectivity of the coupling is preserved across structures and brain states (exploration, immobility, REM). During immobility all structures display a mid gamma-RRo coupling. On the contrary during exploration (and REM sleep in supplementary materials), olfactory bulb and prelimbic cortex displayed mid gamma-RRo, while CA1 and parietal cortex showed a prominent low/high gamma-theta coupling. Hence, theta and RRo seem to implicate different networks. Across behaviors, brain can switch between RRo or theta coupling. In supplementary materials, authors showed phase-amplitude coupling during NREM sleep, however they did not interpret it. I assume they did not manage to disentangle RRo and sleep SO. To be noted, during NREM sleep UP and DOWN occurrences have been shown to be modulated by respiratory phase (Karalis and Sirota, 2018). The second study focused prelimbic cortex activity in a fear-like condition (Biskamp et al., 2017). Authors hang mice by the tail, which induces two types of response, either they struggle and breath irregularly or they stay immobile and have a steady 4 Hz breathing. Authors based all their analysis on that latter very particular state,

strikingly similar to freezing. They showed i) prelimbic cortex expressed a strong RRo, ii) gamma amplitude and extracellular action potentials were modulated by respiration, iii) a higher proportion of putative interneurons are entrained by respiratory rhythm than putative pyramidal, iv) hippocampal theta and prelimbic RRo were phase-phase coupled (two theta cycles for one RRo). Zhong's and Biskamp's works complete each other, since the merge of the studies highlighted the existence of RRo during wakefulness, REM sleep and fear behavior, and they showed local network can be entrained by respiratory rhythm. Similarly, RRo and eAP coupling to respiratory rhythm were observed in the orbitofrontal cortex (Karalis and Sirota, 2018; Kőszeghy et al., 2018) and other mPFC areas (anterior cingulate, infralimbic cortices) (Karalis and Sirota, 2018). Probably inspired by fear-like induced RRo in prelimbic cortex (Biskamp et al., 2017), Adriano Tort proposed a parallel between fear induced oscillations and respiration. Indeed, during rodent fear expression a 4 Hz (Fujisawa and Buzsáki, 2011; Karalis et al., 2016) or a 2-5 Hz oscillations have been well describe to synchronize prefrontal cortex, hippocampus, VTA and basolateral amygdala. Then Adriano Tort proposed this mysterious rhythm to be related to respiration and he initiated a series of "letter to the editor" (Bagur et al., 2018; Kocsis et al., 2018; Lockmann et al., 2016). The exchange resulted in a common admission that RRo strongly bind areas involved in the fear context, probably enabling the expression of fear behaviors. It was also confirmed by an article which specifically aimed to related the 4 Hz freezing induced rhythm and respiration (Bagur et al., 2021; Moberly et al., 2018).

*Full rodent map.* Three studies aimed to depict the possible extent of the respiration-entrained network in rodent brain. The first published provided the wider network with a total of 15 brain areas (including 12 non-olfactory areas) in freely moving mice (A. B. L. Tort et al., 2018). LFPs from all 15 areas (for the complete list, please refer to *Figure 16 C* and its legend) showed significant coherence to both respiratory rhythm and theta rhythm during REM sleep and exploration. However, strength of the coherence highlights a power balance between respiratory rhythm and theta in each area, suggesting some areas are more sensitive to theta and others more sensitive to respiratory rhythm. Nevertheless, this analysis showed each area can bind to either respiratory or to theta rhythms (see *Figure 15 A*). Complementarily, authors computed two-by-two inter-areas coherences to estimate connectivity. They observed significant coherence in respiratory and theta range during REM and exploration, suggesting communication between these 15 areas can be mediated by respiratory rhythm and/or theta rhythm (see *Figure 15 B*). Although, they monitored quiet wake and NREM sleep, authors focused on REM and exploration since the key point of this article was to demonstrate that theta rhythm and RRo coexist or compete in rodent brain. More importantly, they point out the fact that monitoring respiration is essential to distinguish RRo from other brain rhythms as respiratory frequency is a broadband signal with an important variability. By the way, they dedicate a review to that point (A. B. Tort et al., 2018). Conjointly, during quiet wake gamma in a large network couples with respiration (see *Figure 16 C*) (A. B. L. Tort et al., 2018). Then, came Rojas' study who monitored LFP from 4 non-olfactory structures in freely moving rats (Rojas-Líbano et al., 2018). Three areas were common with Tort. The study differs in that he monitored one novel area (primary motor cortex), and he interested in quiet wake. He showed RRo in M1, V1 and hippocampus during quiet wake. Inconsistently with previous literature (Ito et al., 2014) he observed no RRo in S1 during quiet wake. Last study, in which I participated, provided the analysis of 7 areas (all in common with Tort) in freely moving rats during all four brain states, namely exploration, quiet wake, NREM and REM (Girin et al., 2021). As a first step, we sorted our data according brain state and then looked for RRo. As a result, we observed significant coherence in all areas and during all states. However, quiet wake was the only state during which i) RRo were clearly visible and ii) RRo were prominent in all areas (see *Figure 16 A*). We then used a 5% CO<sub>2</sub> enriched air to change respiratory pattern without altering brain state. The most striking result was the wide appearance of RRo during NREM sleep. Since we preserved brain states, while increasing respiratory frequency and amplitude,

we hypothesize RRo emergence is due to respiratory pattern rather than the brain state itself. Therefore, in a second step, we analyzed the data according to respiratory parameters, without taking brain state into account. We showed that a particular respiratory pattern (long and deep inspirations) optimizes RRo occurrence in all brain areas. It turned out that inspiration duration and amplitude of respiratory cycles associated to quiet wake respiratory pattern are close to that optimal pattern, which explains why respiratory modulation is so much extended during quiet wake (see *Figure 16 B*).

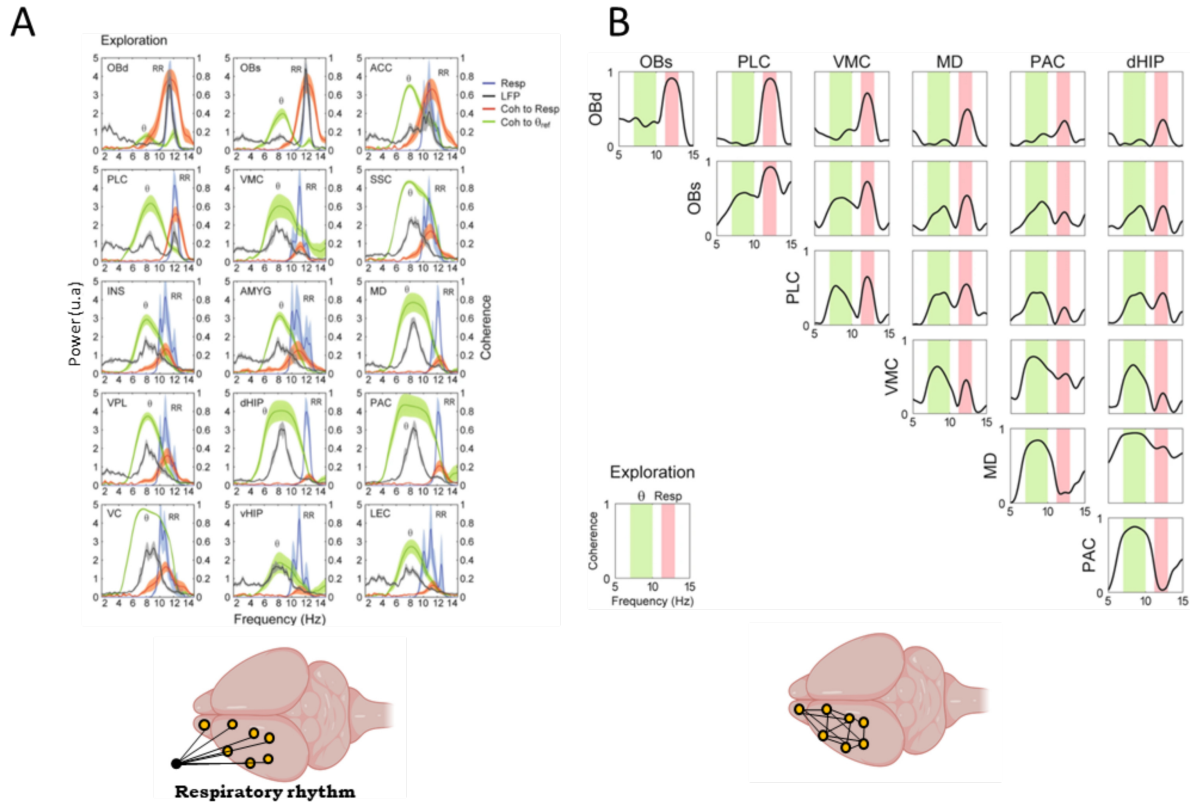


*Figure 15 : Rodent respiratory modulation brain map. A. All presented rodent areas can be coherent with either respiration or theta. This analysis shows all structures can bind to respiratory rhythm. Extracted from A. B. L. Tort et al., 2018. B. Most areas can be two-by-two coherent on respiratory range. This analysis suggests couples of areas can be bind by respiratory rhythm. Extracted from A. B. L. Tort et al., 2018. ACC: anterior cingulate cortex, AMYG: central nucleus of amygdala, dHIP: dorsal CA1, INS: insular cortex, LEC: lateral entorhinal cortex, MD: mediodorsal thalamus, PAC: parietal cortex, PLC: prelimbic cortex, OB: olfactory bulb (surface or deep), SSC: somatosensory cortex, VC: visual cortex, vHIP: central CA1, VMC: vibrissal motor cortex, VPL: ventral posterior thalamus*

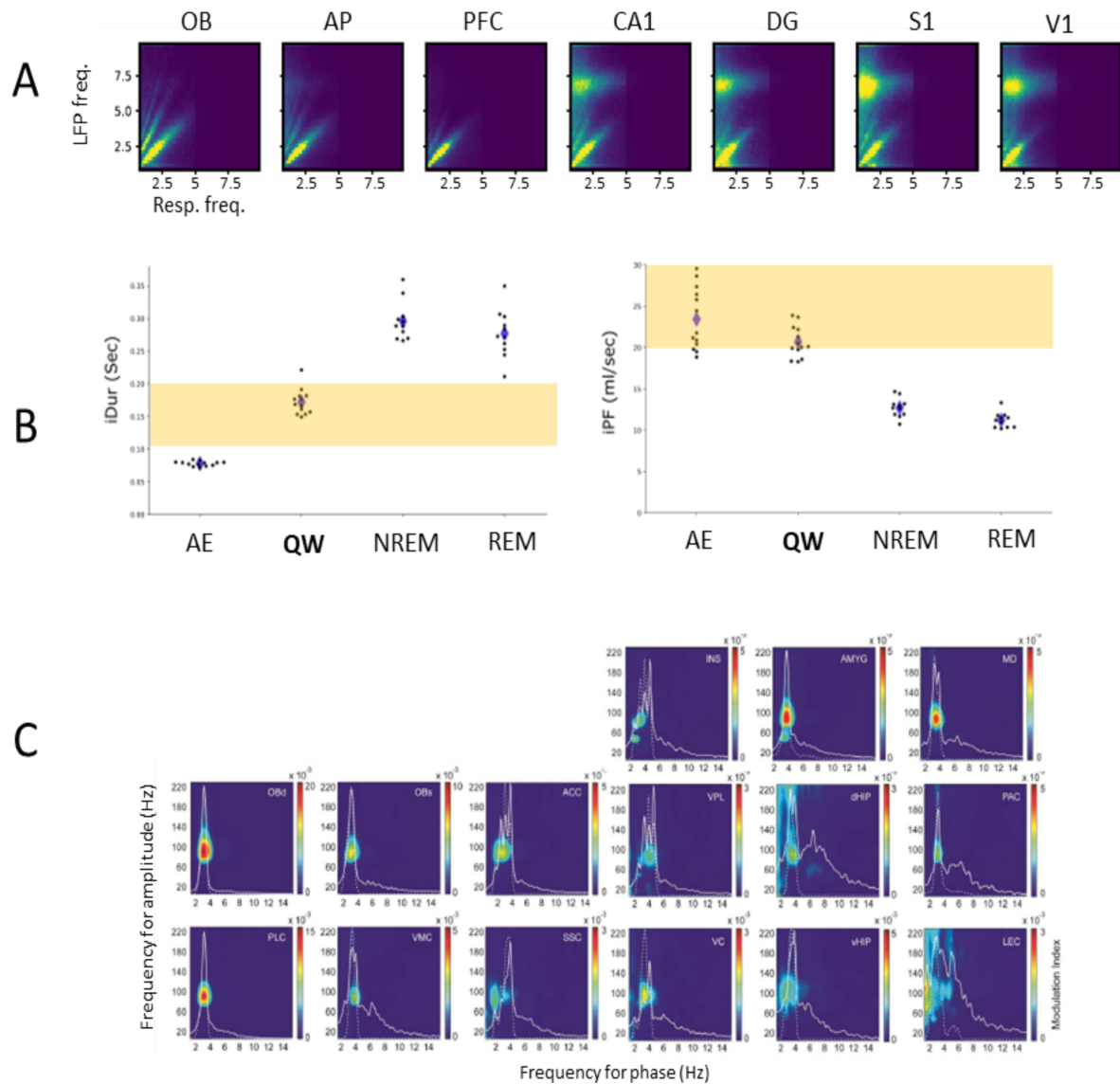
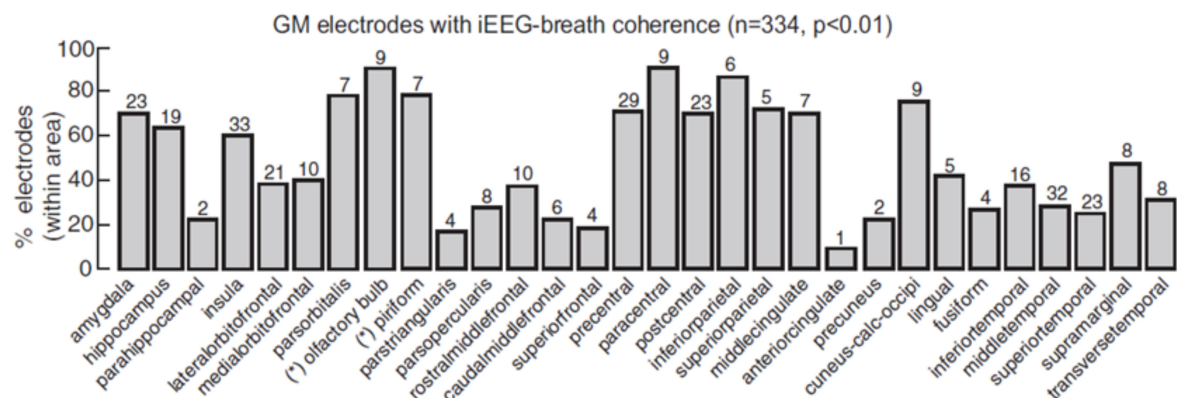


Figure 16 : Quiet wake in rodents corresponds to brain-wide respiratory entrainment. A. LFP low frequency couples to respiratory frequency in all recorded areas. Extracted from Girin et al., 2021 B. Respiratory parameters across brain states. Yellow band high the parameter range which is associated with strongest coupling diagonal. Quiet wake is the only state fitting in the two ranges. Adapted from Girin et al., 2021. C. Additionally to the development of RRo in low frequency, gamma oscillations are brain-wide paced to respiration during quiet wake. Extracted from supplementary materials of A. B. L. Tort et al., 2018. ACC: anterior cingulate cortex, AE: active exploration, AMYG: central nucleus of amygdala, AP: anterior piriform cortex, DG: dentate gyrus, dHIP: dorsal CA1, INS: insular cortex iDur: inspiratory duration, LEC: lateral entorhinal cortex, MD: mediodorsal thalamus, PAC: parietal cortex, PFC/PLC: prefrontal cortex, OB: olfactory bulb (surface or deep), QW: quiet wake, S1/SSC: somatosensory cortex, V1/VC: visual cortex, vHIP: central CA1, VMC: vibrissal motor cortex, VPL: ventral posterior thalamus

*Full human map.* To be noted, resting human breathing is about 0.3 Hz, which is much slower than rodents (2-3Hz). Surprisingly the first RRo observed in human brain directly came from intracranial EEG recordings (Zelano et al., 2016). I would have expected first data coming from less invasive technics like scalp EEG. Whatever, authors benefited from patients implanted in the piriform cortex, the amygdala and the hippocampus. They observed RRo in these three areas in all patients. Additionally, higher frequency oscillations (delta, theta, beta and gamma) couples with respiratory cycle. One year later, a study increased the number of coherent areas to respiration from 3 to 30 (see *Figure 17*) (Herrero et al., 2018). Amongst these 30 areas, 9 displayed also gamma coupling with respiratory rhythm. Additionally, primary motor activity is modulated by respiratory phase (Kluger and Gross, 2020; Park et al., 2020).



*Figure 17 : Human respiratory modulation brain map. Most human areas in which coherence to respiratory rhythm is observed. Extracted from Herrero et al., 2018. GM: Grey matter*

I just described the current map of respiratory modulation in rodent and human brain. It appears almost the whole brain is “under influence”. This is really interesting, but it raises several questions: Where does it come from? Does it really do something? These questions will be tackled in the following paragraph.

### 1.3.2 The possible routing of Respiration-related oscillations across the brain

As I previously explained, respiratory modulation can come from the “nose” or from respiratory centers. The nasal pathway is for now the most studied for the simple reason that is it easy to interfere with. Tools used to impair nasal inputs are tracheotomy (Ito et al., 2014; Lockmann et al., 2016; Yanovsky et al., 2014), bulbectomy (Biskamp et al., 2017), destruction of the nasal epithelium (Karalis and Sirota, 2018; Moberly et al., 2018), or inhibition of the olfactory bulb (Liu et al., 2017; Moberly et al., 2018) in the animal and mouth breathing (Arshamian et al., 2018; Zelano et al., 2016). Tools to increase nasal inputs are air puffs (Piarulli et al., 2018; Rojas-Libano et al., 2018), CO2 enriched air (Girin et al., 2021) or odors (Tsanov et al., 2014). On the other hand, it is obviously difficult to play with respiratory centers and maintain an animal normally alive. Furthermore, disturbing respiratory centers will consequently impact nasal airflow. I read only two articles in which authors developed a setup to uncouple ventilation and respiratory center activity (Bertrand and Hugelin, 1971; Vibert et al., 1979). To suppress all lung movements in cats, authors performed a vagotomy and a spinal section at C7 vertebra while a paralyzing agent was injected. Animals were ventilated, and respiratory center was monitored through phrenic nerve activity. After surgery, anesthesia was stopped, and recording began. On a theoretical basis, the setup is clever, but the protocol is heavy, and I think, it would not go through current ethical process review.

### Nasal pathway.

As a quick reminder from 1.2.3 – Respiratory rhythm shapes neuronal activity in the olfactory system, respiration-rhythmed olfactory inputs reach the olfactory cortex. The olfactory cortex project then to the prefrontal cortex, the amygdala, the hippocampus, the thalamus (Clugnet and Price, 1987; Price, 1985). Therefore, the important divergence of olfactory cortex projections made the nasal pathway a promising way for respiratory modulation spreading. Furthermore, almost all traces of respiratory modulation in the olfactory system disappear after tracheotomy. Consequently, such manipulation should also disrupt brain wide respiratory modulation, if the olfactory system is indeed the propagator. Experiments involving olfactory inputs disruption showed abolishment of respiratory modulation in brain LFP oscillations. RRo in prelimbic cortex disappeared after OSN destruction (Biskamp et al., 2017; Karalis and Sirota, 2018; Moberly et al., 2018), bulbectomy (Biskamp et al., 2017), while they decreased after obstruction of one nostril (Moberly et al., 2018). RRo-gamma coupling was suppressed after OSN destruction (Karalis and Sirota, 2018). In barrel cortex of awake mice bulbectomy abolished RRo (Ito et al., 2014). Complementarily, authors performed double tracheotomy on anesthetized mice. Lungs respiration followed respiratory centers, whereas another frequency was imposed in the nasal cavity. RRo in the barrel cortex followed nasal respiration. Hippocampal RRo were abolished by tracheotomy (Lockmann et al., 2016; Yanovsky et al., 2014). In human, when subject were asked to breathe through the mouth, RRo disappeared in the piriform cortex, the amygdala and the hippocampus (Zelano et al., 2016). On the contrary, stimulation of olfactory system reveals interesting findings. A 13 Hz optogenetic stimulation of the olfactory epithelium induces a 13 Hz rhythm in OB and prelimbic LFP (Moberly et al., 2018). A CSD (current source density) study in the hippocampus, revealed that RRo sinks are located in the same layer than evoked-response induced by lateral olfactory tract and perforant path stimulations (Lockmann et al., 2016). This overlay suggests hippocampal RRo is due to olfactory inputs. All these results show a strong role for nasal inputs in the respiratory modulation spreading.

### Central pathway.

Although few studies tackled the question of a central propagation of respiratory modulation, some interesting cues are already present in literature. The impressive study on ventilated, vagotomized, paralyzed cats showed units driven by respiratory centers rhythm in the reticular formation, the subthalamus and the thalamus (Vibert et al., 1979). Additionally, in a recent study, freely moving mice with destroyed olfactory epithelium showed reduction of respiratory driven units in the prelimbic cortex (54% to 46%), the CA1 (~70% to ~40%), DG (~75% to ~50%) and the thalamus (~50% to ~35%). However you can note, a still consequent number of neurons are bound to respiration (Karalis and Sirota, 2018). For unknown reasons oscillations are dramatically affected by nasal pathway perturbations, while firing still display respiratory synchronization. These results strikingly remind work of Pager and Ravel in the OB (Ravel et al., 1987; Ravel and Pager, 1990). Furthermore, olfactory epithelium destruction suppress one of the two sink in the hippocampus, suggesting the hippocampus receives both nasal and central respiratory influence (Karalis and Sirota, 2018). Nonetheless, this result in not strictly in line with previous CSD (Lockmann et al., 2016; Yanovsky et al., 2014), since tracheotomy fully suppressed respiration-related sink. Difference might be explained by the fact that one result was observed in urethane anesthetized mice (Lockmann et al., 2016; Yanovsky et al., 2014) while the other in freely moving mice (Karalis and Sirota, 2018). Since inspiratory preBötzing (350 neurons in rats (Del Negro et al., 2018)) project to the locus coeruleus (Yackle et al., 2017) we could expect neuromodulation centers to amplify and spread the central respiratory modulation. All these cues suggest the brain is influenced by both nasal and central respiratory pathway.

### 1.3.3 And so what? What functions support this respiratory modulation?

The role of the brain respiratory modulation is not clear. So far, in rodents no articles aimed at studying the link between respiration and non-olfactory behaviors. However, respiration-related brain activity is well documented. On the contrary, human studies proposed protocols to exhibit respiratory modulation of non-olfactory cognition. However, neural correlates during task are for now poor. Nonetheless, recent evidence supports the idea of respiratory rhythm being masterclock, which mediate cross-areas coordination.

#### Communication through synchronization.

As with theta rhythm and the sleep slow waves, RRo is thought to synchronize distant brain areas, hence allowing functional exchange between concerned areas. Recent literature tends to support this idea. As a reminder from 1.1.3.4 Long-range communication a coordinator rhythm should be able to synchronize two areas and enable a synchrony in high frequency oscillations. Several studies showed RRo can couple to higher frequency in rodents (Biskamp et al., 2017; Cavelli et al., 2020; Ito et al., 2014; Karalis and Sirota, 2018; Rojas-Líbano et al., 2018; A. B. L. Tort et al., 2018; Yanovsky et al., 2014; Zhong et al., 2017) as well as in humans (Herrero et al., 2018; Zelano et al., 2016). Conjointly, neurons firing can also correlate with respiratory rhythm (Biskamp et al., 2017; Chi et al., 2016; Ito et al., 2014; Jung et al., 2019; Karalis and Sirota, 2018; Köszeghy et al., 2018; Tsanov et al., 2014; Yanovsky et al., 2014). Furthermore, brain areas can be two-by-two synchronized by respiratory rhythm (A. B. L. Tort et al., 2018). However, to confidently posit that RRo could set up a communication channel between areas, there miss the proof that high frequencies between areas are synchronized. Nonetheless, current evidences made the hypothesis very likely. Still according to 1.1.3.4 Long-range communication, the slow rhythm needs to have a fine spatial resolution, enabling precise spatial selection. RRo have been observed in different cortical and subcortical areas (Girin et al., 2021; Rojas-Líbano et al., 2018; A. B. L. Tort et al., 2018). Furthermore, RRo display different dynamic across hippocampal layers (Chi et al., 2016; Lockmann et al., 2016; Yanovsky et al., 2014). Consequently, respiratory rhythm can entrain precise subsets of neurons. All together, these arguments show RRo check almost all long-range coordinator rhythm requirements. In line with this view, literature provides two supporting examples (described in 1.3.1 What is the extent of respiratory modulation in the non-olfactory brain?): orofacial behaviors coordination (Kleinfeld et al., 2014) and fear expression (Fujisawa and Buzsáki, 2011; Karalis et al., 2016; Lockmann and Tort, 2018; Roy et al., 2017). Rodents display two other well-described coordinator rhythms, namely theta rhythm and sleep slow waves. These two rhythms are well segregated in time, meaning that they present poor overlap in time, indeed sleep slow waves occurs mainly during NREM sleep and theta rhythm occurs mainly during REM sleep and wakefulness. On the contrary, RRo can occur in all brain states, hence RRo can potentially compete with either theta or sleep slow waves. Then, how are these coordinators rhythms coordinated? Is there a real competition? Are they completely independent? Is there some synergy between them? Tort's lab focus most of their publications on the RRo/theta competition (Jung et al., 2019; A. B. L. Tort et al., 2018; Yanovsky et al., 2014; Zhong et al., 2017), while other authors showed they can be tied together (Biskamp et al., 2017; Köszeghy et al., 2018). The interaction between RRo and sleep slow waves has not been studied.

#### Respiratory rhythm and cognition.

Recent studies clearly evidenced a relation between respiratory rhythm and cognition. In 2016, besides showing respiratory modulation in human hippocampus, Zelano and colleagues (Zelano et al., 2016) performed cognitive tasks on healthy subject. Authors setup a memory-related task to test hippocampal RRo relevance. The task consisted in a first phase of encoding and a second phase of retrieval. During the encoding a set of

images was presented. Some images were presented only during inspiration, some others were presented only during expiration. During retrieval, new images were added to the set and at each image presentation, subjects were asked if they recognized it. Again, images were presented in inspiration or in expiration. Images that were encoded during inspiration and were retrieved also during inspiration were more accurately recognized compared to images encoded during expiration and retrieved during expiration. Authors did the same two tasks with a group of subjects that were asked to breathe through the mouth. Mouth breathing condition greatly altered performance. For the first-time nasal respiration has been correlated with non-olfactory cognitive performances. Complementarily, visual memory retrieval showed performance (response time and accuracy) decreased when retrieval occurred in expiration (Nakamura et al., 2018). Lastly about memory, the relation between nasal respiration and the consolidation of odor memory has been studied (Arshamian et al., 2018). Odors were presented, then one hour later odors were tested. During the hour of rest, one group breathe through the nose, the odor through the mouth. Recognition was significantly lower for mouth breathing group. To explain the link between respiratory rhythm and memory, Heck emphasize that hippocampus is significantly modulated by respiration (Heck et al., 2019). Indeed, the awake hippocampus displays RRo and gamma/firing phase-locking to respiration (Chi et al., 2016; Herrero et al., 2018; Zelano et al., 2016; Zhong et al., 2017), while the sleeping hippocampus produces sharp waves and ripples preferentially at inspiration (Karalis and Sirota, 2018; Liu et al., 2017). Memory was not the only cognitive act to be tested. Perl and colleagues (Perl et al., 2019) produces a very smart study using non-olfactory tasks. In the first instance, authors let the subject initiate the trials. Subjects systematically began tasks at inspiration. With a second group of subjects, task onset was randomly triggered, allowing to cover the respiratory cycle. Performance were higher when task onset occurred in inspiration. Consistently, Zelano showed fear expressing faces were faster recognized when images were presented in inspiration compared to expiration. All together, these results suggest the brain is more “ready to work” in inspiration. Moreover, the brain seems to “know it”, since we unconsciously initiate cognitive effort at inspiration. At rest EEG signals displayed different connectivity networks in inspiration and expiration, which could potentially explain the inspiration-expiration difference in readiness (Perl et al., 2019). Then during cognitive tasks, authors observed an increased activity in task-related areas. This activity is correlated with performance (Perl et al., 2019). This awesome study is the only one to correlate cognition, respiratory rhythm and brain activity (Perl et al., 2019).

### **1.3.4 Respiratory modulation across species?**

Currently, models used to track respiratory modulation in non-olfactory areas are mice and rats, while far behind lay humans and cats. Occurrence of RRo and respiration coupled gamma in various brain areas is conserved across species, which, in my opinion, reinforces the idea respiratory rhythm must not be considered as a side rhythm. Although, respiratory modulation can be observed in these all four animals, flagrancy in LFPs greatly varies between models. For example, in mice RRo are prominent. One could hypothesize these differences can be correlated with how preponderant olfactory sense is for the animal (low RRo in human and high RRo in mice). However, even in close species like mice and rats, substantial differences can be observed as illustrated by the two comodulograms shown (see *Figure 18*). Another huge difference between these species is the respiratory frequency range. Rodents respiration range between 1 and 12Hz (Girin et al., 2021), cats respiration range between 0.3 and 0.8Hz (Cavelli et al., 2020), humans respiration range between 0.1 and 0.4 (Boiten et al., 1994; Krieger et al., 1990). On the contrary brain rhythms ranges do not change much between species (Buzsáki and Draguhn, 2004). Therefore, what mean an RRo for a rodent, a cat or a human? Since respiratory parameters are adapted to the physiology of the animal, RRo may also support specialized functions for each specie.

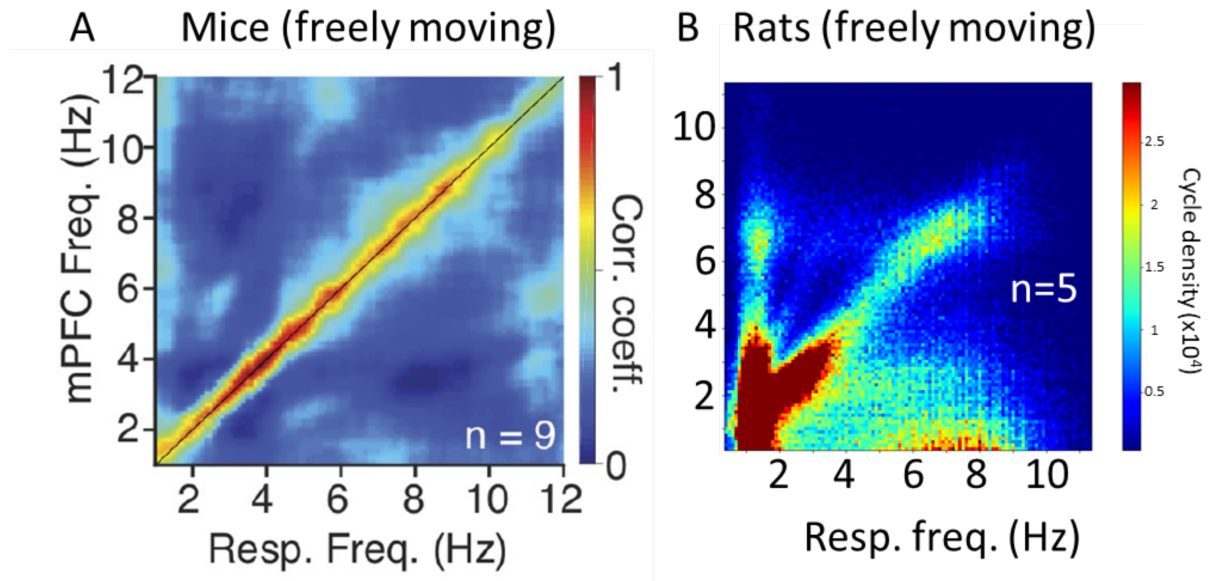


Figure 18 : Even closely related species displays pronounced difference in RRo preponderancy. A. mPFC LFP-respiration covariation matrix from freely moving mice Only diagonal presents high as if respiration imposes LFP low frequency mPFC. Extracted from Karalis and Sirota, 2018. B. mPFC LFP-respiration covariation matrix from freely moving rats. A diagonal is clearly visible show. ng indeed RRo are an important part of mPFC oscillations, but mPFC produces also various respiration-unrelated oscillations. Extracted from personal data.

## **2. Questions and objectives.**

## 2.1 Context

In the team, we actively participated in the demonstration of respiratory modulation of LFP oscillations, spiking activity and sub-threshold oscillations in the olfactory system (Briffaud et al., 2012; Buonviso et al., 2003; Cenier et al., 2009; Courtiol et al., 2011; David et al., 2009; Fourcaud-Trocmé et al., 2018; Litaudon et al., 2003). In the light of the broad projections of olfactory system to rest of the brain, we expected the respiratory modulation to extend beyond olfactory system. Plenty of studies unraveled respiratory modulation in the **LFP** of many non-olfactory areas in rodent brain (Chi et al., 2016; Ito et al., 2014; Köszeghy et al., 2018; Maier et al., 2020; A. B. L. Tort et al., 2018; Yanovsky et al., 2014; Zhong et al., 2017). Like the other teams, we made the hypothesis that the respiratory rhythm could represent a common clock, which could serve as brain-wide temporal reference facilitating neuronal assembly formation. However, to validate this theory some investigation is necessary. We questioned two points. 1) We wondered if such respiratory modulation could also exist in other signals than the LFP, which is a signal sensitive to volume conduction. 2) If widespread neurons use respiratory rhythm as common clock to coordinate their activity, it may be due to the existence of a brain-wide respiratory modulation of neuronal excitability. It has been proposed that all cells in the brain receive a depolarizing signal during the expiration and an hyperpolarizing signal during inspiration (Jerath et al., 2015). Therefore, this common excitability variation, controlled by respiration, would promote information exchange during expiration. However, to date, no evidence is available in favor of this theory. Our first study was then designed to tackle these two points.

## 2.2 Are non-olfactory neurons really affected by respiratory modulation?

Since we wanted to track respiratory modulation in a signal prevented from volume conduction and to monitor cell excitability, we logically decided to lead an intracellular study. We planned to record intracellular activity in freely breathing urethane-anesthetized rats. We chose to record in areas where respiratory modulation was well documented, namely mPFC, the S1 and the hippocampus. Additionally, since we have the intimate conviction that nasal respiration plays a key role in the brain-wide spreading of respiratory modulation, we made the hypothesis that, the more posterior an area is in the anteroposterior axis of the brain, the less susceptible it is to the respiratory drive. Therefore, we also recorded in the V1. Respiration was simultaneously monitored with a nasal airflow captor placed on right nostril. According to literature of the moment, respiratory modulation seems to depend on brain state (Viczkó et al., 2014; Yanovsky et al., 2014) and on nasal respiration (Yanovsky et al., 2014; Zelano et al., 2016). Therefore, I also recorded LFP to monitor brain state and I delivered odors to enhance activation of nasal pathway. We were the first to lead an intracellular study in these areas to characterize respiratory modulation in membrane potential and cell firing. Result gave rise to an article, currently under submission.

## 2.3 May the respiratory rhythm bind distant brain areas?

When I was acquiring intracellular data, another PhD student in the team performed LFP recordings in seven brain areas of freely moving rats throughout sleep/wake cycles (Girin et al., 2021). He showed each vigilance state is associated to a characteristic respiratory regime. Additionally, quiet waking is the only state during which all recorded areas shows a strong coupling to respiration. Finally, it turned out it is the specific respiratory regime developed during quiet waking rather than the state itself, which results in a strong and large respiratory drive of the brain.

Since I participated to these analyses, I wanted to take advantage of this data set to go further in the question and ask to what extent the respiratory modulation we observed

could occur simultaneously in the different areas. Especially, since my intracellular study revealed that, although a great number of cells displayed membrane potential RRo, their phase-locking with respiration presented a high variability. Thus, the hypothesis of a brain-wide depolarization/hyperpolarization cycle related to respiratory rhythm seemed not to hold. Nonetheless, one can rather imagine that respiration-related long-range communication involve transient synchronization of areas by respiration. Unfortunately, in Girin et al., 2021 all areas were analyzed independently, so a piece of the puzzle was missing to assess if respiratory rhythm could really bind areas together. If respiratory rhythm is indeed a common clock, multiple areas must be able to simultaneously synchronize to respiration. This is the question I try to answer in the second study

## **2.4 May the respiratory rhythm shapes assemblies?**

To follow the idea that respiratory rhythm could be a master clock, I still have to show that respiratory rhythm can synchronize firing between distant areas. As a first step, I need to know to what extent individual neurons firing can be modulated by respiration. However, my point is to test if breathing rhythm can be used as a temporal basis for cell assembly formation. So, in a second step, I have to verify if neurons from distant regions and modulated by respiration could fire together in a short time window (0-10ms).

To tackle this question, I needed an experimental setup enabling the recording of spikes and respiration in non-anesthetized animals, which we had not. So, I developed a head-fixed setup, in which recording chamber allowed to lower at least two electrodes simultaneously. Respiration was monitored with an airflow captor placed in front of the nostril. During recording session, in addition to respiration, I recorded firing (and LFP) activity in two distinct areas, at the same time. Unfortunately, sanitary crisis seriously delayed setting up of the installation. Nevertheless, I had time to record six animals. I will present here preliminary data from this brand-new setup. Yet, there is still so much more to do with this dataset.

### **3. Results**

## **3.1. Respiratory modulation of intracellular activity in non-olfactory neurons**

### **3.1.1 Context and summary**

As previously depicted (2. Questions and objectives.), many recent studies unraveled respiratory modulation in the LFP of non-olfactory areas. We had in mind the idea that excitability of all neurons in the brain could synchronously fluctuate at respiratory frequency, as a very general rule in the brain. To tackle this point, we decided to record membrane potential of neurons in non-olfactory areas. Before we started recordings, only one study had observed membrane potential RRo in three out fourteen hippocampal cells (Yanovsky et al., 2014). After we initiated the experiment another three cells popped up, two in parietal cortex (A. B. L. Tort et al., 2018; Zhong et al., 2017) and one in mPFC (Zhong et al., 2017). We undertook to record neurons from mPFC, S1, hippocampus and V1. According to literature of the moment, we strongly expected to detect respiratory modulation in membrane potential of neurons from mPFC, S1 and hippocampus. We chose to record V1 because, in terms of connectivity, V1 is far from the nose. Consequently, we are the first to attempt to rigorously track respiratory modulation in membrane potential activity of non-olfactory neurons.

Our intracellular study evidenced membrane potential RRo in neurons of all four structures. Prevalence of RRo amongst membrane potential activity was variable between areas and between cells. Episodes of membrane potential RRo were generally transient (five respiratory cycles in average). However, we did not find a stable preferred phase for respiration-related depolarization, but on the contrary a cell-dependent variability. For most cells of mPFC, S1 and V1, these episodes were accompanied by a respiration phase-locked firing. Occurrence of membrane potential RRo increased when LFP displayed also a respiratory dynamic. Oppositely, internal excitability state had weak influence on the occurrence of membrane potential RRo. Although, this study rejected the hypothesis of a brain-wide respiration-related fluctuation of neuronal excitability, we highlighted that neurons of each of these four areas can synchronize to respiration.

### **3.1.2 Results**

Results gave rise to a publication, currently under submission.

# Respiratory modulation in the brain: deep in the cells

Maxime Juventin<sup>1</sup>, Mickael Zbili<sup>1</sup>, Nicolas Fourcaud-Trocmé<sup>1</sup>, Samuel Garcia<sup>1</sup>, Nathalie Buonviso<sup>1\*</sup> and Corine Amat<sup>1\*</sup>

<sup>1</sup> Lyon Neuroscience Research Center (CRNL) Inserm U 1028, CNRS UMR 5292, University Lyon1, 69675 Bron, France

**Juventin M, Zbili M, Fourcaud-Trocmé N, Garcia S, Buonviso N and Amat C.** Respiratory modulation in the brain: deep in the cells. - In recent years, several studies have tended to show a respiratory drive in numerous brain areas so that the respiratory rhythm could be considered as a master clock promoting communication between distant brain areas. However, contrary to what is described in the olfactory system, it is not known if respiration related oscillation (RRO) could exist in the membrane potential (MP) of neurons in non-olfactory structures neither if it can structure spiking discharge. Here, we asked to what extent respiratory modulation could shape cellular activity, including MP and spiking activity, in non-olfactory areas. To this purpose, we co-recorded MP and LFP activities in different non-olfactory brain areas, namely the median prefrontal cortex (mPFC), the primary somatosensory cortex (S1), primary visual cortex (V1), and hippocampus (HPC), in urethane-anesthetized rats. Using respiratory cycle by respiratory cycle analysis, we observed that both MP and spiking discharges could be respiration-modulated in all recorded areas, but more transiently than what we previously described in the olfactory bulb. Particularly, respiratory modulation of MP was highly variable both between structures and between cells, very transient for most of cells (mean episode duration of 5 consecutive cycles) and largely influenced by LFP state. Moreover, even if internal excitability state had a weak influence on the proportion of respiration-modulated cells at the whole population level, moderate hyperpolarization of a cell in mPFC and S1 reduced the strength of its modulation. In conclusion, our demonstration that respiration can even influence MP and spike discharge of cells in non-olfactory brain areas suggest an existing cabling supporting conduction of respiration-related inputs to the whole brain

**NEWS & NOTEWORTHY:** In very different mammal brain areas, we evidenced a strong respiratory coupling between MP and spike discharge. Our results show that, at very different places in the brain, the MP of neurons can be depolarized and hyperpolarized according to the respiratory rhythm. These findings contribute to bring evidence that respiratory rhythm could be used as a common clock to set the dynamics of large-scale networks on a same slow rhythm.

freely breathing anesthetized rat, respiratory rhythm, respiratory related oscillation, intracellular activities, membrane potential

## INTRODUCTION

In recent years, a resurgence of publications has proposed respiration as a master clock for brain rhythms, following many observations that reported the breathing rhythm as being able to modulate complex behaviors or cognitive process (Heck et al. 2017, 2019; Maric et al. 2020; Zaccaro et al. 2018). The exploratory behavior of rodents, consisting in rhythmical sampling of the environment, is a perfect example since the onset of each respiratory cycle initiates a “snapshot” of the orofacial sensory environment, comprising sniffing, whisking and head movements (Cao et al. 2012; Kurnikova et al. 2017; Moore et al. 2013). Similarly, licking synchronizes with breathing (Lu et al. 2013; Welzl and Bureš 1977). In humans, respiration modulates memory consolidation (Arshamian et al. 2018), associative learning (Waselius et al. 2019), cognitive performances (Nakamura et al. 2018; Perl et al. 2019; Zelano et al. 2016), sensory perception (Iwabe et al. 2014), and motor behaviors (Li et al. 2012; Li and Laskin 2006). Respiratory phase influences the initiation of a voluntary action (Park et al. 2020) or a cognitive task and its performance (Perl et al. 2019). All these data therefore suggest that the brain could have at least one processing mode depending on the respiratory phase.

Parallel to this literature on the effects of breathing on behavior has appeared an equally important literature on a respiratory drive of brain activity, both in human and rodent. In human, intracerebral EEG-breathing coherence has been observed notably in the hippocampus, amygdala, insula and the parietal lobe (Herrero et al. 2018; Zelano et al. 2016) and inhalation phase is correlated with an increase in the power of delta oscillations (Zelano et al. 2016). In rodent, a respiration-locked local field potential (LFP) oscillation has been described in the hippocampus (Yanovsky et al. 2014), the somatosensory cortex (Ito et al. 2014), the prefrontal cortex (Biskamp et al. 2017; Kőszeghy et al. 2018), neocortical regions up to visual cortex and even subcortical areas (Girin et al. 2021; Tort et al. 2018). In several brain regions, respiration also modulates other rhythms. In the hippocampus, the timing of hippocampal slow-wave ripples is respiration-coupled (Liu et al. 2017). In the somatosensory cortex, delta oscillations are respiration-locked while gamma power is respiration-modulated (Ito et al. 2014). In the prefrontal cortex, fast gamma LFP oscillations (Zhong et al. 2017) and unitary activities (Biskamp et al. 2017) are phase-coupled with respiration.

This respiratory drive, described in such a large cerebral network, is at the moment assumed to arise in the activation of the olfactory bulb (OB) *via* mechanic stimulation of olfactory receptor cells by nasal

respiratory airflows (Grosmaître et al. 2007). Indeed, respiration-brain activity coupling dissipates in human when subjects breathe through the mouth (Zelano et al. 2016) or in rodents when OB is silenced (Ito et al. 2014; Liu et al. 2017; Lockmann et al. 2016; Yanovsky et al. 2014). This respiration-related activity is transmitted to the OB where it has been largely described (For review, Buonviso et al. 2006): respiration modulates both LFP and individual cells activities, including spiking discharge and membrane potential dynamics. In LFP signal, fast rhythms occurrence is shaped by the slow respiration-related oscillation (RRo), beta and gamma waves alternating on expiratory and inspiratory phases, respectively (Buonviso et al. 2003; Cenier et al. 2009). Mitral/tufted cells spiking discharge is strongly patterned by respiratory rhythm both in anesthetized (Briffaud et al. 2012; Cenier et al. 2009; Courtiol et al. 2011a; David et al. 2009) and awake rodent (Cury and Uchida 2010; Gschwend et al. 2012). Importantly, even the membrane potential of mitral/tufted cells is impacted by respiration (Ackels et al. 2020; Briffaud et al. 2012; Fourcaud-Trocmé et al. 2018). Particularly, RRo of membrane potential constrain fast oscillations to occur concomitantly with LFP signal, hence favoring interaction between fast LFP and spiking (Fourcaud-Trocmé et al. 2018). We and others have demonstrated that most of OB respiratory modulation is related to the amplitude of the inspiratory airflow (Courtiol et al. 2011a, 2011b; Esclassan et al. 2012; Oka et al. 2009). Respiratory influence is also present, to a lesser extent, in the olfactory cortex at the LFP and cellular levels (Piriform cortex: Courtiol et al. 2019; Litaudon et al. 2003, 2008; Miura et al. 2012; Olfactory tubercle: Carlson et al. 2014). Directly in contact with nasal respiratory airflows, the olfactory system is thus strongly impacted by respiration dynamics.

Oppositely, while LFP activity in non-olfactory regions has been described as respiration-modulated, very little is known about respiratory modulation of individual cell activities. Only a few reports described spiking discharge modulated by respiration (Biskamp et al. 2017; Köszeghy et al. 2018). To our knowledge, only a BioRxiv preprint reported intracellular recordings in parietal cortex (Jung et al. 2019). There are no studies showing that the membrane potential (MP) of cells in non-olfactory regions can oscillate with respiration nor, as we have shown in mitral/tufted cells of the OB, that this slow respiration-related oscillation of MP can structure spiking discharge. Here we asked to what extent respiratory modulation could shape cellular activity, including MP and spiking activity, in non-olfactory areas. To this purpose, we co-recorded membrane potential and LFP activities in widespread brain areas, namely the median prefrontal cortex (mPFC), the primary somatosensory cortex (S1), primary visual cortex (V1), and hippocampus (HPC), in urethane-anesthetized rats. Using respiratory cycle by respiratory cycle analysis, we tracked respiratory modulation of cellular activities. We observed that both MP and spiking discharges could be respiration-modulated in all recorded areas, but more transiently than what we previously described in the OB (Briffaud et al. 2012). Particularly, respiratory modulation of MP was highly variable both between structures and between cells, very transient for most of cells and largely influenced by LFP state. Moreover, even if internal excitability state had a weak influence on the proportion of respiration-modulated cells at the whole population level, moderate hyperpolarization of a cell in mPFC and S1 reduced the strength of its modulation.

## MATERIALS AND METHODS

### Experimental procedures

#### Animal care

The 25 male Wistar rats (325.2±32.1g, Charles River) used were housed in groups of four in a temperature (22±1 °C) and humidity (55±10%) controlled room and exposed to a 12/12 h light/dark cycle

(light onset, 6:00 am). Experiments were conducted during the light period (between 9:00 am and 3:00 pm). Food and water were available *ad libitum*. All experiments were carried out in accordance with Directive 2010/63/EU of the European Parliament and of the Council of the European Union regarding the protection of animals used for scientific purposes and in compliance with the ARRIVE guidelines. The experimental protocols were approved by the National Ethics Committee “Animal Experimentation Committee of Univ. Claude Bernard Lyon 1—CEEA-55” (Agreement APAFIS #17088).

#### Animal preparation

Rats were anesthetized with an intraperitoneal injection of urethane (1.5 g/kg), then, placed in a stereotaxic apparatus. Respiration was recorded with a homemade bidirectional airflow sensor placed at the entrance of the right nostril. Positive and negative flows corresponded respectively to inspirations and expirations. Body temperature was kept at 37 °C using a heating pad (Harvard Apparatus, Holliston, MA USA). A craniotomy of about 3x3 mm was performed above the site of recording: median prefrontal cortex, primary visual cortex, somatosensory barrel cortex or hippocampus. Dura was removed, and Ringer’s lactate solution was regularly applied onto the brain to prevent from drying. At the end of the experiments, rats were euthanized by intracardiac injection of Dolethal®.

#### In vivo Electrophysiological Recordings

We made simultaneous intra- and extracellular recordings in freely breathing anesthetized rats. Intracellular recordings (n = 69 cells) were performed in four different areas of the left hemisphere: the medial prefrontal cortex (mPFC, AP: 3.1±0.4 mm, MD: 0.7±0.2 mm), the primary somatosensory cortex (S1, AP: -2.4±0.4 mm, MD: 5.0±0.1 mm), the primary visual cortex (V1, AP: -5.3±0.2 mm, MD: 4.5±0.8 mm) and the hippocampus (HPC, -3.5±0.7 mm, MD: 2.6±0.7 mm). Borosilicate glass capillaries (o.d. = 1.5 mm; i.d. = 0.86 mm, Harvard Apparatus, Holliston, MA, USA) were pulled with a horizontal puller (model P-97, Sutter Instruments, Novato, CA, USA). The micropipettes were filled with a 2 M potassium acetate solution, and their resistances ranged from 50 to 120 MΩ. Microelectrodes were lowered using a piezo manipulator (PM-10, World Precision Instruments, Sarasota, FL, USA). The electrophysiological signal was amplified and low-pass filtered at 10 kHz by an intracellular amplifier (Axoclamp 2B, Axon Instruments, Foster City, CA, USA). The signal was then digitalized at 25 kHz (NI USB-6211, National Instruments, Austin, TX, USA) and stored on a computer using NeuroLabscope, a homemade software.

#### Internal polarity state

Internal polarity states (studied in Fig 4) were visually encoded based on sign (positive or negative) and intensity of direct current (DC) injection, amplitude of MP variation and firing activity. We identified 4 states: strong hyperpolarization (Hyp2), light hyperpolarization (Hyp1), basal level (Base), depolarization (Dep). A cell was not systematically recorded under each of the 4 states. *A posteriori* verification comforted our classification. Whatever the structure (Fig 4.A), basal level (Base) represented the state where none (N = 42 cells) or a very low stabilizing current (-0.07±0.06 nA, N = 14 cells) was injected. Hyp1 level corresponded to a MP hyperpolarization around 7 mV from basal level at which the spike discharge decreased by 60%. This level was achieved via a -0.28±0.04 nA (N = 29 cells) DC injection. Hyp2 level corresponded to a MP hyperpolarization around 12 mV from basal level at which the spike discharge decreased by 90% to 100%. This level was achieved via a -0.41±0.04 nA (N = 36 cells) DC injection. Dep level corresponded to a MP depolarization around 7 mV from basal level at which the spike discharge increased by at least

10%. This level was achieved via a  $0.17 \pm 0.04$  nA ( $N = 22$  cells) DC injection. For the cell-by-cell analysis (Fig 4B Base-Hyp1), to limit influence of external factors, we selected pair of recordings close in time. In mPFC, cells ( $N = 9$  cells) received  $-0.17 \pm 0.02$  nA for Hyp1 which resulted in a hyperpolarization of  $7.6 \pm 2.5$  mV and a spike discharge decrease of  $74.4 \pm 7.5$  %. Latency between end of Base recording and beginning of Hyp1 recording was  $3.2 \pm 1$  min. In S1, cells ( $N = 4$  cells) received  $-0.19 \pm 0.06$  nA for Hyp1 which resulted in a hyperpolarization of  $8.4 \pm 5.2$  mV and a spike discharge decrease of  $50.0 \pm 26.6$  %. Latency between end of Base recording and beginning of Hyp1 recording was  $3.3 \pm 1.4$  min. In V1, cells ( $N = 3$  cells) received  $-0.22 \pm 0.06$  nA for Hyp1 which resulted in a hyperpolarization of  $13.9 \pm 7.6$  mV and a spike discharge decrease of  $55.2 \pm 13.1$  %. Latency between end of Base recording and beginning of Hyp1 recordings was  $2.3 \pm 0.8$  min. In HPC, cells ( $N = 3$  cells) received  $-0.26 \pm 0.05$  nA for Hyp1 which resulted in a hyperpolarization of  $7.6 \pm 3.0$  mV and a spike discharge decrease of  $50.5 \pm 10.0$  %. Latency between end of Base and beginning of Hyp1 recordings was  $1.3 \pm 0.2$  min.

Local field potential (LFP) was recorded simultaneously with all intracellular recordings using silicon probes (Neuronexus Technology, Ann Arbor, MI, USA) placed as close as possible to the glass microelectrode. The signal was amplified, and low-filtered at 5 kHz with a homemade amplifier.

### Data analysis

All following analyses have been made using homemade Python scripts.

#### *Respiratory signal processing*

Respiratory cycles were detected as previously described in . Briefly, respiratory signal was high-pass filtered to reduce noise, then zero-crossing points were detected to delineate inspiration and expiration start points. Finally, time of each respiratory cycle was linearly converted to phases ranging from 0 to 1. To summarize, all respiratory cycles were detected, inspiration and expiration phases were well determined, and respiratory phases were computed.

#### *Rescaling time basis of signals with respiratory phase*

We wanted to track variations of signals of interest (LFP, MP, AP discharge) related to respiratory rhythm. However, respiratory cycles displayed duration variability, and inspiration-expiration ratio from two cycles of same duration could differ. Thus, the respiratory phase was the appropriate time scale to reduce jitter due to respiratory cycle variability. Similarly to Roux et al., 2006., we rescaled signals of interest as a function of respiratory phase. Briefly, after having detected respiratory cycles, signal during each cycle was interpolated into a 2000 points vector. To account for the asymmetry of respiratory cycles, the mean inspiration ratio (inspiration duration/cycle duration) was computed for each recording. Cycle by cycle interpolation preserved the ratio, *i.e.*, for a 0.33 ratio, interpolation attributed 33% of the 2000 points to the inspiration and the rest to the expiration. This rescaling allowed the construction of respiration triggered MP average (Fig 1C bottom) or respiration triggered AP histogram (FIG 1C top). We made one exception to construct Fig 3B as we wanted to compare the preferred phase of depolarization between cells, we rescaled all recordings with the same ratio 0.4 in order to align all cell respiratory phases.

#### *Time dynamics of respiration-related MP oscillations*

The method described hereafter aimed at determining if a given signal followed the respiratory rhythm on a cycle-by-cycle basis. It was

applied to AP-removed membrane potential and LFP signals. To remove APs, single APs were cut from 4ms before to 5 ms after the peak. Burst were cut from 30ms before the first AP to 30 ms after the last AP. Cut signal was replaced with a linear interpolation between the two extremities. Several cutting lengths were tested. Visually satisfying parameters were kept.

First step: Identification of local oscillation related to respiration. Signal of interest was rescaled towards respiratory phase as explained previously. As we wanted to follow the time dynamics of respiratory oscillations, we scanned recordings with windows of 4 respiratory cycles, with an overlap of 3 cycles between consecutive windows. In each window we computed respiration triggered median signal, which amplitude should be high when signal oscillations are synchronized to respiration. To question the existence of such a local respiratory related oscillation, we compared median signal waveform amplitude with surrogate amplitudes ( $N = 500$ ). One surrogate of one window was built as follow: we randomly created 2 pairs of cycle (for example cycles 1&3, and 4&2). For one pair we phase shifted with a random ( $\phi_1$ ) phase the first cycle. The other cycle of the pair was phase shifted with the opposed phase ( $\phi_1 + \pi$ ). Second pair underwent the same transformation, with another random phase-shift ( $\phi_2$ ). By doing so, within each pair (phase-opposing) and between pairs (random phase-shifting) respiratory influence was neutralized when averaging, thus surrogate data contained only the signal part unrelated to respiration. We considered a local waveform was respiratory related if window median signal amplitude was larger than 95<sup>th</sup> percentile of surrogate amplitudes. This algorithm allowed to classify local signal in each window as respiratory-related or not.

Second step: Refinement from local oscillation to individual cycles. To reduce false-detection and to increase time precision, we wanted this encoding to be realized cycle by cycle. From the windows previously identified as respiratory related windows, we wanted to extract the cycles which really contributed to this respiratory waveform. To ensure that individual cycles within the window looked like the local waveform, we computed for each cycle the scalar product between the cycle signal and the window median signal. Since we focused on waveform, not on amplitude, we z-scored the signals before performing the scalar product ( $(X - \text{mean}(X)) / \text{std}(X)$ ). We assessed significance by comparing the result to scalar products between the cycle signal and 500 surrogated window signals (we kept the previous surrogates). We considered the individual cycle sufficiently similar to the local waveform if the scalar product value was greater than the 95<sup>th</sup> percentile of surrogated scalar product values. If so, score of this cycle was incremented by 1. Since a cycle may be scanned up to four times (in four consecutive windows), score of individual cycle ranged from 0 to 4. We classified cycles in three respiratory related categories as follow: 0 and 1: non-modulated cycles, 2: undetermined, 3 and 4: modulated cycles. Finally, we eliminated all single or doublet cycles identified as respiratory entrained, and they were transferred to the undetermined category. Indeed, we considered that respiratory related events of strictly less than 3 consecutive cycles were not physiologically relevant and too much susceptible to false detection.

For each cell we were then able to compute the probability of respiratory entrainment (expressed in percent), defined as the ratio between the number of respiration-related cycles and the total number of cycles. For further analysis, we considered a cell to be sensitive to respiration if respiratory entrainment was strictly higher than 2.5%. This threshold avoided overestimation of respiration-sensitive cells for long recording. Overall, the method has been designed to reduce false detection to the minimum; therefore we may underestimate the respiratory entrainment.

### *Respiration triggered membrane potential*

Using the classification method described in the previous paragraph, we could isolate membrane potential cycles related to respiration. These cycles were then stacked, and we computed the median signal. For each respiration-sensitive cell, the amplitude of respiration-related oscillations was defined as the maximum/minimum difference of this median signal. For the 4 examples in Figure 1, 95% confidence intervals represent the sum of standard error ( $1.91 \cdot \text{SEM}$ ) at the minimum and the maximum points. To analyze preferred phase of the depolarization, we computed the median respiration-triggered signal, then we extracted the mean vector and finally we kept its angle. For this latter analysis we only used respiration sensitive cells whose signal contained strictly more than 5 respiratory-related cycles.

### *Respiration triggered spiking pattern*

AP times were rescaled to a respiratory cycle phase basis. Therefore, AP were identified by the number of the respiratory cycle they belong to, and their respiratory phase within that cycle. Once respiratory cycles were classified in respiratory-related categories, we could sort AP according to these categories. Then, for each cell and each respiratory-related category we built respiration triggered discharge histogram. For each cell, three experts, independently, visually encoded spiking patterns associated to each respiratory-related category. Spiking patterns were classified as: respiration driven or not, and with not enough spikes to be determined. Classification was inspired from Buonviso et al. 2006.

### *Power spectrum*

For the 4 examples in Figure 1, Morlet wavelet time-frequency maps (0.4-6Hz) for respiratory signal and AP-removed membrane potential were computed for whole recordings. Then we extracted the 4s time windows showed in the figure and computed the mean across time by frequency to estimate the power spectrum. Spectra were normalized by their sum to get a density.

### *Extracellular signal (LFP) processing*

LFP signal was 0.3Hz high pass filtered. Then, similarly to membrane potential oscillations, LFP-respiration relationship was classified cycle by cycle. Using this classification, the relationship to respiratory rhythm was then compared between MP and LFP.

### *Conditional probabilities*

In Fig5D, we looked at the conditional probability to observe MP RRo relative to LFP dynamics. In other words, we split recording according to LFP RRo encoding. On the one hand we computed MP RRo probability within cycles identified as LFP RRo (without % cycles threshold), and on the other hand we still computed the MP RRo probability but this time within cycles identified as LFP activity not related to respiration (other LFP activity). Fig5E is the complementary view since we computed the conditional probability to observe LFP RRO according to MP dynamics (RRo or other activity).

### *Statistics*

Statistics were made with Scipy (version 1.4.1) python package (scipy.stats.wilcoxon, scipy.stats.mannwithneyu, scipy.stats.kruskal). All averages are presented under the format  $\text{mean} \pm \text{SEM}$ . If not, it is explicitly mentioned.

## RESULTS

### **Evidence for a respiratory modulation of cell membrane potential in non-olfactory structures**

*In vivo* intracellular activities recordings were obtained from 4 non-olfactory structures in 25 freely breathing anesthetized rats; specifically, 34 cells were recorded in median prefrontal cortex (mPFC,  $N = 9$  rats), 13 cells in somatosensory cortex (S1,  $N = 4$  rats), 5 cells in visual cortex (V1,  $N = 4$  rats) and, 17 cells in hippocampus (HPC,  $N = 8$  rats). The respiratory frequency ranged from 1.44 Hz to 2.08 Hz ( $1.78 \pm 0.03$  Hz,  $N = 25$  rats).

In all these four areas, we found cells with a respiration-related oscillation (RRo) of their membrane potential (MP) and a respiration-related (RR) spiking discharge, as shown on the raw data examples (Fig.1A). Indeed, the filtered respiratory signal (light gray) fits the raw traces of the intracellular MP oscillations. In Fig.1B, the power spectral density analysis of the MP signal (black PSD) exhibits a clear power peak at the respiratory frequency (grey PSD) which confirms that MP follows respiratory rhythm in these examples.

In order to properly characterize the relation between MP and respiratory rhythm, we developed a cycle-by-cycle method for detecting the respiratory cycles at which MP oscillated at the respiratory rhythm (see materials and methods for details). We plotted the median of respiration-triggered membrane potential (Fig.1C bottom panels) and the histograms of spiking occurrence during these cycles (Fig.1C top panels). In the examples of Figure 1, MP RRo are large (median amplitude  $\pm$  95% confidence interval: mPFC =  $5.5 \pm 0.9$  mV, S1 =  $14.5 \pm 2.1$  mV, V1 =  $8.8 \pm 2.2$  mV, HPC =  $3.1 \pm 0.8$  mV; Fig.1C bottom panels), and APs occurrences are clearly related to respiratory cycle (top panels in Fig.1C). Moreover, on these examples, MP RRo and firing pattern are similarly phase-locked to respiration, suggesting a strong correlation between MP RRo and the associated firing. Indeed, spikes appeared on the top of the oscillation, where the MP is the most depolarized.

Thus, we evidenced that a respiratory modulation can be expressed in the intracellular activity (MP and spiking) of cells in the four non-olfactory areas we recorded. The next step was to better characterize this MP respiratory modulation in each structure.

We first quantified the percentage of cells exhibiting MP RRo at rest. As explained in Methods, we defined an MP as being respiration-entrained only if we observed at least 3 consecutive RRo cycles. The first step was to measure the percentage of respiratory cycles eliciting an MP RRo in each cell for the 4 structures (Fig. 2A, MP RRo cycles,

MP No RRo cycles and MP which is at the limit to be classified as RRo respectively black, white and grey bars, see methods), then to draw the cumulative distribution of RRo MP cycles percentage across cells for each structure (Fig. 2B). From these representations, we chose to classify a cell as respiratory entrained if it expressed at least 2.5% of

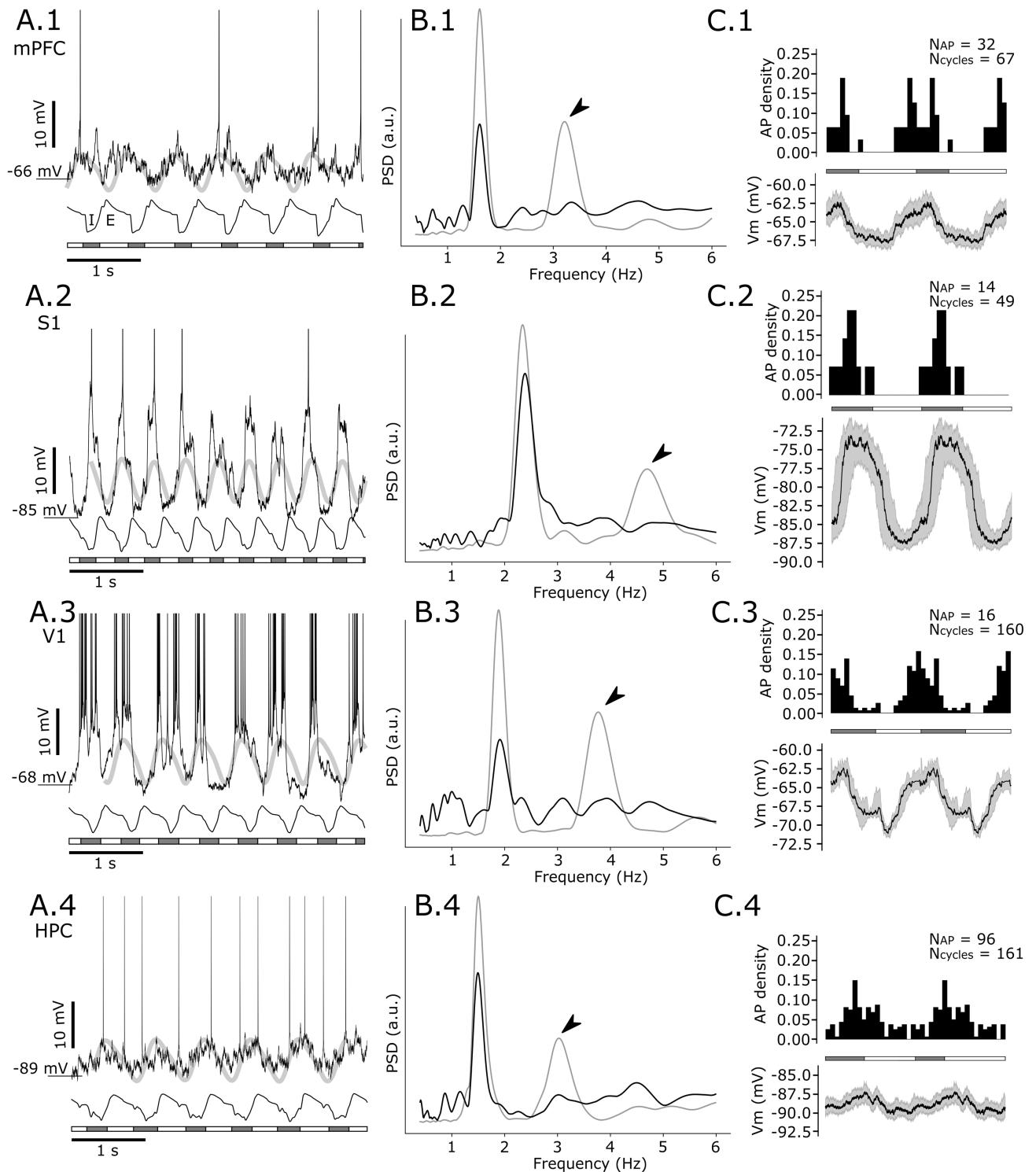


**Figure 1 : Intracellular activity of widespread brain areas correlates with respiratory rhythm. A. Raw traces of intracellular activity from mPFC, S1, V1 and HPC (respectively subpanels 1, 2, 3, 4). A panels:** Top trace: intracellular raw trace in black, overlaid with a filtered (3 Hz low pass) respiratory signal, in grey, which has been time-shifted to highlight MP RRo. Mid trace: Respiratory signal. Bottom: Respiratory phase, with grey bars representing inspiration phases, white bars representing expiration phases. Time scale bar = 1s, amplitude scale bar = 10 mV. E = expiration, I = inspiration. AP have been truncated. **B panels:** MP (black) and respiratory signal (grey) power density spectrum over the 4s of signal presented in A. Arrow heads highlight 1<sup>st</sup> harmonic of the spectrum. **C panels** Respiration-triggered AP firing histogram (top) and respiration triggered MP (bottom). Data of respiration-triggered figures are extracted from several cycles during which MP is identified as correlated with respiration. Cycles and AP numbers are indicated on the right top. To visually reinforce oscillatory behavior, plots have been duplicated. Respiratory phase is reminded in between the two respiration-triggered figures. Grey and white bars correspond respectively to inspiration and expiration. Bottom: respiration triggered MP where black line corresponds to the median, shaded areas delineate the 25<sup>th</sup> and 75<sup>th</sup> percentiles.

RRO cycles (red lines in 2A1-2A4). Under such conditions, respiration-entrained cells represented 53.1% of cells (17/32) in mPFC, 60% (6/10) in S1, 50% (2/4) in V1, and 80% (8/10) in HPC. Therefore, the three cortical structures (mPFC, S1 and V1) presented equivalent proportions of respiration-entrained cells while HPC presented a higher proportion. More specifically, the cumulative percentage curves (Fig. 2B) show that 20% of the cells in S1 and mPFC had about 20% of their MP cycles modulated by respiration, more than 20% of HPC cells had about 75% of their cycles modulated, and no cell in V1 had more than 25% modulated cycles.

As seen in Fig.2A 1-4, the percentages of MP RRo cycles, varied greatly from cell to cell in a same structure and between structures. Indeed, if we take into account only the cells exhibiting more than 2.5% of cycles with RRo MP (above horizontal lines), the percentage of RRo MP cycles ranged from 2.7% to 90.5% in mPFC (18.6±5.4%, N = 17 cells) and from 3.2% to 88.9% in HPC (29.5±11.4%, N = 8 cells), while

it only extended from 6.5 to 33.3% in S1 (15.4±3.6%, N = 6 cells) and from 17.2 to 25.8% in V1 (21.5±3.1%, N = 2 cells) (Fig.2C). Note that three neurons (one in mPFC and two in HPC) exhibited an extreme proportion of MP RRo cycles (more than 90%). The low percentage of MP RRo cycles for some cells is certainly due to our highly selective method for detecting RRo cycles (see material and methods). Due to the great variability between cells, no significant difference in proportion of MP RRo cycles between structures was observed (Fig.2C, Kruskal Wallis test,  $p = 0.70$ ,  $H(3) = 1.45$ ).

To go further, we quantified for each entrained cell at resting MP (Base) the average duration of respiration-entrained episodes (*i.e.*, the number of consecutive cycles that presented MP RRo). As shown in Figure 2D, there was no significant difference in the duration of respiration-entrained episodes between structures (Fig. 2D, Kruskal Wallis test,  $p = 0.18$ ,  $H(3) = 4.77$ ). In fact, the average number of consecutive MP RRo cycles was around five regardless of the structure (mPFC: 5.2±0.3,

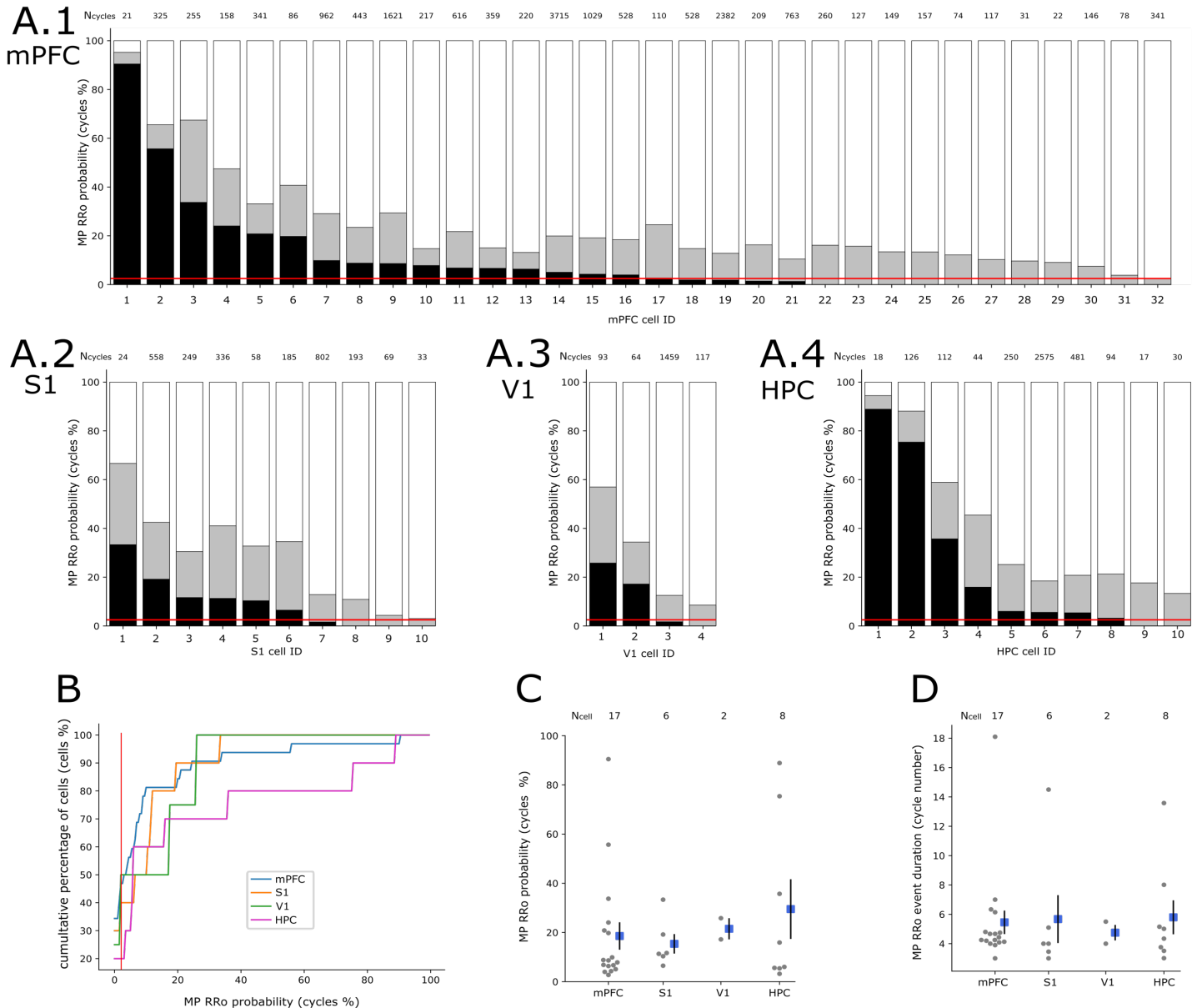


**Figure 2 : A significant number of cells in each structure exhibit MP RRo, yet individual episodes are short.** Only recordings at basal MP are considered. **A.** Distribution of MP encoding by cell in mPFC, S1, V1 and HPC (respectively subpanels 1, 2, 3, 4). Black, grey and white, bars correspond to the probability of RRo cycles, undetermined cycles and no RRo cycles respectively. Red lines indicate our 2.5% threshold. On the top of each bar is indicated the total number of recorded respiratory cycles. **B.** Cumulative distribution of RRo percentages of each structure. Blue, orange, green and pink curves correspond to mPFC, S1, V1 and HPC respectively. Red lines highlight our 2.5% threshold. **C.** MP RRo probabilities across structures. Grey points represent MP RRo probability for individual cells, blue squares represent the mean by structure and black line represent SEM. Only cells with RRo probability above 2.5% are considered. No significant difference is observed (Kruskal-Wallis test,  $p = 0.69$ ,  $H(3) = 1.45$ ,  $N_{mPFC} = 17$ ,  $N_{S1} = 6$ ,  $N_{V1} = 2$ ,  $N_{HPC} = 8$ ). **D.** MP RRo episode duration across structures. Grey points represent mean MP RRo episode duration of individual cells, blue squares represent the mean by structure and black lines represent SEM. The same cell pool as in B is used. No significant difference is observed (Kruskal-Wallis test,  $p = 0.80$ ,  $H(3) = 0.98$ ,  $N_{mPFC} = 17$ ,  $N_{S1} = 6$ ,  $N_{V1} = 2$ ,  $N_{HPC} = 8$ )

N = 17 cells; S1: 4.9±0.6, N = 6 cells; V1: 4.8±0.4, N = 2 cells; HPC: 6.0±0.6, N = 8 cells).

Taken together, these results show that at least 50% of cells of each recorded structures exhibited MP RRo. However, this respiratory entrainment of MP was 1) highly variable both between structures and between cells, 2) very transient for most cells (with mean episode duration of 5 cycles).

Then, to further explore the intrinsic dynamics of these RRo events, we studied both their amplitudes and phases. We first measured the amplitude of the median respiration-triggered MP (see material and methods for details) for each entrained cell (Fig. 3A). In order to reduce the noise in the median respiration-triggered MP, we restricted the analysis to cells with at least 5 RRo cycles (Fig. 3A, B). This revealed that amplitude of MP RRo was higher in S1 (11.2±2.5 mV, N = 6 cells) compared to mPFC (3.5±0.4 mV, N = 16 cells), HPC (3.7±0.5 mV, N = 7 cells), and V1 (5.6±1.5 mV, N = 2 cells) (Fig.3 A). Statistical threshold was not reached except for S1 compared to mPFC and HPC (Kruskal Wallis test,  $p = 0.02$ ,  $H(3) = 9.62$ , *post hoc* Mann-Whitney U test S1–mPFC:  $p = 0.002$  and S1–HPC:  $p = 0.01$ ), probably due to the small sample sizes.

To pursue, we characterized the respiratory phase of the MP RRo. As already suggested by the illustrative examples in Fig 1, MP RRo phases were not unique. Indeed, whereas MP exhibited maximal depolarized values around the transition phase between inspiration and expiration in S1 and HPC examples (Fig.1C, 2 and 1C, 4), MP of mPFC and V1 examples exhibited hyperpolarized values at this same respiratory phase (Fig. 1C1 and 1C3). For a complete analysis, we extracted, for each cell, the phase of the most depolarized value of the median MP RRo (see Fig1, panels C-bottom for examples of median MP RRo). Fig 3 B displays for each structure, the phase for each cell. Globally these phases seem to be distributed according to two preferential values, between 130-170 degree and 315-340 degree, approximately corresponding respectively to I/E transition (at 140 degree) and the end of expiration before E/I transition point (E/I at 0 degree). For mPFC and S1, the majority of the vectors were distributed pretty much equally

between the two phases, whereas for HPC 4/7 vectors were locked close to I/E transition, while the three others presented a different phase between end of expiration and beginning of inspiration.

Area	MP activity	RR discharge		No RR discharge		Total cells
		N <sub>cell</sub>	%	N <sub>cell</sub>	%	
mPFC	RRo	4	80%	1	20%	5
	No RRo	6	28.57%	15	71.43%	21
S1	RRo	4	80%	1	20%	5
	No RRo	1	14.29%	6	85.71%	7
V1	RRo	1	50%	1	50%	2
	No RRo	1	33.3%	2	66.6%	3
HPC	RRo	1	25%	3	75%	4
	No RRo	3	37.5%	5	62.5%	8

**Table 1 : Neocortical areas show stronger coupling between MP and spiking than hippocampus.** For each cell, spikes were segregated depending if they occur during a MP RRo respiratory cycle or a no RRo respiratory cycles. Respiration triggered discharge histograms were computed for the two MP categories. Histograms are then classified as either RR discharge or no RR discharge. Results are presented for each area and each MP activity. Line “N<sub>cell</sub>” represents the number of cell in each discharge class. Line “%” represents the percentage of cell in each discharge class relative to the total number of cells associated to a MP activity.

Finally, we looked in details at the relationship between MP RRo and spiking discharge. Table 1 presents the different association’s possibilities between MP (RRo or no RRo) and discharge (RR discharge and No-RR discharge). To construct this table, we considered the distribution of spikes as a function of respiratory phase (see Fig 1 C, top panels) using previously described method used in olfactory bulb (Briffaud et al. 2012; Cenier et al. 2009) (see Material and Methods for details). For a given cell, we segregated spikes occurring during respiratory cycles presenting a RRo MP from those occurring during respiratory cycles presenting a no RRo MP. The two spike distributions were then classified as either respiration-related (RR) discharge or non-respiration-related (no RR) discharge. Table 1 summarizes this classification across cells for each structure. It shows the percentages

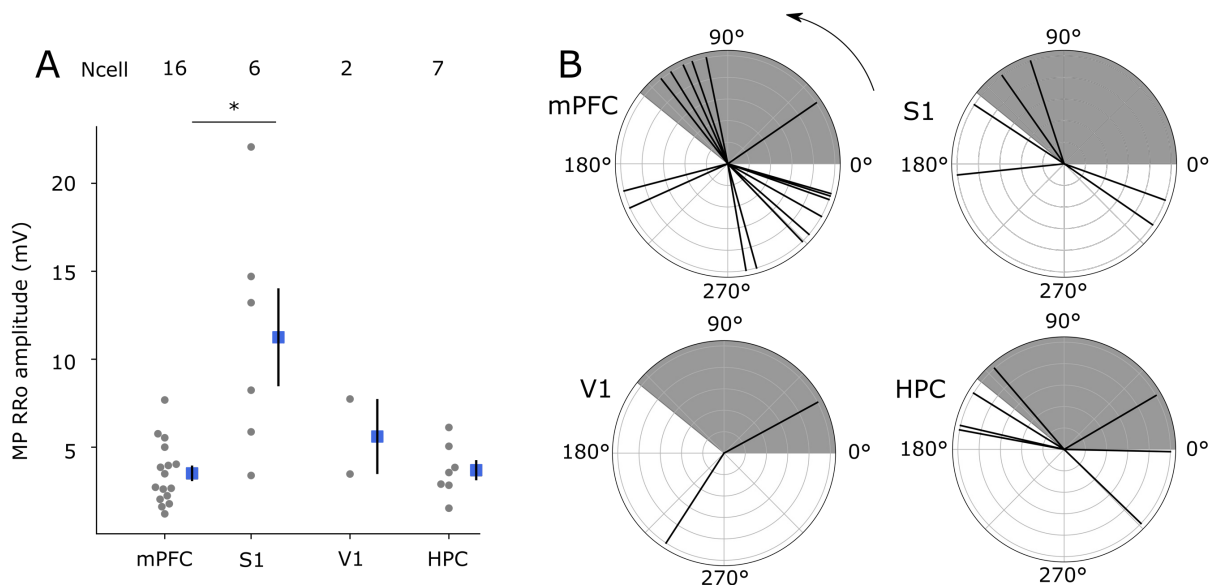


**Figure 3 : MP RRo phase and amplitude characteristics. Only recordings at basal MP are considered. A. MP RRo amplitude across structures.** Grey points represent MP RRo amplitude of individual cells, blue squares represent the mean by structure and black line represent SEM. Significant differences are observed (Kruskal-Wallis test,  $p = 0.02$ ,  $H(3) = 9.62$ ,  $N_{mPFC} = 16$ ,  $N_{S1} = 6$ ,  $N_{V1} = 2$ ,  $N_{HPC} = 7$ ). *Post hoc* two-sided Mann-Whitney U test reveals amplitude of MP RRo is higher in S1 cells than in mPFC ones,  $p = 0.002$ . Only cells with MP RRo probability above 2.5% and strictly more than 5 cycles are considered. **B. MP RRo preferred respiratory-phase across structures.** Preferred phases are presented in a trigonometric circle, time progressing is anticlockwise. Shaded and white areas, correspond respectively to inspirations and expirations.

of each association between spiking discharge patterns (columns) and respiration-triggered MP types (lines). In mPFC and S1, the RRo MP was mostly associated with the RR discharge pattern (80% for both structures) and conversely the No RRo MP was mostly associated with the No RR discharge pattern (71.4% and 85.7% respectively). Results about V1 follow the same trend with a smaller cell number. Results about HPC did not show the same association profile. Indeed, only 25% of the MP RRo was associated with RR discharge pattern.

In summary, we showed that respiration-related membrane potential oscillations were larger for cells in S1. Their respiratory phases were mainly around I/E and E/I transitions for mPFC and S1 cells, while mainly around I/E transition for HPC cells. Moreover, respiratory coupling between MP and spiking discharge was much more frequent in mPFC and S1 (71.4% and 85.7% respectively) than in HPC (25%).

Faced with the transient nature of MP RRo and their variability in amplitude and phase, we asked if parameters such as cell intrinsic state or local network state could influence respiration entrainment of MP.

### Influence of intrinsic excitability and network activity on the respiratory modulation of membrane potential

Our second aim was then to examine to what extent RRo MP could be influenced by (i) intracellular excitability, and (ii) by local field potential (LFP) state.

#### (i) Effect of intracellular excitability.

First, we studied the effect of excitability level on the probability for MP to be respiration-modulated. Briefly, we tested two hyperpolarization levels (Hyp1 and Hyp2) and one depolarized level (Dep) by progressive direct intracellular DC current injection. As described in materials and methods, we used 3 criteria (firing, MP value, and injected current) to classify these excitability states.

Fig 4A shows the proportions of respiration-entrained cells in each structure, as a function of internal excitability levels. mPFC and HPC displayed relatively stable proportions across the four different excitability levels ( $52.6 \pm 5.1\%$ ,  $N = 4$  excitability levels; and  $82.0 \pm 5.4\%$ ,  $N = 4$  excitability levels; respectively). On the contrary, S1 dropped to 0% (0/4 cells) in Hyp2 and showed disparate proportions in other levels (Hyp1 = 20%, base = 60%, Dep = 25%). V1 showed

stable proportion between base and Hyp1 levels (50%) and an increase to 80% at Hyp2 level. Thus, when looking at the whole population, excitability level did not clearly impact the proportion of respiration-entrained cells.

Then, we compared the percentages of MP RRo cycles for a same cell when it was hyperpolarized from base to Hyp1 level (Fig. 4B). This cell-by-cell analysis was necessary because of the great variability of MP RRo cycles proportion at base level within a same structure (cf. Fig 2). This analysis indicated that, in mPFC and S1, the percentage of MP RRo cycles was considerably reduced when hyperpolarizing the cell (mPFC: Base:  $5.7 \pm 2.9\%$ , Hyper1:  $1.6 \pm 1.1\%$ , Wilcoxon test  $p = 0.02$ ,  $Z = 0.0$ ,  $N = 9$  cells) (S1: Base:  $15.7 \pm 7.1\%$ , Hyper1:  $1.0 \pm 0.6$ , Wilcoxon test  $p = 0.07$ ,  $Z = 1.0$ ,  $N = 4$  cells).

These data showed that, even if internal excitability state had a weak influence on the proportion of respiration-entrained cells at the whole population level, moderate hyperpolarization of a cell, in PFC and S1, decreased its MP RRo cycle percentage.

#### (ii) Effect of LFP state.

Since it is now well established that LFP in these brain structures can be respiration-entrained (Girin et al. 2021; Tort et al. 2018), we then questioned how MP and LFP respiratory rhythms could interact. Raw data in Fig. 5A1 shows an example where neither MP nor LFP were respiration-entrained. At this moment, MP and LFP signals appeared very different. Conversely, for the same cell, a few minutes later (Fig. 5A2, after 2 min), respiratory frequency appeared simultaneously in MP and LFP signals. The similarity between both signals is highlighted when superimposing filtered respiratory signal (light grey traces on MP and LFP raw signals).

LFP RRo cycles were detected in the same way than MP RRo cycles, in order to be able to compare their temporal dynamics (see Methods). We found LFP RRo cycles in the four structures. Fig. 5B displays the mean percentage of LFP RRo cycles per recording (grey dots) and the percentages per structure (blue squares). mPFC showed a much higher percentage of LFP RRo cycles (up to 74%, with a mean of  $32.9 \pm 5.1\%$ ,  $N = 20$  cells) than S1 ( $14.8 \pm 11.4\%$ ,  $N = 3$  cells), V1 ( $15.4 \pm 9.4$ ,  $N = 2$  cells), or HPC ( $11.3 \pm 3.8\%$ ,  $N = 4$  cells). Nonetheless, the differences were not significant, certainly due to low effectives (Kruskal Wallis test,  $p = 0.14$ ,  $H(3) = 5.38$ ). In the way that we did for the MP recordings, we quantified for each LFP recording the mean duration of

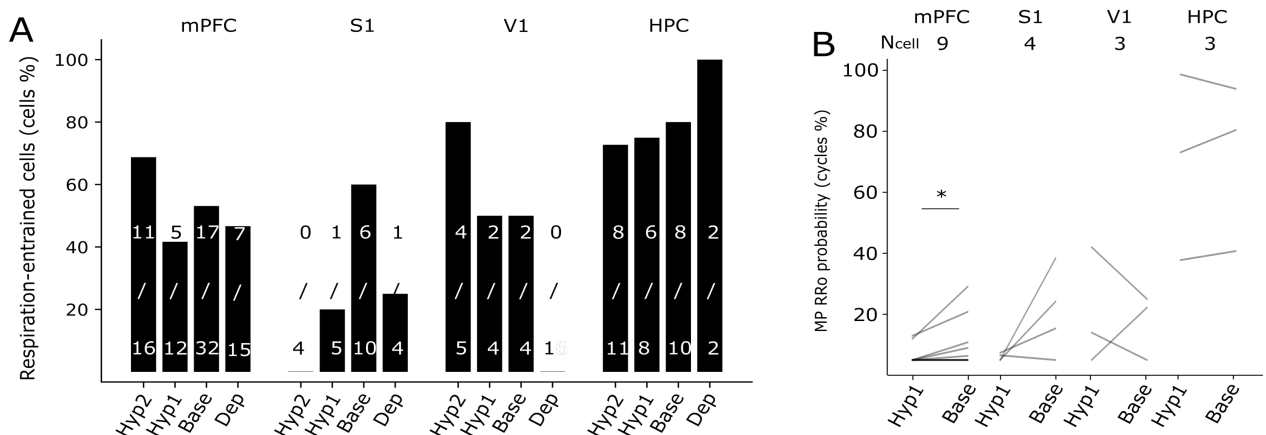


**Figure 4 : Internal excitability level has weak influence on percentage of respiration coupled cells on the whole population but decrease percentage of RRo MP cycles when cell by cell analysis. A. Percentage of respiration-coupled cells across structures and internal excitability states.** Numbers of cells appear in each black bar. **B. Individual cell evolution of MP RRo probability across hyper1-to-base states.** Only cells recorded in hyper1 and base conditions are presented. Recordings must be close in time (<7 min see methods). For mPFC, RRo probability is higher in hyper1 than in base (Wilcoxon paired test,  $p = 0.04$ ,  $N = 9$ ).

respiration-entrained episodes. The mean number of consecutive LFP RRo cycles (Fig.5C) was significantly higher for mPFC ( $11.0 \pm 2.2$ ,  $N = 20$  cells) than for S1 ( $3.7 \pm 0.3$ ,  $N = 3$  cells), and HPC ( $4.2 \pm 0.4$ ,  $N = 4$

cells) (Kruskal Wallis test  $p = 0.01$ ,  $H(3) = 10.51$ , *post hoc* Mann-Whitney U test mPFC-S1:  $p = 0.01$  and mPFC-HPC:  $p = 0.01$ )

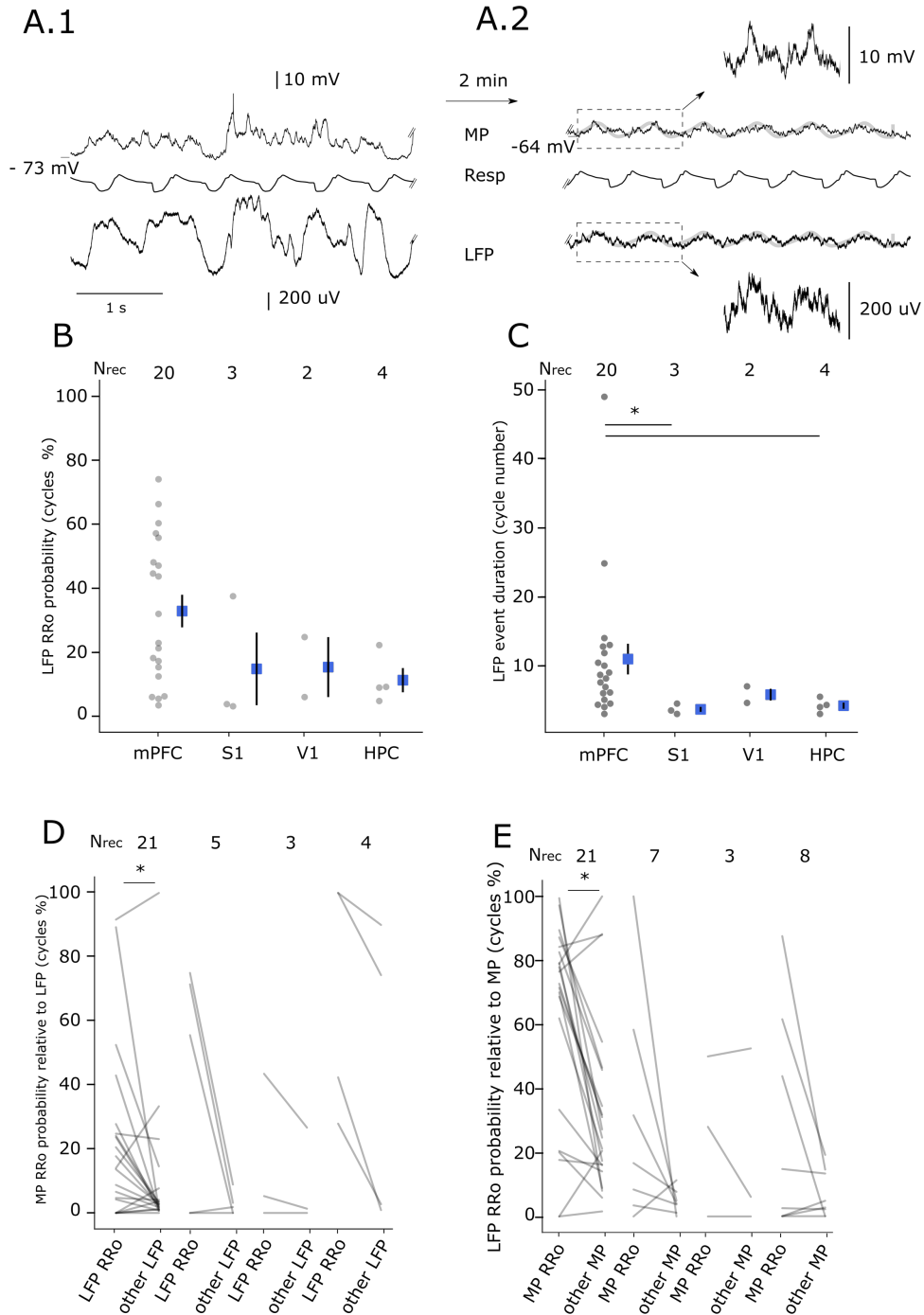


**Figure 5 : MP RRo probability increases when RRo are concomitantly present in LFP.** Only recordings at basal MP are considered. **A.** MP (Top), respiratory signal (mid) and LFP (bottom) raw traces of the same cell when LFP and MP do not display RRo (A1) and two minutes later when LFP and MP display RRo (A2). On A2 panel, light grey traces show filtered and time-shifted respiratory signal superimposed on MP and LFP traces. Time scale bar: 1s. **B** LFP RRo probability across structures. Grey points represent LFP RRo probability, blue squares represent the mean by structure and black line represent SEM. Only LFPs with RRo probability above 2.5% are considered. No significant difference is observed (Kruskal-Wallis test,  $p = 0.14$ ,  $H(3) = 5.38$ ,  $N_{mPFC} = 20$ ,  $N_{S1} = 3$ ,  $N_{V1} = 2$ ,  $N_{HPC} = 4$ ). **C** LFP RRo episode duration across structures. Grey points represent mean LFP RRo duration of individual traces, blue squares represent the mean by structure and black lines represent SEM. The same pool of traces as in B is used. Significant differences are observed (Kruskal-Wallis test,  $p = 0.01$ ,  $H(3) = 10.51$ ,  $N_{mPFC} = 17$ ,  $N_{S1} = 6$ ,  $N_{V1} = 2$ ,  $N_{HPC} = 8$ ). mPFC presents longer LFP RRo episodes than S1 (Mann-Whitney U test,  $p = 0.01$ ) and HPC (Mann-Whitney U test,  $p = 0.009$ ). **D.** Conditional probability of MP RRo given LFP dynamics. Columns “LFP RRo” represent the probability to observe MP RRo when LFP is also RRo. On the other hand, columns “other LFP” represent MP RRo probability when LFP is no RRo. Only cell recordings during which LFP presented both RRo and other oscillations were analyzed. In mPFC, MP RRo probability increases when LFP is RRo (Wilcoxon test,  $p = 0.02$ ,  $Z = 44$ ). **D.** Conditional probability of LFP RRo given MP dynamics. Columns “MP RRo” represent the probability to observe LFP RRo when MP is also RRo. On the other hand, columns “other MP” represent LFP RRo probability when MP is no RRo. Only cell presenting both MP RRo and other oscillations were analyzed. In mPFC, LFP RRo probability increases when MP is RRo (Wilcoxon test,  $p = 0.002$ ,  $Z = 27$ )

Then, we observed to what extent LFP and MP respiration-entrainment could be correlated. To do so, we calculated the percentage MP RRo cycles when the LFP displayed RRo or not (fig. 5D). It clearly emerged that, independently of the structure considered, the MP had a higher probability to display RRo when the LFP displayed RRo. For mPFC, the increased MP RRo probability when LFP switched from no RRo to RRo was significant (Wilcoxon test  $p = 0.02$ ,  $Z = 44$ ,  $N = 21$  cells). HPC exhibited the same tendency, and, to a lesser extent, S1 and V1 also. These results strongly suggest that LFP state could strongly influence MP. Reciprocally, we wondered if the probability that the LFP displayed RRo could be different when the MP displayed RRo or not (fig. 5E). Here we found that in mPFC, S1 and HPC, the LFP had a higher probability to display RRo when the MP displayed RRo, but this result was statistically significant only for mPFC (Wilcoxon test mPFC:  $p = 0.002$ ,  $Z = 27$ ,  $N = 21$  cells). This confirms that, most of the time, the respiratory modulation of a cell MP is coherent with the respiratory modulation of its network environment. Note that the absence of statistical significance in regions others than mPFC is probably due to the small sample size.

To summarize, we observed that the respiratory modulation of MP activity is largely influenced by that of LFP.

## DISCUSSION

While many studies have recently evidenced a respiration-related activity in LFPs of many brain regions (Biskamp et al. 2017; Girin et al. 2021; Ito et al. 2014; Kőszeghy et al. 2018; Liu et al. 2017; Tort et al. 2018; Yanovsky et al. 2014; Zhong et al. 2017), our study is the first to describe a respiratory-related oscillation in the MP activity in mPFC, S1, V1 and HPC. We defined a cell MP as respiratory modulated if at least 2.5% of its respiration-based cycles were respiration-locked. In such conditions, we showed for the first time a respiration-related oscillation of MP in a large proportion of cells (53.1% in mPFC, 60% in S1, 50% in V1, and 80% in HPC). Before us, very sparse and scarce data existed reporting MP oscillations coherent with LFP respiration-related oscillation ((Tort et al. 2018; Zhong et al. 2017): 1 cell recorded in parietal cortex; Yanovsky et al. 2014: 3 cells out of 7 recorded in dentate gyrus after brainstem stimulation). Our study goes much further by comparing the probability of MP respiration-related oscillations in four different brain regions and by detailing how such oscillation could be influenced by excitability state or network activity.

We first evidenced that the proportions of cells expressing MP respiration-related oscillations were disparate between brain regions. In fact, 20% of recorded cells in S1 and mPFC showed about 20% of their MP cycles modulated by respiration, while more than 20% of HPC cells had about 75% of their cycles modulated, and no cell in V1 had more than 25% modulated cycles. The amplitude of MP RRo was larger in S1 than in other brain regions. Respiratory coupling between MP and spiking discharge was much more frequent in mPFC and S1 (100% and 80% respectively) than in HPC (25%). Interestingly, extracellularly recorded spiking activity in S1 has been previously described as rhythmically correlated with respiration (Ito et al., 2014). This stronger relation between respiration and S1 barrel cortex cells could have something to do with the fact that respiration binds different orofacial rhythms as whisking and sniffing particularly during olfactory search (Kleinfeld et al. 2014; Moore et al. 2013; Ranade et al. 2013).

We expected cells in mPFC to display more clearly respiration-related oscillations in their MP, given the strong modulation of LFP described in this region in the freely moving animal (Bagur et al. 2021; Dupin et al. 2019; Girin et al. 2021; Karalis et al. 2016). Indeed, neither the duration of MP respiration-modulated episodes nor the amplitude of MP RRo is more pronounced in mPFC than in the three other areas.

The fact that anesthetics have voltage-dependent effects on resting MP (MacIver and Kendig 1991) could lower MP sensitivity to respiration. However, even in the awake head-fixed mouse, Kőszeghy et al. 2018 reported that spiking discharges of neurons in mPFC are much less coupled to breathing than neurons in orbito-frontal cortex. This different probability of respiration-related oscillation between LFP and intracellular signals raises the question of a possible contamination of LFP signals by volume conduction coming from distant generators (Kajikawa and Schroeder 2011; Parabucki and Lampl 2017).

Oppositely, we showed a very clear respiration-related activity in MP of HPC cells (80% of cells expressed RRo and 20% of them displayed at least 75% of modulated cycles). This probably reflects the strong relation between olfactory and limbic structures. Very recently, Zhou et al. (2021) reported that human hippocampal connectivity is stronger with olfactory cortex than other sensory cortices and that olfactory-hippocampal connectivity oscillates with nasal breathing. Interestingly, several recordings of HPC neurons exhibiting MP RRo revealed that, when emitted in bursts, action potentials were locked to the I/E transition point of respiratory cycle while single action potentials were more loosely distributed over the respiratory cycle (data not shown). It is commonly admitted that bursts could facilitate synaptic transmission (Miles 1990) and induce synaptic plasticity, LTP or LTD, depending on the theta oscillatory cycle phase of the burst (Huerta and Lisman 1995). The fact that the MP of HPC cells could be paced by breathing could thus influence place cells coding notably during sniffing where respiratory and theta rhythms are in the same frequency range (Girin et al. 2021; Tort et al. 2018).

Although the small sample size of recorded cells in V1, 50% of them showed episodes of RRo MP. In these cells, the percentage of RRo MP did not exceed more than about 25% of total cycles. This confirms the observation that LFP in posterior areas are less susceptible to respiratory drive (Girin et al. 2021; Tort et al. 2018). It is nevertheless interesting to observe that, even in a region as posterior as V1 and so probably connected to the olfactory input, respiration can affect subthreshold activity.

We previously showed that the MP of mitral/tufted cells, the principal neurons of the olfactory bulb, is strongly respiration-modulated (Briffaud et al. 2012). We cannot compare the percentages of modulated cells between the non-olfactory structures recorded here and olfactory bulb neurons because we did not use the same experimental paradigm, neither the same detection method nor data processing. However, it can be noted that hyperpolarization of mPFC and S1 cells appears to reduce the number of cells exhibiting RRo MP. On the contrary, in the olfactory bulb, hyperpolarization induced an increase in the proportion of respiratory modulated cells, which could suggest a reversal potential of RRo MP more hyperpolarized in non-olfactory structures than in olfactory bulb. It would be necessary to undertake a fine characterization of the different types of RRo that may exist (as in mitral/tufted cells) in order to be able to formulate hypotheses. However, we could postulate that a greater inhibition would be implicated in the oscillatory dynamics of these non-olfactory cells. Indeed, it has been shown that inhibitory interneurons appear to be more respiratory modulated than pyramidal neurons (Biskamp et al. 2017: mPFC; Karalis and Sirota 2018: mPFC and CA1 but not dentate gyrus). It would be of great interest to test the possibility that the consequence of a hyperpolarization results in rather an increase or a decrease of the respiratory modulation would come from the fact that the respiratory influence could rather impinge on inhibitory interneurons (as it could be in mPFC) or on a balanced excitatory-inhibitory network (as in OB). We previously showed the importance of excitation in respiratory modulation of spiking discharges and MP in the OB that mostly occurred through peripheral afferents on in

mitral/tufted cells (Briffaud et al. 2012). This is confirmed by results of a preliminary experiment in mPFC showing that the amplitude of MP RRo decreases when the naris of the animal is blocked (data not shown).

We have been able to evidence RRo MP thanks to our detection method (see material and methods) which allowed us to detect even transient oscillations. Indeed, it is one of our major results that MP RRo episodes were temporary, often not exceeding five respiratory cycles in duration whatever the brain region, whereas the LFP RRo episodes were variable between regions, with duration up to 10 cycles in mPFC and between 3 and 6 cycles for other structures. This longer RR-LFP episode duration in mPFC could be due to its anatomic connections with olfactory bulb which put the mPFC much more often under the influence of olfactory pathway. Then, the respiratory rhythm may take over more often than other rhythms. Alternating populations of cells could transiently express respiratory modulation in their MP resulting in a longer duration of LFP respiratory modulation. In other structures, the competition between several other LFP rhythms (such as slow rhythm or theta) probably does not favor the emergence of this rhythm. Additionally, for all the structures, the sensitivity of each individual cell MP to LFP respiratory modulation likely differs according to its excitability state, limiting episodes of MP RRo to short durations. This could be supported by our observation that cells could show less RRo MP when hyperpolarized (see Fig.4B).

Although our study focused on the respiratory rhythm, the influence of other LFP rhythms on cellular activity (MP and discharge) should not be ignored. For examples, in few cases, we observed a spiking discharge that was RR while MP displayed no RRo. We could suppose that if the spiking discharge is influenced by a rhythm twice slower or twice faster than the respiratory rhythm, they will appear locked on respiratory cycle on spike histograms. We also observed more complicated patterns with several rhythms nested. For example, on the LFP spectrum analysis of Fig 1B3.3 we can distinguish a slow oscillation (around 1 Hz) which could compete with the respiratory rhythm.

Overall, our results evidenced a consequent proportion of RRo within electrophysiological signals, which could only have been revealed thanks to respiration co-recording. We evidenced a strong respiratory coupling between MP and spike discharge in PFC, S1 and V1 (and to a lesser extent in HPC). Furthermore, MP and LFP RRo dynamics showed strong covariations. Even if our experiments in anesthetized animal are purely descriptive, our results show that, at very different places in the brain, the MP of neurons can be depolarized and hyperpolarized according to the respiratory rhythm. These findings contribute to bring evidence that respiratory rhythm could be used as a common clock to set the dynamics of large-scale networks on a same slow rhythm.

#### AUTHOR CONTRIBUTIONS

C.A. and N.B. conceived and designed research; M.J. and M.Z. performed experiments; M.J., N.F.-T., and S.G. analyzed data; M.J., N.F.-T., N.B. and C.A. interpreted results of experiment; M.J. and C.A. prepared figures. M.J., N.B. and C.A. drafted manuscript; M.J., M.Z., N.F.-T., N.B. and C.A. edited and revised manuscript; M.J., M.Z., N.F.-T., S.G., N.B. and C.A. approved final version of manuscript.

#### REFERENCES

**Ackels T, Jordan R, Schaefer AT, Fukunaga I.** Respiration-locking of olfactory receptor and projection neurons in the mouse olfactory bulb and its modulation by brain state. *Front Cell Neurosci* 14: 220, 2020.

**Arshamian A, Iravani B, Majid A, Lundström JN.** Respiration modulates olfactory memory consolidation in humans. *J Neurosci* 38: 10286–10294, 2018.

**Bagur S, Lefort JM, Lacroix MM, de Lavilléon G, Herry C, Chouvaeff M, Billand C, Geoffroy H, Benchenane K.** Breathing-driven prefrontal oscillations regulate maintenance of conditioned-fear evoked freezing independently of initiation. *Nat Commun* 12: 1–15, 2021.

**Biskamp J, Bartos M, Sauer J-F.** Organization of prefrontal network activity by respiration-related oscillations. *Sci Rep* 7: 1–11, 2017.

**Briffaud V, Fourcaud-Trocmé N, Messaoudi B, Buonviso N, Amat C.** The relationship between respiration-related membrane potential slow oscillations and discharge patterns in mitral/tufted cells: what are the rules? *PLoS One* 7: e43964, 2012.

**Buonviso N, Amat C, Litaudon P.** Respiratory modulation of olfactory neurons in the rodent brain. *Chem Senses* 31: 145–154, 2006.

**Buonviso N, Amat C, Litaudon P, Roux S, Royet J-P, Farget V, Sicard G.** Rhythm sequence through the olfactory bulb layers during the time window of a respiratory cycle. *Eur J Neurosci* 17: 1811–1819, 2003.

**Cao Y, Roy S, Sachdev RN, Heck DH.** Dynamic correlation between whisking and breathing rhythms in mice. *J Neurosci* 32: 1653–1659, 2012.

**Carlson KS, Dillione MR, Wesson DW.** Odor-and state-dependent olfactory tubercle local field potential dynamics in awake rats. *J Neurophysiol* 111: 2109–2123, 2014.

**Cenier T, David F, Litaudon P, Garcia S, Amat C, Buonviso N.** Respiration-gated formation of gamma and beta neural assemblies in the mammalian olfactory bulb. *Eur J Neurosci* 29: 921–930, 2009.

**Courtioi E, Amat C, Thevenet M, Messaoudi B, Garcia S, Buonviso N.** Reshaping of bulbar odor response by nasal flow rate in the rat. *PLoS One* 6: e16445, 2011a.

**Courtioi E, Buonviso N, Litaudon P.** Odorant features differentially modulate beta/gamma oscillatory patterns in anterior versus posterior piriform cortex. *Neuroscience* 409: 26–34, 2019.

**Courtioi E, Hegoburu C, Litaudon P, Garcia S, Fourcaud-Trocmé N, Buonviso N.** Individual and synergistic effects of sniffing frequency and flow rate on olfactory bulb activity. *J Neurophysiol* 106: 2813–2824, 2011b.

**Cury KM, Uchida N.** Robust odor coding via inhalation-coupled transient activity in the mammalian olfactory bulb. *Neuron* 68: 570–585, 2010.

**David FO, Hugues E, Cenier T, Fourcaud-Trocmé N, Buonviso N.** Specific entrainment of mitral cells during gamma oscillation in the rat olfactory bulb. *PLoS Comput Biol* 5: e1000551, 2009.

**Dupin M, Garcia S, Boulanger-Bertolus J, Buonviso N, Mouly A-M.** New insights from 22-kHz ultrasonic vocalizations to characterize fear responses: relationship with respiration and brain oscillatory dynamics. *Eneuro* 6, 2019.

- Esclassan F, Courtiol E, Thévenet M, Garcia S, Buonviso N, Litaudon P.** Faster, deeper, better: the impact of sniffing modulation on bulbar olfactory processing. *PLoS One* 7: e40927, 2012.
- Fourcaud-Trocmé N, Briffaud V, Thévenet M, Buonviso N, Amat C.** In vivo beta and gamma subthreshold oscillations in rat mitral cells: origin and gating by respiratory dynamics. *J Neurophysiol* 119: 274–289, 2018.
- Grin B, Juventin M, Garcia S, Lefèvre L, Amat C, Fourcaud-Trocmé N, Buonviso N.** The deep and slow breathing characterizing rest favors brain respiratory-drive. *Sci Rep* 11: 1–15, 2021.
- Grosmaître X, Santarelli LC, Tan J, Luo M, Ma M.** Dual functions of mammalian olfactory sensory neurons as odor detectors and mechanical sensors. *Nat Neurosci* 10: 348–354, 2007.
- Gschwend O, Beroud J, Carleton A.** Encoding odorant identity by spiking packets of rate-invariant neurons in awake mice. *PLoS One* 7: e30155, 2012.
- Heck DH, Kozma R, Kay LM.** The rhythm of memory: how breathing shapes memory function. *J Neurophysiol* 122: 563–571, 2019.
- Heck DH, McAfee SS, Liu Y, Babajani-Feremi A, Rezaie R, Freeman WJ, Wheless JW, Papanicolaou AC, Ruszinkó M, Sokolov Y.** Breathing as a fundamental rhythm of brain function. *Front Neural Circuits* 10: 115, 2017.
- Herrero JL, Khuvis S, Yeagle E, Cerf M, Mehta AD.** Breathing above the brain stem: volitional control and attentional modulation in humans. *J Neurophysiol* , 2018.
- Huerta PT, Lisman JE.** Bidirectional synaptic plasticity induced by a single burst during cholinergic theta oscillation in CA1 in vitro. *Neuron* 15: 1053–1063, 1995.
- Ito J, Roy S, Liu Y, Cao Y, Fletcher M, Lu L, Boughter JD, Grün S, Heck DH.** Whisker barrel cortex delta oscillations and gamma power in the awake mouse are linked to respiration. *Nat Commun* 5: 3572, 2014.
- Iwabe T, Ozaki I, Hashizume A.** The respiratory cycle modulates brain potentials, sympathetic activity, and subjective pain sensation induced by noxious stimulation. *Neurosci Res* 84: 47–59, 2014.
- Jung F, Yanovsky Y, Brankač J, Tort AB, Draguhn A.** Respiration competes with theta for modulating parietal cortex neurons. *BioRxiv* 707331, 2019.
- Kajikawa Y, Schroeder CE.** How local is the local field potential? *Neuron* 72: 847–858, 2011.
- Karalis N, Dejean C, Chaudun F, Khoder S, Rozeske RR, Wurtz H, Bagur S, Benchenane K, Sirota A, Courtin J.** 4-Hz oscillations synchronize prefrontal–amygdala circuits during fear behavior. *Nat Neurosci* 19: 605–612, 2016.
- Karalis N, Sirota A.** Breathing coordinates limbic network dynamics underlying memory consolidation. *Available SSRN 3283711* , 2018.
- Kleinfeld D, Moore JD, Wang F, Deschênes M.** The brainstem oscillator for whisking and the case for breathing as the master clock for orofacial motor actions. In: *Cold Spring Harbor symposia on quantitative biology*. Cold Spring Harbor Laboratory Press, 2014, p. 29–39.
- Köszeghy Á, Lasztóczy B, Forro T, Klausberger T.** Spike-timing of orbitofrontal neurons is synchronized with breathing. *Front Cell Neurosci* 12: 105, 2018.
- Kurnikova A, Moore JD, Liao S-M, Deschênes M, Kleinfeld D.** Coordination of orofacial motor actions into exploratory behavior by rat. *Curr Biol* 27: 688–696, 2017.
- Li S, Laskin JJ.** Influences of ventilation on maximal isometric force of the finger flexors. *Muscle Nerve* 34: 651–655, 2006.
- Li S, Park W-H, Borg A.** Phase-dependent respiratory-motor interactions in reaction time tasks during rhythmic voluntary breathing. *Motor Control* 16: 493–505, 2012.
- Litaudon P, Amat C, Bertrand B, Vigouroux M, Buonviso N.** Piriform cortex functional heterogeneity revealed by cellular responses to odours. *Eur J Neurosci* 17: 2457–2461, 2003.
- Litaudon P, Garcia S, Buonviso N.** Strong coupling between pyramidal cell activity and network oscillations in the olfactory cortex. *Neuroscience* 156: 781–787, 2008.
- Liu Y, McAfee SS, Heck DH.** Hippocampal sharp-wave ripples in awake mice are entrained by respiration. *Sci Rep* 7: 1–9, 2017.
- Lockmann AL, Laplagne DA, Leão RN, Tort AB.** A respiration-coupled rhythm in the rat hippocampus independent of theta and slow oscillations. *J Neurosci* 36: 5338–5352, 2016.
- Lu L, Cao Y, Tokita K, Heck DH, Boughter Jr JD.** Medial cerebellar nuclear projections and activity patterns link cerebellar output to orofacial and respiratory behavior. *Front Neural Circuits* 7: 56, 2013.
- MacIver MB, Kendig JJ.** Anesthetic effects on resting membrane potential are voltage-dependent and agent-specific. *Anesthesiology* 74: 83–88, 1991.
- Maric V, Ramanathan D, Mishra J.** Respiratory regulation & interactions with neuro-cognitive circuitry. *Neurosci Biobehav Rev* 112: 95–106, 2020.
- Miles R.** Synaptic excitation of inhibitory cells by single CA3 hippocampal pyramidal cells of the guinea-pig in vitro. *J Physiol* 428: 61–77, 1990.
- Miura K, Mainen ZF, Uchida N.** Odor representations in olfactory cortex: distributed rate coding and decorrelated population activity. *Neuron* 74: 1087–1098, 2012.
- Moore JD, Deschênes M, Furuta T, Huber D, Smear MC, Demers M, Kleinfeld D.** Hierarchy of orofacial rhythms revealed through whisking and breathing. *Nature* 497: 205–210, 2013.
- Nakamura NH, Fukunaga M, Oku Y.** Respiratory modulation of cognitive performance during the retrieval process. *PLoS One* 13: e0204021, 2018.
- Oka Y, Takai Y, Touhara K.** Nasal airflow rate affects the sensitivity and pattern of glomerular odorant responses in the mouse olfactory bulb. *J Neurosci* 29: 12070–12078, 2009.

**Parabucki A, Lampl I.** Volume conduction coupling of whisker-evoked cortical LFP in the mouse olfactory bulb. *Cell Rep* 21: 919–925, 2017.

**Park H-D, Barnoud C, Trang H, Kannape OA, Schaller K, Blanke O.** Breathing is coupled with voluntary action and the cortical readiness potential. *Nat Commun* 11: 1–8, 2020.

**Perl O, Ravia A, Rubinson M, Eisen A, Soroka T, Mor N, Secundo L, Sobel N.** Human non-olfactory cognition phase-locked with inhalation. *Nat Hum Behav* 3: 501–512, 2019.

**Ranade S, Hangya B, Kepecs A.** Multiple Modes of Phase Locking between Sniffing and Whisking during Active Exploration. *J Neurosci* 33: 8250–8256, 2013.

**Roux SG, Garcia S, Bertrand B, Cenier T, Vigouroux M, Buonviso N, Litaudon P.** Respiratory cycle as time basis: An improved method for averaging olfactory neural events. *J Neurosci Methods* 152: 173–178, 2006.

**Tort ABL, Ponsel S, Jessberger J, Yanovsky Y, Brankačk J, Draguhn A.** Parallel detection of theta and respiration-coupled oscillations throughout the mouse brain. *Sci Rep* 8: 6432, 2018.

**Wasselius T, Wikgren J, Penttonen M, Nokia MS.** Breathe out and learn: expiration-contingent stimulus presentation facilitates associative learning in trace eyeblink conditioning. *Psychophysiology* 56: e13387, 2019.

**Welzl H, Bureš J.** Lick-synchronized breathing in rats. *Physiol Behav* 18: 751–753, 1977.

**Yanovsky Y, Ciatipis M, Draguhn A, Tort AB, Brankačk J.** Slow oscillations in the mouse hippocampus entrained by nasal respiration. *J Neurosci* 34: 5949–5964, 2014.

**Zaccaro A, Piarulli A, Laurino M, Garbella E, Menicucci D, Neri B, Gemignani A.** How breath-control can change your life: a systematic review on psycho-physiological correlates of slow breathing. *Front Hum Neurosci* 12: 353, 2018.

**Zelano C, Jiang H, Zhou G, Arora N, Schuele S, Rosenow J, Gottfried JA.** Nasal respiration entrains human limbic oscillations and modulates cognitive function. *J Neurosci* 36: 12448–12467, 2016.

**Zhong W, Ciatipis M, Wolfenstetter T, Jessberger J, Müller C, Ponsel S, Yanovsky Y, Brankačk J, Tort AB, Draguhn A.** Selective entrainment of gamma subbands by different slow network oscillations. *Proc Natl Acad Sci* 114: 4519–4524, 2017.

**Zhou G, Olofsson JK, Koubeissi MZ, Menelaou G, Rosenow J, Schuele SU, Xu P, Voss JL, Lane G, Zelano C.** Human hippocampal connectivity is stronger in olfaction than other sensory systems. *Prog Neurobiol* 201: 102027, 2021.

## 3.2. Role of the respiratory rhythm in supporting the long-range communication in the brain

### 3.2.1 Context

Our previous intracellular study revealed that subthreshold and spiking activity of neurons in non-olfactory regions can indeed be modulated by respiration even during anesthesia.

In a second step, it was necessary to ask whether this respiratory rhythm could serve a binding function for distant brain areas. In other words, could distant brain regions be simultaneously modulated by respiration? Indeed, even if several groups evidenced a respiratory drive in different cortical and sub-cortical regions, none of them reported if this modulation could be simultaneous in these different regions. My second study aimed at bridging this gap.

For this purpose, I took advantage of the data collected by another student of the team, Baptiste Girin, and for which I took an active part in their processing. Results were published and can be found in annexes (6.1 Co-author published article). Very briefly, in this study, LFP activity were recorded in seven areas, in freely moving rats. The brain regions targeted were olfactory bulb (OB), anterior piriform cortex (aPCX), medial prefrontal cortex (mPFC), CA1 and DG regions of hippocampus, primary barrel cortex (S1), and primary visual cortex (V1). Recordings were performed during four brain states: quiet waking (QW), exploration (EX), slow wave sleep (SWS) and rapid eyes movements sleep (REM). Animals were placed in a plethysmograph during recordings so that respiration was acquired in a non-invasive way. We showed that low frequency (<10 Hz) band of LFP could correlate with respiration during all four brain states and in all seven brain areas. Nonetheless, LFP coupling to respiration was exacerbated during QW. By having the animals breathe a 5% CO<sub>2</sub>-enriched air, we were able to modify their breathing patterns while maintaining the different brain states. This allowed us to conclude that respiration patterns (mainly inspiratory amplitude and duration) better explained LFP-respiration coupling than brain state itself. Finally, we concluded that the long and deep respiration regime, associated with QW state, favored coupling between respiration and the brain activity.

Going back to my original question, while all areas were analyzed independently in Girin et al.'s study, I developed for my second study a series of analysis to test to what extent the respiratory modulation observed in the different areas could occur simultaneously. I tackled if binding function of respiratory rhythm could be mediated by cross-areas synchronization of low and high frequencies LFP oscillations.

In a first step, I will track binding in LFP low frequency band. And, if such binding exists, I will verify if it also exists in high frequency bands, which would render long-range communication effective. These two points motivated the further analyses I performed on the dataset from Girin et al., 2021.

### 3.2.2. Methods

#### **Experimental procedures.**

The same dataset that Girin et al., 2021, was used. For procedures, please refer to Girin et al., 2021. For the following analysis, I used two pools of animals. For analyses treating areas independently (respiration-related oscillations (RRO) probabilities, cycle-frequency map) I used all available animals (N = 11 rats). Otherwise, when I studied connectivity between areas (respiration-bound network, RRO and gamma connectivity) I reduced the pool of animals so that all animals had the same implanted areas. This latter pool contained four rats and six areas (mPFC, aPCX, S1, V1, CA1, DG).

## Respiratory signal

Acquisition and processing is the same than the one used in Girin et al., 2021.

## State scoring

Four brain states were scored in Girin et al., 2021, namely quiet waking (QW), active exploration (EX), slow waves sleep (SWS) and REM sleep (REM). This previous scoring was re-used in the present study. These files associated a brain state score at every time point. However, since I proposed a cycle-by-cycle analysis, I attributed to each respiratory cycle a brain state score. To do so, for each respiratory cycle I reported the brain state in which the cycle was observed.

## Electrophysiological signals analysis

Data were analyzed with python custom-written scripts.

*Detection of Respiration-Related oscillations (RRo).* For each LFP signal, the RRo detection method returned a respiratory cycle-by-respiratory cycle scoring of RRo presence. The method was almost the same than the one developed for the intracellular study. The only difference relied on the deformation from time-based signal to respiratory phase-based signal. Contrarily to the anesthetized preparation, waveform of respiration varied in the awake animal, especially its symmetry. Therefore, during deformation no fixed inspiration ratio was imposed (inspiratory duration / cycle duration). For detail, please refer to page 3 (inserted page 58 of the manuscript) of the intracellular publication, section “time dynamics of respiration-related MP oscillations”.

*RRo probabilities.* RRo probabilities represented the proportion of respiratory cycles displaying RRo amongst a “selection” of respiratory cycles. Selection of respiratory cycles depended on the question. I could easily select respiratory cycles according to a brain state or to specific inspiration duration or amplitude values, since RRo scorings of each brain area, brain state scoring, and inspiration amplitude and duration were all by-cycle vectors (see Table 1). Probabilities were averaged across animals (number of animals depended on the area of interest).

Respiratory cycle	C <sub>1</sub>	C <sub>2</sub>	...	C <sub>N-1</sub>	C <sub>N</sub>
Area <sub>1</sub> RRo	0	1	...	0	0
...	..	..	...	...	...
Area <sub>z</sub> RRo	1	1	...	1	0
Brain state	QW	QW	...	SWS	SWS
Inspiration duration (s)	0.15	0.16	...	0.2	0.29
Inspiration amplitude (mL.s <sup>-1</sup> )	27	26	...	24	15

Table 1 : Illustration of data organization for computing RRo probabilities. RRo scoring ( $Z$  represented the number of implanted areas for this fictive animal); all parameters (brain state scoring and respiration parameters) of an animal were described for each respiratory cycle ( $N$  represented the number respiratory cycles for this fictive animal). Blue cells highlight the selection of respiratory cycles occurring during QW. For presented data, Area<sub>1</sub> displayed a RRo probability of 50% (1/2), while Area<sub>z</sub> displayed a RRo probability of 100% (2/2). Green cells represented the selection of respiratory cycles with inspiration duration between 0.15 and 0.20 s, and inspiration amplitude between 20 and 30 mL.s<sup>-1</sup>. For presented data, Area<sub>1</sub> displayed a RRo probability of 33% (1/3), while Area<sub>z</sub> displayed a RRo probability of 100% (3/3).

*Respiration-related network (RR network) size probabilities.* Size of RR network corresponded to the number of areas displaying simultaneously RRo in their LFP. The size of the RR network was computed as the sum of all RRo scoring (see Table 2). With this encoding, I proceeded like in the paragraph *RRo probabilities* to compute RR network size probabilities. Probabilities were averaged across animals ( $N = 4$  animals).

Respiratory cycle	C <sub>1</sub>	C <sub>2</sub>	...	C <sub>N-1</sub>	C <sub>N</sub>
aPCX RRo	0	1	...	1	0
mPFC RRo	0	1	...	1	0
DG RRo	1	1	...	1	0
CA1 RRo	1	1	...	0	0
S1 RRo	0	1	...	0	0
V1 RRo	1	1	...	0	0
RR network size	3	6	...	3	0
Brain state	QW	QW	...	SWS	SWS
Inspiration duration (s)	0.15	0.16	...	0.2	0.29
Inspiration amplitude (mL.s <sup>-1</sup> )	27	26	...	24	15

Table 2 : Illustration of data organization for computing RR network size probabilities. Fictive RRo scorings of the six areas (in grey) were used to compute the size of RR network across respiratory cycles (in black) for one fictive animal. For presented data (four cycles), probability of a RR network size of 3 areas was 50% (2/4), and probability of a RR network size of 6 areas was 25% (1/4). Selection of cycles was processed like in RRo probabilities paragraph.

*Phase-frequency map.* For LFP of each area, I computed a wavelet-based time-frequency signal in high frequency range (12-140 Hz with a 2 Hz frequency step). Signal was rescaled from time to respiratory phase as described in (Roux et al., 2006). Then, I selected respiratory cycles that displayed RRo. A second selection sorted these respiratory cycles according to their brain state. For each brain state, phase-frequency signal was averaged across respiratory cycles resulting in a mean phase-frequency map (similar aspect than maps presented *Figure 23*). Each line (*i.e.*, each frequency bin) of the mean map was divided by mean power of the line. This normalization allowed to visually highlight which high frequencies bands were modulated by respiratory phase. Finally, these maps were averaged across animals and presented *Figure 23*.

*RRo connectivity.* Respiration-related connectivity between areas in low frequency LFP was estimated with RRo synchronization. For each pair of areas, RRo connectivity was computed as the probability of simultaneous RRo in both involved areas. Probabilities were averaged by animals. Width of bounds in *Figure 24A* correlated with mean probability.

*Gamma2 connectivity.* Respiration-related connectivity between areas in high frequency LFP was estimated for the Gamma2 band (60-90 Hz). More precisely, during RRo episodes, I measured if Gamma2 oscillations of two areas displayed stable phase difference as proposed in Varela et al., 2001. For each area of a pair, LFP was band-pass filtered (55-100 Hz), and phase was extracted with a Hilbert transform. Phase difference was obtained by subtraction of Gamma2 phases from each area. Phase difference (time series) was rescaled from time to respiratory phase (respiratory phase series). Then, I selected respiratory cycles that displayed simultaneously RRo in both areas (see *RRo connectivity*). A second selection sorted these respiratory cycles according to the associated brain state. For each brain state, I vertically stacked phase difference signal by respiratory cycles, and I computed length of mean vector for each respiratory phase (see *Table 3*). If length of mean vector tended toward 1, it meant phase difference was stable. Otherwise, if length of mean vector tended toward 0, phase difference was variable. Therefore, length of mean vector measured the stability of Gamma2 phase difference throughout respiratory phase (see *Table 3* and inset in *Figure 24*). However, rather than absolute values of stability, I was truly interested in a modulation of stability signal by respiratory phase (inset in *Figure 24*). To test significance of such respiratory modulation I proceeded in two steps. First, I computed the mean vector of stability signal and I kept its length. Secondly, I repeated the algorithm described above with 200 surrogates (phase difference signal was randomly phase-shifted at each respiratory cycle). If length of true mean vector was strictly superior to 95<sup>th</sup> percentile of surrogated lengths, the stability signal was considered modulated in the Gamma2 range. I named “Gamma2 modulation

index” the length of the mean vector. Gamma2 modulation index was kept and averaged across animals. Width of bounds in *Figure 24B* correlated with mean length.

$C_1$	..	..	..	..	..
$C_2$	..	..	..	..	..
...	..	..	..	..	..
$C_{Y-1}$	..	..	..	..	..
$C_Y$	..	..	..	..	..
Respiratory phase	0 ( $\varphi_1$ )	0.0025 ( $\varphi_2$ )	...	0.9975 ( $\varphi_{399}$ )	1 ( $\varphi_{400}$ )
Length of mean vector	$L\varphi_1$	$L\varphi_1$	...	$L\varphi_{399}$	$L\varphi_{400}$

*Table 3 : Illustration of data organization for computing Gamma2 synchronization in one pair of area in one brain state. In grey, fictive data of phase difference were vertically stacked, respiratory cycle-by-respiratory cycle. For this fictive pair of areas, Y respiratory cycles presented simultaneously RRo during the brain state of interest. Data were aligned on respiratory phase, which we defined with 400 points (first dark line). For each respiratory phase (each column), mean vector was computed from the Y respiratory cycles, and its lengths (L) was extracted (second dark line).*

#### Statistics.

Kruskal-Wallis and Mann-Whitney U tests were performed with Scipy python package (Scipy version: 1.5.4, functions: `scipy.stats.mannwhitneyu`, `scipy.stats.kruskal`). Averaging are presented under the form  $\text{mean} \pm \text{sem}$ . If not, it will be explicitly mentioned.

### 3.2.3. Results

Results of Girin et al., 2021 piqued my curiosity, I couldn't stop asking myself: did brain areas coupled to respiration simultaneously, as if respiratory rhythm was common reference point? However, with the analyses performed in Girin et al., 2021 it was tricky to tackle the simultaneity of respiratory modulation. Therefore, I decided to perform parallel and complementary analyses. To detect LFP-respiration coupling I used the detection method developed for my intracellular study, rather than a spectral-based detection as used in Girin et al., 2021. Indeed, when I was developing my detection methods, I tried spectral-based detection. However, I did not keep this means of detection because raw signal inspection indicated this method overestimated RRo. On the contrary, the intracellular methods tended to underestimate RRo. In a first approach of freely moving dataset, I preferred to use a method which underestimate respiratory modulation to limit false detection.

#### *The RRo detection method developed for intracellular recordings in anesthetized preparation transposed to LFP signals in freely moving animals: comforting results*

To track such RRo cross-areas synchronization I transposed the RRo detection method developed for my intracellular study. This detection was applied independently to each recorded area, as a result RRo scorings of all areas were commonly aligned to respiratory cycles (see *Table 1*). Therefore, for each respiratory cycle it was easy to identify the areas simultaneously synchronized to respiration. But before acceding to respiration-related (RR) network dynamics, I wanted to ensure my RRo detection method gave similar results than those Girin's publication (Girin et al., 2021). *Figure 19* presents RRo probabilities throughout brain areas and brain states. RRo probabilities of all areas display a state-dependence (Kruskal Wallis test; OB:  $p=4 \cdot 10^{-4}$ ,  $H(5)=18.3$ , aPCX:  $p=8 \cdot 10^{-7}$ ,  $H(10)=31.2$ , mPFC:  $p=8 \cdot 10^{-4}$ ,  $H(4)=16.8$ , CA1:  $p=8.8 \cdot 10^{-8}$ ,  $H(10)=35.7$ , DG:  $p=7.2 \cdot 10^{-6}$ ,  $H(10)=26.9$ , S1:  $p=3.2 \cdot 10^{-6}$ ,  $H(8)=28.3$ , V1:  $p=2.9 \cdot 10^{-6}$ ,  $H(8)=28.5$ ). Looking more into details indicates RRo probabilities are higher during QW than during SWS and REM for all areas, (*post hoc* Mann-Whitney U test, see *Table 4*). The same observation can be made for EX. Thus, all structures present higher RRo probabilities during wakefulness than during sleep. Noteworthy, RRo are more frequent during QW than during EX only in aPCX and mPFC. So, for these two areas RRo probabilities decrease from QW, to EX, to SWS and finally to

REM. The five other areas (OB, CA1, DG, S1, V1) present equivalent RRo probabilities between QW and EX. Consistently with Girin's covariation matrices and coherence analyses, RRo are observed in all areas and during all brain states. However, RRo are particularly present during QW in all areas. Consequently, my RRo detection method gives results very similar to Girin's et al hence I will use it to track the dynamic of the RR network.

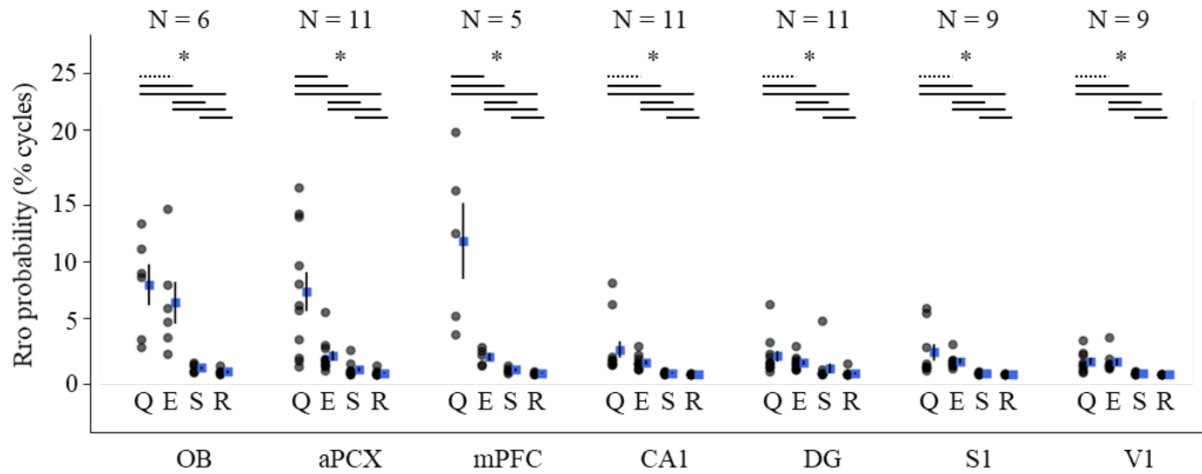


Figure 19: RRo occurrence in all areas presents state-dependent probabilities. RRo probability represents the number of respiratory cycles displaying RRo in one area for a given brain state divided by the number of respiratory cycles associated to the brain state. Grey dots correspond to RRo probability of one animal in one area and one state. Blue squares and vertical black lines represent animals' average, respectively sem, for one area in one state. Horizontal black lines represent significant ( $p \leq 0.05$ ) difference between two states with post-hoc Mann-Whitney U test. Dashed horizontal black lines highlight the few non-significant differences.

		EX	SWS	REM
OB	QW	0.288	<b>2x10<sup>-3</sup></b>	<b>2x10<sup>-3</sup></b>
	EX		<b>2x10<sup>-3</sup></b>	<b>2x10<sup>-3</sup></b>
	SWS			<b>0.033</b>
aPCX	QW	<b>3x10<sup>-3</sup></b>	<b>21x10<sup>-4</sup></b>	<b>5x10<sup>-5</sup></b>
	EX		<b>8x10<sup>-4</sup></b>	<b>6x10<sup>-5</sup></b>
	SWS			<b>0.024</b>
mPFC	QW	<b>6x10<sup>-3</sup></b>	<b>6x10<sup>-3</sup></b>	<b>6x10<sup>-3</sup></b>
	EX		<b>0.011</b>	<b>6x10<sup>-3</sup></b>
	SWS			<b>0.030</b>
CA1	QW	0.095	<b>4x10<sup>-5</sup></b>	<b>4x10<sup>-5</sup></b>
	EX		<b>4x10<sup>-5</sup></b>	<b>4x10<sup>-5</sup></b>
	SWS			<b>4x10<sup>-4</sup></b>
DG	QW	0.256	<b>6x10<sup>-4</sup></b>	<b>1x10<sup>-4</sup></b>
	EX		<b>6x10<sup>-4</sup></b>	<b>1x10<sup>-4</sup></b>
	SWS			<b>6x10<sup>-3</sup></b>
S1	QW	0.330	<b>2x10<sup>-4</sup></b>	<b>2x10<sup>-4</sup></b>
	EX		<b>2x10<sup>-4</sup></b>	<b>2x10<sup>-4</sup></b>
	SWS			<b>3x10<sup>-3</sup></b>
V1	QW	0.396	<b>3x10<sup>-4</sup></b>	<b>2x10<sup>-4</sup></b>
	EX		<b>2x10<sup>-4</sup></b>	<b>2x10<sup>-4</sup></b>
	SWS			<b>7x10<sup>-3</sup></b>

Table 4 : Values of Mann-Whitney U test from Figure 19. Significant p-value are highlighted in bold.

*Simultaneous respiration-related oscillations mainly occur during quiet waking state.*

Now, I focused the analysis on the simultaneous occurrence of RRo throughout brain areas. Since recording sites of some animals were missing, I selected only animals with identical recording sites to avoid bias in this analysis. From the eleven available rats, I kept only four of them. Yet, I kept six areas, only the OB was missing for these animals. I named RR network the ensemble of brain areas simultaneously exhibiting RRo. So, the extension of the RR network could range from 1 to 6 areas for these animals.

I first studied the probability that RRo occur simultaneously in a 1-6 areas network throughout brain states (Figure 20). All animals presented a RR network of at least 3 areas. Larger networks were consistently, *i.e.*, in all animals, observed only during QW and EX. RR networks of 4 areas were observed in three animals during SWS and in two animals during REM. Above, it dropped to two animals during SWS and one animal in REM. Consequently, large RR network seems more consistently observed in wakefulness than during sleep.

RR networks of 1, 3, 4 and 5 areas showed a state-dependence (Kruskal Wallis test; 1 area:  $p=0.02$ ,  $H(3)=9.4$ , 2 areas:  $p=0.06$ ,  $H(3)=7.3$ , 3 areas:  $p=0.05$ ,  $H(3)=12.7$ , 4 areas:  $p=0.02$ ,  $H(3)=10.1$ , 5 areas:  $p=0.05$ ,  $H(3)=8.0$ , 6 areas:  $p=0.3$ ,  $H(3)=4.1$ ). Results were particularly interesting for networks larger than 3 areas. Indeed, probability of occurrence of a >3 areas RR network during EX, SWS and REM were close to zero contrarily to QW (3 areas:  $4.0\pm 1.1\%$ , 4 areas:  $2.2\pm 0.9\%$ , 5 areas:  $1.2\pm 0.6\%$ , 6 areas:  $0.3\pm 0.2\%$ ). Furthermore, probabilities of 3, 4 and 5 areas RR network were often significantly higher during QW than during the other brain states (see Table 5 and Figure 20). These results show that respiratory rhythm can effectively bind large network through RRo synchronization. However, these large RR networks preferentially emerge during QW.

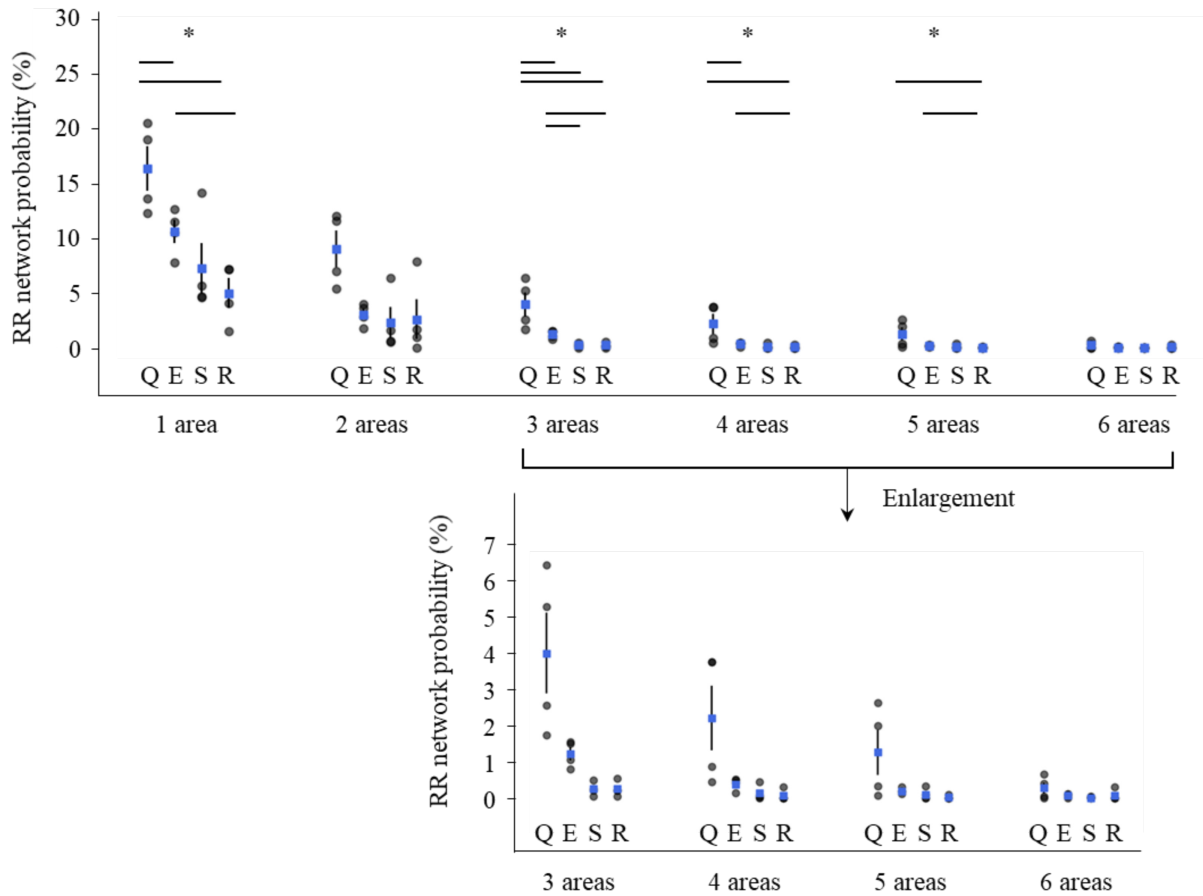


Figure 20 : RR network presents state-dependent probabilities. RR network probability represents the number of respiratory cycles displaying RRo in  $N$  areas ( $1 \leq N \leq 6$ ) for a given brain state divided by the number of respiratory cycles associated to the brain state. Since RRo probabilities decrease when network size increases, an enlargement is proposed for the large network ( $N \geq 3$  areas). Grey dots correspond to probability of RR network of size  $N$  for one animal in one state. Blue squares, respectively vertical black lines, represent animals' average, respectively sem, for one area in one state. Horizontal black lines represent significant ( $p \leq 0.05$ ) difference between two states with post-hoc Mann-Whitney U test.

		EX	SWS	REM
<b>RR network of 1 area</b>	QW	<b>0.030</b>	0.056	<b>0.015</b>
	EX		0.156	<b>0.015</b>
	SWS			0.333
<b>RR network of 2 areas</b>	QW			
	EX			
	SWS			
<b>RR network 3 areas</b>	QW	<b>0.015</b>	<b>0.015</b>	<b>0.015</b>
	EX		<b>0.015</b>	<b>0.015</b>
	SWS			0.443
<b>RR network 4 areas</b>	QW	0.056	<b>0.030</b>	<b>0.015</b>
	EX		0.056	<b>0.030</b>
	SWS			0.230
<b>RR network of 5 areas</b>	QW	0.156	0.055	<b>0.030</b>
	EX		0.155	<b>0.013</b>
	SWS			0.310
<b>RR network of 6 areas</b>	QW			
	EX			
	SWS			

Table 5 : Values of Mann-Whitney U test from Figure 20. When Kruskal-Wallis test was not significant ( $p > 0.05$ ), Mann-Whitney test was not computed. Significant p-value are highlighted in bold.

Intermediate inspiration durations and amplitudes favor occurrence of simultaneous respiration-related oscillations.

As mentioned earlier, a key point of this dataset is the precision in amplitude and in time of the respiratory signal we collected. In Girin's study, it allowed to unravel a particular respiratory regime, consisting in intermediate inspiration duration (0.1-0.2 s) and amplitude (20-30 mL.s<sup>-1</sup>), which maximizes LFP-respiration coupling in all areas (Girin et al., 2021). In the same optic, I wanted to tackle whether large network formation strictly depends on brain state or if it rather depended on particular respiratory parameters. To answer, I investigated RR network size as a function of respiratory regimen. I explored respiratory regimen by varying simultaneously inspiration amplitudes and durations, in other words I navigated along X and Y axis of 2D map of probabilities presented Figure 21.

Figure 21 depicts a 2D map of probabilities for each RR network size, which probabilities are color-coded from blue (low values) to yellow (high values). Maps are overlaid with four colored contour curves representing the median distribution of respiratory cycles associated to each brain state (QW: black, EX: magenta, SWS: red, REM: orange). To be noted, I chose to study the RR network size as a function of the inspiration duration - inspiration amplitude pair because 1) this pair allows the best segregation of the four brain states, and 2) this pair is the optimal pair to investigate LFP-respiration coupling (Girin et al., 2021). Figure 3 reveals that the probability map for a 1 area-size RR network displayed a broad distribution, which spreads over respiratory regimen of all four brain states. Nonetheless, one could observe a slight attraction of higher probabilities around an inspiration duration of about 0.2 s and an inspiration amplitude about of 10 mL.s<sup>-1</sup>. Visual investigation of the other maps revealed with great interest, that the larger the RR network size, the higher probabilities concentrated in a zone of the map corresponding to QW state.

I named “concentration of probabilities” the sum of probabilities within a contour area over the sum of all probabilities. This concentration has been quantified for each state and each network sizes and is represented in (*Figure 22*). This representation shows that the larger the RR network size, the stronger QW-associated respiratory regime attract probabilities. While concentration of probabilities tended to increase with RR network size in QW, it maintained a stable low level during SWS and dropped during EX and REM. In addition to the quantification, one should qualitatively have a look on probability maps of large network ( $\geq 3$  areas). Although high probabilities concentrated mainly in QW area, *Figure 21* showed this concentration is not uniform. Indeed, distribution of probabilities draws an optimum, centered at intermediate inspiration duration (0.2 s) and amplitude (10 mL.s<sup>-1</sup>). This suggests that, amongst the respiratory patterns adopted during QW, only those with intermediate inspiration duration and amplitude maximized probabilities to entrain a large network. To be noted, a part of SWS-associated regime (0.15 s < inspiration duration < 0.25s, and 15 mL.s<sup>-1</sup> < inspiration amplitude < 20 mL.s<sup>-1</sup>) overlapped with the optimum. Consequently, some SWS respiratory patterns enabled large RR networks, which explained why SWS maintained a stable concentration of probabilities in *Figure 22*. This showed that respiratory patterns optimizing large RR networks were not exclusive to QW. Hence, this suggests that respiratory parameters prevail on brain states. All together, these results show that an intermediate inspiration duration (0.15-0.25s) and amplitude (15-30 mL.s<sup>-1</sup>), a pattern often developed during QW, favors the formation of large RR networks.

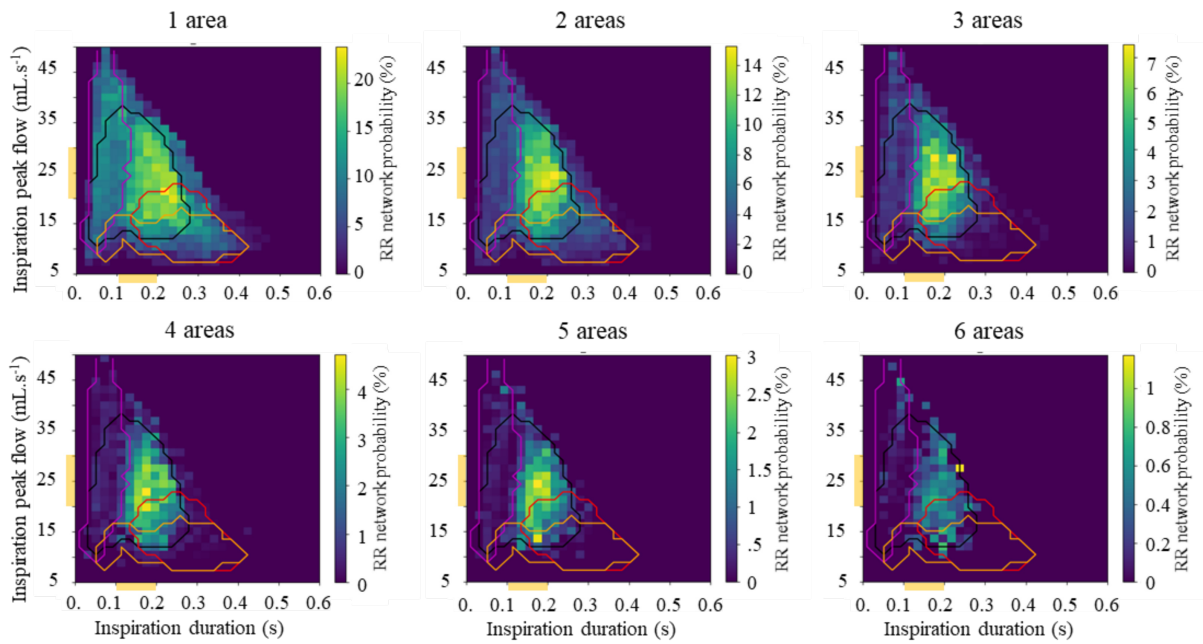


Figure 21 : Large RR networks were favored by respiratory pattern characteristic of quiet waking. RR network probability represents the number of respiratory cycles  $RR_0$  in  $N$  areas ( $N$  ranged from one area to six areas included) for a given bin of inspiration duration and amplitude divided by the number of respiratory cycles in the bin. Each map corresponds to the average from the four animals. Probability are color-coded, and please, note that each map has its own scale. Black, magenta, red and orange curves represent the median distribution of respiratory cycles associated to respectively quiet waking, exploration, SWS and REM sleep. Yellow rectangles on X and Y axis highlight the optimal respiratory parameters range observed in (Girin et al., 2021)

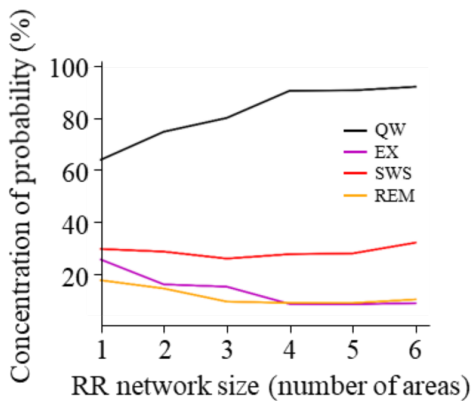


Figure 22 : Quantification of Figure 21. For each brain state, concentration of RR network probability was quantified by computing the sum of the RR network probabilities within contour divided by the sum of all RR network probabilities.

*During QW, cross-area RRo binding enables a Gamma2 synchronization.*

Respiratory rhythm can indeed bind distant brain areas through low frequency LFP oscillations. However, an efficient long-range communication rhythm should be able to synchronize local activities (i.e., high frequency LFP oscillations) in distant areas (1.1.3.4 Long-range communication). In this view, I aimed to identify high frequency oscillations, which can be modulated by respiration. More precisely, I look for phase amplitude coupling in LFP signals, namely the modulation of high frequency envelopes by the respiration's phase. According to literature (A. B. L. Tort et al., 2018; Zhong et al., 2017), I expected such phase-amplitude coupling in 80-120 Hz (called Gamma2 in Zhong et al., 2017). For each brain area and during each brain state, I selected respiratory cycles during which I observed RRo. Cycle-frequency map of these cycles were averaged. *Figure 23* shows qualitative respiratory phase-high frequency amplitude coupling. At a first sight, I identified four high frequency bands displaying heterogeneity throughout respiratory phase:

- Gamma3 band (110-40 Hz) highlighted by purple arrow heads in *Figure 23*
- Gamma2 band (60-90 Hz) highlighted by red arrow heads in *Figure 23*
- Gamma1 band (42-52 Hz) highlighted by yellow arrow heads in *Figure 23*
- Beta band (12-25 Hz) highlighted by blue arrow heads in *Figure 23*

Beta modulation was only visible during QW, but in all areas. Gamma3 modulation seemed to occur mainly during EX and only in V1, S1, DG, and CA1. Gamma1 and 2 were considerably modulated during QW and EX in all areas. In a lesser extent, one still distinguished Gamma1 and 2 modulations in the OB, aPCX and mPFC during SWS and REM. To be noted, phase-locking of Gamma1 and 2 anti-phased for a given brain state. However, one could observe a phase-shift between QW and EX. For example, the nice gamma2 burst that occurred during the late inspiration (respiratory phase $\approx$ 0.4) in QW, occurred during late expiration respiratory phase $\approx$ 0.8) in EX.

Given that 1) Gamma2 modulation was observed in numerous areas and brain state, 2) For a given brain state, when the gamma2 was present, it was well aligned in respiratory phase across areas, I focused my analyses on cross-area synchronization in gamma2 band.

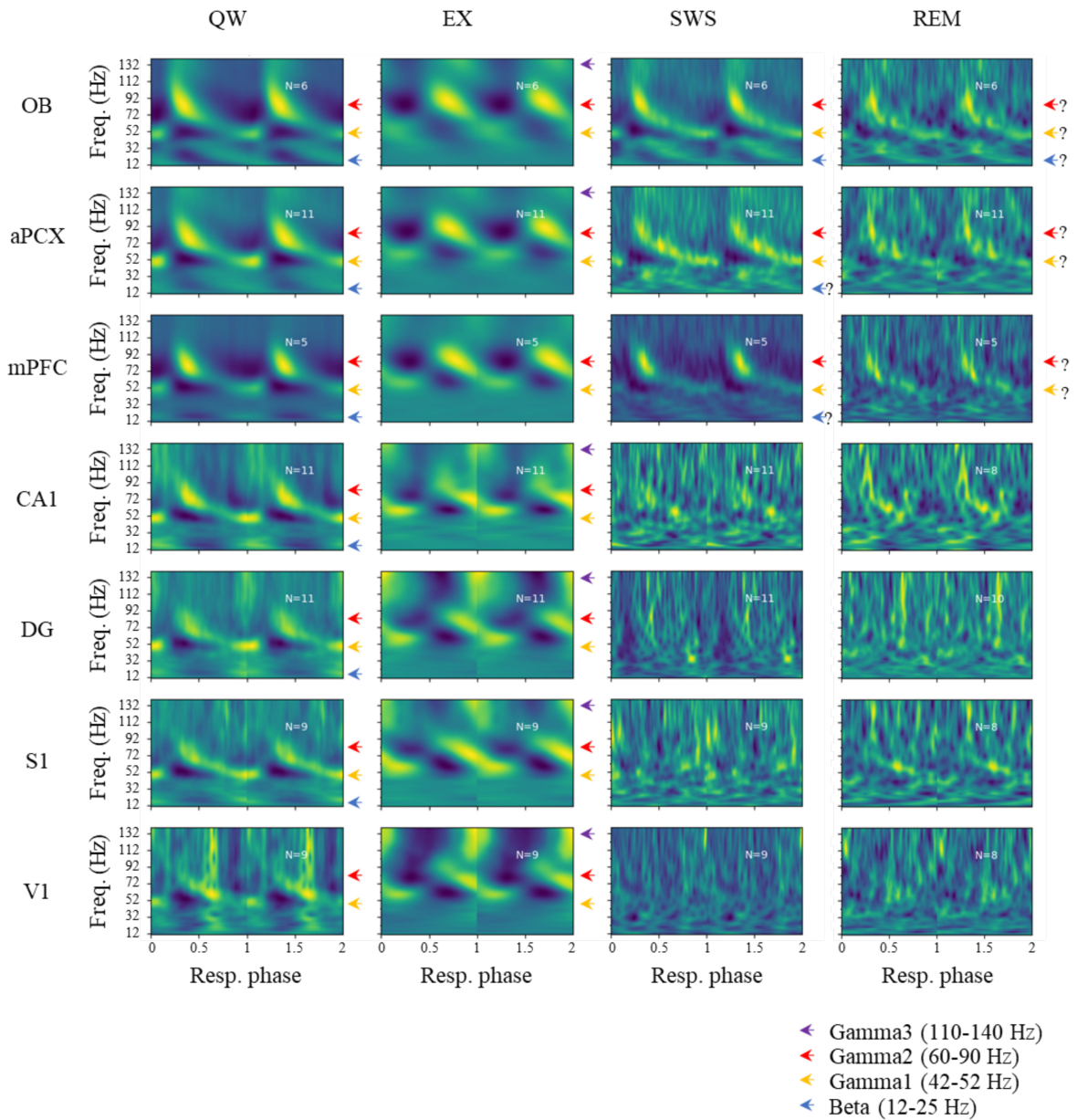


Figure 23 : Several LFP high frequency bands appeared modulated by respiratory phase. Phase-frequency maps were computed for one mean cycle (see methods, section phase-frequency maps) and duplicated to improve visual aspect. White incrustated text indicates the number of animals per areas and state. Blue, yellow, red and purple arrow heads highlight amplitude modulation by respiratory phase of Beta (12-25 Hz), Gamma1 (42-52 Hz), Gamma2 (60-90 Hz), and Gamma3 (110-140 Hz) bands respectively.

In this final step, I wanted to tackle if respiratory rhythm could simultaneously synchronize high and low frequencies LFP of distant areas. Therefore, for a pair of area, 1) I identified respiratory cycles during which RRo occurred in both areas ( *Figure 24A*), and 2) for these respiratory cycles, I looked for Gamma2 synchronization ( *Figure 24B*).

*Figure 24A* showed RRo-mediated connectivity network. Width of links between areas represent the probability to observe RRo co-occurrence. Consistently with previous results, RRo were more frequent during QW. During QW, network connectivity was particularly dense, *i.e.*, all areas were interconnected, and each pair was observed in all four animals. Nonetheless, V1 co-varied rarely with other areas, it seemed less integrated to the respiratory network. During EX, while probabilities are globally lower than during QW, network is still robust since each pair is observed in all four animals also. On the contrary, for SWS and REM, probabilities are low and numerous pairs have not been detected in all animals.

*Figure 24B* showed Gamma2 synchronization network during RRo synchronization. A link between two areas means that cross-area Gamma2 synchronization was significantly modulated by respiratory phase (in strictly more than one animal). Width of the link represents Gamma2 modulation index (see methods, section *Gamma2 connectivity*). In brief 1) I measured the stability of Gamma2 phase difference (curves in inset of *Figure 24B*). The peak observed at 0.4 indicates an enhanced Gamma2 synchronization between mPFC and S1 at this respiratory phase. During QW, inspiration corresponds the respiratory phases from 0 to about 0.4. Therefore, late inspiration promoted Gamma2 synchronization. To go further, I wanted to quantify this respiratory modulation of Gamma2 synchronization 2) To quantify strength of this respiratory modulation, I computed mean vectors of each stability curve. I named Gamma2 modulation index the length of a mean vector (see Gamma2 modulation index values in inset of *Figure 24B*). Gamma2 modulation index were kept only if they were higher than 95<sup>th</sup> percentile of surrogated Gamma2 modulation indices (N = 200 randomly phase-shifted surrogates).

*Figure 24B* showed QW was associated to a complete network. Indeed, most pairs of areas were represented, and they were observed in several animals. Nonetheless, pairs V1-S1, V1-CA1, and DG-S1 showed weaker connection, since they were observed only in two animals. Connectivity networks of the other brain states were too patchy to be interpreted. Therefore, these results showed that waking synchronization by respiratory rhythm of distant brain areas in low frequency LFP (RRo connectivity) was accompanied by a Gamma2 synchronization, only during quiet waking. Consequently, respiratory rhythm can coordinate local activities of distant areas, hence one could propose that respiratory rhythm is able to setup long-range communication channel throughout the brain. Now, whether it is used or not, remain to be determined.

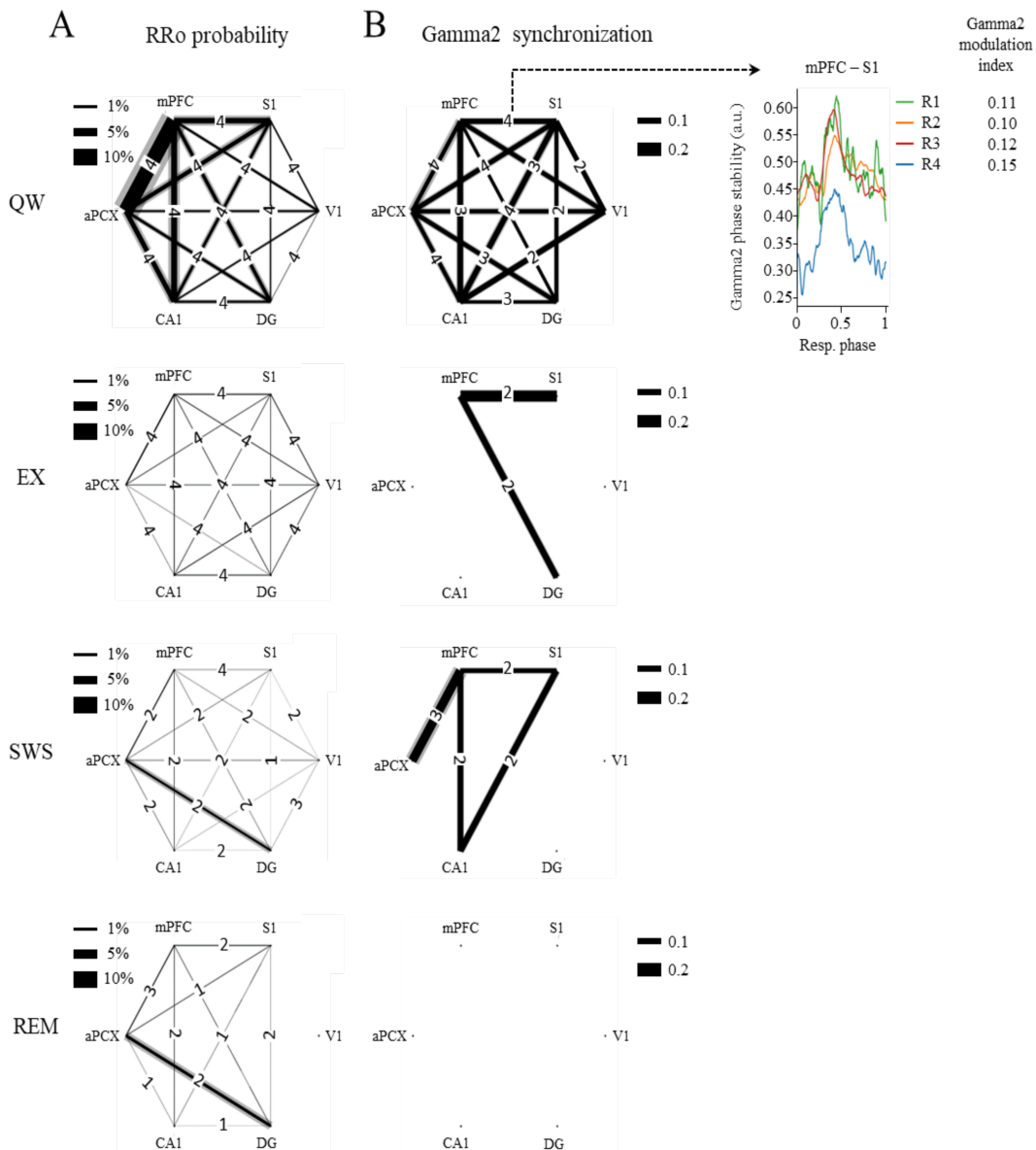


Figure 24 : Respiratory rhythm can bind most areas simultaneously in low and high frequency bands during quiet waking. **A.** RRo co-occurrence network. Width of black lines represent animals' average of RRo co-occurrence probability (expressed in %). Grey lines represent sem, however variability is low, thus they are often not visible. In the middle of each line is indicated the number of animals in which the connectivity has been observed. **B.** Gamma2 synchronization network. Width of black lines represent animals' average of Gamma2 modulation index. Grey lines represent sem, however variability is low, thus they are often not visible. In the middle of each line is indicated the number of animals in which the connectivity has been observed. Top right corner proposes an example of stability signal from which Gamma2 modulation index is computed. In this case, all animals presented significantly modulated stability signals.

### 3.2.4. Conclusion and perspectives

This study is the first to study long-range synchronization mediated by respiratory rhythm. I showed that multiple areas could express simultaneously RRo. Amongst a pool of six areas, I observed all sizes of network. Events of very large network (five or six in my case), although rare, existed. This shows that respiratory rhythm can coordinate brain areas with a great flexibility. Nonetheless, flexibility of respiratory drive is strongly affected by respiratory regime. Indeed, short and deep inspirations (characteristic of exploration respiration), as well as long and shallow inspirations (characteristic of sleep respiration) were mainly associated with small networks ( $\leq 3$  areas in my case). On the contrary, intermediate inspiration duration and amplitude (characteristic of quiet waking) were associated with all sizes of networks, **which suggests a high flexibility of brain areas coordination**. Complementarily, several high frequency bands were modulated in amplitude by respiratory phase when LFP displayed RRo. It was the case in all areas, however mainly during wakefulness. Gamma2 band (60-90Hz) stood out with its remarkable modulation and its conserved phase-locking across brain areas. After quantification, it turned out that synchronization of distinct areas in Gamma2 range was significantly modulated by respiratory phase during quiet waking. Therefore, synchronization of distinct areas by RRo observed during quiet waking was followed in Gamma2 band, which suggests respiratory rhythm could effectively setup long-range communication channel. All together, these results showed quiet waking benefits from a particular respiratory regime, which optimizes brain-wide respiratory drive. RRo are frequent and observed in all recorded areas (Girin et al., 2021). Complementarily, RRo can bind all areas, which results in variable RR network size. In association with these low frequency binding, binding was also observed Gamma2 band. These findings reinforce the idea that respiratory rhythm could serve as a brain-wide clock, especially during quiet waking.

With the present study, I only quantified Gamma2 synchronization for a question of time. However, can the other high frequency also present cross-area synchronization? Gamma1 band was promising, since strength of envelope's modulation (*Figure 23*) seemed consequent and the modulation appeared in all areas during quiet waking and exploration. Therefore, I expect similar results than those observed for Gamma2. If so, it would be really interesting, since Gamma1 and Gamma2 presented a phase-opposition. It would mean that several respiratory phases could carry information. Consequently, one respiratory cycle could multiplex several information. In the olfactory bulb, similar observation had been made for gamma (inspiration locked) and beta (expiration locked) (Buonviso et al., 2003). It was proposed that inspiratory gamma burst mediates feedforward information transfer, while expiratory beta burst mediates feedback information transfer. Therefore, one can wonder if respiratory modulation of high frequency bands could also support bidirectional information transfer outside of the olfactory system. Nonetheless, for now I do not have idea to tackle this question. About high frequency oscillations, another study on OB came to my mind. Authors showed that high frequency dynamics of the OB strongly depended on respiration airflow and frequency (Courtiol et al., 2011a, 2011b). On the one hand, high airflow favored gamma bursts, while low airflow favored beta bursts (Courtiol et al., 2011a). On the other hand, high respiratory frequency decreased gamma occurrence (Courtiol et al., 2011b). Therefore, high frequencies LFP oscillations in the olfactory system depend on respiratory parameters. Since the OB seems the main entrance of the brain-wide respiratory drive, it would be interesting to investigate how respiratory parameters impact non-olfactory high frequencies. In a first sight, one could compare quiet waking and exploration phase-frequency map *Figure 23*. Olfactory areas (aPCX and OB) presented respiratory modulation in beta band during quiet waking, which disappeared during exploration. The same observation was made for the non-olfactory areas. In the present study, I studied respiratory modulation of high frequency LFP oscillation only as a function of brain states. However, to tackle if intermediate inspiration duration and amplitude also favor

high frequency synchronization, it would be interesting to quantify respiratory modulation of high frequency oscillation as a function of respiratory regimes rather than brain states. And ultimately, we should study high frequency synchronization throughout respiratory regime.

This second study focused on the detection of RRo amongst brain rhythms. Yet, sleep slow waves and theta rhythm are other prominent coordinator rhythm. Consequently, by focusing on RRo I get only a snapshot of the coordination of brain areas. To my knowledge, only Tort's team were interested in deciphering the competition between theta rhythm and RRo during REM sleep and exploration. I plan to enlarge my analysis to also detection theta rhythm and sleep slow waves. I made the following assumption: I imagine that at each instant, one area is subjected to the influence of several coordinators, namely theta and RRo during wakefulness and REM, and sleep slow waves and RRo during SWS. I hope to be able to quantify time dynamic of this balance.

### 3.3. May respiratory rhythm shape neural assemblies?

#### 3.3.1. Context

I previously showed on the one hand that neurons can individually display respiratory modulation in firing and membrane potential slow oscillations, in anesthetized rats. On the other hand, I showed LFP from distant brain areas can simultaneously synchronize to respiratory frequency, in conscious rats. Then, it would be tempting to propose that respiratory rhythm could shape neural assemblies. To tackle this question, it will be necessary to evidence that neurons firing could synchronize to respiration in distant areas, in conscious animals. Icing on the cake, this brain-wide firing synchronization could correlate during some behaviors. However, in first instance, we only studied if respiration-related assemblies could spontaneously occur throughout sleep/wake cycle. Since, LFP associated to quiet waking presented the wider, the stronger (Girin et al., 2021) and the more synchronous (3.2. Role of the respiratory rhythm in supporting the long-range communication in the brain) respiratory modulation, we therefore expected quiet waking to be the most appropriate moment to observe respiration-related assemblies.

To follow this idea, I needed a setup enabling to record firing activity of distant brain areas, in non-anesthetized rats, which we did not have. To build the setup we had several choices to do.

- The first choice concerned the type of electrodes. I needed numerous recording sites to maximize the probability to record assemblies. Additionally, I needed electrodes with good penetration profile. The smoothest the penetration, the more stable the tissue and thus the better the recording. Moreover, the fewer damage, the more recording sessions were possible. I rapidly eliminated wire-based electrodes for gaining interest in silicon probe. I chose Neuronexus probe for the flexibility of their recording sites geometry.
- The next choice concerned the preparation: head-fixed are freely moving? I wanted to record several areas, six precisely. If I decided to implant electrode (fixed or on micro-drive), it would mean I use six electrodes per animal. It would represent an amount of about 8.000 € per animal, which we could not afford. I could implant less electrodes, but price per animals will still be elevated and few areas will be recorded. I therefore chose a head-fixed setup. Electrodes were cleaned and reused between. Overall, 7 electrodes were used for 9 rats. Trade-off we had to make, was that we recorded areas two-by-two, hence we could not record a network of areas.
- The third choice concerned the area of interest. I wanted to stay close to areas implanted in Girin et al., 2021, namely the olfactory bulb (OB), the anterior piriform cortex (aPCX), the medial prefrontal cortex (mPFC), primary somatosensory cortex in the barrel field (S1), primary visual cortex (V1), CA1 and dentate gyrus (DG). I excluded the OB because non-anesthetized respiratory modulation is well characterized there, and it is too close from the eyes. Lowering electrodes could stress the animal. V1 was too posterior for the implant I designed. The, I recorded in mPFC, aPCX, CA1, DG and S1. I added to this list an anterior cortex receiving direct inputs from olfactory cortex: the orbitofrontal cortex (OFC). The implant was design to allow simultaneous recording of one anterior area (mPFC, OFC, aPCX) and one posterior (CA1, DG, S1).
- The fourth question concerned the pairing of areas. Three pairs were defined and were recorded several times to have a chance to reach statistical threshold. I paired mPFC (prelimbic cortex (pL) was targeted) and CA1, since literature suggest a bidirectional communication (Ferraris et al., 2018; Roy et al., 2017). I paired OFC and DG, since they both receives direct projection from olfactory system (Clugnet and Price, 1987; Price, 1985). I paired aPCX and S1, because they belong to the two most important sensory system in rodents.
- Lastly, I had to find a way to identify electrodes tracks. Additionally, I wanted to record several times each pair, thus I needed to be able to differentiate each descent. I found a kit of three fluorescent dyes, so I could record up to three time a pair.

### 3.3.2. Methods

#### Experimental procedure

**Animal care.** Four female and two male Sprague Dawley rats (Charles River, Germany, 250-300 g at the arrival) were used and housed in group of three in a temperature ( $22\pm 1$  °C) and humidity ( $55\pm 10$  %) controlled room and exposed to a 12/12 h light/dark cycle (light onset 7:00 am). Experiments were conducted during light period. Food and water were available *ad libitum*. All experiments were carried out in accordance with Directive 2010/63/EU of the European Parliament and of the Council of the European Union regarding the protection of animals used for scientific purposes and in compliance with the ARRIVE guidelines. The experimental protocols were approved by the National Ethics Committee “Animal Experimentation Committee of Univ. Claude Bernard Lyon 1—CEEA-55” (Agreement APAFIS #17088).

**Contention device.** Contention device was designed with help of and was inspired from Damien Gervasoni (Gervasoni, 2000). Device was composed of an implantable piece and a contention plate (Figure 25A). The implantable piece was a 22x22x2 mm 3D printed square. In the center, a 14x14 mm clearance was left to manage a recording chamber, giving the implant a U shape. This part is now referred as the U-piece. At each corner, a screw (steel) was screwed and glued. Aluminum spacers (5 mm height) were put around the screws. The U-piece fitted with the contention plate, to which it was secured with four bolts. Contention plate was fixed to stereotaxic apparatus. All 3D models were designed (OpenSCAD software) and printed (Ultimaker2 printer) by me. Polylactic acid (PLA) was used for 3D printing.

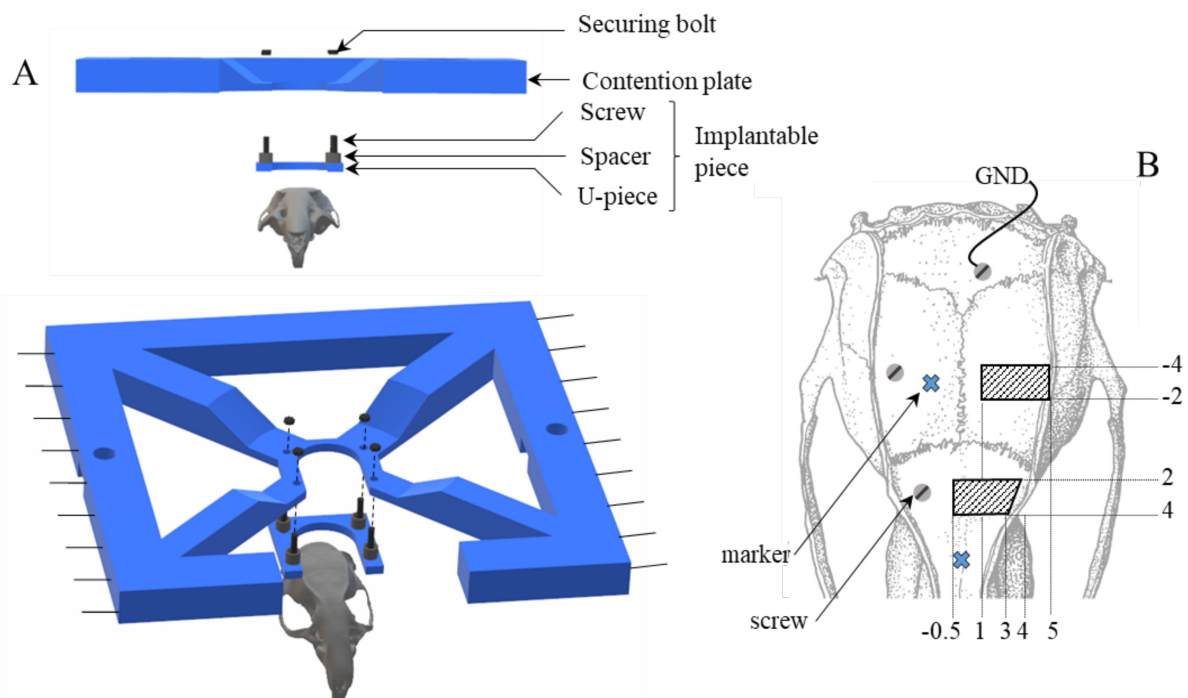


Figure 25 : Preview of the contention device and implant. A. Contention device. 3D printed are colored in blue. Lateral black lines symbolize anchoring to stereotaxic apparatus. Screw and bolt (steel) are colored in black. Spacer (aluminum) are colored in dark grey. Skull is colored is light grey. Skull model was found on [www.thingiverse.com](http://www.thingiverse.com). B. Map of implantation. Three anchor screws (grey circle) were inserted. Posterior one was used as reference. Two stereotaxic markers (blue cross) were cemented. Hatched areas represent craniotomy windows. Coordinates are given relative to bregma position. Anterior and left coordinates are positive. Skull image was extracted from Paxinos and Watson, 2006.

*Animal preparation.* Preparation consisted in five steps: acclimation, habituation to the experimenter, implantation and recovery, habituation to the immobilization, recording.

- After their arrival, animals were kept alone for one week of acclimation.
- After this period, rats and experimenter got used to each other for one week.
- Implantation consisted in building an anchoring stud. Animals were anesthetized with isoflurane. Once anesthesia was induced, animals were placed in stereotaxis apparatus. Non-steroid anti-inflammatory (Carprofen: 0.5 mg/kg) and analgesic (Buprenorphine: 3 mg/kg) drugs were administered subcutaneously. During at least thirty minutes (estimated delay for drug action), no painful act was made. Fifteen minutes before incision, local analgesic was injected subcutaneously (Lidocain: 200  $\mu$ L). Then scalp was incised, and periosteum was cautiously removed. Three anchor screws were inserted in the bone (*Figure 25B*). One in the right frontal bone, one in the right parietal bone, and one in the supraoccipital bone. The latter one served as reference. Reference electrode consisted in a bare Ag wire soldered on one side to a screw and the other side to a mini female banana plug. After screws were placed, two windows were marked with pencil. The anterior window allowed to target prelimbic cortex (pL), orbitofrontal cortex (OFC) and anterior piriform cortex (aPCX). The posterior window allowed to target CA1, dentate gyrus (DG) and the primary somatosensory cortex (S1) (*Figure 25B*). Then, a layer of SuperBond was applied on screws and over the skull. Windows and bregma were preserved from SuperBond. At that moment, two stereotaxic markers, made from stainless steel needles, were implanted, in case of Bregma degradation. Anterior marker was grossly positioned and cemented. Then, its distance to bregma was a posteriori stereotactically measured. Procedure was repeated for posterior marker. The next step consisted in cementing the U-piece to the skull. To ensure horizontality and stereotaxic positioning, U-piece was mounted on the contention plate. Once positioned, dental cement was applied to attach U-piece to the skull. Skull above delimited windows was carefully preserved from cement. U-piece and bare Ag reference wire were cautiously enveloped with cement. Only mini banana plug was accessible. To avoid bone infection, a thin layer of transparent SuperBond was applied over delimited windows. Hours following surgery, rats were isolated in a recovery room to let animals some rest and not to stress fellows. Once animals were fully awake, they were placed back to their homecage. However, a bulkhead was added to avoid physical contact between healthy animals and surgery recovering animals. Bulkhead was maintained at least five days to allow wound to heal. Analgesic coverage was maintained for three days with subcutaneous injection of non-steroid anti-inflammatory drug (Carprofen: 0.5mg/kg). After a 12 days recovery, and if animals were in good shape, habituation to contention began.
- The aim was to reach four hours of quiet contention, with sleep and wake periods. The first two days were dedicated to short but numerous manual habituations to contention (four to five times per day, five to thirty minutes). Each contention was rewarded with a bit of sweet Corn Flakes. Following days, animals were placed in the full contention system. Once animals were able to stay one-hour quiet, nasal respiration sensor was introduced. Tube of the sensor must touch rat's nostril to get an exploitable signal. As this sensor induced stress and discomfort, habituation to the sensor was the hardest part. Habituation lasted  $13.5 \pm 0.5$  days ( $N = 6$  rats). Habituation was considered as efficient when animals stayed quiet for four hours, three days on a row.
- Animals underwent their second surgery to remove bone and dura over delimited windows. As for the implantation, animals were anesthetized with Isoflurane, complementarily subcutaneous injections of carprofen and buprenorphine were made. Skull and the layer of Superbond were drilled over delimited windows. A drop of lidocaine was placed on the dura. Then, using a hook and the sharp edge of a needle, dura was cut and removed. When the two windows were proceeded, a piece of hemostatic sponge (Bloxang) soaked with 10% Betadine solution was

placed over the windows. To protect from dehydration and pathogen entry, recording chamber was hermetically sealed with bone wax. Like previously, rats were let some hours in a quiet room to wake up. Then they were placed back in their homecage, to which the bulkhead was added. The day after craniotomy, animals were let to recover and were injected with carprofen. The next day, recordings began.

*Recording sessions.* Recording session started at 2 pm and lasted about four hours. First, animals were fixed in contention system. Bandage (bone wax and hemostatic sponge) was removing, and recording chamber was cleaned. Electrodes were stereotactically placed above areas of interest. Then, electrodes were lowered one by one to the areas of interest. At first, electrodes were rapidly lowered (about 10  $\mu\text{m/s}$ ), then approximately 1000  $\mu\text{m}$  descending speed dropped to 1  $\mu\text{m/s}$ . When electrodes were in place, tissue were let 20 min to accommodate deformation. Then, nasal respiration sensor was placed, and data were acquired. Each rat had nine recording sessions and six targeted areas. Areas were recorded by pairs. Prelimbic cortex (pL) - CA1 pair was recorded during sessions 1,4 and 7, Orbitofrontal cortex (OFC) - dentate gyrus (DG) pair during sessions 2,5 and 8, and Anterior piriform cortex (aPCX) - primary somatosensory cortex (S1) pair during sessions 3,6 and 9. After recording, electrodes were removed, recording chamber was cleaned and finally sealed with a new bandage. Electrodes were dipped overnight in an agitated 10% Decon90 solution at 40 °C.

*LFP and respiration recording.* Signals were acquired at 30 kHz with an OpenEphys board, to which two 32-channel Intan amplifier (RHD32 with accelerometer) and an I/O analogical board were linked. LFP were recorded with Neuronexus silicon probes (A1x32-Poly3-10mm-50-177, A1x32-Poly2-10mm-50s-177). Respiration was monitored with a homemade air flow sensor. OpenEphys software and homemade python scripts were used for real-time visualization and data storage.

*Histology.* Prior to recordings, electrodes were dipped in either DiI, DiO or DiD dye until human eye observed colorization of probe tip. After the nine recording sessions, rats were killed with lethal injection of pentobarbital. Animals were flushed with phosphate-buffered alkaline, perfused with paraformaldehyde (4%). Brains were removed, postfixed overnight, cryoprotected (sucrose 30%), and frozen. Brains were sliced (40  $\mu\text{m}$  coronal section) with a cryostat. Slices were mount with DAPI. Slides are still under observation.

## **Data Analysis**

*Respiratory signal.* Nasal sensor on awake animal gave a nice respiratory signal, as long as the tube of the captor is close enough to the nostril. Nostril twitching provoked slight modification of airflow direction, which significantly impacted signal amplitude. Furthermore, distance from nostril to captor greatly influences signal amplitude. Throughout recordings, captor placement was not reproducible. Therefore, amplitude of respiratory signal could not be compared between recordings and between animal. On the contrary, nostril twitches did not alter much signal shape, consequently temporal markers of respiratory cycles are stable over time. Therefore, we could only use the temporal components of the signal. The detection of respiratory cycles was achieved with the same algorithm described in Girin et al., 2021 and (Courtiol et al., 2011b). This algorithm performs two main operations: signal smoothing for noise reduction, and detection of zero-crossing points to define accurately the inspiration and expiration phase starting points. For each respiratory cycle, inspiration duration and expiration duration were measured. Instantaneous respiratory frequency was determined as the inverse of the respiratory cycle (inspiration plus expiration) duration. Respiratory regimen developed by rats during contention were identified by computing 2D histograms of inspiration duration and respiratory frequency. In *Figure 26 A* and *B*, heights of histogram have been log-scaled to counterbalance the important distribution heterogeneity.

*Scoring of putative brain states.* I could not score brain states in a classical manner, as done in Girin et al., 2021 for followings reasons. 1) I had no camera or pupil tracker to estimate if animal slept. 2) With nasal sensor, I could not trust respiration amplitude values to distinguish sleep and wakefulness. 3) I did not implanted EMG in order not to burden preparation. To overcome this issue, I used respiratory pattern as a proxy to define brain state. From our freely moving rats dataset (Girin et al., 2021), we observed that each brain state was characterized by specific respiratory patterns (see colored contour curves in *Figure 21* and *Figure 26A*). Therefore, by comparing of respiratory patterns of freely moving and head-fixed respirations, we tried to retrieve brain state in head-fixed preparation with respiration only. To be noted, the combination inspiration duration / inspiration amplitude would better segregate brain states (see colored contour curves in *Figure 21*). Unfortunately, as previously explained, respiration amplitude is not sufficiently well captured by our sensor in the head-fixed preparation to be relevant. Hence, we used the second-best segregation combined parameters, namely inspiration duration and respiratory frequency (*Figure 8*). To be noted, in freely moving rats, respiratory parameters distribution drew a hyperbole (*Figure 8A*). This form is due to the fact that physiological respiration displayed almost constant inspiration ratios (inspiration duration over cycle duration). Yet, visualizing a constant inspiration ratio on graph whose axes are inspiration duration and respiratory frequency has for consequence to draw hyperboles, as demonstrated below.

$$\text{inspiration ratio} = \text{constant} = \frac{\text{inspiration duration}}{\text{cycle duration}}$$

$$\text{constant} = \text{inspiration duration} \times \text{respiratory frequency}$$

$$\text{respiratory frequency} = \frac{\text{constant}}{\text{inspiration duration}}$$

Therefore, to identify putative brain states we used thresholds for frequency (horizontal lines), inspiration duration (vertical lines) and inspiration ratio (hyperboles). We defined as

- putative exploration state (pEX): every respiratory cycle with a frequency superior to 4 Hz and an inspiration ratio inferior to 0.6
  - putative quiet waking state (pQW): every respiratory cycle with a frequency inferior to 4 Hz, an inspiration duration inferior to 0.25 s, and an inspiration ratio between 0.2 and 0.6
  - putative sleep state (pSleep): every respiratory cycle with an inspiration duration superior to 0.25s, and an inspiration ratio inferior to 0.6
  - putative discomfort state (pDiscomfort) every respiratory cycle with a frequency inferior to 2 Hz, an inspiration duration inferior to 0.15s, and an inspiration ratio inferior to 0.2.
- Head-fixed respiratory parameters distribution did not display a hyperbolic shape but rather a L-shape (*Figure 8B*). The angle (very short inspiratory and low frequency) recalled us respiratory pattern observed during freezing (*Figure 5* from Dupin et al., 2019). We separated these respiratory cycles from pQW, in case they were associated with stress or just a body position discomfort.

*LFP processing.* For each recording, the 64 channels were down sampled to 5000 Hz, highpass filtered (0.8 Hz, order = 2), and split into two data files, one per electrode. Then, for each electrode, coherence to respiration was computed for the 32 channels in the 1-10 Hz band. Time-frequency (0.6 Hz to 12 Hz by 0.05 Hz step) signal was computed for channel with the highest coherence (highest area under the curve), and rescaled to respiratory phase as described in Roux et al., 2006 and in freely moving study ([3.2.2. Methods](#) – phase-frequency maps). To estimate the spectrum for each respiratory cycle, phase-frequency maps were averaged along respiratory phase axis. Then, to obtain power spectrum density, spectra were divided by the sum of average spectrum. To build *Figure 27*, by-cycle power spectrum densities from i) one animal, ii) one area and iii) one putative brain state were averaged. To build *Figure 28*, major frequency of each spectrum is extracted. Therefore, for every respiratory cycle I assessed its respiratory frequency and

its major LFP frequency. Then, for each i) animal, ii) area and iii) putative brain state by-cycle LFP-respiration covariation matrices were computed. Matrices were averaged across animals.

*Spike sorting.* To identify and isolate single units, SpikeInterface software (<https://github.com/SpikeInterface/spikeinterface>) was used (Buccino et al., 2020). SpikeInterface enables to flexibly use various spike sorters. We used Tridesclous, the sorter developed in the lab, and with the help of benchmarks we chose to also use Kilosort2 (Pachitariu et al., 2016). These software take into account geometry of recording sites when high density electrodes are used. Both software used the same algorithm, namely template matching. Briefly, it consists in two steps. First, a catalog of spike waveform is built. A waveform corresponds to the fingerprint on the electrode of a putative action potential (AP) (like in *Figure 5A*). Indeed, AP of one neuron can be perceived on multiple recording sites of a high-density electrodes. To determine these waveforms, LFP of each recording site is high pass filtered and negative peaks are detected. All peaks simultaneously detected over close recording sites constitute a waveform. Once all waveforms were detected, they were clustered. In theory, one cluster contained AP from one and only one neuron. Waveform of a cluster were averaged to get a template for the cluster. This first step was not necessarily run on the whole recording. The second step of the algorithm consist in the template-matching. For each detected peak, algorithm test which template matched the best. The spike was then attributed to most comparable cluster. Once spike sorting was finished, we computed for each cluster two quality metrics: ISI violation and signal-noise ratio. ISI violation corresponds to the rate of the refractory period violation, *i.e.*, the number of spikes within refractory period by unit of time. This metric estimated whether the cluster was pure (contains only one cell) or if it was rather a multi-unit cluster. Signal-noise ratio corresponds to the amplitude of the spike relatively to the actual noise of the signal. This metric estimated indirectly the quality of the sorting. The more ample the spike, the safer will be the sorting. We based our automatic curation on following threshold:

- ISI violation < 0.05 Hz
- and signal-noise ratio > 5 standard deviation

*Criteria for classifying a firing pattern as respiratory modulated.* For each cell (*i.e.*, cluster), spike times were converted to respiratory phase as described in the intracellular study (see Cenier et al., 2009 and page 3 of intracellular publication, section *Rescaling time basis of signals with respiratory phase*, page 58 of manuscript). We wanted to tackle if particular respiratory regime (we expected pQW) could favor respiration-related discharge of neurons. Consequently, we scanned respiratory regime through combination inspiration duration and respiratory frequency, and we looked for respiratory modulation. Following algorithm was repeated for each combination of respiratory parameters. If the bin contained enough respiratory cycles ( $N > 30$  cycles) and if the cell fired enough ( $N > 100$  spikes) during these cycles, mean vector of spike distribution was computed. Vector length represented the strength of respiratory modulation. Angle represented the preferred phase of firing. To assess significance of respiratory modulation, we repeated the same algorithm for 200 surrogates (each spike was randomly phase-shifted). If length of true mean vector was superior the 95<sup>th</sup> percentile of surrogated mean vector lengths, cell was considered modulated for this combination of inspiration duration and respiratory frequency. If so, length and angle were kept. Once all respiratory patterns were ranged, the cell presented four maps:

- A map of “presence” which indicated in which bins the cluster fired enough to be tested.
- A map of “respiratory modulation” which stored bins where respiratory modulation was identified.
- A map of “respiratory modulation strength” which stored length of mean vector for modulated bins
- A map of “angle”, storing angle of mean vector for modulated bins.

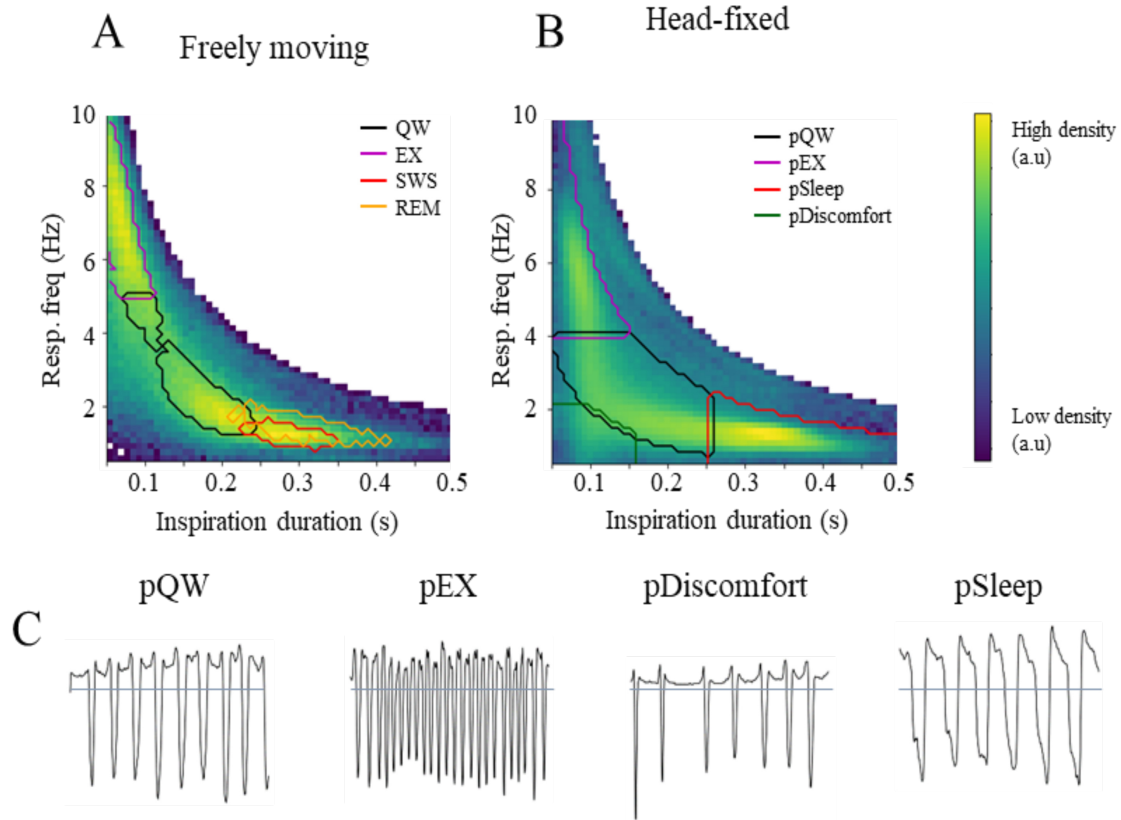
To build *Figure 30*, for one area, maps of respiratory modulation of all cells from a same area, irrespective of animal, were summed. Same process was made with maps of presence. To assess the proportion of modulated cell throughout respiratory regime, the summed map of respiratory modulation was divided by the summed map of presence. To build *Figure 31*, for one area, maps of respiratory modulation strength of all cells from a same area, irrespective of animal, were averaged. If a bin contained less than 10 cells, average was not plotted. To build *Figure 32*, for one area, maps of respiratory modulation angle of all cells from a same area, irrespective of animal, were concatenated. To assess stability of preferred phase of firing, mean vector was computed for each bin. If bin contained more than 10 cells, length of mean vector was plotted. As a reminder, if length was close to 1, it meant cells preferentially discharge at close respiratory phases.

### 3.3.3. Results

Following results are preliminary, but the aim is to expose the potential this dataset represents.

In a first time, we wanted to characterize respiration, spectral properties and respiratory modulation of low frequency LFP properties from head-fixed preparation, with previous study (Girin et al., 2021) as point of comparison

*Breathing characteristics in the head-fixed rat.* First, we compared breathing characteristics in freely moving and head-fixed preparations. *Figure 19* *Figure 26* A and B showed 2D distribution of inspiration duration and respiratory frequency in freely moving (A) and head-fixed (B) rat preparation. Although global distributions were very similar, some differences could be observed. Freely moving rats presented an important density between 7-10Hz and at low inspiration duration, contrarily to head-fixed rats. Indeed, we observed head-fixed rats sniffed at lower frequency than freely moving rats, consistently with literature on rats (Girin et al., 2021; Wesson et al., 2008). Furthermore, head-fixed rats displayed a consequent density of respiratory cycles of long inspiration (>0.35 s) and low frequency (1 Hz), which was not observed in freely moving animals. They also presented some respiratory cycles with low frequency (1-2Hz) and short inspiration duration (inferior to 0.15s), resulting in very low inspiration ratio (inferior to 0.2). This new pattern slightly rubbed out the hyperbole shape in favor to a more angular shape. This pattern evoked us respiration associated to fear that another student in team recorded (*Figure 5* from Dupin et al., 2019). When animals produced ultrasonic vocalization, she observed a very short inspiration and a long expiration during which ultrasound were emitted. Although I took great care of my animals and I rendered the habituation the smoothest possible, it is possible that at some moment animals are annoyed to be restrain, resulting in development of stress. Nonetheless, we did not recorded ultrasound (we must add it to the installation) and thus we cannot be sure this respiratory pattern indicated a state of stress. Another possible explanation is that rat's body was in a position which hindered respiration. In both hypotheses, this respiratory pattern seemed to attest of a discomfort. We named this state "putative discomfort".



	pQW	pEX	pDiscomfort	pSleep
insp. dur. (s)	$0.17 \pm 0.01$	$0.09 \pm 0.001$	$0.12 \pm 0.01$	$0.33 \pm 0.001$
freq (Hz)	$1.85 \pm 0.05$	$4.94 \pm 0.15$	$1.44 \pm 0.11$	$1.27 \pm 0.02$
insp. ratio	$0.31 \pm 0.01$	$0.12 \pm 0.01$	$0.17 \pm 0.02$	$0.42 \pm 0.01$

Figure 26 : Characterization of respiration during contention and identification of putative brain states. A. 2D distribution of respiratory parameters in freely moving rats ( $N = 11$  rats). Median distribution of respiratory parameters associated to each brain state (QW: black, EX: magenta, SWS: red, REM: orange) are presented with contour curves. B. 2D distribution of respiratory parameters in head-fixed rats ( $N = 6$  rats). From this distribution, brain states were identified as putative. Respiratory parameters corresponding to each putative brain state are highlighted by contour curves (pQW: black, pEX, magenta, pSleep: red, pDiscomfort: green). C. Raw traces of respiratory signal. Horizontal lines highlight the zero-airflow, corresponding to transition between inspiration (down) and expiration (up). Inspiration duration (insp. dur.), respiratory frequency (freq) and inspiration ratio (insp. ratio.) of presented cycles are described in table (mean  $\pm$  sem).

*LFP characteristics of the different brain states in the head-fixed rat.* We then characterized LFP spectral activities of each putative brain states. As visible in Figure 9, during pQW, all areas presented a high spectral density in theta band (around 7 Hz), which was particularly pronounced in CA1 and DG. All areas, S1 excluded, displayed a wide density peak between 1 and 4 Hz, which correlated with respiratory frequency distribution. S1 showed the particularity to express a strong 4-5 Hz oscillation. During pEX, OFC, aPCX and pL displayed high spectral density in respiratory frequency range. CA1 and DG presented a peak of density in theta band. On the contrary, S1 displayed a flat distribution, no particular oscillations seemed to emerge. Spectral activities of pDiscomfort were very similar to pQW. To be noted, fear expression is correlated with development of a strong 4 Hz oscillation related to respiration in mice mPFC and in the hippocampus (Bagur et al., 2021; Karalis et al., 2016; Roy et al., 2017). Hence, if pDiscomfort was related to a state of stress we would expect development of this 4 Hz oscillation. Consequently, it is likely that respiration associated to pDiscomfort is due to a physical discomfort rather than stress. During pSleep all areas, excepted S1, displayed a high density delta band (1-4 Hz). S1 continued to express a strong 4 Hz oscillation. pQW and pEX spectrums are credible for wakefulness spectrums. pDiscomfort should probably be included in pQW. The high delta power in pSleep recalled SWS spectrums. REM sleep could not be isolated with this process. REM sleep respiration is greatly variable and overlap with SWS and QW. Thus, pSleep and pQW probably contained episodes of REM. In conclusion, spectrums were coherent with the expected brain states although they had been extracted only from respiratory parameters distribution.

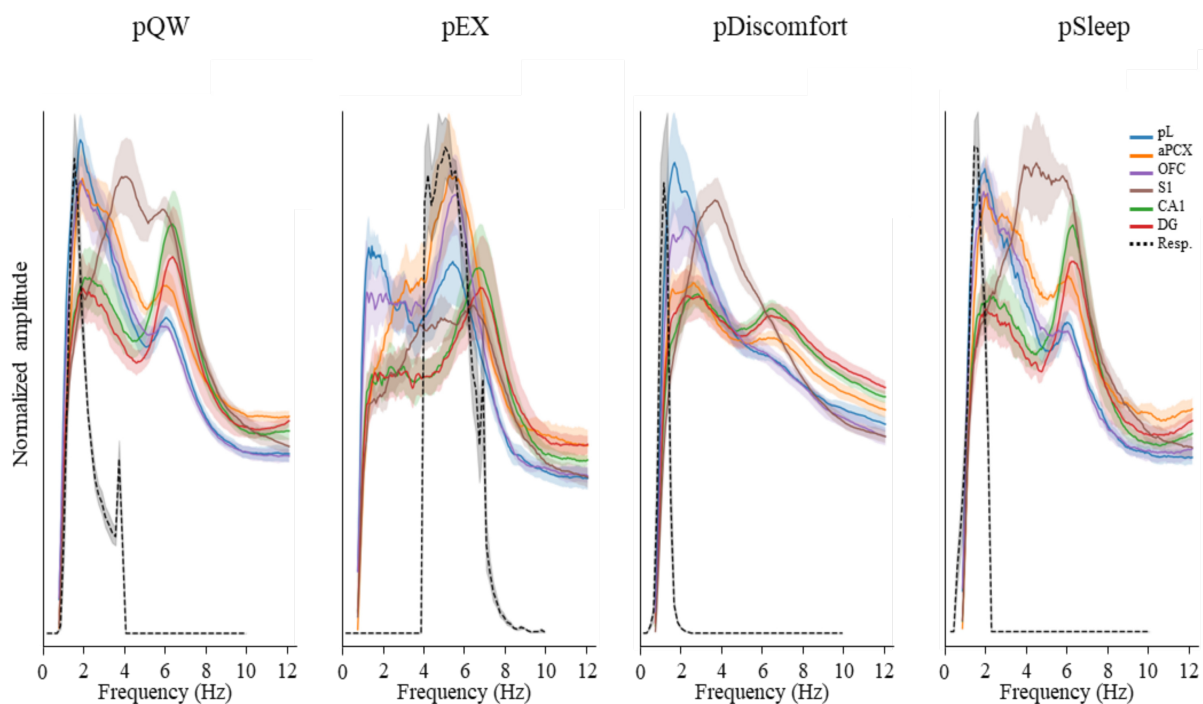


*Figure 27 : LFP spectral characterization of putative brain states. Power spectrum densities (pL: blue, aPCX: orange, OFC: magenta, S1: brown, CA1: green, DG: red) are overlaid with respiratory frequency histogram (black dashed line). Full lines and dashed lines represent average across animals (N=6) Shaded areas represent sem across animals (N=6). A spectrum was associated to each respiratory cycle. For one area and one animal, respiratory cycles were sorted in putative brain states according to conditions mentioned previously. Spectrums of cycles associated to a state were averaged.*

*Characterization of LFP respiratory modulation.* Lastly, we characterized respiratory modulation of low frequency LFP. To do so, we computed LFP-respiration covariation matrices, represented in Figure 10. As a reminder, density on the matrix diagonal means respiration and main LFP oscillation displayed the same frequency. Here, pQW was associated with clear diagonal in all areas. To be noted, this by-cycle analysis revealed LFP-respiration coupling which was not visible on power spectrum density. Though, the 4 Hz oscillation in S1 was still visible and was independent from respiration. These matrices are strikingly similar to the QW matrices in Girin et al., 2021. pEX displayed moderated coupling for OFC, aPCX, and pL. On the contrary CA1, DG, and S1 were not coupled. Hence, anterior areas coupled to respiration, while posterior ones were not, like EX matrices in Girin et al., 2021. During pDiscomfort, over-diagonal ( $y = 2*x$ ,  $y = 3*x$ , etc.) were more pronounced than diagonal. Over-diagonal could be explained by the existence of harmonics. For non-sinusoidal oscillations, wavelet convolution is high at fundamental frequency. However, convolution still fits for multiple of fundamental frequency. These multiples are called harmonics. Here, since we computed wavelet-based time-frequency signal, analysis was sensitive to harmonics. Particularly, in the case of pDiscomfort which corresponded to very asymmetrical respiratory cycle (inspiration ratio is below 0.2). Consequently, if LFP showed respiratory coupling, one could expect that LFP RRo were also asymmetrical. If these assumptions are true, over-diagonal would attest of the presence of RRo. Otherwise, it would mean that LFP displayed cross-frequency coupling in low frequencies LFP, which according to raw signal observation was very unlikely. To come back to matrices, over-diagonals were clear in pL, OFC and aPCX, but subtle in CA1 and DG. On the contrary S1 did not present coupling. Consequently, excepted for S1, respiratory modulation during pDiscomfort was close from what happened during pQW. This result is another evidence suggesting pDiscomfort correspond to QW rather to a state of stress. Finally, most points of pSleep matrices were vertically arranged, showing LFP frequency were independent from respiration. Nonetheless, a diagonal stepped out when close looking in pL, OFC, aPCX and DG. Hence, respiratory regime associated to pSleep enabled respiratory coupling. As a reminder SWS matrices in (Girin et al., 2021), displayed much smaller respiratory frequency range and no diagonals were observed. However, REM matrices presented diagonals. These diagonals in my data could have two other interpretations. 1) Wide frequency range associated to pSleep could suggest that pSleep actually contained episodes of QW. Hence arbitrary borders between pQW and pSleep could be improved 2) Borders between pQW and pSleep were correct, but points on diagonal corresponded to REM episodes.

Altogether, results on respiration, spectral properties and respiratory modulation of low frequency LFP suggest that head-fixed preparation does not present major difference as compared to freely moving. So now, we will go for spikes analysis.

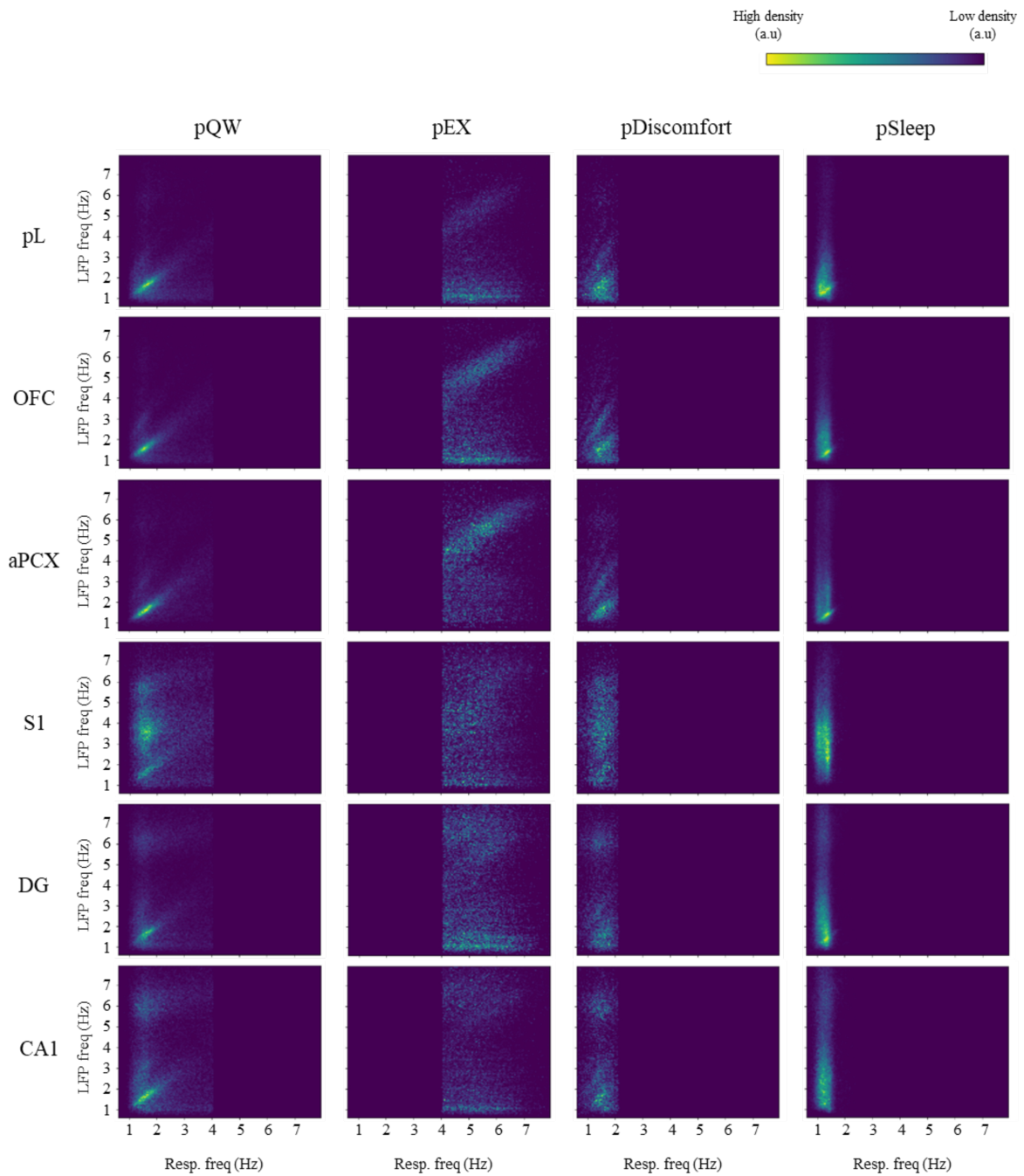


Figure 28 : Characterization of LFP respiratory modulation by LFP-respiration covariation matrices throughout putative brain states. Covariation matrices, averaged across the six rats, were obtained for every area and putative brain state. A spectrum was associated to each respiratory cycle. Major frequency was extracted. For one area and one animal, respiratory cycles were sorted in putative brain states according to conditions mentioned previously. Major LFP frequency and respiratory frequency of cycles associated to a state were used to compute covariation matrix.

*Characterizing respiratory modulation in neuronal firing.* This part of the results is largely unfinished. It still requires a lot of pre-processing of the data that I did not have time to do. I will only present here some preliminary results to show the kind of analysis I would like to do later.

Spikes were sorted with SpikeInterface software, with which we used two sorters: Tridesclous and Kilosort2. The two sorters gave similar results, however only figures from Tridesclous sorting are presented below. After sorting, automatic curation was applied so that we kept only cells with signal to noise ratio above 5 and ISI (inter-spike interval) violation below 0.05. However, an additional manual curation would be necessary to improve the sorting, which I do not have the time to do within the deadlines imposed by the PhD defense. Hence, following results are not definitive. I will rather expose how we plan to tackle the question of respiration-based neuronal assemblies.

In a first time, we characterized respiratory modulation of neurons firing as a function of respiratory regime. For each cell, we inspected respiration-related firing pattern according to inspiration duration and respiratory frequency. Spike times were rescaled to respiratory phase as previously done in (see Cenier et al., 2009 and page 3 of intracellular publication, section *Rescaling time basis of signals with respiratory phase*, page 58 of manuscript). For each inspiration duration – respiratory frequency combination of respiratory parameters, we computed mean vector from distribution of selected spikes. Length of the mean vector reflected the strength of respiratory modulation, and angle represented preferred respiratory phase of firing. If firing pattern was modulated by respiration, mean vector length should be great. Length of the mean vector was compared to 200 surrogates to assess significance. If firing pattern was significantly modulated by respiration, length and angle of mean vector was kept. To get enough respiratory cycles and spikes per bin, bins were broadened (9 bins x 9 bins matrices for *Figure 29*, *Figure 30*, *Figure 31*, and *Figure 32*, while 60 bins x 60 bins matrices for *Figure 26*) compared to *Figure 26*. Respiratory parameters distribution was recomputed in *Figure 29* with broaden bins to keep reference point.

Using this method, we aimed at tackling the following questions: is there a respiratory regimen favoring respiration-related firings? Is there a respiratory regimen associated with strong respiration-related firing? Do neurons preferentially fire at the same phase of respiration?

We first estimated the density of modulated firing as a function of respiratory regimen. For this purpose, we counted the number of cells identified as modulated by respiratory rhythm in each bin and divided it by the number of cells observed in this bin. Results are presented in *Figure 30*. OFC, aPCX and S1 displayed high proportions (between 40 and 80%) of modulated cells. DG presented intermediate proportions (between 20 and 50%), while pL and CA1 displayed very low proportions (between 0 and 20%). Results for pL were surprising, since other authors observed consequent percentage of modulated cells there (Biskamp et al., 2017; Karalis and Sirota, 2018; Kőszeghy et al., 2018) All areas presented homogenous distribution of proportions, hence no particular respiratory regime tended to drive more cells.

We then estimated the strength of respiratory modulation for each respiratory regimen. Mean vector length of modulated cells were averaged for each bin. Results are presented *Figure 31*. OFC, aPCX, S1 and DG presented weaker respiratory modulation in respiratory regimen associated to pSleep. On the contrary, we observed the strongest respiratory modulation in OFC, aPCX, S1, and DG during respiratory regimen associated to pQW and pDiscomfort. Still in OFC, aPCX, S1, and DG, during pEX-associated respiration, neurons displayed intermediate strength. CA1 displayed same tendency, although less marked. pL displayed too few modulated cells for interpretations.

Finally, we wanted to estimate to what extent cells were susceptible to fire together, at the same respiratory phase. For each bin, stability of mean vector angles was estimated. The closer to 1, the closer cells fired in respiratory phase. This analysis should indicate us in which respiratory regimen, respiration-related assemblies are the more susceptible. Nonetheless, it would not be direct evidence, just suggestions. Results are shown *Figure 32*. S1 and aPCX displayed high stability during respiratory regimes corresponding to

pQW and pEX, while OFC, pL, CA1 and DG presented highest stability during respiratory regimes corresponding to pQW and pDiscomfort.

Together, these results showed that although pQW did not present particularly high proportion of modulated cells, these modulated cells displayed stronger respiratory modulation of their discharge compared to the other putative brain states. Additionally, these modulated cells displayed few variabilities in preferred respiratory phase of firing, which could suggest a potential synchronization.

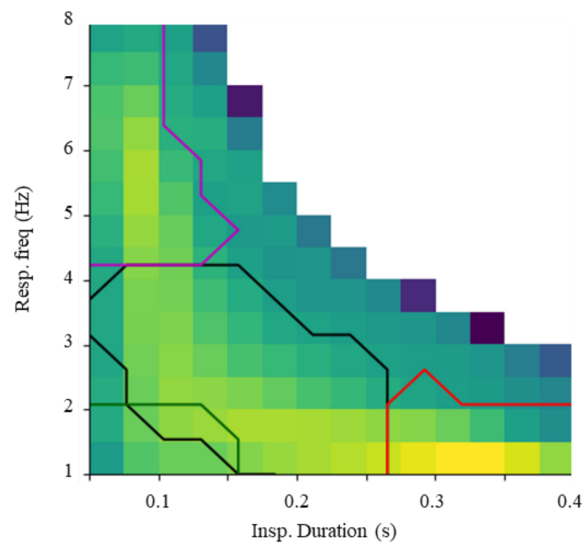


Figure 29 : Inspiration duration and respiratory frequency 2D distribution in head-fixed preparation. Figure 26 B (60 bins x 60 bins matrices) was recomputed with same bins that following map of firing respiratory modulation (9 bins x 9 bins matrices).

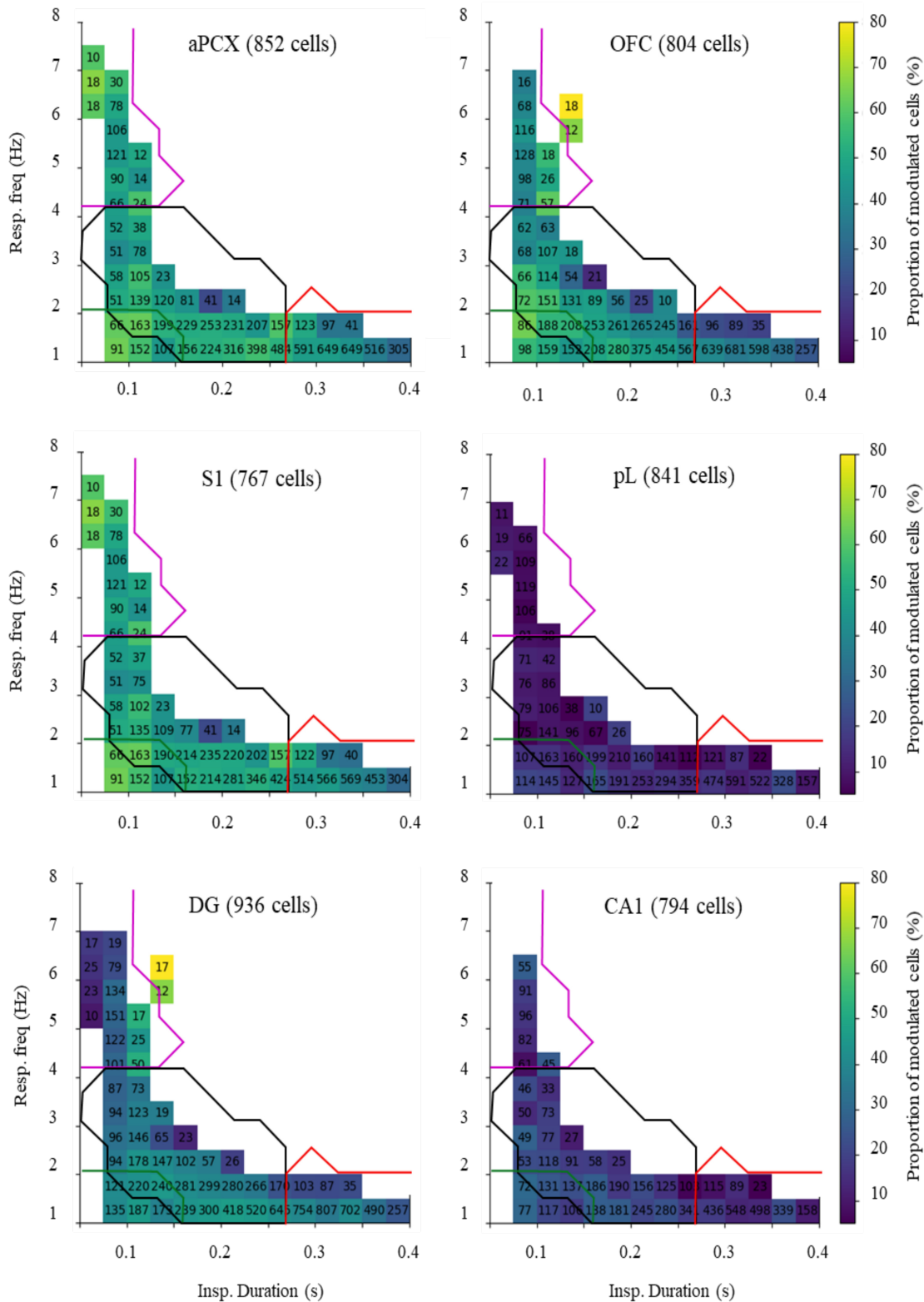


Figure 30 : Probability of respiration-modulated cell firing as a function of inspiration duration and respiratory frequency. Color of each bin represents the percentage of cells displaying respiratory modulated firing over the number of cells detected in this bin. Numbers correspond to the number of detected cells in each bin. Total number of cells is specified next to area's name.

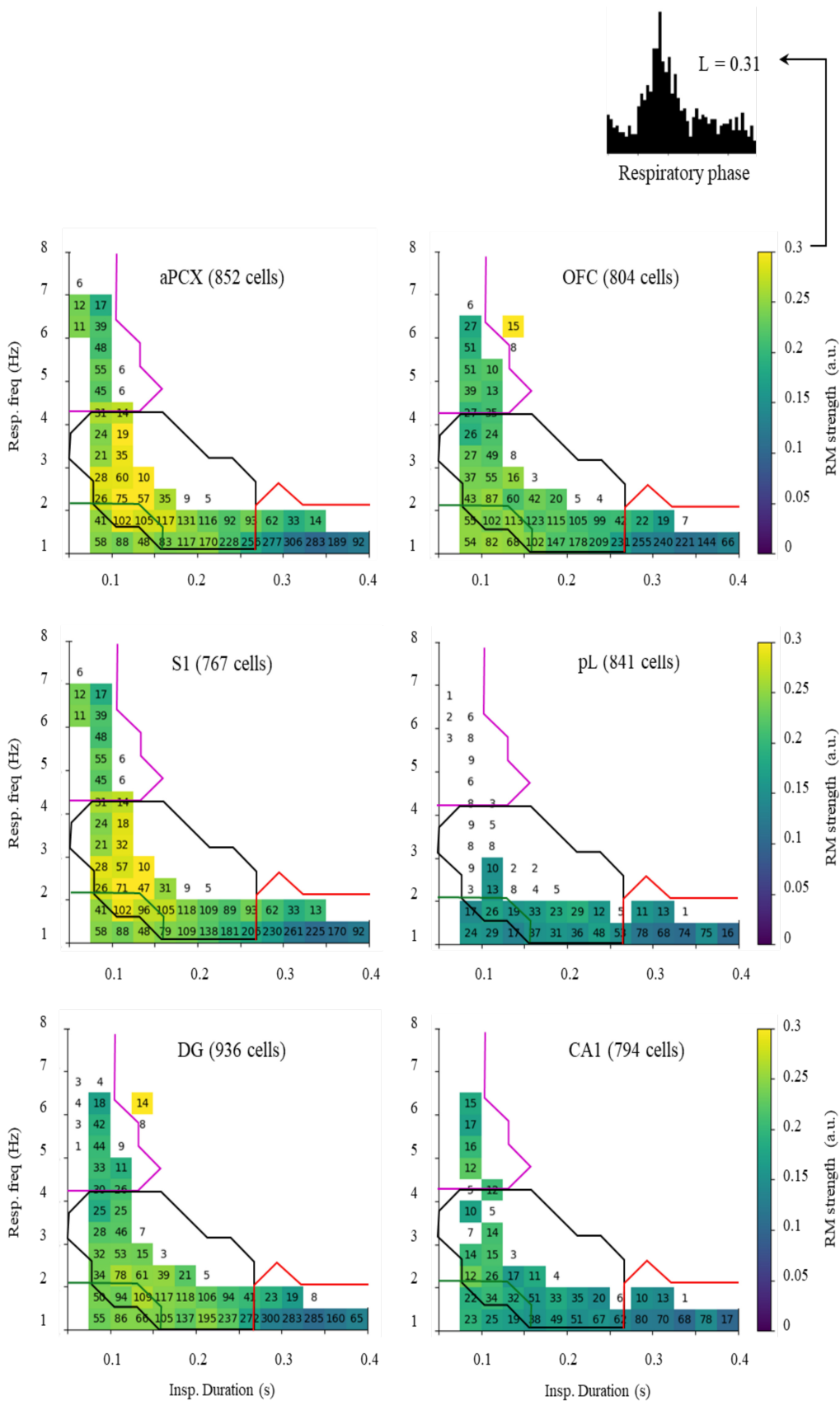


Figure 31 : Strength of respiration- modulated cell firing as a function of inspiration duration and respiratory frequency. Color of each bin represents the average length of mean vectors from modulated cell. To illustrate color scale, an example of histogram for which mean vector length was 0.31 (top right). Numbers correspond to the number of modulated cells in each bin. Total number of cells is specified next to area's name.

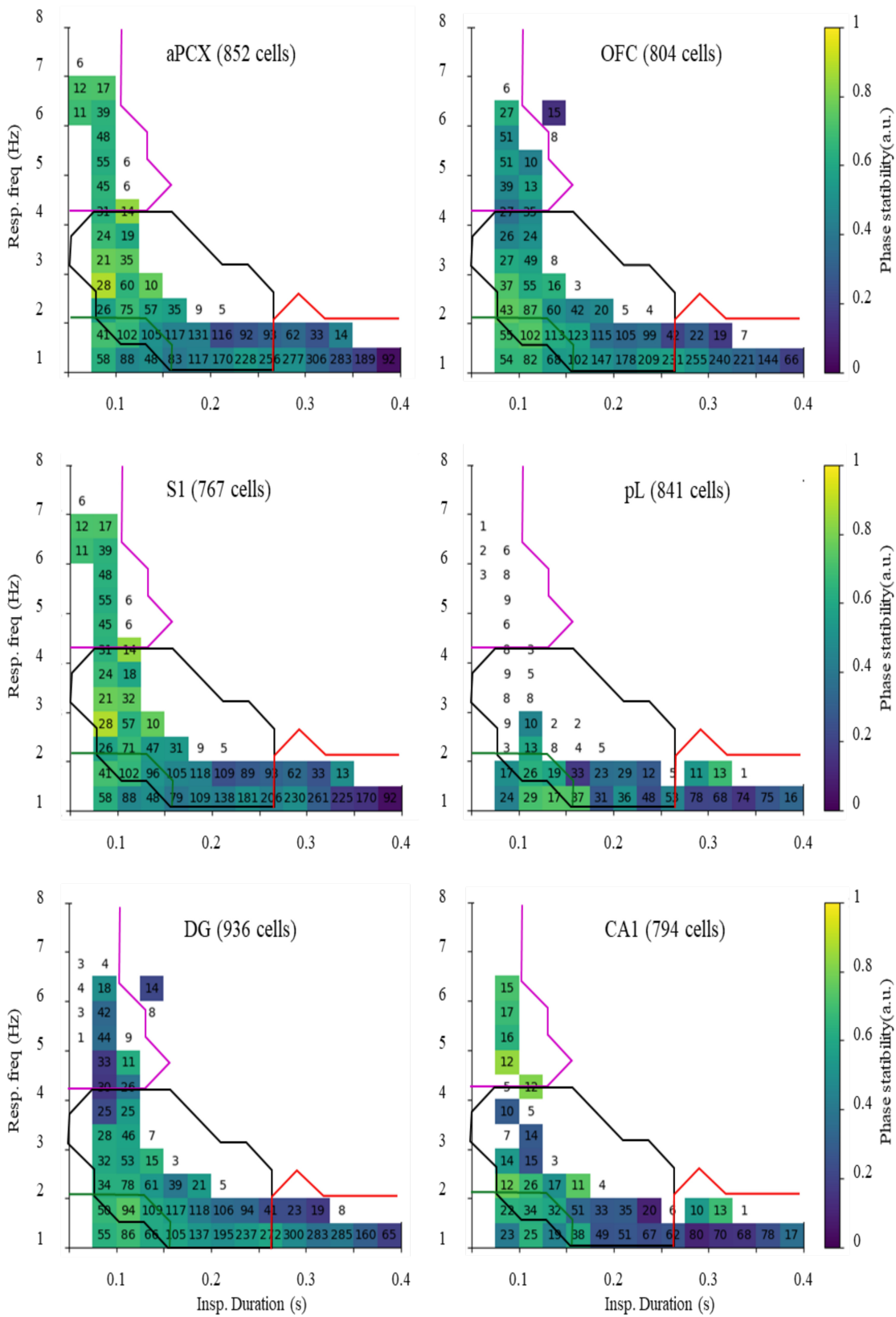


Figure 32 : Preferred-phase stability of respiratory modulated cell firing as a function of inspiration duration and respiratory frequency. Color of each bin represents the mean vector length of cell preferred firing phases. Numbers correspond to the number of modulated cells in each bin. Total number of cells is specified next to area's name.

### 3.2.4. Conclusion and perspectives

In conclusion, gross comparison with freely moving preparation did not evidence major impairment of respiratory modulation in the head-fixed rat. Respiration regimen between both preparations were close. However, sniffing was slower, putative sleep presented longer inspiration and quiet waking could present periods with extremely short inspiration (putative discomfort). Respiratory modulation of low frequency LFP presented important similarity with freely moving. Namely, quiet waking was associated with a wide and important LFP-respiration coupling. During sniffing, only olfactory (here aPCX) and anterior (here OFC and pL) areas showed LFP-respiration coupling. Coupling was greatly reduced during sleep. These observations showed the head-fixed preparation I developed was relevant to study brain-wide respiratory modulation. However, a more precise comparison would be necessary. About spiking behavior, it seemed that quiet respiration (respiratory frequencies from 1.5 to 3 Hz, and inspiration durations from 0.1 to 0.15 s) maximizes the strength of respiratory modulation. This strength tended to be associated with stable preferred respiratory phase of firing.

This dataset is quite new, and as previously mentioned, presented analysis were only preliminary. I will now detail what further analysis is planned. In first instance, we need to properly score brain states. To do so, we will use LFP and respiratory signals. Then, we will properly compare this head-fixed setup with sleeping literature to ensure animals did not present anomalies in sleep/wake cycle, suggesting they were not comfortable. Yet, during its PhD, Damien Gervasoni showed head-fixed and freely moving displayed similar sleep (Gervasoni, 2000). Since Damien himself taught me how to proceed with rats restraining, we could expect similar results. Finally, we will compare and quantify difference in brain-wide LFP respiratory modulation with freely moving. In low frequency band, have RRo the same occurrence for the common areas? In high frequency band, do I observe the same beta, gamma<sub>1</sub>, 2 and 3 than I observed in the freely moving prep? Then, we should be able now if head-fixed preparation was a good choice to study respiratory modulation.

Since we expect the respiratory rhythm to be a long-range communication rhythm, following cascade should be observed: respiratory rhythm should induce RRo in low frequency LFP, which modulates amplitude of high frequency LFP oscillations, and finally, phase of high frequency LFP should modulate assemblies' firing. Therefore, we will get interest in high frequency LFP. We plan to detect cycle-by-cycle high frequency oscillations, and precisely extract their phases. Therefore, we will tackle the existence of such cascade if spikes phase-lock high frequency oscillations, which themselves phase-lock RRo.

The ultimate objective of this dataset is to study assembly formation. First, we need to improve spike sorting. Discussions with Samuel Garcia, our expert in spike sorting and developer of SpikeInterface and Tridesclous, led to the observations, that, currently, no good spike sorter exists. Benchmarks revealed that all sorters have weaknesses and assets. A possibility to approach truth would be to use several existing sorters with complementary assets. However, this idea is for now only idealistic. Short term and concrete solutions to improve spike sorting consist in manual curation, which I will shortly go into it. In addition, to cluster curation, I need to finish microscope observations of brain slices, to ensure my area of interest have been successfully targeted.

Finally, we need to detect neurons assemblies. To do so, I plan to detect neurons which fire within a time window compatible with assembly, namely 0-15 ms. Python and Matlab scripts already exist for such detection, I will use them to extract part of code I am interested in. Then, I will investigate whether these assemblies can be modulated by respiratory rhythm. As showed in 3.2. Role of the respiratory rhythm in supporting the long-range communication in the brain, during QW low and high frequency LFP get synchronized to respiration simultaneously in distant brain areas. Therefore, if we observe respiration-related cell assemblies, we expect to observe them mainly during QW. If we are right, which functions could support such respiration-mediated communication,

especially during quiet waking, a state corresponding to a nothing-doing state? Though, as demonstrated by sleep literature, it not because the animal does nothing in appearance that the brain does not work. An interesting study on human cognition and respiration could give a possible perspective. Authors tested consolidation of olfactory hippocampal-dependent memory with a protocol involving a step of odor presentation, a 1h-step of consolidation and a final step of odor recognition (Arshamian et al., 2018). Authors compared two groups, one group could only breath through the nose during the 1h consolidation, and the other group could only breath through the mouth. As a result, nose-breather displayed better recognition memory than mouth-breather. We could interpret these results as follow. During the hour of consolidation, subjects waited in a room, where there was nothing to do, which could be assimilated to quiet waking. In case of mouth-breather, respiratory drive is greatly decreased (Biskamp et al., 2017; Ito et al., 2014; Yanovsky et al., 2014; Zelano et al., 2016). In the present study, respiration-mediated binding between olfactory areas and hippocampus was probably weakened. Authors proposed the same explanation in their discussion: “Although this study did not measure brain oscillations, we propose that one possibility for the reduction in  $d'$  ( $d'$  is the index used by the authors to measure recognition index) could be the decreased communication between sensory (i.e., olfactory bulb) and memory networks (i.e., hippocampus) during consolidation when air is redirected to the mouth” By extrapolation, I suggest that decreasing respiratory drive during quiet waking should alter wakefulness consolidation. Like slow waves of sleep reinforce memory consolidation after wakefulness experience (Rasch and Born, 2013), I suggest than respiratory drive associated to quiet waking reinforce memory consolidation of immediate experience. Therefore, we could imagine a memory system in several steps. Immediately after an experience, brains pre-consolidate memory during quiet waking and with respiratory rhythm. Then, when the animal falls asleep, sleep slow waves take the relay for a more intense and long-lasting memory consolidation during SWS (= NREM).

## **4. Discussion**

## 4.1. Respiratory modulation and respiration monitoring

When studying respiratory modulation of neural activity, monitoring of respiration is mandatory. Monitoring can be direct, through measurement of air flows or air pressure variations. Other devices measure respiration indirectly through chest extension or nasal air temperature (expired air is warmer than inspired one). In literature, one can observe air flow captors in front of nostril (used for my intracellular and head-fixed studies, and Buonviso et al., 2003; Cenier et al., 2009; Courtiol et al., 2011a, 2011b), thermistor in front of nostril (Chi et al., 2016; Ito et al., 2014) or intranasal (Biskamp et al., 2017; Chi et al., 2016; Liu et al., 2017; Lockmann and Tort, 2018; A. B. L. Tort et al., 2018; Zhong et al., 2017), and plethysmograph (freely moving study of Girin et al., 2021; Tort et al., 2021). The choice of the device is important because, on the one hand one should favor direct measurement to avoid artifacts, on the other hand one should limit invasive method not to alter the phenomenon of interest. In particular, since brain-wide respiratory modulation seems to strongly depend on respiratory regime (Girin et al., 2021), one really do not want to interfere with the mechanics of respiration. Therefore, when one study respiratory modulation I would recommend 1) to favor device allowing to monitor time and amplitude dynamic of respiration. It would grant access accurate description of respiratory regime, 2) to limit invasive device. Implantation of intranasal thermistor induces inflammation in nasal cavity, which should certainly cause trouble to air flows. Similarly, the use of head-fixed preparation slightly alters respiratory regime, so this preparation might not be the best to study respiratory modulation. As discussed in the study 3, it would be necessary to properly compare respiratory modulation properties in freely moving and head-fixed preparations.

Nowadays, the best solution to monitor respiration is the plethysmography. It consists in a box of small volume, in which air pressure is isolated from the atmosphere. Therefore, variation of air pressure within the airtight chamber is mainly due to lung inflations and deflations. Displacements of the animal induce air movement, but it does not create vacuum or volume expense, hence it poorly affects pressure signal. Consequently, positive and negative pressure values reflect respectively inspiration and expiration, hence temporal dynamic of respiration is easily extracted. Additionally, pressure values correlate with breathed volume ( $PV = nRT$ , P: pression, V: volume, n: Avogadro constant, R: perfect gas constant, T: temperature), therefore amplitude dynamic is accessible. Most importantly, the device monitors absolute values of pressure variation, consequently these values are comparable between recording sessions (for a same animal) and between animals. The main issue with plethysmography is that airtight chamber is small. As the chamber is sealed, it imposes the use of wireless recording system. Indeed, a small volume enable a better monitoring of air pressure variations. Therefore, possible behavioral tasks are limited. For example, it is not possible to test spatial navigation. Though, former student of the lab developed olfactory Go-no-Go tasks (Courtiol et al., 2014, 2011b). So, it not impossible to do behavior, but there are spatial limitations. These two constraints probably explain why plethysmography is not much used in the field.

Recently, respiration monitoring device emerged, and has a great potential. The principle of respiration monitoring is not new, it is just a piezo belt around the chest. However, for rats (and rats only) developers (Etisense) made two great enhancements:

- The belt is sewn on a jacket. Front of the jacket has three holes, one for the head and two for the fore legs. At the back of the jacket there is one hole for the trunk. Contrarily to classic belt, piezo captor stays in place when the rat moves.
- The device is wireless and is not so big. Therefore, animal can freely walk, and experimenter does not worry for the wires being chewed. Consequently, there is no spatial limitations for behavioral tests with such device.

I assisted to a demonstration, and the quality of the signal is striking. Temporal dynamic (inspiration and expiration timing) could easily be extracted. In addition, Etisense' algorithm computes an estimation of breathed volume. It would be interesting to test whether this estimation is reproducible between recording sessions and between animals. If it the case, it means that we could follow temporal and amplitude dynamics

in freely moving rats without spatial restrictions (problem of plethysmography) and without being invasive (problem of intranasal thermistor). Icing on the cake, device includes an electrocardiogram monitoring, which gives additional information about animal's physiology. However, there is no input or output to enable a synchronization with electrophysiological signal, which constitute a major issue. Consequently, for now, the device is useless for studies on respiratory modulation of the brain. Additionally, device generate an inductive field, and we don't know if it could parasite LFP recordings. Nonetheless, we will keep an eye on this promising device.

When I conceived the head-fixed setup, I had to choose the respiration monitor device. At that occasion, we tried the Etisense' jacket. But since, synchronization was impossible with LFP, we rapidly gave out this solution. We tried pressure sensor placed between animal's stomach and hammock. However, animal was free enough to remove the sensor. Plethysmography was not possible because the whole setup (stereotaxic apparatus and micromanipulator) was too voluminous. We did not envisage to implant thermistor in the nasal cavity not to burden the preparation too much. The best choice was then to use a sensor in front of the nostril. We chose an airflow sensor rather than a thermistor, because it offers a direct measure of respiration. Although nasal sensor made habituation tougher, it was the best solution for respiration monitoring.

## **4.2. Respiratory drive: One respiratory phase to bind them all (the brain areas)?**

We expect the respiratory rhythm to be a common temporal reference to numerous brain areas. To achieve such function, one hypothesis was that all neurons could be able to commonly undergo hyperpolarization and depolarization variation at respiratory frequency. Jerath et al., 2015 posit that membrane potential slightly hyperpolarizes during each inspiration and slightly depolarizes during each expiration, by way of slowly adapting stretch receptors and oxygenation and that such depolarization could be a source of respiratory drive. Conversely, based on following evidences, we were rather expecting depolarization during inspiration. Perception of pain on the hand decreases during expiration and increases during inspiration (Iwabe et al., 2014). This process has no link with olfaction or respiration. Yet, a depolarization during inspiration and a hyperpolarization during expiration in the pain sensory system could explain such difference in the perception. In addition to sensory processes, cognition seems also improved during inspiration. Fear expression on human faces were better recognized during inspiration (Zelano et al., 2016). Authors of the same study also tackled memory encoding and retrieval. In a first step of encoding, authors presented pictures. Some pictures were presented during inspiration and others during expiration. Few minutes later, authors presented another set of pictures. Some pictures were already presented during encoding, others were new. During this retrieval phase, pictures were presented during inspiration or during expiration. Results showed memory accuracy was higher for pictures retrieved during inspiration. However, respiratory phase had no significant influence during encoding. Another group studied relationship between respiratory phase and human cognitive performance in three non-olfactory tasks (Perl et al., 2019). One lexical recognition task consisted in the presentation of a series of letters, subject should answer if series corresponded to a real word or not. One mathematical task for which subjects had to tell if equation was correct or not. And one visuospatial task for which subjects had to tell if presented shape could exist in nature. In a first experiment, subjects were let free to initiate the task. It turned out that subjects spontaneously initiated task at inspiration. In a second experiment (with other subjects), start of trials was imposed and was triggered either in inspiration or in expiration. Visuospatial tasks showed higher performance when performed in inspiration rather than in expiration. We could interpret these results as follow: when possible the brain initiates working in inspiration, which corresponds to the moment the brain is the readier to work. This brain readiness could be explained by a brain-wide depolarization during inspiration. Indeed, if all neurons

undergo simultaneously a slight depolarization during inspiration, one can imagine formation of cell assemblies is easier and thus communication gets more efficient. However, my intracellular study in anesthetized rats goes against this Jerath's hypothesis since we showed depolarization did not occur with a consistent respiratory phase, even within a single area. As an example, for one hippocampal cell with hyperpolarizing current, I even observed phase-locking could change over time. Figure 33A showed depolarization occurred during expiration, while 60 seconds later depolarization phase-locked to inspiration. However, this intracellular study was led on anesthetized animals. Would it be confirmed in conscious animal? This is what we plan to tackle with head-fixed preparation.

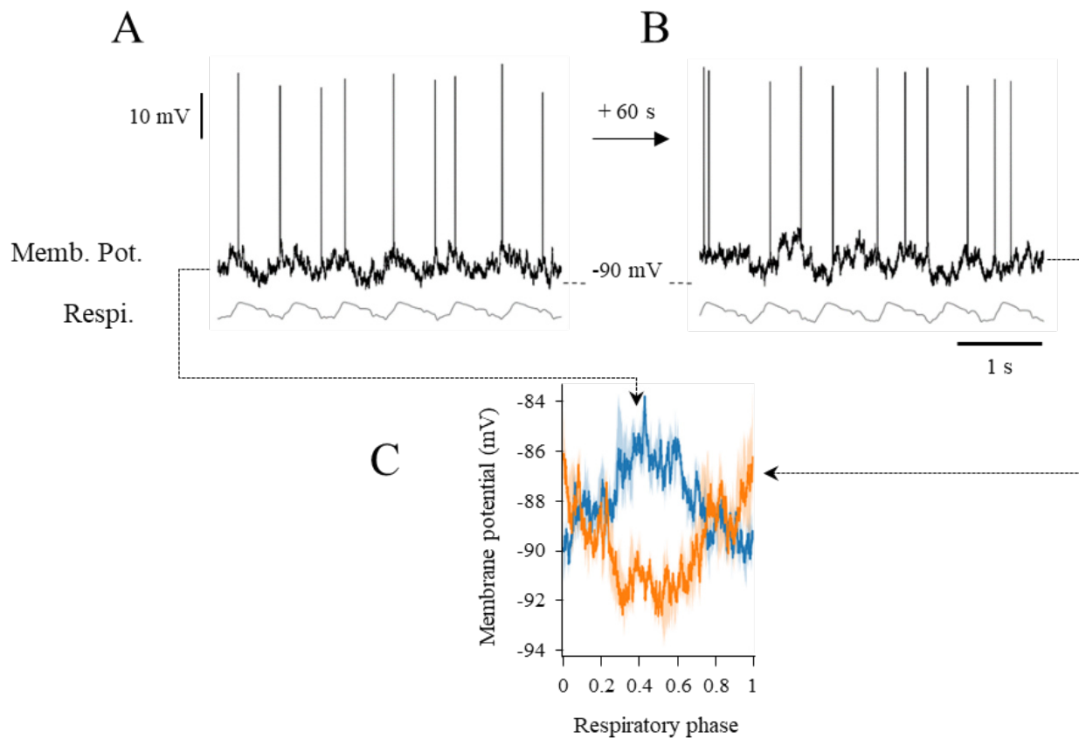


Figure 33 : Radical shift of RRo phase-locking to respiration. A. Raw membrane potential (top) and respiration (bottom) signals. Inspiration is down, expiration is up. Vertical scale bar: 10 mV, horizontal scale bar: 1s. B. Signal of the same cell than in A, but 60 seconds later. C. Respiration-triggered averaged membrane potential. Signal of the six respiratory cycles presented in A and B were averaged. Blue, respectively orange, curve represents the average from A, respectively B. Shaded areas represent SEM. Inspiration goes from 0 to 0.4, expiration goes to 0.4 to 1

Similarly, mitral and tufted cells, principal neurons of the olfactory bulb, displayed also depolarization at variable respiratory phases (Ackels et al., 2020; Briffaud et al., 2012) under anesthesia, which was also observed in head-fixed mice (Ackels et al., 2020). Virginie Briffaud, a former PhD student of Corine Amat precisely studied respiratory modulation of membrane potential waveform in the olfactory bulb (Briffaud et al., 2012). Although she did not focus on respiratory phase, raw traces presented in figures 1 and 10 of the Briffaud et al., 2012, showed cells with depolarization locked either to inspiration or to expiration. Contrarily to my non-olfactory neuron, she did not observe cells which phase-shifted their phase-locking to respiration under spontaneous condition (no odor). A recent study went further by showing these differences in phase-locking could be due to different cell populations (Ackels et al., 2020). Mitral cells displayed depolarization during inspiration, while tufted cells displayed depolarization during expiration (Ackels et al., 2020). Consequently, each population has its own respiratory phase. In parallel, high frequency LFP oscillations in the olfactory system displayed a similar segregation throughout respiratory phase. Indeed, gamma burst occurs just after inspiration and beta burst during expiration (Buonviso et al., 2003). Consequently, the

end of inspiration is characterized by LFP gamma oscillations and depolarization of mitral cells, while expiration is characterized by LFP beta oscillations and tufted cells depolarization. On this basis, one could hypothesize that within a respiratory cycle parallel information could be coded by distinct populations (here mitral vs tufted cells), at distinct respiratory phases (late inspiration vs expiration) and at distinct frequency (here gamma vs beta). Therefore, respiratory modulation in the olfactory system seems to enable a multiplexing of information.

With these arguments, I could interpret the variability of depolarization's phase I observed in my intracellular study as a clue indicating respiratory rhythm could extend multiplexing of information to the rest of the brain. But is there other evidence in literature? Since respiratory modulation literature rely mostly on LFP, to evidence multiplexing we should look for brain areas displaying phase-locking with several high frequency LFP oscillations. Other authors commonly reported a strong phase amplitude coupling between 70-90 Hz oscillations and RRo in most brain areas (Biskamp et al., 2017; Ito et al., 2014; Karalis and Sirota, 2018; A. B. L. Tort et al., 2018; Zhong et al., 2017). Less recurrently phase amplitude coupling was also reported in 20-40Hz (mice' baso-lateral amygdala, nucleus accumbens: Karalis and Sirota, 2018), 40-50 Hz (mice' insular cortex, amygdala: Tort et al., 2018), 30-50 Hz (cat's OB, PFC, S1, V1, parietal cortex: Cavelli et al., 2020). However, these studies showed most areas displayed phase amplitude coupling with a single high frequency band, thus my hypothesis does not seem to be supported by others. On the contrary, my phase-amplitude coupling analyses in freely moving (see *Figure 23*) and head-fixed datasets (data not shown) revealed at least two distinct high frequency bands modulated by respiratory rhythm in each brain area. This difference could have the following explanations. 1) To compute my phase amplitude coupling map I used only respiratory cycles displaying RRo, therefore these cycles present in low frequency LFP a strong respiratory modulation. Consequently, I may have selected moments of strongest respiratory modulation, which highlight the complete range of high frequency coupling. 2) Contrarily to others, I extract respiratory phase directly on respiratory signal and not on a Hilbert transform of LFP signal (previously filtered in respiratory frequency range). I may have fewer jitter in the estimation of respiratory phase. Therefore, I should be able to detect finer phase-amplitude coupling. 3) Most of other authors used mice, therefore difference can rely on species. Though, whatever the reason why I observed multiple phase-amplitude couplings, I should lead further investigations to consolidate the multiplexing hypothesis. Do other (than Gamma2) high frequency bands also mediate cross-area synchronization (like in *Figure 24*)? If so, do they occur at the same respiratory phase or each high frequency band has its own respiratory phase? Complementarily, using the head-fixed dataset I could study relationship between cell assemblies and respiratory phase. Are there also multiple respiratory phases which shape cell assemblies? What would be the relationship between cell assemblies firing and high frequency oscillations?

The hypothesis that respiratory rhythm could support a multiplexing of information is tempting, since it would give a lot of weight to the respiratory rhythm is brain's activity. However, for now it is just a personal hypothesis, which is not supported by current literature.

### 4.3. Does an interaction between slow rhythms exists?

Brain activity consists in a complex imbrication of plenty of rhythms. During these three years of PhD, I only focused on respiratory-related oscillations (RRo). However, this rhythm coexists and competes with other slow rhythms, like theta rhythm and sleep slow waves in rodents. I did not extensively study these two rhythms, so I could not quantify interactions between these two and respiratory rhythm. Though, Tort's lab is used to study RRo and theta rhythm. They showed that all brain areas (at least the fifteen they recorded) showed coherence to both hippocampal theta and respiratory rhythms (A. B. L. Tort et al., 2018). In addition, these two rhythms selectively coupled with distinct high frequency oscillations, namely respiratory rhythm couples with an 80-120 Hz, while theta rhythm coupled with 40-80 Hz and 120-160 Hz gammas (Zhong et al., 2017). Hence, although theta rhythm and RRo coexists in all brain areas, their activities do not compete for synchronizing with high frequency oscillations. In addition, they recorded firing activity in hippocampus (Chi et al., 2016), parietal cortex and medial prefrontal cortex (Zhong et al., 2017). In these three areas, they observed cells which firing exclusively phase-locked theta, other which exclusively phase-locked respiratory rhythm, and a last category of cells which firing phase-locked both rhythms. Consequently, for exclusive cells one could imagine that both rhythms compete, but only one won the race. On the contrary, for cells which simultaneously phase-locked the two rhythms, we could imagine a coupling between theta and respiratory rhythm. This can be explained by a phase-phase coupling between respiratory and theta rhythm (Biskamp et al., 2017). Authors showed that mice expressing fear (hang by the tail) displayed a phase-phase coupling between LFP RRo of prefrontal cortex and hippocampal theta, in a 2:1 ratio (2 theta cycles for 1 respiratory cycle). To be noted, during REM sleep, variations of theta frequency were found to be preceded by variations in respiratory frequency (Tort et al., 2021). Therefore, respiratory rhythm influenced theta rhythm. We could hypothesize that particular respiratory regime could bring theta and respiratory frequencies to be multiple (e.g., ratio 2:1, 3:1), which would facilitate phase-phase coupling. I observed possibly related phenomenon in my intracellular dataset. In HPC (N = 1 cell), S1 (N = 1 cell), and in V1 (N = 1 cell) I observed cellular activities whose bursts (spikes with inter-spike intervals shorter than 20 ms) displayed phase-locking to respiratory rhythm, while single spikes did not. Single spikes could then phase-lock another rhythm, for example theta. These examples suggest that cells firing could simultaneously code two different information.

Very little is known about interaction between rhythms associated to SWS and respiratory rhythm, excepted that sharp-waves and ripples phase-locked to inspiration (Liu et al., 2017). Nonetheless, in my intracellular dataset, I observed in two mPFC cells a potential coupling between slow wave activity and respiratory rhythm. These cells marked me because their firing pattern displayed a very nice respiratory modulation although their membrane potentials were not driven by respiratory rhythm. On the contrary membrane potential displayed slow oscillations (about 1 Hz), but at some moment membrane potential slow oscillation was exactly the half of respiratory frequency (see *Figure 34*). Therefore, action potentials occurring during UP phase of the oscillation were also phase-locked to respiration, but they occurred one out of two respiratory cycles (ratio 2:1, two respiratory cycle for one slow oscillation). Was this a real coupling? Or did it happen by accident?

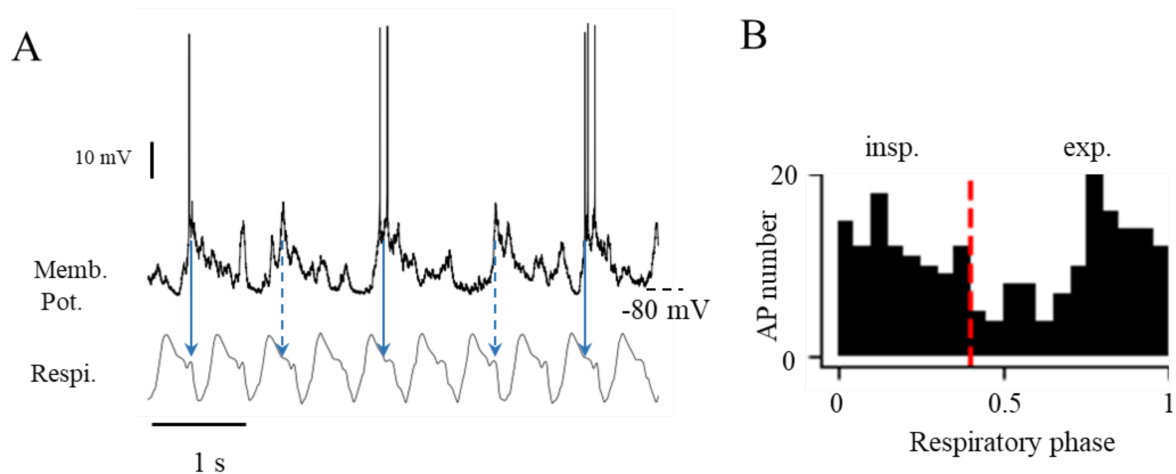


Figure 34 : Interaction between slow rhythm? A. Raw membrane potential (top) and respiration (bottom) signals. Inspiration is down, expiration is up. Full blue arrows highlight where in the respiratory cycle action potentials occur. Dashed blue arrows highlight where in the respiratory cycle depolarization occur, although no action potential was triggered. Vertical scale bar: 10 mV, horizontal scale bar: 1s. B. Respiration-related firing histogram associated to slow oscillations observed in A. Although, membrane potential did not oscillate at respiratory frequency, firing displayed respiratory modulation.

Further work is necessary to study interactions between slow rhythms (theta, sleep slow waves and respiratory rhythm). I would not be surprising that interaction between slow rhythm exists. Phase-phase coupling, presented above, is one possibility to coordinate slow rhythms. I do not know what the implications of such cross-talks could be, but I will definitely look for such interactions in the head-fixed dataset. One hypothesis, with example of theta and respiratory rhythms coordination, could be the following: In its brain-wide study, Adriano Tort showed influence of respiratory rhythm was strong in anterior areas and gradually decreased from anterior to posterior (A. B. L. Tort et al., 2018). Theta rhythm displayed the opposite spatial distribution. In such conditions, one could imagine that a respiratory rhythm could shape preferentially an anterior network of areas, while theta rhythm shape a posterior one. Interaction between respiration-related and theta oscillations could facilitate anteroposterior information transfer, hence a facilitated brain-wide information treatment. Another possibility will consist in considering the range of coordinator rhythms (theta rhythm, sleep slow waves, respiratory rhythm) as a referral system. Depending on the drive (theta rhythm, sleep slow waves, respiratory rhythm), a neuron could be involved in different assemblies, and therefore participate in communication with different brain areas. In addition, the drive would be adapted to behavioral needs.

#### 4.4. Origin and propagation of respiratory modulation?

The rediscovery of brain respiratory modulation has been accompanied by hypotheses about its origins. These origins can be divided in peripheral and central categories.

##### Peripheral origin.

Although respiratory rhythm is generated by brainstem nuclei, the mechanics of ventilation generates airflows and body movements which are perceived by sensory neurons. Respiration is then perceived i) in a proprioceptive manner by stretch-sensitive neurons in lungs, diaphragm, chest, ii) in an interoceptive manner by brain and systemic chemoreceptor ( $O_2$  and  $CO_2$ ), and iii) in an exteroceptive manner in the nasal cavity by olfactory sensory neurons (chemo and mechanoreception: Grosmaître et al., 2007)

*Body-wide sensing of respiration.*

In Jerath et al., 2015, authors proposed several means for the brain to sense respiration. Stretch receptors in lungs, diaphragm, and chest perceive the advancement in respiratory cycle, which information goes up to the brain (Jerath et al., 2015). Additionally, respiration-paced variations in blood concentration of O<sub>2</sub> and CO<sub>2</sub> can be perceived by chemoreceptors in brainstem and carotids (Jerath et al., 2015; Neubauer and Sunderram, 2004). All these respiration-related information reach the integration center of autonomic nervous system, namely the nucleus tractus solitarii (Jerath et al., 2015). Then, nucleus tractus solitarii could certainly spread a brain-wide respiratory modulation. Although these hypotheses are very likely to impact respiratory modulation of the brain, there are no way to test this hypothesis, yet. Indeed, this mechanism has extremely distributed (lungs, brain, carotids) and varied (mechano and chemo receptors) sensors, thus it is difficult to study.

#### Nasal pathway.

Currently, the nasal respiration is the most supported hypothesis for the origin of brain-wide respiratory modulation. Briefly (for more detail, see 1.3.2 The possible routing of Respiration-related oscillations across the brain), respiratory rhythm represents more than a simple modulation in the olfactory system, activity of olfactory system is shaped by respiratory rhythm. In addition, olfactory system has wide projections to the rest of the brain (frontal neocortices, limbic system, thalamus), which are supposed to take parts in propagation of respiration-paced inputs. In addition, this nasal pathway can easily be manipulated (downregulation by tracheotomy(Ito et al., 2014; Yanovsky et al., 2014), DREAD-mediated silencing of olfactory bulbs (Liu et al., 2017), and upregulation by air puff (Ito et al., 2014), optogenetic stimulation of olfactory bulb (Moberly et al., 2018)). Interestingly, cutting nasal pathway greatly weakens respiratory modulation from the brain, nonetheless it does eradicate it. Therefore, nasal respiration plays a major, but not unique, role for brain's respiratory modulation.

To argue in favor of the importance of the nasal pathway, during my intracellular study, I delivered odors to the animal when I was recording a cell. The idea was to boost nasal

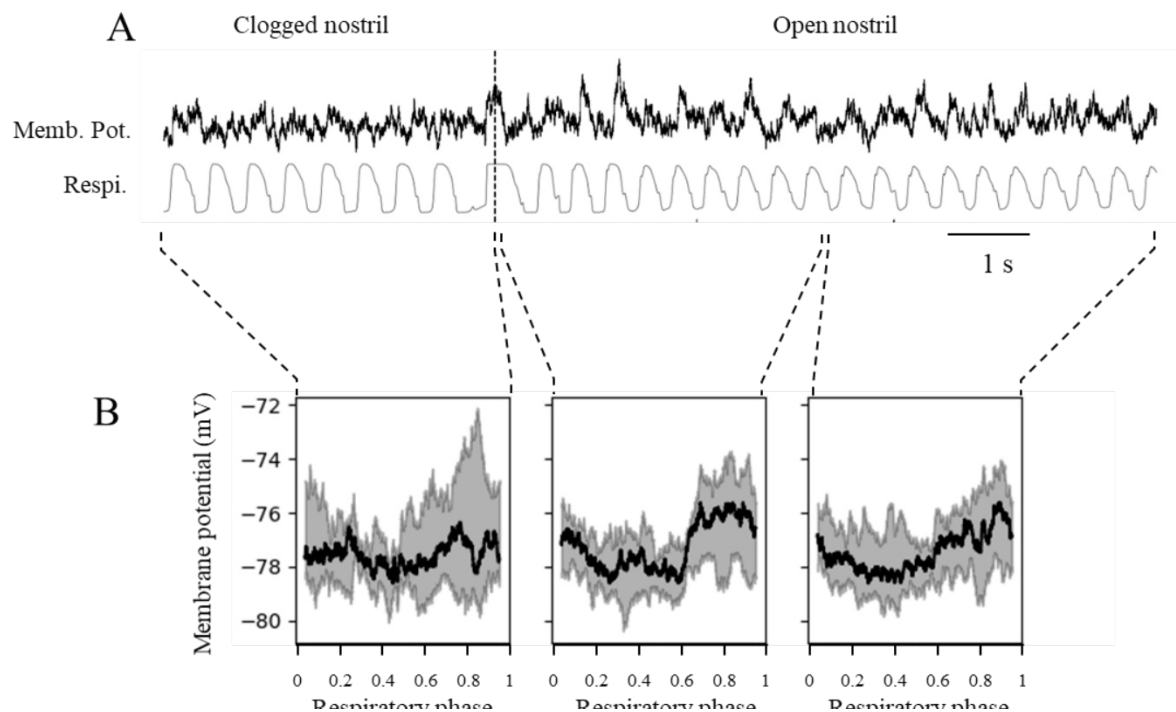


Figure 35 : Nasal respiration influences the brain deep to membrane potential oscillation. A Raw membrane potential (top) and respiration (bottom) signal around nostril reopening. Vertical dashed line indicates nostril reopening. Left to the dashed line, nostril is clogged. Right to the dashed line nostril is open. Horizontal scale: 1s. B. Respiration-triggered average membrane potential prior to nostril reopening (left), at reopening (middle) and ten respiratory cycles after reopening (right). Black line corresponds to median signal. Grey shaded area corresponds to sem of signal.

pathway with natural stimulation. Unfortunately, this protocol did not lead to strong effects. This can be explained by the fact that an odorant stimulation during anesthesia is maybe not strong enough to activate non-olfactory regions. Additionally, it has been showed that there is a olfactory gating during slow wave activity during urethane anesthesia, cortical olfactory neurons were less responsive to odors (Murakami et al., 2005). We envisaged to perform tracheotomy, but we faced several issues. With a simple tracheotomy (no more nasal respiration, not reversible), if we did not observed traces of respiratory modulation, we could not know if the recorded cell lacked nasal inputs or if the cell was just not sensitive to respiratory rhythm. Therefore, we should have use reversible tracheotomy. But we worried about manipulating close animal's head while a cell was impaled. We chose an alternative method. For some cells, we plugged one nostril while the other was used to monitor respiration (see *Figure 35*). Results were very interesting but not reproducible. For some cells, when nostril (left) was plugged, membrane potential (left hemisphere) RRo disappeared, while it rapidly reappeared at nostril re-opening (see *Figure 35*). Unfortunately, we lacked a control to ensure nostril was sealed, we should have put an electrode in the right olfactory bulb to record LFP. If LFP got flat, we would have been sure nostril was hermetically sealed. We think that the quality of our obstruction explains the poorly reproducible but interesting results.

With the freely moving dataset, we used CO<sub>2</sub>-enriched air to disturb respiratory regime, and consequently nasal airflows. This method was efficient and non-invasive, but it did not uncouple central from nasal respiration. Therefore, we could not disentangle the origin of respiratory modulation. We thought to add to the freely moving and head-fixed preparations, a DREADD-mediated inhibition of the olfactory bulb. We would have proceeded as follow: At least one month before first recording, we should have infected both olfactory bulbs with Adeno-associated Virus containing inhibitory DREADD receptor sequences. Then we should have waited for viral expression (about one month). Then, at animal's implantation (contention implant or telemetry implant), one would have added bilateral LFP electrodes in olfactory bulb. These LFP would have enabled to monitor the silencing of nasal pathway when Clozapine N-oxide would have been injected.

### Central origin

Although respiration can be sensed by the body (exteroception, interception and proprioception), the respiratory rhythm originates from rhythmic activity of brainstem nuclei. As depicted in 1.2.1 – Respiratory rhythm generation, respiration generator is composed of several nuclei. Here, I will focus on the most described nucleus, namely the preBötzing complex which paces inspiration. In addition to its respiratory functions, preBötzing complex has been shown to play a role of common clock for orofacial movements (whisking, chewing, licking) during exploration (Kleinfeld et al., 2014). Briefly, orofacial movements synchronize to respiration during exploration. In parallel, neurons of preBötzing complex synapse on motor nuclei (in the brainstem) involved in these orofacial movements. It was proposed the inspiration-paced inputs of preBötzing complex forced the synchronization of these movements (Kleinfeld et al., 2014). This demonstration of respiratory rhythm being a coordinator is extremely precise and convincing, but it highlights a very local coordination since observed projections stayed in the brainstem. Hence this study could not explain a large-scale respiratory modulation of the brain orchestrated by the preBötzing complex. However, there are at least two routes which could enable a larger spread of this respiratory modulation. First, during exploration orofacial movements (including whisking) synchronize with respiration. Therefore, orofacial sensory neurons convey respiration-paced inputs to the thalamus, then to the primary somatosensory cortex (including barrel field), and then association cortices. Secondly, preBötzing complex projects, synapses and positively regulates the locus coeruleus (Yackle et al., 2017), a noradrenergic nucleus which projects to the whole brain. In addition, knocking down a very specific sub-population of preBötzing neurons projecting to locus coeruleus, does not affect respiration parameters but strongly affects activity of mice. Mice displayed much more quiet waking (Yackle et al., 2017). Therefore,

locus coeruleus could be a relay enabling an amplification and a spreading of central respiratory modulation. If so, one can wonder what would look like the activation map of modulated brain areas? Does it provide a brain-wide ON/OFF respiratory modulation? Such case would be possible if locus coeruleus projections were uniform. Or on the contrary, is there a fine spatial control? Such case would be possible if locus coeruleus presented topographic projections. For example, the ventral part would project to anterior brain areas, while dorsal part projects to posterior brain areas. Then one could imagine, that depending on which part of locus coeruleus is activated by preBötzinger complex, different brain areas could be bound by respiratory rhythm. Recent literature suggests locus coeruleus presents a modular organization, where each module projects to different targets (Chandler et al., 2019), which favor the hypothesis of a fine spatial selection of respiratory modulation spreading. Currently, evidences support the hypothesis that locus coeruleus could spread a respiratory modulation from inspiration generator (preBötzinger complex) via noradrenergic neuromodulation (Yackle et al., 2017). Therefore, it would be interesting to study relation between neuromodulation and respiration. Other neuromodulation centers could also be involved.

For now, we know that nasal respiration is the main source of the brain's respiratory drive. However, it is not the only pathway enabling spreading of respiratory modulation to the whole brain. Nonetheless, no other pathways have been identified, yet.

#### 4.5. General conclusion

The ensemble of results I produced are in line with the way of thinking which attempts to give credit to respiratory rhythm in brain's functioning. Although considered for a long time as an annoying artifact, respiratory rhythm is now proposed to enable long-range communication between brain areas. Since 2014, accumulating number of studies argued in favor of such function. Respiratory rhythm drives low frequency of numerous brain areas and is capable of cross-frequency coupling with high frequency oscillations. In addition, I brought evidence supporting cross-areas synchronization mediated by respiration rhythm. Contrarily to other coordinator rhythms (theta rhythm, sleep slow waves), respiratory rhythm is a vital function, therefore it never stops. For this reason it was proposed to be global clock, common to all neurons (Buonviso et al., 2006; Fontanini and Bower, 2006; Kleinfeld et al., 2014). If we were right, we could wonder why evolution selected respiratory rhythm as the brain clock. Attributing a new function to an already existing rhythm is economically advantageous. Then, since it is a vital function, it is secured rhythm. The respiratory rhythm is also adapted to physiology, which has two consequences. Respiration is adapted to the animal (generally the bigger the animal, the slower the respiration), and respiration adapts to physiological needs (physical effort, rest, sleep) Finally, as described previously, at least two clocks, one nasal and an unidentified one, exist in the brain. Therefore, it is a robust system.

For us, humans, why is it interesting to study respiratory modulation of the brain? The respiratory rhythm is the only rhythm that we can voluntarily control. Coupled with the fact that the way of breathing can affect brain activity (Girin et al., 2021; Piarulli et al., 2018), breathing could represent a tool to consciously act on the brain. Although virtue of respiration on mental health is known since a lot time, and put into practice in Pranaya yoga (Jerath et al., 2006; Zaccaro et al., 2018), neural mechanism began only to understand. Consequently, if respiratory rhythm constitutes indeed an important means for neural communication, one can wonder to what extend respiratory disease (*e.g.*, sleep apnea) impact brain activities at long term. Complementarily, since nasal respiration seems fundamental, the same question for olfactory disorders whether permanent (congenital anosmia) or temporal (viral anosmia due to cold or coronaviruses) could be asked. A more positive view would propose reparatory and olfactory exercises as a potential cure for mental health (Zaccaro et al., 2018) and why not for neural disorders like epilepsy. Calming neurons through a calm nasal respiration?

## **5. Bibliography**

- Abeles, M., 1982. Role of the cortical neuron: integrator or coincidence detector? *Isr. J. Med. Sci.* 18, 83–92.
- Achermann, P., Borbély, A.A., 1997. Low-frequency (<1Hz) oscillations in the human sleep electroencephalogram. *Neuroscience* 81, 213–222. [https://doi.org/10.1016/S0306-4522\(97\)00186-3](https://doi.org/10.1016/S0306-4522(97)00186-3)
- Ackels, T., Jordan, R., Schaefer, A.T., Fukunaga, I., 2020. Respiration-locking of olfactory receptor and projection neurons in the mouse olfactory bulb and its modulation by brain state. *Front. Cell. Neurosci.* 14, 220.
- Adamantidis, A.R., Gutierrez Herrera, C., Gent, T.C., 2019. Oscillating circuitries in the sleeping brain. *Nat. Rev. Neurosci.* 20, 746–762. <https://doi.org/10.1038/s41583-019-0223-4>
- Adrian, E.D., 1950. The electrical activity of the mammalian olfactory bulb. *Electroencephalogr. Clin. Neurophysiol.* 2, 377–388.
- Adrian, E.D., 1942. Olfactory reactions in the brain of the hedgehog. *J. Physiol.* 100, 459–473.
- Albo, Z., Di Prisco, G.V., Vertes, R.P., 2003. Anterior thalamic unit discharge profiles and coherence with hippocampal theta rhythm. *Thalamus Relat. Syst.* 2, 133–144.
- Arshamian, A., Iravani, B., Majid, A., Lundström, J.N., 2018. Respiration modulates olfactory memory consolidation in humans. *J. Neurosci.* 38, 10286–10294.
- Azouz, R., Gray, C.M., 2000. Dynamic spike threshold reveals a mechanism for synaptic coincidence detection in cortical neurons in vivo. *Proc. Natl. Acad. Sci.* 97, 8110–8115.
- Bagur, S., Lacroix, M.M., de Lavilléon, G., Lefort, J.M., Geoffroy, H., Benchenane, K., 2018. Harnessing olfactory bulb oscillations to perform fully brain-based sleep-scoring and real-time monitoring of anaesthesia depth. *PLoS Biol.* 16, e2005458.
- Bagur, S., Lefort, J.M., Lacroix, M.M., de Lavilléon, G., Herry, C., Chouvaeff, M., Billand, C., Geoffroy, H., Benchenane, K., 2021. Breathing-driven prefrontal oscillations regulate maintenance of conditioned-fear evoked freezing independently of initiation. *Nat. Commun.* 12, 1–15.
- Bakkum, D.J., Frey, U., Radivojevic, M., Russell, T.L., Müller, J., Fiscella, M., Takahashi, H., Hierlemann, A., 2013. Tracking axonal action potential propagation on a high-density microelectrode array across hundreds of sites. *Nat. Commun.* 4, 2181. <https://doi.org/10.1038/ncomms3181>
- Battaglia, F.P., 2004. Hippocampal sharp wave bursts coincide with neocortical “up-state” transitions. *Learn. Mem.* 11, 697–704. <https://doi.org/10.1101/lm.73504>
- Bazelot, M., Dinocourt, C., Cohen, I., Miles, R., 2010. Unitary inhibitory field potentials in the CA3 region of rat hippocampus. *J. Physiol.* 588, 2077–2090. <https://doi.org/10.1113/jphysiol.2009.185918>
- Benchenane, K., Peyrache, A., Khamassi, M., Tierney, P.L., Gioanni, Y., Battaglia, F.P., Wiener, S.I., 2010. Coherent theta oscillations and reorganization of spike timing in the hippocampal-prefrontal network upon learning. *Neuron* 66, 921–936.

- Berg, R.W., Kleinfeld, D., 2003. Vibrissa movement elicited by rhythmic electrical microstimulation to motor cortex in the aroused rat mimics exploratory whisking. *J. Neurophysiol.* 90, 2950–2963.
- Berger, H., 1929. Über das elektroencephalogramm des menschen. *Arch. Für Psychiatr. Nervenkrankh.* 87, 527–570.
- Bertrand, F., Hugelin, A., 1971. Respiratory synchronizing function of nucleus parabrachialis medialis: pneumotoxic mechanisms. *J. Neurophysiol.* 34, 189–207.
- Biskamp, J., Bartos, M., Sauer, J.-F., 2017. Organization of prefrontal network activity by respiration-related oscillations. *Sci. Rep.* 7, 1–11.
- Boiten, F.A., Frijda, N.H., Wientjes, C.J., 1994. Emotions and respiratory patterns: review and critical analysis. *Int. J. Psychophysiol.* 17, 103–128.
- Bonnefond, M., Kastner, S., Jensen, O., 2017. Communication between brain areas based on nested oscillations. *eneuro* 4.
- Bouret, S., Sara, S.J., 2002. Locus coeruleus activation modulates firing rate and temporal organization of odour-induced single-cell responses in rat piriform cortex. *Eur. J. Neurosci.* 16, 2371–2382.
- Bressler, S.L., 1987. Relation of olfactory bulb and cortex. I. Spatial variation of bulbocortical interdependence. *Brain Res.* 409, 285–293.
- Briffaud, V., Fourcaud-Trocmé, N., Messaoudi, B., Buonviso, N., Amat, C., 2012. The relationship between respiration-related membrane potential slow oscillations and discharge patterns in mitral/tufted cells: what are the rules? *PLoS One* 7, e43964.
- Brown, R.P., Gerbarg, P.L., 2009. Yoga breathing, meditation, and longevity. *Ann. N. Y. Acad. Sci.* 1172, 54.
- Buccino, A.P., Hurwitz, C.L., Garcia, S., Magland, J., Siegle, J.H., Hurwitz, R., Hennig, M.H., 2020. SpikeInterface, a unified framework for spike sorting. *Elife* 9, e61834.
- Buonviso, N., Amat, C., Litaudon, P., 2006. Respiratory modulation of olfactory neurons in the rodent brain. *Chem. Senses* 31, 145–154.
- Buonviso, N., Amat, C., Litaudon, P., Roux, S., Royet, J.-P., Farget, V., Sicard, G., 2003. Rhythm sequence through the olfactory bulb layers during the time window of a respiratory cycle. *Eur. J. Neurosci.* 17, 1811–1819.
- Buzsáki, G., Anastassiou, C.A., Koch, C., 2012. The origin of extracellular fields and currents — EEG, ECoG, LFP and spikes. *Nat. Rev. Neurosci.* 13, 407–420. <https://doi.org/10.1038/nrn3241>
- Buzsáki, G., Bickford, R.G., Ponomareff, G., Thal, L.J., Mandel, R., Gage, F.H., 1988. Nucleus basalis and thalamic control of neocortical activity in the freely moving rat. *J. Neurosci. Off. J. Soc. Neurosci.* 8, 4007–4026.
- Buzsáki, G., Draguhn, A., 2004. Neuronal oscillations in cortical networks. *science* 304, 1926–1929.

- Buzsáki, G., Geisler, C., Henze, D.A., Wang, X.-J., 2004. Interneuron Diversity series: Circuit complexity and axon wiring economy of cortical interneurons. *Trends Neurosci.* 27, 186–193. <https://doi.org/10.1016/j.tins.2004.02.007>
- Buzsáki, G., Wang, X.-J., 2012. Mechanisms of Gamma Oscillations. *Annu. Rev. Neurosci.* 35, 203–225. <https://doi.org/10.1146/annurev-neuro-062111-150444>
- Cang, J., Isaacson, J.S., 2003. In vivo whole-cell recording of odor-evoked synaptic transmission in the rat olfactory bulb. *J. Neurosci.* 23, 4108–4116.
- Canolty, R.T., Edwards, E., Dalal, S.S., Soltani, M., Nagarajan, S.S., Kirsch, H.E., Berger, M.S., Barbaro, N.M., Knight, R.T., 2006. High gamma power is phase-locked to theta oscillations in human neocortex. *science* 313, 1626–1628.
- Canolty, R.T., Knight, R.T., 2010. The functional role of cross-frequency coupling. *Trends Cogn. Sci.* 14, 506–515.
- Cao, Y., Roy, S., Sachdev, R.N., Heck, D.H., 2012. Dynamic correlation between whisking and breathing rhythms in mice. *J. Neurosci.* 32, 1653–1659.
- Cardin, J.A., Carlén, M., Meletis, K., Knoblich, U., Zhang, F., Deisseroth, K., Tsai, L.-H., Moore, C.I., 2009. Driving fast-spiking cells induces gamma rhythm and controls sensory responses. *Nature* 459, 663–667.
- Carnevali, L., Sgoifo, A., Trombini, M., Landgraf, R., Neumann, I.D., Nalivaiko, E., 2013. Different patterns of respiration in rat lines selectively bred for high or low anxiety. *PloS One* 8, e64519.
- Caton, R., 1875. Electrical currents of the brain. *J. Nerv. Ment. Dis.* 2, 610.
- Cavelli, M., Castro-Zaballa, S., Gonzalez, J., Rojas-Líbano, D., Rubido, N., Velásquez, N., Torterolo, P., 2020. Nasal respiration entrains neocortical long-range gamma coherence during wakefulness. *Eur. J. Neurosci.* 51, 1463–1477.
- Cenier, T., David, F., Litaudon, P., Garcia, S., Amat, C., Buonviso, N., 2009. Respiration-gated formation of gamma and beta neural assemblies in the mammalian olfactory bulb. *Eur. J. Neurosci.* 29, 921–930.
- Chandler, D.J., Jensen, P., McCall, J.G., Pickering, A.E., Schwarz, L.A., Totah, N.K., 2019. Redefining noradrenergic neuromodulation of behavior: impacts of a modular locus coeruleus architecture. *J. Neurosci.* 39, 8239–8249.
- Chaput, M.A., 2000. EOG responses in anesthetized freely breathing rats. *Chem. Senses* 25, 695–701.
- Charpak, S., Mertz, J., Beaurepaire, E., Moreaux, L., Delaney, K., 2001. Odor-evoked calcium signals in dendrites of rat mitral cells. *Proc. Natl. Acad. Sci.* 98, 1230–1234.
- Chi, V.N., Müller, C., Wolfenstetter, T., Yanovsky, Y., Draguhn, A., Tort, A.B., Brankač, J., 2016. Hippocampal respiration-driven rhythm distinct from theta oscillations in awake mice. *J. Neurosci.* 36, 162–177.
- Chrobak, J.J., Buzsáki, G., 1998. Gamma oscillations in the entorhinal cortex of the freely behaving rat. *J. Neurosci.* 18, 388–398.

- Clemens, Z., Mölle, M., Erőss, L., Jakus, R., Rásonyi, G., Halász, P., Born, J., 2011. Fine-tuned coupling between human parahippocampal ripples and sleep spindles. *Eur. J. Neurosci.* 33, 511–520.
- Clemens, Z., Mölle, M., Erőss, L., Barsi, P., Halász, P., Born, J., 2007. Temporal coupling of parahippocampal ripples, sleep spindles and slow oscillations in humans. *Brain* 130, 2868–2878. <https://doi.org/10.1093/brain/awm146>
- Clugnet, M.-C., Price, J.L., 1987. Olfactory input to the prefrontal cortex in the rat. *Ann. N. Y. Acad. Sci.* 510, 231–235.
- Cohen, M.X., Elger, C.E., Fell, J., 2008. Oscillatory activity and phase–amplitude coupling in the human medial frontal cortex during decision making. *J. Cogn. Neurosci.* 21, 390–402.
- Cole, S., Voytek, B., 2019. Cycle-by-cycle analysis of neural oscillations. *J. Neurophysiol.* 122, 849–861. <https://doi.org/10.1152/jn.00273.2019>
- Cole, S.R., Voytek, B., 2017. Brain oscillations and the importance of waveform shape. *Trends Cogn. Sci.* 21, 137–149.
- Colgin, L.L., 2013. Mechanisms and Functions of Theta Rhythms. *Annu. Rev. Neurosci.* 36, 295–312. <https://doi.org/10.1146/annurev-neuro-062012-170330>
- Colgin, L.L., Denninger, T., Fyhn, M., Hafting, T., Bonnevie, T., Jensen, O., Moser, M.-B., Moser, E.I., 2009. Frequency of gamma oscillations routes flow of information in the hippocampus. *Nature* 462, 353–357.
- Courtiol, E., Amat, C., Thevenet, M., Messaoudi, B., Garcia, S., Buonviso, N., 2011a. Reshaping of bulbar odor response by nasal flow rate in the rat. *PLoS One* 6, e16445.
- Courtiol, E., Hegoburu, C., Litaudon, P., Garcia, S., Fourcaud-Trocmé, N., Buonviso, N., 2011b. Individual and synergistic effects of sniffing frequency and flow rate on olfactory bulb activity. *J. Neurophysiol.* 106, 2813–2824.
- Courtiol, E., Lefèvre, L., Garcia, S., Thévenet, M., Messaoudi, B., Buonviso, N., 2014. Sniff adjustment in an odor discrimination task in the rat: analytical or synthetic strategy? *Front. Behav. Neurosci.* 8, 145.
- Cox, R., van Driel, J., de Boer, M., Talamini, L.M., 2014. Slow oscillations during sleep coordinate interregional communication in cortical networks. *J. Neurosci.* 34, 16890–16901.
- Crunelli, V., Hughes, S.W., 2010. The slow (< 1 Hz) rhythm of non-REM sleep: a dialogue between three cardinal oscillators. *Nat. Neurosci.* 13, 9–17.
- Csicsvari, J., Hirase, H., Mamiya, A., Buzsáki, G., 2000. Ensemble Patterns of Hippocampal CA3-CA1 Neurons during Sharp Wave-Associated Population Events. *Neuron* 28, 585–594. [https://doi.org/10.1016/S0896-6273\(00\)00135-5](https://doi.org/10.1016/S0896-6273(00)00135-5)
- Csicsvari, J., Jamieson, B., Wise, K.D., Buzsáki, G., 2003. Mechanisms of gamma oscillations in the hippocampus of the behaving rat. *Neuron* 37, 311–322.
- Daoudal, G., 2003. Long-Term Plasticity of Intrinsic Excitability: Learning Rules and Mechanisms. *Learn. Mem.* 10, 456–465. <https://doi.org/10.1101/lm.64103>

- Datiche, F., Cattarelli, M., 1996. Reciprocal and topographic connections between the piriform and prefrontal cortices in the rat: a tracing study using the B subunit of the cholera toxin. *Brain Res. Bull.* 41, 391–398.
- DeCoteau, W.E., Thorn, C., Gibson, D.J., Courtemanche, R., Mitra, P., Kubota, Y., Graybiel, A.M., 2007. Learning-related coordination of striatal and hippocampal theta rhythms during acquisition of a procedural maze task. *Proc. Natl. Acad. Sci.* 104, 5644–5649.
- Del Negro, C.A., Funk, G.D., Feldman, J.L., 2018. Breathing matters. *Nat. Rev. Neurosci.* 19, 351–367.
- Deschênes, M., Moore, J., Kleinfeld, D., 2012. Sniffing and whisking in rodents. *Curr. Opin. Neurobiol.* 22, 243–250.
- Descilo, T., Vedamurtachar, A., Gerbarg, P.L., Nagaraja, D., Gangadhar, B.N., Damodaran, B., Adelson, B., Braslow, L.H., Marcus, S., Brown, R.P., 2010. Effects of a yoga breath intervention alone and in combination with an exposure therapy for post-traumatic stress disorder and depression in survivors of the 2004 South-East Asia tsunami. *Acta Psychiatr. Scand.* 121, 289–300. <https://doi.org/10.1111/j.1600-0447.2009.01466.x>
- Destexhe, A., Contreras, D., Steriade, M., 1999. Spatiotemporal Analysis of Local Field Potentials and Unit Discharges in Cat Cerebral Cortex during Natural Wake and Sleep States. *J. Neurosci.* 19, 4595–4608. <https://doi.org/10.1523/JNEUROSCI.19-11-04595.1999>
- Dupin, M., Garcia, S., Boulanger-Bertolus, J., Buonviso, N., Mouly, A.-M., 2019. New insights from 22-kHz ultrasonic vocalizations to characterize fear responses: relationship with respiration and brain oscillatory dynamics. *Eneuro* 6.
- Edmonds, W.A., Kennedy, T.D., Hughes, P.A., Calzada, P.J., 2009. A single-participants investigation of the effects of various biofeedback-assisted breathing patterns on heart rate variability: a practitioner’s approach. *Biofeedback* 37, 141–146.
- Eeckman, F.H., Freeman, W.J., 1990. Correlations between unit firing and EEG in the rat olfactory system. *Brain Res.* 528, 238–244.
- Fell, J., Axmacher, N., 2011. The role of phase synchronization in memory processes. *Nat. Rev. Neurosci.* 12, 105–118.
- Fellin, T., Halassa, M.M., Terunuma, M., Succol, F., Takano, H., Frank, M., Moss, S.J., Haydon, P.G., 2009. Endogenous nonneuronal modulators of synaptic transmission control cortical slow oscillations in vivo. *Proc. Natl. Acad. Sci.* 106, 15037–15042. <https://doi.org/10.1073/pnas.0906419106>
- Fernandez, L.M.J., Comte, J.-C., Le Merre, P., Lin, J.-S., Salin, P.-A., Crochet, S., 2017. Highly Dynamic Spatiotemporal Organization of Low-Frequency Activities During Behavioral States in the Mouse Cerebral Cortex. *Cereb. Cortex* 27, 5444–5462. <https://doi.org/10.1093/cercor/bhw311>
- Ferraris, M., Ghestem, A., Vicente, A.F., Nallet-Khosrofiyan, L., Bernard, C., Quilichini, P.P., 2018. The nucleus reuniens controls long-range hippocampo–prefrontal gamma synchronization during slow oscillations. *J. Neurosci.* 38, 3026–3038.

- Fontanini, A., Bower, J.M., 2006. Slow-waves in the olfactory system: an olfactory perspective on cortical rhythms. *Trends Neurosci.* 29, 429–437.
- Fontanini, A., Bower, J.M., 2005. Variable coupling between olfactory system activity and respiration in ketamine/xylazine anesthetized rats. *J. Neurophysiol.* 93, 3573–3581.
- Fontanini, A., Spano, P., Bower, J.M., 2003. Ketamine-xylazine-induced slow (< 1.5 Hz) oscillations in the rat piriform (olfactory) cortex are functionally correlated with respiration. *J. Neurosci.* 23, 7993–8001.
- Fourcaud-Trocmé, N., Briffaud, V., Thévenet, M., Buonviso, N., Amat, C., 2018. In vivo beta and gamma subthreshold oscillations in rat mitral cells: origin and gating by respiratory dynamics. *J. Neurophysiol.* 119, 274–289.
- Fox, S.E., Wolfson, S., Ranck, J.B., 1986. Hippocampal theta rhythm and the firing of neurons in walking and urethane anesthetized rats. *Exp. Brain Res.* 62, 495–508.
- Freeman, W.J., 1978. Spatial properties of an EEG event in the olfactory bulb and cortex. *Electroencephalogr. Clin. Neurophysiol.* 44, 586–605.
- Freeman, W.J., 1975. Mass action in the nervous system. Citeseer.
- Freeman, W.J., 1959. Distribution in time and space of prepyriform electrical activity. *J. Neurophysiol.* 22, 644–665.
- Freeman, W.J., Schneider, W., 1982. Changes in spatial patterns of rabbit olfactory EEG with conditioning to odors. *Psychophysiology* 19, 44–56.
- Fries, P., 2015. Rhythms for Cognition: Communication through Coherence. *Neuron* 88, 220–235. <https://doi.org/10.1016/j.neuron.2015.09.034>
- Fries, P., 2005. A mechanism for cognitive dynamics: neuronal communication through neuronal coherence. *Trends Cogn. Sci.* 9, 474–480.
- Frysinger, R.C., Harper, R.M., 1990. Cardiac and respiratory correlations with unit discharge in epileptic human temporal lobe. *Epilepsia* 31, 162–171.
- Frysinger, R.C., Harper, R.M., 1989. Cardiac and respiratory correlations with unit discharge in human amygdala and hippocampus. *Electroencephalogr. Clin. Neurophysiol.* 72, 463–470. [https://doi.org/10.1016/0013-4694\(89\)90222-8](https://doi.org/10.1016/0013-4694(89)90222-8)
- Frysinger, R.C., Harper, R.M., 1986. Cardiac and respiratory relationships with neural discharge in the anterior cingulate cortex during sleep-waking states. *Exp. Neurol.* 94, 247–263.
- Fujisawa, S., Buzsáki, G., 2011. A 4 Hz oscillation adaptively synchronizes prefrontal, VTA, and hippocampal activities. *Neuron* 72, 153–165.
- Gent, T.C., Bandarabadi, M., Herrera, C.G., Adamantidis, A.R., 2018. Thalamic dual control of sleep and wakefulness. *Nat. Neurosci.* 21, 974–984.
- Gerbarg, P.L., Brown, R.P., 2005. Yoga: A breath of relief for Hurricane Katrina refugees. *Curr. Psychiatry* 4, 55–67.

- Gervasoni, D., 2000. Neuromodulation de l'activité des neurones monoaminergiques au cours du cycle veille-sommeil: Approches électrophysiologique et pharmacologique chez le rat vigile. (PhD Thesis). Université Claude Bernard-Lyon I.
- Gervasoni, D., Lin, S.-C., Ribeiro, S., Soares, E.S., Pantoja, J., Nicolelis, M.A., 2004. Global forebrain dynamics predict rat behavioral states and their transitions. *J. Neurosci.* 24, 11137–11147.
- Girardeau, G., Zugaro, M., 2011. Hippocampal ripples and memory consolidation. *Curr. Opin. Neurobiol., Behavioural and cognitive neuroscience* 21, 452–459. <https://doi.org/10.1016/j.conb.2011.02.005>
- Girin, B., Juventin, M., Garcia, S., Lefèvre, L., Amat, C., Fourcaud-Trocmé, N., Buonviso, N., 2021. The deep and slow breathing characterizing rest favors brain respiratory-drive. *Sci. Rep.* 11, 1–15.
- Glickfeld, L.L., Roberts, J.D., Somogyi, P., Scanziani, M., 2009. Interneurons hyperpolarize pyramidal cells along their entire somatodendritic axis. *Nat. Neurosci.* 12, 21–23.
- Gray, C.M., Engel, A.K., König, P., Singer, W., 1992. Synchronization of oscillatory neuronal responses in cat striate cortex: temporal properties. *Vis. Neurosci.* 8, 337–347.
- Gray, C.M., König, P., Engel, A.K., Singer, W., 1989. Oscillatory responses in cat visual cortex exhibit inter-columnar synchronization which reflects global stimulus properties. *Nature* 338, 334–337.
- Gray, C.M., Singer, W., 1989. Stimulus-specific neuronal oscillations in orientation columns of cat visual cortex. *Proc. Natl. Acad. Sci.* 86, 1698–1702.
- Grosmaître, X., Santarelli, L.C., Tan, J., Luo, M., Ma, M., 2007. Dual functions of mammalian olfactory sensory neurons as odor detectors and mechanical sensors. *Nat. Neurosci.* 10, 348–354.
- Gross, M.J., Shearer, D.A., Bringer, J.D., Hall, R., Cook, C.J., Kilduff, L.P., 2016. Abbreviated resonant frequency training to augment heart rate variability and enhance on-demand emotional regulation in elite sport support staff. *Appl. Psychophysiol. Biofeedback* 41, 263–274.
- Gruzelier, J.H., Thompson, T., Redding, E., Brandt, R., Steffert, T., 2014. Application of alpha/theta neurofeedback and heart rate variability training to young contemporary dancers: State anxiety and creativity. *Int. J. Psychophysiol.* 93, 105–111.
- Hagiwara, S., Szabo, T., Enger, P.S., 1965. Physiological properties of electroreceptors in the electric eel, *Electrophorus electricus*. *J. Neurophysiol.* 28, 775–783.
- Hahn, M.A., Heib, D., Schabus, M., Hoedlmoser, K., Helfrich, R.F., 2020. Slow oscillation-spindle coupling predicts enhanced memory formation from childhood to adolescence. *Elife* 9, e53730.
- Harris, K.D., Csicsvari, J., Hirase, H., Dragoi, G., Buzsáki, G., 2003. Organization of cell assemblies in the hippocampus. *Nature* 424, 552–556.
- Hasenstaub, A., Shu, Y., Haider, B., Kraushaar, U., Duque, A., McCormick, D.A., 2005. Inhibitory postsynaptic potentials carry synchronized frequency information in active cortical networks. *Neuron* 47, 423–435.

- He, B.J., Snyder, A.Z., Zempel, J.M., Smyth, M.D., Raichle, M.E., 2008. Electrophysiological correlates of the brain's intrinsic large-scale functional architecture. *Proc. Natl. Acad. Sci.* 105, 16039–16044. <https://doi.org/10.1073/pnas.0807010105>
- Hebb, D.O., 1949. *The organization of behavior; a neuropsychological theory.* Wiley Book Clin. Psychol. 62, 78.
- Heck, D.H., Kozma, R., Kay, L.M., 2019. The rhythm of memory: how breathing shapes memory function. *J. Neurophysiol.* 122, 563–571.
- Helfrich, R.F., Lendner, J.D., Mander, B.A., Guillen, H., Paff, M., Mnatsakanyan, L., Vadera, S., Walker, M.P., Lin, J.J., Knight, R.T., 2019. Bidirectional prefrontal-hippocampal dynamics organize information transfer during sleep in humans. *Nat. Commun.* 10, 1–16.
- Helfrich, R.F., Mander, B.A., Jagust, W.J., Knight, R.T., Walker, M.P., 2018. Old brains come uncoupled in sleep: slow wave-spindle synchrony, brain atrophy, and forgetting. *Neuron* 97, 221–230.
- Herrero, J.L., Khuvis, S., Yeagle, E., Cerf, M., Mehta, A.D., 2018. Breathing above the brain stem: volitional control and attentional modulation in humans. *J. Neurophysiol.*
- Homma, I., Masaoka, Y., 2008. Breathing rhythms and emotions. *Exp. Physiol.* 93, 1011–1021.
- Hughes, S.W., L\Horincz, M.L., Parri, H.R., Crunelli, V., 2011. Infralow (< 0.1 Hz) oscillations in thalamic relay nuclei: basic mechanisms and significance to health and disease states, in: *Progress in Brain Research.* Elsevier, pp. 145–162.
- Igarashi, K.M., Ieki, N., An, M., Yamaguchi, Y., Nagayama, S., Kobayakawa, K., Kobayakawa, R., Tanifuji, M., Sakano, H., Chen, W.R., 2012. Parallel mitral and tufted cell pathways route distinct odor information to different targets in the olfactory cortex. *J. Neurosci.* 32, 7970–7985.
- Isomura, Y., Sirota, A., Özen, S., Montgomery, S., Mizuseki, K., Henze, D.A., Buzsáki, G., 2006. Integration and Segregation of Activity in Entorhinal-Hippocampal Subregions by Neocortical Slow Oscillations. *Neuron* 52, 871–882. <https://doi.org/10.1016/j.neuron.2006.10.023>
- Ito, H.T., Moser, E.I., Moser, M.-B., 2018. Supramammillary nucleus modulates spike-time coordination in the prefrontal-thalamo-hippocampal circuit during navigation. *Neuron* 99, 576–587.
- Ito, H.T., Zhang, S.-J., Witter, M.P., Moser, E.I., Moser, M.-B., 2015. A prefrontal-thalamo-hippocampal circuit for goal-directed spatial navigation. *Nature* 522, 50–55.
- Ito, J., Roy, S., Liu, Y., Cao, Y., Fletcher, M., Lu, L., Boughter, J.D., Grün, S., Heck, D.H., 2014. Whisker barrel cortex delta oscillations and gamma power in the awake mouse are linked to respiration. *Nat. Commun.* 5, 3572. <https://doi.org/10.1038/ncomms4572>
- Iwabe, T., Ozaki, I., Hashizume, A., 2014. The respiratory cycle modulates brain potentials, sympathetic activity, and subjective pain sensation induced by noxious stimulation. *Neurosci. Res.* 84, 47–59. <https://doi.org/10.1016/j.neures.2014.03.003>

- Jacobs, J., Kahana, M.J., Ekstrom, A.D., Fried, I., 2007. Brain Oscillations Control Timing of Single-Neuron Activity in Humans. *J. Neurosci.* 27, 3839–3844. <https://doi.org/10.1523/JNEUROSCI.4636-06.2007>
- Janakiramaiah, N., Gangadhar, B.N., Murthy, P.N.V., Harish, M.G., Subbakrishna, D.K., Vedamurthachar, A., 2000. Antidepressant efficacy of Sudarshan Kriya Yoga (SKY) in melancholia: a randomized comparison with electroconvulsive therapy (ECT) and imipramine. *J. Affect. Disord.* 57, 255–259.
- Jensen, O., Colgin, L.L., 2007. Cross-frequency coupling between neuronal oscillations. *Trends Cogn. Sci.* 11, 267–269.
- Jerath, R., Crawford, M.W., Barnes, V.A., Harden, K., 2015. Widespread depolarization during expiration: A source of respiratory drive? *Med. Hypotheses* 84, 31–37.
- Jerath, R., Edry, J.W., Barnes, V.A., Jerath, V., 2006. Physiology of long pranayamic breathing: neural respiratory elements may provide a mechanism that explains how slow deep breathing shifts the autonomic nervous system. *Med. Hypotheses* 67, 566–571.
- Jessberger, J., Zhong, W., Brankačk, J., Draguhn, A., 2016. Olfactory bulb field potentials and respiration in sleep-wake states of mice. *Neural Plast.* 2016.
- Jones, B.E., Moore, R.Y., 1977. Ascending projections of the locus coeruleus in the rat. II. Autoradiographic study. *Brain Res.* 127, 23–53.
- Jung, F., Yanovsky, Y., Brankačk, J., Tort, A.B., Draguhn, A., 2019. Respiration competes with theta for modulating parietal cortex neurons. *BioRxiv* 707331.
- Kahana, M.J., Seelig, D., Madsen, J.R., 2001. Theta returns. *Curr. Opin. Neurobiol.* 11, 739–744. [https://doi.org/10.1016/S0959-4388\(01\)00278-1](https://doi.org/10.1016/S0959-4388(01)00278-1)
- Kamondi, A., Acsády, L., Buzsáki, G., 1998. Dendritic Spikes Are Enhanced by Cooperative Network Activity in the Intact Hippocampus. *J. Neurosci.* 18, 3919–3928. <https://doi.org/10.1523/JNEUROSCI.18-10-03919.1998>
- Karalis, N., Dejean, C., Chaudun, F., Khoder, S., Rozeske, R.R., Wurtz, H., Bagur, S., Benchenane, K., Sirota, A., Courtin, J., 2016. 4-Hz oscillations synchronize prefrontal-amygdala circuits during fear behavior. *Nat. Neurosci.* 19, 605–612.
- Karalis, N., Sirota, A., 2018. Breathing coordinates limbic network dynamics underlying memory consolidation. Available SSRN 3283711.
- Karavidas, M.K., Lehrer, P.M., Vaschillo, E., Vaschillo, B., Marin, H., Buyske, S., Malinovsky, I., Radvanski, D., Hassett, A., 2007. Preliminary results of an open label study of heart rate variability biofeedback for the treatment of major depression. *Appl. Psychophysiol. Biofeedback* 32, 19–30.
- Kharya, C., Gupta, V., Deepak, K.K., Sagar, R., Upadhyav, A., Kochupillai, V., Anand, S., 2014. Effect of controlled breathing exercises on the psychological status and the cardiac autonomic tone: Sudarshan Kriya and Prana-Yoga. *Indian J Physiol Pharmacol* 58, 210–220.
- Kleinfeld, D., Moore, J.D., Wang, F., Deschênes, M., 2014. The brainstem oscillator for whisking and the case for breathing as the master clock for orofacial motor actions, in: *Cold Spring Harbor Symposia on Quantitative Biology*. Cold Spring Harbor Laboratory Press, pp. 29–39.

- Kluger, D.S., Gross, J., 2020. Depth and phase of respiration modulate cortico-muscular communication. *NeuroImage* 222, 117272.
- Kocsis, B., Pittman-Polletta, B.R., Roy, A., 2018. Respiration-coupled rhythms in prefrontal cortex: beyond if, to when, how, and why. *Brain Struct. Funct.* 223, 11–16.
- König, P., Engel, A.K., Singer, W., 1996. Integrator or coincidence detector? The role of the cortical neuron revisited. *Trends Neurosci.* 19, 130–137. [https://doi.org/10.1016/S0166-2236\(96\)80019-1](https://doi.org/10.1016/S0166-2236(96)80019-1)
- Köszegehy, Á., Lasztóczy, B., Forro, T., Klausberger, T., 2018. Spike-timing of orbitofrontal neurons is synchronized with breathing. *Front. Cell. Neurosci.* 12, 105.
- Kreiter, A.K., Singer, W., 1992. Oscillatory neuronal responses in the visual cortex of the awake macaque monkey. *Eur. J. Neurosci.* 4, 369–375.
- Krieger, J., Maglasiu, N., Sforza, E., Kurtz, D., 1990. Breathing during sleep in normal middle-aged subjects. *Sleep* 13, 143–154.
- Lakatos, P., Shah, A.S., Knuth, K.H., Ulbert, I., Karmos, G., Schroeder, C.E., 2005. An oscillatory hierarchy controlling neuronal excitability and stimulus processing in the auditory cortex. *J. Neurophysiol.* 94, 1904–1911.
- Latchoumane, C.-F.V., Ngo, H.-V.V., Born, J., Shin, H.-S., 2017. Thalamic spindles promote memory formation during sleep through triple phase-locking of cortical, thalamic, and hippocampal rhythms. *Neuron* 95, 424–435.
- Lecci, S., Fernandez, L.M., Weber, F.D., Cardis, R., Chatton, J.-Y., Born, J., Lüthi, A., 2017. Coordinated infraslow neural and cardiac oscillations mark fragility and offline periods in mammalian sleep. *Sci. Adv.* 3, e1602026.
- Lehrer, P.M., Vaschillo, E., Vaschillo, B., Lu, S.-E., Eckberg, D.L., Edelberg, R., Shih, W.J., Lin, Y., Kuusela, T.A., Tahvanainen, K.U., 2003. Heart rate variability biofeedback increases baroreflex gain and peak expiratory flow. *Psychosom. Med.* 65, 796–805.
- Lehrer, P.M., Vaschillo, E., Vaschillo, B., Lu, S.-E., Scardella, A., Siddique, M., Habib, R.H., 2004. Biofeedback treatment for asthma. *Chest* 126, 352–361.
- Lin, I.M., Tai, L.Y., Fan, S.-Y., 2014. Breathing at a rate of 5.5 breaths per minute with equal inhalation-to-exhalation ratio increases heart rate variability. *Int. J. Psychophysiol.* 91, 206–211.
- Litaudon, P., Amat, C., Bertrand, B., Vigouroux, M., Buonviso, N., 2003. Piriform cortex functional heterogeneity revealed by cellular responses to odours. *Eur. J. Neurosci.* 17, 2457–2461.
- Liu, Y., McAfee, S.S., Heck, D.H., 2017. Hippocampal sharp-wave ripples in awake mice are entrained by respiration. *Sci. Rep.* 7, 1–9.
- Lockmann, A.L., Laplagne, D.A., Leão, R.N., Tort, A.B., 2016. A respiration-coupled rhythm in the rat hippocampus independent of theta and slow oscillations. *J. Neurosci.* 36, 5338–5352.
- Lockmann, A.L., Tort, A.B., 2018. Nasal respiration entrains delta-frequency oscillations in the prefrontal cortex and hippocampus of rodents. *Brain Struct. Funct.* 223, 1–3.

- Lörincz, M.L., Gunner, D., Bao, Y., Connelly, W.M., Isaac, J.T., Hughes, S.W., Crunelli, V., 2015. A distinct class of slow ( 0.2–2 Hz) intrinsically bursting layer 5 pyramidal neurons determines UP/DOWN state dynamics in the neocortex. *J. Neurosci.* 35, 5442–5458.
- Lüthi, A., 2014. Sleep spindles: where they come from, what they do. *The Neuroscientist* 20, 243–256.
- Macrides, F., Eichenbaum, H.B., Forbes, W.B., 1982. Temporal relationship between sniffing and the limbic theta rhythm during odor discrimination reversal learning. *J. Neurosci.* 2, 1705–1717.
- Maier, E., Lauer, S., Brecht, M., 2020. Layer 4 organization and respiration locking in the rodent nose somatosensory cortex. *J. Neurophysiol.* 124, 822–832.
- Manabe, H., Kusumoto-Yoshida, I., Ota, M., Mori, K., 2011. Olfactory cortex generates synchronized top-down inputs to the olfactory bulb during slow-wave sleep. *J. Neurosci.* 31, 8123–8133.
- Manning, J.R., Jacobs, J., Fried, I., Kahana, M.J., 2009. Broadband shifts in local field potential power spectra are correlated with single-neuron spiking in humans. *J. Neurosci.* 29, 13613–13620.
- Margrie, T.W., Schaefer, A.T., 2003. Theta oscillation coupled spike latencies yield computational vigour in a mammalian sensory system. *J. Physiol.* 546, 363–374.
- Massimini, M., Huber, R., Ferrarelli, F., Hill, S., Tononi, G., 2004. The Sleep Slow Oscillation as a Traveling Wave. *J. Neurosci.* 24, 6862–6870. <https://doi.org/10.1523/JNEUROSCI.1318-04.2004>
- Mizrahi-Kliger, A.D., Kaplan, A., Israel, Z., Bergman, H., 2018. Desynchronization of slow oscillations in the basal ganglia during natural sleep. *Proc. Natl. Acad. Sci.* 115, E4274–E4283.
- Mizuseki, K., Sirota, A., Pastalkova, E., Buzsáki, G., 2009. Theta oscillations provide temporal windows for local circuit computation in the entorhinal-hippocampal loop. *Neuron* 64, 267–280.
- Moberly, A.H., Schreck, M., Bhattarai, J.P., Zweifel, L.S., Luo, W., Ma, M., 2018. Olfactory inputs modulate respiration-related rhythmic activity in the prefrontal cortex and freezing behavior. *Nat. Commun.* 9, 1–10.
- Mölle, M., Born, J., 2011. Slow oscillations orchestrating fast oscillations and memory consolidation. *Prog. Brain Res.* 193, 93–110.
- Mölle, M., Eschenko, O., Gais, S., Sara, S.J., Born, J., 2009. The influence of learning on sleep slow oscillations and associated spindles and ripples in humans and rats. *Eur. J. Neurosci.* 29, 1071–1081.
- Mölle, M., Yeshenko, O., Marshall, L., Sara, S.J., Born, J., 2006. Hippocampal Sharp Wave-Ripples Linked to Slow Oscillations in Rat Slow-Wave Sleep. *J. Neurophysiol.* 96, 62–70. <https://doi.org/10.1152/jn.00014.2006>
- Moore, J.D., Deschênes, M., Furuta, T., Huber, D., Smear, M.C., Demers, M., Kleinfeld, D., 2013. Hierarchy of orofacial rhythms revealed through whisking and breathing. *Nature* 497, 205–210.

- Moser, D., Anderer, P., Gruber, G., Parapatics, S., Loretz, E., Boeck, M., Kloesch, G., Heller, E., Schmidt, A., Danker-Hopfe, H., 2009. Sleep classification according to AASM and Rechtschaffen & Kales: effects on sleep scoring parameters. *Sleep* 32, 139–149.
- Muehlroth, B.E., Sander, M.C., Fandakova, Y., Grandy, T.H., Rasch, B., Shing, Y.L., Werkle-Bergner, M., 2019. Precise slow oscillation–spindle coupling promotes memory consolidation in younger and older adults. *Sci. Rep.* 9, 1–15.
- Murakami, M., Kashiwadani, H., Kirino, Y., Mori, K., 2005. State-dependent sensory gating in olfactory cortex. *Neuron* 46, 285–296.
- Nakamura, N.H., Fukunaga, M., Oku, Y., 2018. Respiratory modulation of cognitive performance during the retrieval process. *PloS One* 13, e0204021.
- Narikiyo, K., Manabe, H., Mori, K., 2014. Sharp wave-associated synchronized inputs from the piriform cortex activate olfactory tubercle neurons during slow-wave sleep. *J. Neurophysiol.* 111, 72–81.
- Neske, G.T., 2016. The Slow Oscillation in Cortical and Thalamic Networks: Mechanisms and Functions. *Front. Neural Circuits* 9. <https://doi.org/10.3389/fncir.2015.00088>
- Neubauer, J.A., Sunderram, J., 2004. Oxygen-sensing neurons in the central nervous system. *J. Appl. Physiol.* 96, 367–374. <https://doi.org/10.1152/jappphysiol.00831.2003>
- Ni, H., Zhang, J., Harper, R.M., 1990. Respiratory-related discharge of periaqueductal gray neurons during sleep-waking states. *Brain Res.* 511, 319–325.
- Nir, Y., Staba, R.J., Andrillon, T., Vyazovskiy, V.V., Cirelli, C., Fried, I., Tononi, G., 2011. Regional slow waves and spindles in human sleep. *Neuron* 70, 153–169.
- Noble, D.J., Hochman, S., 2019. Hypothesis: Pulmonary Afferent Activity Patterns During Slow, Deep Breathing Contribute to the Neural Induction of Physiological Relaxation. *Front. Physiol.* 10, 1176. <https://doi.org/10.3389/fphys.2019.01176>
- O’Keefe, J., Recce, M.L., 1993. Phase relationship between hippocampal place units and the EEG theta rhythm. *Hippocampus* 3, 317–330. <https://doi.org/10.1002/hipo.450030307>
- Onisawa, N., Manabe, H., Mori, K., 2017. Temporal coordination of olfactory cortex sharp-wave activity with up-and downstates in the orbitofrontal cortex during slow-wave sleep. *J. Neurophysiol.* 117, 123–135.
- Pachitariu, M., Steinmetz, N.A., Kadir, S.N., Carandini, M., Harris, K.D., 2016. Fast and accurate spike sorting of high-channel count probes with KiloSort. *Adv. Neural Inf. Process. Syst.* 29, 4448–4456.
- Pagliardini, S., Funk, G.D., Dickson, C.T., 2013. Breathing and brain state: urethane anesthesia as a model for natural sleep. *Respir. Physiol. Neurobiol.* 188, 324–332.
- Palva, J.M., Palva, S., Kaila, K., 2005. Phase synchrony among neuronal oscillations in the human cortex. *J. Neurosci.* 25, 3962–3972.
- Pappenheimer, J.R., 1977. Sleep and respiration of rats during hypoxia. *J. Physiol.* 266, 191–207.

- Park, H.-D., Barnoud, C., Trang, H., Kannape, O.A., Schaller, K., Blanke, O., 2020. Breathing is coupled with voluntary action and the cortical readiness potential. *Nat. Commun.* 11, 1–8.
- Park, Y.-J., Park, Y.-B., 2012. Clinical utility of paced breathing as a concentration meditation practice. *Complement. Ther. Med.* 20, 393–399.
- Parri, H.R., Gould, T.M., Crunelli, V., 2001. Spontaneous astrocytic Ca<sup>2+</sup> oscillations in situ drive NMDAR-mediated neuronal excitation. *Nat. Neurosci.* 4, 803–812.
- Paxinos, G., Watson, C., 2006. *The rat brain in stereotaxic coordinates: hard cover edition.* Elsevier.
- Perl, O., Ravia, A., Rubinson, M., Eisen, A., Soroka, T., Mor, N., Secundo, L., Sobel, N., 2019. Human non-olfactory cognition phase-locked with inhalation. *Nat. Hum. Behav.* 3, 501–512.
- Philippot, P., Chapelle, G., Blairy, S., 2002. Respiratory feedback in the generation of emotion. *Cogn. Emot.* 16, 605–627.
- Piarulli, A., Zaccaro, A., Laurino, M., Menicucci, D., De Vito, A., Bruschini, L., Berrettini, S., Bergamasco, M., Laureys, S., Gemignani, A., 2018. Ultra-slow mechanical stimulation of olfactory epithelium modulates consciousness by slowing cerebral rhythms in humans. *Sci. Rep.* 8, 1–17.
- Popa, D., Duvarci, S., Popescu, A.T., Léna, C., Paré, D., 2010. Coherent amygdalocortical theta promotes fear memory consolidation during paradoxical sleep. *Proc. Natl. Acad. Sci.* 107, 6516–6519.
- Poskanzer, K.E., Yuste, R., 2011. Astrocytic regulation of cortical UP states. *Proc. Natl. Acad. Sci.* 108, 18453–18458.
- Price, J.L., 1985. Beyond the primary olfactory cortex: olfactory-related areas in the neocortex, thalamus and hypothalamus. *Chem. Senses* 10, 239–258.
- Rasch, B., Born, J., 2013. About Sleep's Role in Memory. *Physiol. Rev.* 93, 681–766. <https://doi.org/10.1152/physrev.00032.2012>
- Ravel, N., Caille, D., Pager, J., 1987. A centrifugal respiratory modulation of olfactory bulb unit activity: a study on acute rat preparation. *Exp. Brain Res.* 65, 623–628.
- Ravel, N., Pager, J., 1990. Respiratory patterning of the rat olfactory bulb unit activity: nasal versus tracheal breathing. *Neurosci. Lett.* 115, 213–218.
- Rojas-Libano, D., Wimmer del Solar, J., Aguilar-Rivera, M., Montefusco-Siegmund, R., Maldonado, P.E., 2018. Local cortical activity of distant brain areas can phase-lock to the olfactory bulb's respiratory rhythm in the freely behaving rat. *J. Neurophysiol.* 120, 960–972.
- Roumis, D.K., Frank, L.M., 2015. Hippocampal sharp-wave ripples in waking and sleeping states. *Curr. Opin. Neurobiol.* 35, 6–12. <https://doi.org/10.1016/j.conb.2015.05.001>
- Roux, S.G., Garcia, S., Bertrand, B., Cenier, T., Vigouroux, M., Buonviso, N., Litaudon, P., 2006. Respiratory cycle as time basis: an improved method for averaging olfactory neural events. *J. Neurosci. Methods* 152, 173–178.

- Roy, A., Svensson, F.P., Mazeh, A., Kocsis, B., 2017. Prefrontal-hippocampal coupling by theta rhythm and by 2–5 Hz oscillation in the delta band: The role of the nucleus reuniens of the thalamus. *Brain Struct. Funct.* 222, 2819–2830.
- Sageman, S., 2004. Breaking through the despair: spiritually oriented group therapy as a means of healing women with severe mental illness. *J. Am. Acad. Psychoanal. Dyn. Psychiatry* 32, 125–141.
- Sakakibara, M., Hayano, J., Oikawa, L.O., Katsamanis, M., Lehrer, P., 2013. Heart rate variability biofeedback improves cardiorespiratory resting function during sleep. *Appl. Psychophysiol. Biofeedback* 38, 265–271.
- Sanchez-Vives, M.V., McCormick, D.A., 2000. Cellular and network mechanisms of rhythmic recurrent activity in neocortex. *Nat. Neurosci.* 3, 8.
- Scheffzük, C., Kukushka, V.I., Vyssotski, A.L., Draguhn, A., Tort, A.B., Brankačk, J., 2011. Selective coupling between theta phase and neocortical fast gamma oscillations during REM-sleep in mice. *PloS One* 6, e28489.
- Schomburg, E.W., Anastassiou, C.A., Buzsáki, G., Koch, C., 2012. The Spiking Component of Oscillatory Extracellular Potentials in the Rat Hippocampus. *J. Neurosci.* 32, 11798–11811. <https://doi.org/10.1523/JNEUROSCI.0656-12.2012>
- Schomburg, E.W., Fernández-Ruiz, A., Mizuseki, K., Berényi, A., Anastassiou, C.A., Koch, C., Buzsáki, G., 2014. Theta phase segregation of input-specific gamma patterns in entorhinal-hippocampal networks. *Neuron* 84, 470–485.
- Siapas, A.G., Wilson, M.A., 1998. Coordinated interactions between hippocampal ripples and cortical spindles during slow-wave sleep. *Neuron* 21, 1123–1128.
- Siclari, F., Bernardi, G., Cataldi, J., Tononi, G., 2018. Dreaming in NREM sleep: a high-density EEG study of slow waves and spindles. *J. Neurosci.* 38, 9175–9185.
- Siclari, F., Tononi, G., 2017. Local aspects of sleep and wakefulness. *Curr. Opin. Neurobiol.* 44, 222–227.
- Siepmann, M., Aykac, V., Unterdörfer, J., Petrowski, K., Mueck-Weymann, M., 2008. A pilot study on the effects of heart rate variability biofeedback in patients with depression and in healthy subjects. *Appl. Psychophysiol. Biofeedback* 33, 195–201.
- Sirota, A., Csicsvari, J., Buhl, D., Buzsáki, G., 2003. Communication between neocortex and hippocampus during sleep in rodents. *Proc. Natl. Acad. Sci.* 100, 2065–2069.
- Sirota, A., Montgomery, S., Fujisawa, S., Isomura, Y., Zugaro, M., Buzsáki, G., 2008. Entrainment of neocortical neurons and gamma oscillations by the hippocampal theta rhythm. *Neuron* 60, 683–697.
- Sobel, E.C., Tank, D.W., 1993. Timing of odor stimulation does not alter patterning of olfactory bulb unit activity in freely breathing rats. *J. Neurophysiol.* 69, 1331–1337.
- Sosulski, D.L., Bloom, M.L., Cutforth, T., Axel, R., Datta, S.R., 2011. Distinct representations of olfactory information in different cortical centres. *Nature* 472, 213–216.

- Staresina, B.P., Bergmann, T.O., Bonnefond, M., Van Der Meij, R., Jensen, O., Deuker, L., Elger, C.E., Axmacher, N., Fell, J., 2015. Hierarchical nesting of slow oscillations, spindles and ripples in the human hippocampus during sleep. *Nat. Neurosci.* 18, 1679–1686.
- Stark, R., Schienle, A., Walter, B., Vaitl, D., 2000. Effects of paced respiration on heart period and heart period variability. *Psychophysiology* 37, 302–309.
- Steriade, M., 2006. Grouping of brain rhythms in corticothalamic systems. *Neuroscience* 137, 1087–1106. <https://doi.org/10.1016/j.neuroscience.2005.10.029>
- Steriade, M., 1993. Central core modulation of spontaneous oscillations and sensory transmission in thalamocortical systems. *Curr. Opin. Neurobiol.* 3, 619–625. [https://doi.org/10.1016/0959-4388\(93\)90064-6](https://doi.org/10.1016/0959-4388(93)90064-6)
- Steriade, M., Nunez, A., Amzica, F., 1993a. A novel slow (< 1 Hz) oscillation of neocortical neurons in vivo: depolarizing and hyperpolarizing components. *J. Neurosci.* 13, 3252–3265.
- Steriade, M., Nuñez, A., Amzica, F., 1993b. Intracellular analysis of relations between the slow (< 1 Hz) neocortical oscillation and other sleep rhythms of the electroencephalogram. *J. Neurosci.* 13, 3266–3283.
- Suess, W.M., Alexander, A.B., Smith, D.D., Sweeney, H.W., Marion, R.J., 1980. The effects of psychological stress on respiration: a preliminary study of anxiety and hyperventilation. *Psychophysiology* 17, 535–540.
- Tononi, G., Cirelli, C., 2014. Sleep and the Price of Plasticity: From Synaptic and Cellular Homeostasis to Memory Consolidation and Integration. *Neuron* 81, 12–34. <https://doi.org/10.1016/j.neuron.2013.12.025>
- Tort, A.B., Brankačk, J., Draguhn, A., 2018. Respiration-entrained brain rhythms are global but often overlooked. *Trends Neurosci.* 41, 186–197.
- Tort, A.B., Hammer, M., Zhang, J., Brankačk, J., Draguhn, A., 2021. Temporal relations between cortical network oscillations and breathing frequency during REM sleep. *J. Neurosci.* 41, 5229–5242.
- Tort, A.B.L., Kramer, M.A., Thorn, C., Gibson, D.J., Kubota, Y., Graybiel, A.M., Kopell, N.J., 2008. Dynamic cross-frequency couplings of local field potential oscillations in rat striatum and hippocampus during performance of a T-maze task. *Proc. Natl. Acad. Sci.* 105, 20517–20522. <https://doi.org/10.1073/pnas.0810524105>
- Tort, A.B.L., Ponsel, S., Jessberger, J., Yanovsky, Y., Brankačk, J., Draguhn, A., 2018. Parallel detection of theta and respiration-coupled oscillations throughout the mouse brain. *Sci. Rep.* 8, 6432. <https://doi.org/10.1038/s41598-018-24629-z>
- Totty, M.S., Chesney, L.A., Geist, P.A., Datta, S., 2017. Sleep-dependent oscillatory synchronization: a role in fear memory consolidation. *Front. Neural Circuits* 11, 49.
- Trevelyan, A.J., 2009. The direct relationship between inhibitory currents and local field potentials. *J. Neurosci.* 29, 15299–15307.
- Tsanov, M., Chah, E., Reilly, R., O'Mara, S.M., 2014. Respiratory cycle entrainment of septal neurons mediates the fast coupling of sniffing rate and hippocampal theta rhythm. *Eur. J. Neurosci.* 39, 957–974. <https://doi.org/10.1111/ejn.12449>

- Van Diest, I., Verstappen, K., Aubert, A.E., Widjaja, D., Vansteenwegen, D., Vlemincx, E., 2014. Inhalation/exhalation ratio modulates the effect of slow breathing on heart rate variability and relaxation. *Appl. Psychophysiol. Biofeedback* 39, 171–180.
- Van Essen, D.C., Anderson, C.H., Felleman, D.J., 1992. Information processing in the primate visual system: an integrated systems perspective. *Science* 255, 419–423.
- Vanderwolf, C.H., 1969. Hippocampal electrical activity and voluntary movement in the rat. *Electroencephalogr. Clin. Neurophysiol.* 26, 407–418.
- Vanhatalo, S., Palva, J.M., Holmes, M.D., Miller, J.W., Voipio, J., Kaila, K., 2004. Infralow oscillations modulate excitability and interictal epileptic activity in the human cortex during sleep. *Proc. Natl. Acad. Sci.* 101, 5053–5057. <https://doi.org/10.1073/pnas.0305375101>
- Varela, F., Lachaux, J.-P., Rodriguez, E., Martinerie, J., 2001. The brainweb: phase synchronization and large-scale integration. *Nat. Rev. Neurosci.* 2, 229–239.
- Vibert, J.F., Caille, D., Bertrand, F., Gromysz, H., Hugelin, A., 1979. Ascending projection from the respiratory centre to mesencephalon and diencephalon. *Neurosci. Lett.* 11, 29–33.
- Viczko, J., Sharma, A.V., Pagliardini, S., Wolansky, T., Dickson, C.T., 2014. Lack of respiratory coupling with neocortical and hippocampal slow oscillations. *J. Neurosci.* 34, 3937–3946.
- Vijayan, S., Lepage, K.Q., Kopell, N.J., Cash, S.S., 2017. Frontal beta-theta network during REM sleep. *Elife* 6, e18894.
- von Nicolai, C., Engler, G., Sharott, A., Engel, A.K., Moll, C.K., Siegel, M., 2014. Corticostriatal coordination through coherent phase-amplitude coupling. *J. Neurosci.* 34, 5938–5948.
- von Stein, A., Sarnthein, J., 2000. Different frequencies for different scales of cortical integration: from local gamma to long range alpha/theta synchronization. *Int. J. Psychophysiol.* 38, 301–313. [https://doi.org/10.1016/S0167-8760\(00\)00172-0](https://doi.org/10.1016/S0167-8760(00)00172-0)
- Vyazovskiy, V.V., Olcese, U., Hanlon, E.C., Nir, Y., Cirelli, C., Tononi, G., 2011. Local sleep in awake rats. *Nature* 472, 443–447.
- Welker, W.I., 1964. Analysis of sniffing of the albino rat 1. *Behaviour* 22, 223–244.
- Wesson, D.W., Donahou, T.N., Johnson, M.O., Wachowiak, M., 2008. Sniffing Behavior of Mice during Performance in Odor-Guided Tasks. *Chem. Senses* 33, 581–596. <https://doi.org/10.1093/chemse/bjn029>
- Wilson, D.A., 1998. Habituation of odor responses in the rat anterior piriform cortex. *J. Neurophysiol.* 79, 1425–1440.
- Winson, J., 1974. Patterns of hippocampal theta rhythm in the freely moving rat. *Electroencephalogr. Clin. Neurophysiol.* 36, 291–301. [https://doi.org/10.1016/0013-4694\(74\)90171-0](https://doi.org/10.1016/0013-4694(74)90171-0)
- Wolansky, T., Clement, E.A., Peters, S.R., Palczak, M.A., Dickson, C.T., 2006. Hippocampal Slow Oscillation: A Novel EEG State and Its Coordination with Ongoing

- Neocortical Activity. *J. Neurosci.* 26, 6213–6229. <https://doi.org/10.1523/JNEUROSCI.5594-05.2006>
- Womelsdorf, T., Schoffelen, J.-M., Oostenveld, R., Singer, W., Desimone, R., Engel, A.K., Fries, P., 2007. Modulation of Neuronal Interactions Through Neuronal Synchronization. *Science* 316, 1609–1612. <https://doi.org/10.1126/science.1139597>
  - Wong, R.K.S., Prince, D.A., BASBAUMt, A.I., 1979. Intradendritic recordings from hippocampal neurons. *Proc Natl Acad Sci USA* 5.
  - Xu, W., De Carvalho, F., Clarke, A.K., Jackson, A., 2021. Communication from the cerebellum to the neocortex during sleep spindles. *Prog. Neurobiol.* 199, 101940.
  - Yackle, K., Schwarz, L.A., Kam, K., Sorokin, J.M., Huguenard, J.R., Feldman, J.L., Luo, L., Krasnow, M.A., 2017. Breathing control center neurons that promote arousal in mice. *Science* 355, 1411–1415.
  - Yanovsky, Y., Ciatipis, M., Draguhn, A., Tort, A.B., Brankačk, J., 2014. Slow oscillations in the mouse hippocampus entrained by nasal respiration. *J. Neurosci.* 34, 5949–5964.
  - Ylinen, A., Bragin, A., Nádasdy, Z., Jandó, G., Szabo, I., Sik, A., Buzsáki, G., 1995. Sharp wave-associated high-frequency oscillation (200 Hz) in the intact hippocampus: network and intracellular mechanisms. *J. Neurosci.* 15, 30–46.
  - Yuen, A.W., Sander, J.W., 2010. Can slow breathing exercises improve seizure control in people with refractory epilepsy? A hypothesis. *Epilepsy Behav.* 18, 331–334.
  - Zaccaro, A., Piarulli, A., Laurino, M., Garbella, E., Menicucci, D., Neri, B., Gemignani, A., 2018. How breath-control can change your life: a systematic review on psychophysiological correlates of slow breathing. *Front. Hum. Neurosci.* 12, 353.
  - Zanos, T.P., Mineault, P.J., Pack, C.C., 2011. Removal of Spurious Correlations Between Spikes and Local Field Potentials. *J Neurophysiol* 105, 13.
  - Zelano, C., Jiang, H., Zhou, G., Arora, N., Schuele, S., Rosenow, J., Gottfried, J.A., 2016. Nasal respiration entrains human limbic oscillations and modulates cognitive function. *J. Neurosci.* 36, 12448–12467.
  - Zhang, J.-X., Harper, R.M., Frysinger, R.C., 1986. Respiratory modulation of neuronal discharge in the central nucleus of the amygdala during sleep and waking states. *Exp. Neurol.* 91, 193–207.
  - Zhong, W., Ciatipis, M., Wolfenstetter, T., Jessberger, J., Müller, C., Ponsel, S., Yanovsky, Y., Brankačk, J., Tort, A.B., Draguhn, A., 2017. Selective entrainment of gamma subbands by different slow network oscillations. *Proc. Natl. Acad. Sci.* 114, 4519–4524.
  - Zucker, T.L., Samuelson, K.W., Muench, F., Greenberg, M.A., Gevirtz, R.N., 2009. The effects of respiratory sinus arrhythmia biofeedback on heart rate variability and posttraumatic stress disorder symptoms: a pilot study. *Appl. Psychophysiol. Biofeedback* 34, 135.

## **6. Annexes**

## **6.1 Co-author published article**



OPEN

# The deep and slow breathing characterizing rest favors brain respiratory-drive

Baptiste Girin<sup>1,3</sup>, Maxime Juventin<sup>1,3</sup>, Samuel Garcia<sup>1</sup>, Laura Lefèvre<sup>2</sup>, Corine Amat<sup>1</sup>, Nicolas Fourcaud-Trocme<sup>1,4</sup> & Nathalie Buonviso<sup>1,4</sup>✉

A respiration-locked activity in the olfactory brain, mainly originating in the mechano-sensitivity of olfactory sensory neurons to air pressure, propagates from the olfactory bulb to the rest of the brain. Interestingly, changes in nasal airflow rate result in reorganization of olfactory bulb response. By leveraging spontaneous variations of respiratory dynamics during natural conditions, we investigated whether respiratory drive also varies with nasal airflow movements. We analyzed local field potential activity relative to respiratory signal in various brain regions during waking and sleep states. We found that respiration regime was state-specific, and that quiet waking was the only vigilance state during which all the recorded structures can be respiration-driven whatever the respiratory frequency. Using CO<sub>2</sub>-enriched air to alter respiratory regime associated to each state and a respiratory cycle based analysis, we evidenced that the large and strong brain drive observed during quiet waking was related to an optimal trade-off between depth and duration of inspiration in the respiratory pattern, characterizing this specific state. These results show for the first time that changes in respiration regime affect cortical dynamics and that the respiratory regime associated with rest is optimal for respiration to drive the brain.

Transferring information across distant brain regions is essential for the expression of specific behaviors. The communication through coherence hypothesis<sup>1</sup> recently sets the respiratory rhythm as a global rhythm, potentially influencing behavior by modulating cortical neurodynamics<sup>2,3</sup>. Indeed, number of studies have described breathing as modulating complex behaviors. In animals, respiration notably interacts with vocalizations, whisking and licking<sup>4,5</sup>. In humans, a clear relationship exists between breathing and cognitive processing<sup>6</sup>. Notably, respiration modulates olfactory memory consolidation<sup>6</sup> and cognitive performance during retrieval<sup>7</sup>. Pain processing is gated during exhalation<sup>8</sup>. In experiments with forced breathing, the gripping force is greater during exhalation than during inhalation<sup>9</sup>. The recognition of facial fear expression is faster if the stimulus is presented during the inspiratory phase<sup>10</sup>. Even when no instructions for inspiration are given, subjects inhale spontaneously at the beginning of a cognitive task and these inhalations induce changes in brain network functional connectivity<sup>11</sup>. Importantly, this last study also emphasized the involvement of nasal respiration in improving performance in a visuo-spatial task.

Respiration also modulates ongoing activity in diverse cerebral regions both in rodents<sup>12–17</sup> and humans<sup>10,18</sup>. Such a respiratory drive surely depends on nasal respiration as it is suppressed when nasal airflow is by-passed. In rodents, respiration-locked activity is eliminated in the barrel cortex when nasal airflow is stopped after olfactory bulbectomy<sup>12</sup>; in hippocampus, respiration-related slow rhythm is suppressed under tracheotomy<sup>19,20</sup> and influence of respiration on sharp wave ripples occurrence is eliminated when olfactory bulb (OB) activity is inhibited<sup>15</sup>. In human, oscillatory power in olfactory cortex and limbic structures dissipates when subjects breathe through the mouth<sup>10</sup>. Even if the involvement of a central component cannot be excluded<sup>21</sup>, the main origin of this respiratory drive during nasal breathing is likely to be found in the olfactory receptor cells mechano-sensitivity to pressure changes in the nasal cavity during successive inspirations and expirations<sup>22</sup>.

A respiration-locked activity propagates from the olfactory epithelium to the OB where it has been extensively described. In brief, respiration has been shown to modulate OB local field potential (LFP) fast oscillations<sup>23</sup>, and both unitary discharges<sup>24–26</sup> and membrane potential of principal neurons<sup>27,28</sup>. Interestingly, changes in airflow

<sup>1</sup>Lyon Neuroscience Research Center (CRNL), Inserm U 1028, CNRS UMR 5292, University Lyon 1, 69675 Bron, France. <sup>2</sup>Present address: Medical Research Council Brain Network Dynamics Unit, Nuffield Department of Clinical Neurosciences, University of Oxford, Oxford OX1 3TH, UK. <sup>3</sup>These authors contributed equally: Baptiste Girin and Maxime Juventin. <sup>4</sup>These authors jointly supervised this work: Fourcaud-Trocme and Nathalie Buonviso. ✉email: nathalie.buonviso@cnr.fr

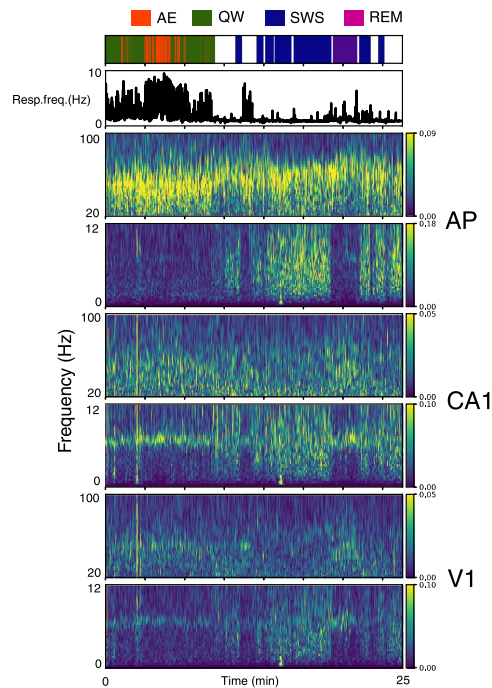


**Figure 1.** Example of a 25 min long recording in anterior piriform cortex (AP), hippocampus CA1 and primary visual cortex (V1) regions. Top panel: states scoring with active exploration (AE, red), quiet awaking (QW, green), slow-wave sleep (SWS, blue), and rapid-eye movements sleep (REM, pink). Periods not scored (not all criteria met, see “Methods”) appear in white. Second panel: Instantaneous respiratory frequency (in Hz). Other panels from top to bottom: For each structure (AP, CA1, V1), time–frequency representation of LFP in the low (0.5–12 Hz) and high (20–100 Hz) frequency range. Warm colors indicate high power.

rate are sufficient to substantially reorganize the OB response: cellular odor-evoked activities and LFP oscillations are strongly modified by nasal flow rate<sup>29–32</sup>. A low/high flow rate favors a beta/gamma regime in the OB, respectively<sup>31</sup>. Nasal airflow rate, but not respiratory frequency, is a key factor that regulates olfactory sensitivity of the OB glomeruli as shown by calcium imaging combined with an artificial sniffing setup<sup>29</sup>.

Yet, nasal airflow varies in both flow rate and frequency according to respiration dynamics. Therefore, if the respiratory drive of the brain originates in nasal airflow movements, then it should vary with respiration dynamics that occur spontaneously during natural conditions. We took advantage of the spontaneous variations of respiration dynamics during waking and sleep states to explore respiratory drive in various brain regions: olfactory bulb (OB), piriform (AP), prefrontal (PFC), somatosensory (S1) and visual (V1) cortices, dorsal CA1 (CA1) and dentate gyrus (DG) hippocampal areas. We analyzed their LFP activity relative to respiratory signal. Importantly, we did not restrict our study to epochs of respiratory steady state as chosen by others<sup>17</sup> but instead included signals from full waking and sleep periods, thus encompassing the wide range of respiratory frequencies expressed by a freely moving animal. This reveals that respiratory regime was state-specific, and that quiet waking was the only vigilance state where both olfactory and non-olfactory structures can be respiration-coupled whatever the respiration frequency (0.8–5 Hz) expressed during this state. We used a CO<sub>2</sub>-enriched air in the plethysmograph to alter the respiratory regime associated with each state. Using a respiratory cycle based analysis, we evidenced that the large and strong brain entrainment during quiet waking was related to its specific respiration regime consisting in an optimal trade-off between depth and duration of inspiration. These results show for the first time that changes in respiratory regime alter the cortical dynamics and that the respiratory regime observed during rest is optimal for respiration to drive the brain.

## Results

Respiration signal, recorded via a whole-body plethysmograph, and LFPs were collected from 13 rats during active exploration (AE), quiet waking (QW), slow-wave sleep (SWS) and rapid-eye movements (REM) episodes (Fig. 1; see “Methods” section for state scoring). Typically, respiratory frequency was higher during awake states

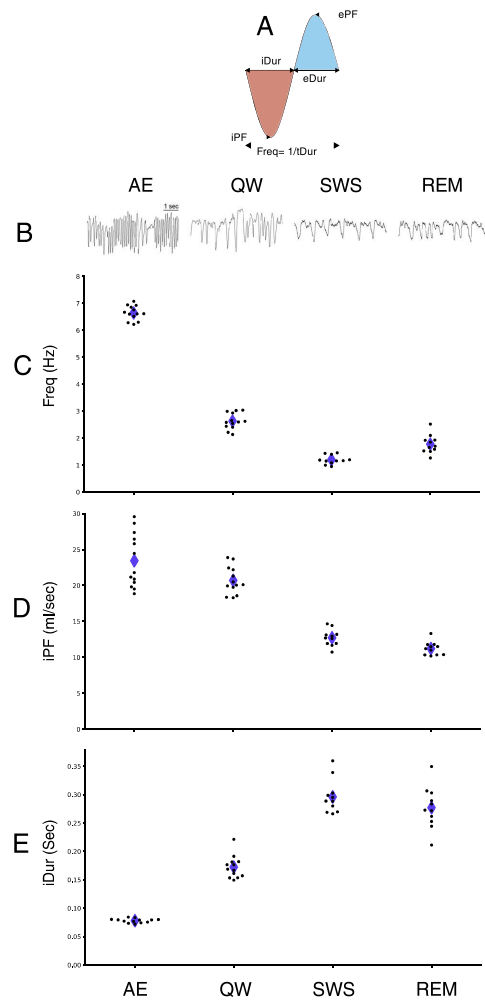


**Figure 2.** Respiration regimes associated with brain states. (A) Schematic representation of measured respiratory features. (B) Examples of respiration raw traces during active exploration (AE), quiet waking (QW), slow-wave sleep (SWS) and rapid eye movements sleep (REM). (C–E) Scatter plot of respiration features measured during each brain state (average per rat): frequency (Freq, C), inspiration peak flow rate (iPF, D), and inspiration duration (iDur, E). Repeated measure ANOVA tests with the 11 rats recorded in all states show significant effects of state on all respiratory features (see main text for details). Black dots: individual values per animal; Purple diamonds: means.

and highly variable, whereas it was low and more stable during sleep states. LFP activities varied both in the low (0.5–10 Hz) and high (20–100 Hz) frequency bands. A major innovation of our study is that we analyzed data from the wide range of 0–10 Hz respiration frequencies, i.e. neither restricting to epochs where respiration frequency did not overlap with theta frequency nor focusing on stationary periods, as proceeded in a similar study<sup>17</sup>. This allowed us to track faithfully respiratory brain entrainment under non-stationary respiration regimes. We first explored to what extent respiratory regime varied with behavioral state by analyzing the following features (Fig. 2A):

- instantaneous respiratory frequency (Freq, in Hz), extracted from inhalation and exhalation durations (iDur, eDur).

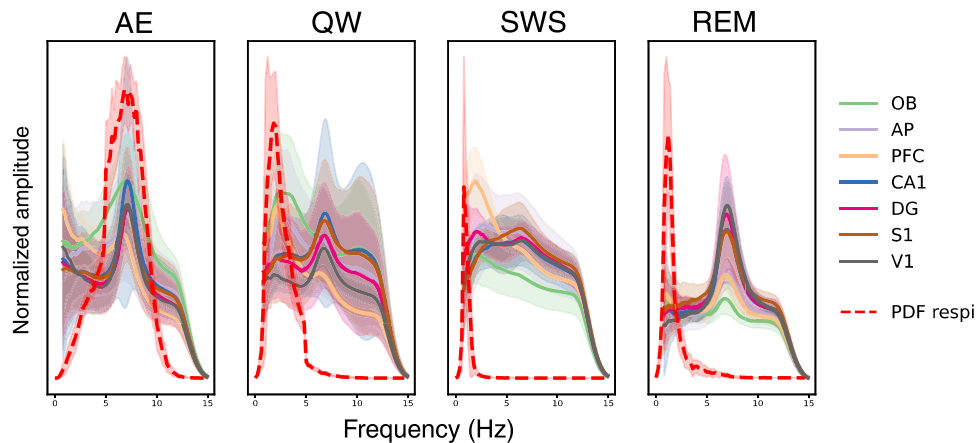


**Figure 3.** Normalized power spectral density of LFP and probability density function (PDF) of respiration frequency during the four brain states (AE active exploration, QW quiet waking, SWS slow-wave sleep, REM rapid eye movements sleep). Normalized spectra of LFP signals recorded in each structure (solid lines) were averaged across rats. Shaded areas display the standard deviations. The probability density function (PDF) of respiration frequencies (dotted red lines) were average across rats, shaded areas display the standard deviations. See sample size (number of rats and sites per state) in Table 1. See “Methods” section for spectrum normalization procedure but note that relative amplitude of spectra across states has been preserved.

– inspiration and expiration peak flow rate (iPF, ePF, respectively, in  $\text{mL s}^{-1}$ ), representing the maximal flow rate.

Representative raw traces (Fig. 2B) illustrate the diversity of respiratory patterns between the different states, which was confirmed at the group level (Fig. 2C–E). All respiration features significantly varied between states (repeated measures ANOVA test: for Freq:  $F_{3,30} = 65.0$ ,  $p < 0.001$ ; for iPF:  $F_{3,30} = 114.4$ ,  $p < 0.001$ ; for iDur:  $F_{3,30} = 344.1$ ,  $p < 0.001$ . Post-hoc paired t-test with Holm correction showed highly significant differences between all state pairs,  $p < 0.001$ , except  $p = 0.019$  between SWS and REM for iDur and  $p = 0.073$  between SWS and REM for iPF. For all tests  $N = 11$  because 2 rats which have not been recorded during SWS and REM states have been excluded, but their data points in awake states are still plotted in Fig. 2C–E). Freq was particularly higher during AE (mean 6.58 Hz, SD 0.24 Hz, Fig. 2C) compared to QW (mean 2.56 Hz, SD 0.27 Hz) as sniffing activity was predominant and characterized by i) high iPF even if highly variable (AE: mean 23.8  $\text{mL/s}$ , SD 3.9  $\text{mL/s}$ ; compared to QW: mean 20.8  $\text{mL/s}$ , SD 2.0  $\text{mL/s}$ , Fig. 2D) and high ePF (AE: mean 19.0  $\text{mL/s}$ , SD 2.5  $\text{mL/s}$ ; compared to QW: mean 14.0  $\text{mL/s}$ , SD 1.5  $\text{mL/s}$ , not shown) and ii) very short iDur (AE: mean 0.08 s, SD 0.004 s; compared to QW: mean 0.18 s, SD 0.02 s, Fig. 2E) and very short eDur (AE mean: 0.097 s, SD 0.006 s; compared to QW: mean 0.31 s, SD: 0.06 s, not shown). iPF was much higher for waking states (AE and QW, see above for values) than for sleep ones (SWS: mean 12.7  $\text{mL/s}$ , SD 1.2  $\text{mL/s}$ ; and REM: mean 11.2  $\text{mL/s}$ , SD 0.9  $\text{mL/s}$ ). Similarly, iDur was shorter for waking states (AE and QW, see above for values) than for sleep ones (SWS: mean 0.30 s, SD 0.03 s; and REM: mean 0.28 s, SD 0.04 s). Then a slow Freq, a low iPF, and a long iDur characterized sleep states. Similar observations and statistical differences were made on expiration features (not shown). To summarize, AE was characterized by a high iPF and a short iDur (related to sniffing activity), whereas both sleep states exhibited a low iPF and a long iDur. QW regime had distinctive features with both iPF and iDur in the mid-range.

Then, we investigated to what extent brain respiratory-drive, as described by others<sup>3</sup>, varied with brain state. We thus tracked respiratory frequency in the LFP recordings of each structure, during each state. Visual inspection of power spectra (Fig. 3) showed no clear overlap between respiration and LFP oscillations frequencies, except during AE where the animals actively explored the environment. Nevertheless, it is difficult in that case to disentangle sniffing-related activity (6.58 Hz, SD 0.24 Hz) from the prominent exploration-related theta rhythm (about 7 Hz, as measured in dorsal CA1 during REM<sup>17</sup>). We observed that theta rhythm (6–8 Hz range, according to peaks in spectra, see Fig. 3) was a major frequency during all states, except during SWS where delta activity (0–5 Hz) dominated. During QW, in addition to a clear theta rhythm in all structures except OB (Fig. 3, green line), spectral analysis evidenced a high power in the delta band (0–5 Hz), in all structures, partly overlapping with respiratory frequencies. During SWS, while respiratory frequency was very slow and constant around 1 Hz, LFP power was high in the whole delta band. Similarly, during REM state, respiration and LFP frequencies poorly overlapped: while LFP power peaked in the theta range (around 7 Hz), respiration frequencies lied in a much lower range (0.5–4 Hz). To summarize, these results suggest that brain respiratory-drive probably varies with brain state even if we could not observe a clear overlapping between respiratory and LFP frequencies.

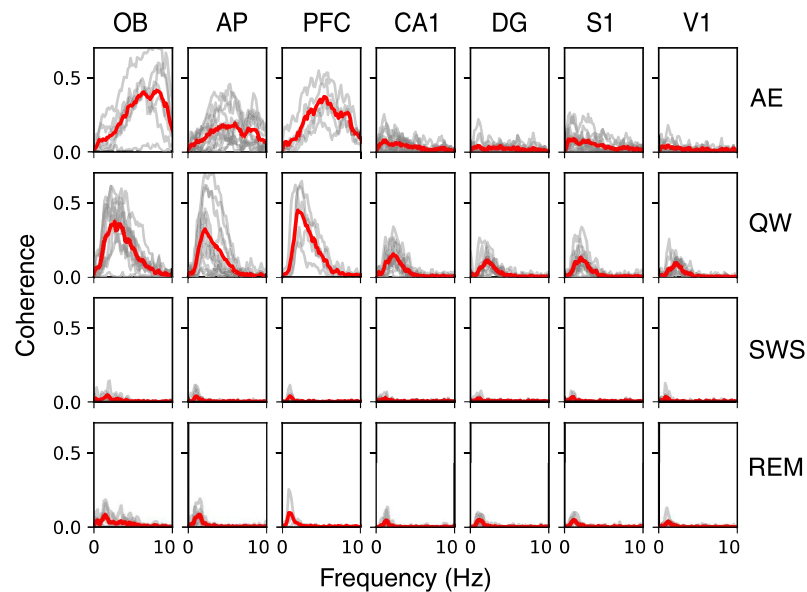


**Figure 4.** Coherence spectra between LFP and Respiratory signals during the four brain states (AE active exploration, QW quiet waking, SWS slow-wave sleep, REM rapid eye movements sleep), in all structures, in the 0.5–10 Hz range. Results obtained from simultaneous recordings in each rat (grey lines) and averaged across animals (red lines). See sample size (number of rats) in Table 1 and p values in Supplementary Table S1.

To go further, we then performed coherence analyses between LFP signals for all the recorded brain regions and respiration in the low frequency band (0.5–10 Hz) during the four states (Fig. 4). As described in “Methods” section, peak coherence values for actual data were compared to surrogates data. Actual and surrogates distributions significantly differed in all recorded regions and all states (see Supplementary Table S1), suggesting that all the recorded areas were respiration-coupled whatever the brain state. However, visual inspection of coherence spectra (Fig. 4) and actual values (Supplementary Table S1) relativized this conclusion since it is obvious that coherence spectra are particularly flat during SWS and REM, whatever the structure. On the contrary, coherence appeared more clearly in waking states (AE and QW, Fig. 4). During AE epochs, the respiration-LFP coherence was high (0.2–0.7) for  $\text{Freq} > 5$  Hz and only in olfactory structures (OB, AP) and PFC. It is noteworthy that QW state was the only state during which coherence spectra appeared not flat in all the recorded areas. During SWS and REM, although power spectra exhibited a high power in the low frequency range (see Figs. 1, 3), the coherence with respiration, even if significant, was very weak (10 times smaller than during QW). To summarize, when analyzing respiration-LFP coherence over a large range of respiratory frequencies, we observed that respiratory drive of brain areas varied with vigilance state, QW state being the state where LFP-respiration coherence is the highest in all the structures.

Then, we searched in which state respiratory frequency could dominate in the LFP signal. We computed covariation maps (2-dimensional distribution of joined LFP-respiration frequencies across time) for all states and recorded structures, as described in “Methods”, focusing on the 0.5–10 Hz frequency range (Fig. 5). This analysis beneficially complements coherence analysis since it allows tracking instantaneous synchrony in the data. A highlighted diagonal in the covariation maps indicates that LFP predominantly oscillated at the respiratory frequency. Significance of these data has been assessed by comparing, for each rat, the coupling index measured in air condition with coupling indices of 100 surrogate maps obtained by shuffling LFP frequencies across time (see Supplementary Fig. S1, Supplementary Table S2, and methods section). During AE, where rats sniffed in the 5–10 Hz range, the predominant LFP frequency clearly followed respiration in olfactory structures and in PFC (see the highlighted diagonal in OB, AP, PFC and Supplementary Table S2). Oppositely, covariation maps in the other structures showed a uniform theta band activity whatever the respiration frequency (see the highlighted horizontal band in CA1, DG, S1, V1) indicating that these areas maintained an activity in the theta range whatever the respiration frequency. During QW, respiration frequency became predominant in the LFPs of all recorded structures as assessed by the highlighted diagonal in the 1–4 Hz range and by the comparison between actual and surrogate coupling index values (Supplementary Fig. S1B and Supplementary Table S2). In four structures (S1, CA1, V1, DG) respiration frequency co-dominated with theta nevertheless (Fig. 5, see the

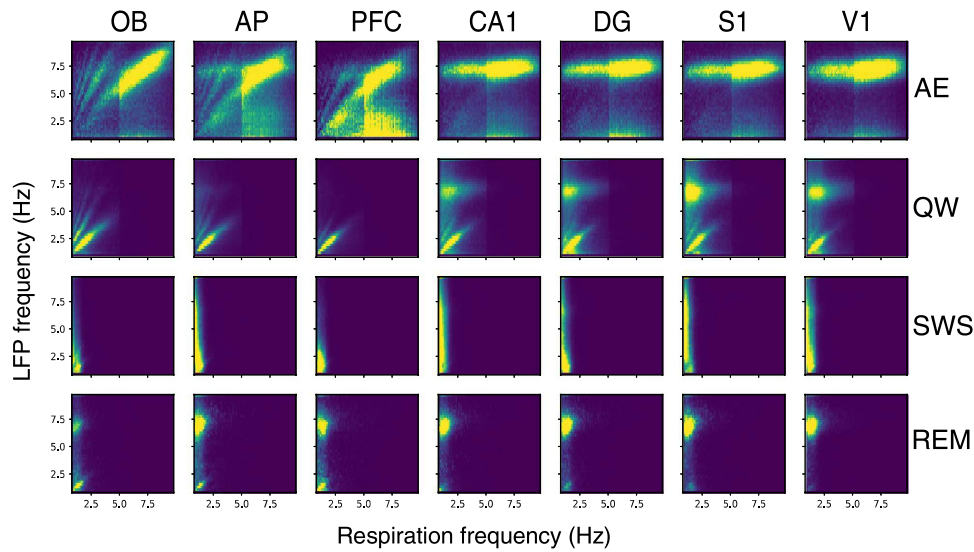


**Figure 5.** Covariation between LFP and respiration frequencies. Covariation maps, averaged across rats, obtained from LFP signals recorded under ambient air in OB, AP, PFC, CA1, DG, S1, and V1. Y-axis represents LFP frequency and X-axis respiratory frequency. The maps are 2-dimensional distributions of joined LFP-respiration frequencies across time (see methods for details), normalized so that the total sum is 1. Point density is represented on a color scale ranging from blue (0) to yellow (map maximum) as the point density increases. For each structure and state, see sample size (number of rats in the average) in Table 1.

yellow spot around 7 Hz). During SWS, the range of respiration frequencies was narrow (see the low variation in Fig. 2C1) so that covariation analysis was not relevant for this state. During REM, LFP predominant frequency was theta and, even if covariation maps showed a highlighted diagonal in OB, AP, PFC and DG (Supplementary Fig. S1A), comparison between actual and surrogate data (Supplementary Fig. S1B) revealed no difference between conditions. These results revealed that LFP mainly oscillated at respiratory frequencies in all the recorded structures only during QW state.

We then explored if the specific respiratory drive of the brain observed during QW could be more related to the specificity of respiration features (frequency and/or peak flow rate) or to that of the QW state itself. To disentangle state vs respiration regime effect, we altered the respiration regime associated with each state using a 5% CO<sub>2</sub>-enriched air in the plethysmograph (n = 5 rats). CO<sub>2</sub> enrichment effectively strongly modified respiratory regime, as summarized in Supplementary Figure S2. Indeed, with addition of CO<sub>2</sub>, Freq significantly varied during AE, QW, and SWS (Supplementary Fig. S2 top panel), iPF greatly increased during all the four states (Supplementary Fig. S2, middle panel), and iDur strongly decreased during SWS and REM (Supplementary Fig. S2, bottom panel). Under such conditions, LFP-respiration coherence was slightly improved (Supplementary Fig. S3), particularly during QW state, in all structures (compare Fig. 4 and Supplementary Fig. S3). Then, covariation maps were also computed for both ambient AIR and CO<sub>2</sub> conditions (n = 5, Supplementary Fig. S4). Under CO<sub>2</sub> condition, covariation maps revealed subtle changes (Supplementary Fig. S4B) that we evidenced by comparing the coupling index between respiration and the predominant LFP frequency in the different structures, during the four states (Fig. 6). As explained in “Methods” section, the coupling index represents the sum of density along the diagonal of the covariation map and varies between 0 and 1 (with 1 being the highest coupling value). Individual data are shown in Fig. 6. The population analysis showed a significant interaction between the condition (AIR or CO<sub>2</sub>) and animal state ( $F_{3,184.5} = 3.53, p = 0.016$ ) but not between condition and structure ( $F_{6,184.5} = 1.70, p = 0.12$ ). We thus looked at results at the animal state level. During AE, the coupling index did not show much changes between ambient AIR and CO<sub>2</sub> conditions (AIR 0.16 vs CO<sub>2</sub> 0.18; T-test,  $t = -1.49, df = 185, p = 0.18$ ) even if olfactory areas and PFC showed a slight increase of coupling index in all the rats. This probably indicates that, even if iPF increased significantly under CO<sub>2</sub> (see Supplementary Fig. S2), LFP frequency in these areas was still dominated by theta rhythm. During QW, the coupling index, already high under AIR condition, markedly increased (AIR 0.33 vs CO<sub>2</sub> 0.42; T-test,  $t = -4.75, df = 185, p < 0.0001$ ), although it increased very modestly in V1. During SWS, even if delta band remained the major frequency, the coupling index increased under CO<sub>2</sub> in most rats and most structures suggesting that respiratory frequency became more predominant under CO<sub>2</sub> compared to AIR condition (AIR 0.22 vs CO<sub>2</sub> 0.30; T-test,  $t = -3.36, df = 185, p = 0.0019$ ). We even observed highlighted diagonal on a short range of respiration frequencies (white arrows, Supplementary Fig. S4B). During REM, while

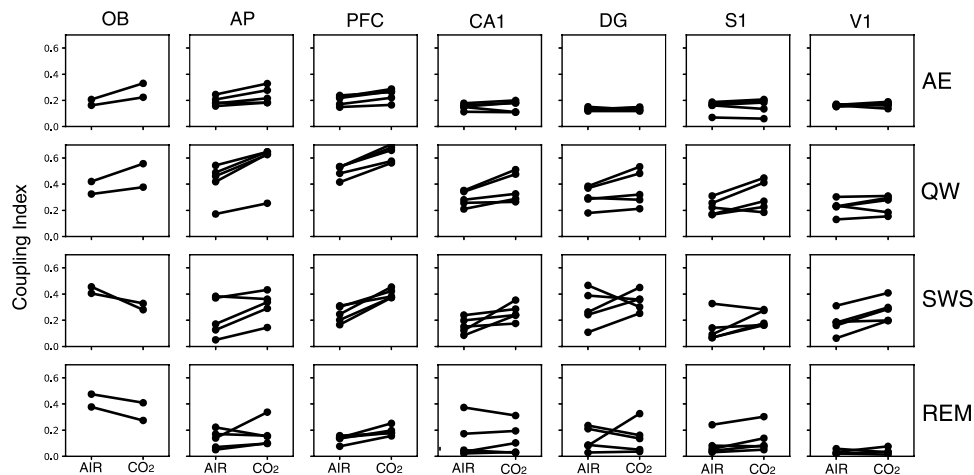


**Figure 6.** Comparison of respiration-LFP coupling between AIR and CO<sub>2</sub> conditions. For each state (lines), each structure (columns), and each rat (black lines), the coupling index is plotted in AIR and CO<sub>2</sub> conditions. AE active exploration, QW quiet waking, SWS slow-wave sleep, REM rapid eye movements sleep.

covariation maps exhibited a clearer and more extended highlighted diagonal (white arrows, Supplementary Fig. S4B), the coupling index in Fig. 6 appeared generally comparable between CO<sub>2</sub> and AIR condition (AIR 0.13 vs CO<sub>2</sub> 0.14; T-test,  $t = -0.56$ ,  $df = 185$ ,  $p = 0.58$ ) except few exceptions (1 rat in AP, all rats in PFC, 1 rat in DG, 2 rats in S1). This is probably because, again here, theta rhythm still dominated, as observed in the covariation maps of all structures except OB (Supplementary Fig. S4). Overall, these results suggest that the strong respiratory brain drive during QW was not related to the neuronal activity characteristics of this peculiar brain state but rather to the respiratory regime associated with this state. Indeed, when extending the respiratory regime of sleep states, via CO<sub>2</sub>-enriched air, to a wider range of frequencies and higher flow rates, respiration frequency became more predominant in LFP signals relative to ambient air condition.

Since CO<sub>2</sub> condition increased both peak flow rate and frequency, the next step was to decipher which of the respiration features was decisive in entraining brain structures to respiration. We focused on two respiration features determining the depth and frequency of respiration: inspiration peak flow rate (iPF) and inspiration duration (iDur). We thus performed a coupling analysis between respiration and LFP frequencies, independently of the brain state, segregating respiratory cycles according to their values of iPF (Fig. 7A) and iDur (Fig. 7B). Both individual and averaged coupling index curves (sample size, see Table 1) followed an inverted-U shape curve: close to zero for low iPF values, it reached a maximum for iPF values around 20 mL s<sup>-1</sup>, then decreased for higher iPF values. This shape was similar for all structures, but with different amplitudes. Indeed, the respiration-LFP coupling as a function of iPF was very strong in olfactory structures and PFC, less so in other areas, but nevertheless still significant (quadratic term significance—i.e. existence of a local maximum—was assessed by comparing generalized mixed-effect linear models with Wald test ( $df = 1$ ): OB:  $\chi^2 = 7.88$ ,  $p = 0.005$ ; CA1:  $\chi^2 = 6.67$ ,  $p = 0.01$ ; PFC:  $\chi^2 = 10.02$ ,  $p = 0.0015$ ; DG:  $\chi^2 = 11.03$ ,  $p = 0.0009$ ; AP:  $\chi^2 = 12.27$ ,  $p = 0.0004$ ; S1:  $\chi^2 = 7.87$ ,  $p = 0.005$ ; V1:  $\chi^2 = 7.88$ ,  $p = 0.005$ ). Similar results were obtained when computing the coupling index as a function of iDur (Fig. 7B). As for iPF, the coupling index indeed evolved following an inverted-U shape curve, optimal for a range of iDur values around 0.15 s (quadratic term was significant for PFC:  $\chi^2 = 6.34$ ,  $p = 0.01$ ; and there were trends for AP:  $\chi^2 = 3.09$ ,  $p = 0.08$ ; and OB:  $\chi^2 = 2.8$ ,  $p = 0.09$ ). To explain the inverted-U shapes of the coupling index curves, we have to consider iPF and iDur simultaneously. In Fig. 7A, the highest values of iPF correspond to the sniffing cycles during AE, which present the shortest iDur. The decreasing phase which followed (Fig. 7B,  $iDur > 0.3$  s) for long iDur values correspond to the sleep states breathing cycles, which also have small iPF values.

Finally, these results show that the best coupling between respiration and LFP frequencies is achieved for inspiration peak flow rate in the range of 20–30 mL/s combined with 0.1–0.2 s inspiration duration. This trade-off between iPF and iDur corresponds to the specific features of respiratory regime associated with the QW state.

## Discussion

We studied how respiration could drive brain areas during spontaneous variations of respiratory regime related to four different behavioral states: active exploration, quiet waking, slow-wave sleep and paradoxical sleep. In addition to confirming previous observations that LFPs in different brain structures can actually be respiration-coupled<sup>12–17</sup>, we unveiled new fundamental findings: (1) a large-scale respiratory drive is a specific characteristic of the quiet waking state, (2) this specificity is due to the respiratory regime associated with this state and not to

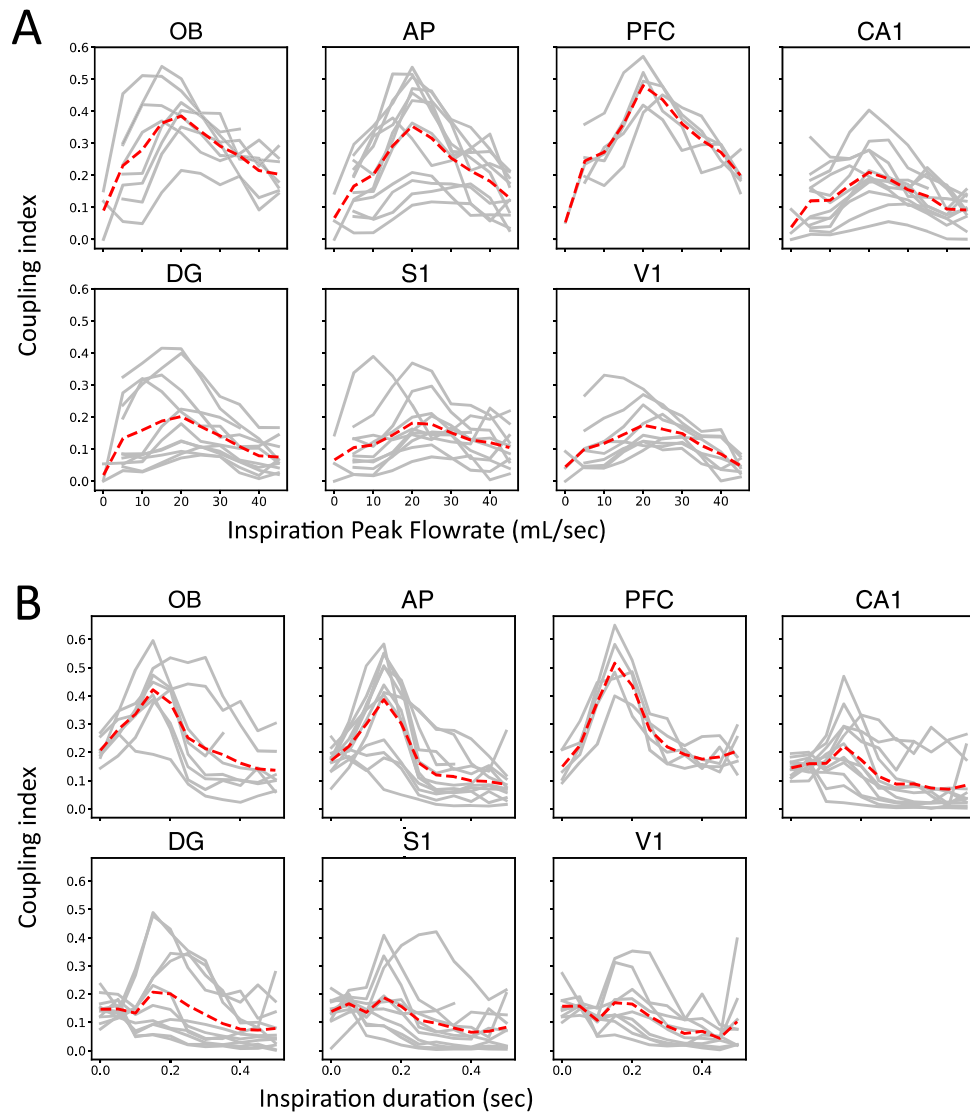


**Figure 7.** Coupling index as a function of inspiration peak flow rate iPF (A) and inspiration duration iDur (B). Data are presented individually for each animal (solid lines, see Table 1 for sample size), and averaged across animals (dotted red lines). The inverted U-shape of coupling index as a function of iPF and iDur was assessed by comparing two generalized mixed linear-models either with or without the quadratic term (see “Methods” for details). The comparison showed that the iPF quadratic term was significant for all areas (Wald test,  $p < 0.02$ , see text for details) and that the iDur quadratic term was significant for some areas (Wald test, PFC:  $p = 0.01$ , and trends for AP and OB,  $p < 0.1$ , see text for details).

Brain structure	AP	ML	DV	n air (AE and QW)	n air (SWS and REM)	n CO <sub>2</sub> (all states)
Olfactory bulb, OB	5.5 <sup>a</sup>	1.5	2	9	7	2
Anterior piriform cortex, AP	2.76	3.5	~6	13	11	5
Dorsal hippocampus CA1, CA1	-2.92	2	~3.5	13	11	5
Dentate gyrus, DG	-4.8	2.8	~3.2	12	10	5
Primary visual cortex, V1	-5.28	4.2	~1.2	9	7	5
Primary somatosensory barrel cortex, S1	-2.4	5	~2	12	10	5
Prefrontal cortex, PFC	3	0.8	~3.5	5	5	5

**Table 1.** Coordinates from bregma (mm) and number of rats (n) in each condition (air and CO<sub>2</sub>). Note that in air condition, we distinguished awake and sleep states because 2 rats were not recorded in sleep states. <sup>a</sup>From naso-frontal suture.

the brain state itself, (3) an optimal respiratory regime for large brain entrainment is a deep and long inhalation (peak flow rate in the range of 20–30 mL/s and duration in the range of 0.1–0.2 s).

We described for the first time that, even if each of the recorded structures can be occasionally entrained by respiration as reported by others<sup>17,33</sup>, a global respiratory drive of the brain only emerged during quiet waking state. A respiratory drive in different brain areas with regard to the brain state has been previously described. However, none of them reported this specificity of the quiet waking state. Indeed, while one study focused on rest periods (similar to the QW state in our study) and exploration (similar to the AE state in our study) to investigate how gamma band activity in distant areas phase-locked to respiratory activity of the olfactory bulb<sup>33</sup>, an EEG study in the cat described the respiratory slow wave in the waking state but did not differentiate rest from exploration<sup>34</sup>. Respiratory drive in different brain areas was also explored but restricted to exploration periods recorded in the animal home cage and REM sleep epochs recorded in a plethysmograph<sup>1</sup>. Furthermore, because in both states theta oscillations and respiration may overlap in frequency, they also chose to analyze only epochs where respiration frequency and theta frequency were not overlapping. We took a different approach by exploring LFP-respiration covariation whatever the brain state, and including all respiratory frequencies. Finally, we have been the first to explore respiratory drive simultaneously in a large brain network, during four brain states, and during the whole duration of recordings. This strategy allowed us to highlight the specificity of the quiet waking state.

We also provided evidence that the global respiratory drive observed during quiet waking is not related to the state itself but rather to the respiratory regime associated. This demonstration has been possible because, using a CO<sub>2</sub>-enriched air in the plethysmograph, we modified the respiratory regimes associated with the different states, thus extending the range of possible respiratory frequencies and amplifying nasal airflow. In such condition, we observed that LFP frequency could reflect respiratory frequency during SWS and REM states, whereas it was not observable in ambient air condition. We concluded that the global brain respiratory drive was determined by respiratory regime and not by the brain state itself. We chose CO<sub>2</sub> over respiratory nuclei stimulation<sup>35</sup> to modify respiratory regime mainly because the method was easier to implement and not invasive. However, CO<sub>2</sub> use remains questionable because of its known effect on locus coeruleus<sup>36,37</sup>, on vegetative functions (increase in heart and respiratory rates), and on other complex behaviors such as anxiety<sup>38</sup>. Nevertheless, the very low concentration used here (5%) did not cause any significant change in the animals' behavior. Once habituated to CO<sub>2</sub> exposure, animals slept normally.

An interesting point in our study is our demonstration of an “optimal” respiratory regime for brain entrainment in rats, consisting in a deep (around 20 mL/sec) and long (around 0.15 s) inspiration. Indeed, a respiratory cycle based analysis allowed us to study LFP-respiration coupling in details. We observed that a deep inspiration alone was not sufficient to entrain non-olfactory structures: if it was the case, we should have observed a large respiratory drive during active exploration where flow rates are the highest (see Fig. 2), with inspiration being very ample but also very short. Similarly, a long inspiration alone was not sufficient to drive non-olfactory areas since SWS and REM states exhibited the longest inspirations while entrainment was restricted to olfactory areas and PFC. During sleep states, inspiration was very long but also very low in amplitude. Finally, the only state presenting an optimal breathing regime, with a deep and long inspiration, is the quiet waking state. We previously showed in the anesthetized tracheotomized rat that the respiratory drive in the OB depended on a trade-off between frequency and flow rate in the nasal cavity<sup>30,32</sup>. The present study extends this finding to non-olfactory areas and more importantly to the ecological condition of freely moving animal. Because brain respiratory-drive disappears when nasal respiration is by-passed or when OB activity is suppressed<sup>10,12,15,19,20</sup>, it is tempting to conclude from our results that the duration and flow rate of the airflows circulating in the nasal cavity, mechanically stimulating the olfactory epithelium<sup>22</sup>, and thus activating the OB, determines the respiratory drive in the brain. In such view, the OB would represent the main driving force of the respiration influence onto the brain. However, given that higher airflows implies a deeper breathing and thus a different recruitment of respiratory centers and motor control, the effect of other pathways cannot be excluded.

We observed that AE state was peculiar in that sense that non-olfactory structures (except PFC) exhibited a kind of resistance to respiratory coupling in the high range of respiration frequency (>5 Hz), even in CO<sub>2</sub> condition. We can formulate different hypotheses to try to explain this phenomenon. First, CO<sub>2</sub> use, while resulted in inspiration depth increase, did not modify inspiration duration during AE (see Supplementary Fig. S2). Since, as described also by others<sup>17</sup>, more posterior areas are less susceptible to respiration drive, we could assume that

these structures would require a longer inspiration duration to be respiration-entrained. Second, AE state is dominated by sniffing epochs where a strong hippocampal theta rhythm coupling has been described<sup>17</sup>. It could be possible that a strong theta coupling preclude respiratory drive in structures where the two rhythms compete. During such episodes, hippocampal theta and respiration frequencies completely overlap (see spectra in Fig. 3) so that it was not possible to disentangle theta-coupling from respiration-coupling in this frequency range<sup>17</sup>. We have also to keep in mind that sniffing act is likely a very different mechanism than a high rate respiration, which involves other brain structures, maybe explaining that non-olfactory brains structures could be less responsive to nasal airflow during this behavior.

Our study pointed out that all brain structures were not respiratory-coupled to the same extent. This has been previously reported that, in either REM or exploration, respiratory drive was most prominent in frontal regions (OB, prelimbic cortex, anterior cingulate cortex)<sup>17,33</sup>. Interestingly, PFC seems particularly sensitive to respiratory drive. Indeed, it is the only non-olfactory structure that appeared respiration-coupled during the four brain states, whatever the respiratory regime. Individual data of LFP-respiration coupling index as a function of inhalation amplitude or duration (Fig. 7) emphasized the strong and systematic coupling of this structure with respiration. PFC has been previously shown to be very well tuned to the 4 Hz respiratory frequency during animal freezing<sup>39–42</sup>. Here, the strong tuning of PFC with respiratory rhythm holds whatever the respiratory frequency as previously evoked<sup>42</sup>. This suggests that PFC could function as a hub structure, able to tune its activity to different areas according to the respiration frequency. Yet, PFC activity is coherent with basolateral amygdala during freezing when the animal breathes in the 2–4 Hz range<sup>39</sup>, but it can also synchronize with hippocampal activity in the 7–8 Hz range<sup>43–45</sup>.

In their review, Heck et al.<sup>46</sup> emphasized the potential role of respiration in organizing cortical activity in memory processes, notably by its ability to phase-lock hippocampal sharp wave ripples during wakening<sup>45</sup>. Our demonstration that brain structures are collectively and strongly susceptible to respiratory drive during quiet waking suggests that memory processes could be favored during this particular rest state. Our further demonstration that nasal airflow dynamics are crucial in the extent of brain entrainment by respiration could explain why memory consolidation is improved by nasal versus oral breathing<sup>6</sup>. The question remains about testing if an equivalent of the quiet state exists in human. We assume that such a state, characterized by a generalized brain entrainment on respiration, could be reached during deep-breathing practice.

The crucial role of the olfactory pathway in brain respiratory-drive is nowadays largely recognized, and particularly well emphasized in review papers<sup>2,46–49</sup>. But credit where credit is due: in their excellent opinion paper, Fontanini and Bower<sup>50</sup> were the first in 2006 to clearly posit that “[...] it might be that the pan-cortical correlations that particularly characterize slow-wave sleep and meditation actually depend on an afferent input signal generated within the olfactory system.” Our work is definitely in line with this thinking and that of a “sniffing brain” they developed. Moreover, our new data answers in the affirmative to the following question<sup>46</sup>: “Does the change in sniff frequency (for rats, rabbits, cats, and mice) or duration (for humans) alter the cortical circuit by driving the OB differently via the olfactory nerve [...]”. Finally, our results suggest that nasal airflow adjustments by variation in respiratory regime could be an effective tool for influencing brain activity. Notably, the slow and deep breathing associated to rest state seems to be an optimal regime to achieve a respiratory drive onto the whole brain.

## Methods

**Experimental procedures.** *Animal care.* Thirteen male Long Evans rats (Janvier Laboratories, Le Genest Saint Isle, France; 8 weeks old, ~250 to 300 g at the start of the experiment) were used and housed in groups of four in a temperature ( $22 \pm 1$  °C) and humidity ( $55 \pm 10\%$ ) controlled room and exposed to a 12/12 h light/dark cycle (light onset, 6:00 am). Experiments were conducted during the light period (between 9:00 am and 3:00 pm). Food and water were available ad libitum. All experiments were carried out in accordance with Directive 2010/63/EU of the European Parliament and of the Council of the European Union regarding the protection of animals used for scientific purposes and in compliance with the ARRIVE guidelines. The experimental protocols were approved by the National Ethics Committee “Animal Experimentation Committee of Univ. Claude Bernard Lyon 1—CEEA-55” (Agreement APAFIS #17088).

*Animal preparation.* Preparation consisted in electrode implantations in different brain areas. Anesthesia was induced by an initial dose of a mixture of chloral hydrate and sodium pentobarbital (intraperitoneal; Equithesin 3 ml/kg) and maintained with additional doses as needed. Rats were administered with anti-inflammatory and analgesic treatment (subcutaneous; carprofen 2 mg/kg or meloxicam 0.2 mg/kg) immediately after surgery and during several postoperative days if necessary. After a minimal 10 days' period of recovery, animals were implanted with monopolar stainless steel LFP recording electrodes (diameter: 100  $\mu$ m, 200–800 k $\Omega$  impedance, California Fine Wire) soldered to a copper wire (diameter: 250  $\mu$ m). Electrodes were positioned stereotactically into the left cortical hemisphere in 6 (n=8 rats) or 7 (n=5 rats) brain areas (see Table 1 for coordinates and sample size) comprising the olfactory bulb (OB), anterior piriform cortex (AP), dorsal part of the hippocampus CA1 (CA1) and dentate gyrus (DG), primary visual cortex (V1), primary somatosensory barrel cortex (S1), and prefrontal cortex (PFC). Electrophysiological activity was recorded while the electrode was lowered. Positioning of the recording electrode in the AP was determined by the shape of evoked field potential induced by stimulation of a bipolar OB electrode placed close to the mitral cell layer. The final location was selected to where the evoked potentials had the largest amplitude (before reversal). The stimulation electrode was then replaced by a monopolar recording electrode in the OB. The depth of the recording electrodes in the OB and CA1 was adjusted using their large multiunit activity, to the level of the mitral cell layer and just below the pyramidal layer, respectively. Positioning of the other recording electrodes tips (DG, S1, V1, PFC) was achieved stereotactically.

cally. Each electrode was individually fixed to the skull using dental cement. A reference wire was connected to a skull golden screw located above the posterior portion of the contralateral cortical hemisphere. Two anchor screws were also inserted in the contralateral side to secure the implant. Each electrode was attached to a 32-pin electrode interface board (EIB, Neuralynx, Inc, USA, ViewPoint France) combined with an omnetics connector and centered on the animal's head.

**LFP and respiration recording.** Signals were acquired by telemetry using a 32 channels wireless recording system (W32 headstage, TBSI, ViewPoint France). Signals were sampled at 15 kHz, amplified (gain 800×) and recorded via an acquisition card (USB-2533, Measurement Computing, Norton, MA). Signals were acquired using custom-made open-source software (pyacq, <https://github.com/pyacq/pyacq>) and stored on a computer for offline analysis.

Respiratory activity was recorded by using whole-body plethysmography. Plethysmograph (EMKA Technologies, France) was previously described in detail<sup>51,52</sup>.

One camera (B/W CMOS PINHOLE camera) was placed in a corner of the cage in order to monitor the animal behavior.

**Recording sessions.** Before starting recording sessions, animals were habituated to the plethysmography cage during 2 sessions of 20 min. At the end of this period, animals were completely familiarized with the environment and did not show any sign of stress.

**Ambient air.** Recording sessions then started. Six sessions (one session per day) of 2 h under ambient air were recorded for each animal. During the first minutes, animals alternated between active exploration and quiet rest. After a certain amount of time, variable between animals (10–30 min), rats started to sleep, with SWS and REM states alternation.

**CO<sub>2</sub>-enriched air.** In some experiments, we used a 5% CO<sub>2</sub>-enriched air in the plethysmograph to change respiration regime. The choice of 5% concentration was based on respiratory physiology experiments, where the CO<sub>2</sub> concentration usually used is 8%<sup>53</sup>. It has been shown that a concentration of 10% can increase immobility bouts in Long-Evans rats, suggesting a certain level of anxiety<sup>54</sup>. We therefore searched for the lowest concentration able to induce a change in the amplitude and/or respiratory frequency. Our criteria were that: (1) animal could fall asleep with the same delay as under ambient air, (2) no signs of stress (no increase in episodes of immobility or grooming) were shown, (3) sniffing frequency returned to baseline in less than 5 min after CO<sub>2</sub> stopping in the plethysmograph. Pilot experiments (n = 4, not shown) allowed us to define 5% CO<sub>2</sub> concentration as meeting all these criteria. Following the three ambient air recording sessions, five animals were recorded during 3 new sessions under CO<sub>2</sub>-enriched air (one session per day). To diffuse CO<sub>2</sub> enriched air, a 10% CO<sub>2</sub>—air container (Air Liquide, France) was connected to the plethysmograph. Pure air was mixed with CO<sub>2</sub> (50/50) so that the final concentration was 5%. Under CO<sub>2</sub>, the recording sessions were limited to 2 h. Exposure of animals three times 2 h was not sufficient to induce chronic hypercapnia<sup>55</sup>.

**Data analysis. Respiratory signal.** Respiratory signals were acquired and extracted using previously described method<sup>51</sup> allowing accurate measurements of different respiratory parameters in behaving animals. The detection of the respiratory cycles was achieved using an enhanced version of the algorithm described in a previous study<sup>56</sup>. This algorithm performs two main operations: signal smoothing for noise reduction, and detection of zero-crossing points to define accurately the inspiration and expiration phase starting points. For each respiratory cycle, inspiration and expiration peak flow rate (iPE, ePF), inspiration duration and expiration duration (iDur, eDur) were measured. Instantaneous respiratory frequency (Freq) was determined as the inverse of the respiratory cycle (inspiration plus expiration) duration.

**States scoring.** Based on video, electrophysiological, and breathing recordings, two well-trained experimenters visually coded four vigilance states by inspection of behaviors, respiration, and associated LFP spectral features (see Fig. 1). State was classified as active exploration (AE) if the animal engaged in exploratory behavior (locomotion, whisking, and sniffing), with a high amplitude and > 5 Hz respiration<sup>33</sup> during at least three cycles, and a cortical LFPs expressing high gamma (30–55 Hz) power density. In quiet waking (QW), the animal was immobile (standing or sitting quietly) with a high amplitude and < 5 Hz respiration, cortical LFPs expressed relatively high gamma activity. In slow wave sleep (SWS), the animal was lying immobile with eyes closed and slow and extremely regular respiratory movements. LFPs were characterized by prominent delta waves (1–4 Hz). In rapid eye movements sleep (REM), the animal was immobile with eyes closed. Breathing was irregular, with epochs of low and slow amplitude alternating with short epochs of higher frequency and amplitude (see Figs. 1 and 2). LFPs were low in amplitude and expressed very high theta and gamma power. Intermediary states, where LFP features were not very clear, were not coded.

**Electrophysiological signals.** Data were analyzed using custom-written scripts with the python language and its scientific ecosystem tool suite.

**Spectral analysis.** The power spectral density (PSD) of the LFP signals was calculated using the continuous Morlet wavelet transform<sup>57</sup> instead of the classical windowed Fourier transform (FFT). The Morlet wavelet estimated the amplitude of the signal across time and frequency. The obtained time–frequency map was then

segmented in periods of interest with variable durations and averaged on the time axis. We made this choice mainly because low frequency analyses require very long windows with FFT methods while the Morlet wavelet transform is a continuous representation along time. Segmenting state periods with varying durations combined with fixed windowed method would be sub-optimal whereas the continuous representation in the Morlet time frequency map makes the process easier and more accurate. The drawback with our approach is that the final PSD is smoother on the frequency domain than a standard FFT. To compare spectra shape across channels and states while removing some variability across rats, we normalized all spectra from the same rat and channel to an average area of 1 across states. We thus obtained spectra whose amplitude was similar across rats and channels, and was still quantitatively comparable across states.

**Coherence analysis.** For the computation, the signal was down sampled to 1000 Hz. LFP-respiration coherence was calculated with a custom-modified version of Scipy coherence function. Indeed, since coherence is based on FFT window method then the outcome is biased by the total duration of the period. In our case, to compensate the great difference in duration between states, we randomly sub-sampled an equal number of non-juxtaposed epochs of each state and then used the classic coherence with no overlap on these epochs (256 epochs of 6 s). Coherence between LFP and respiration was compared against chance using a surrogate-based statistical testing. Surrogate were obtained by preserving the LFP and respiration spectra using a four-steps process: (1) shuffling ( $n=100$ ) of 256 epochs, (2) coherence computing, (3) extraction of the maximum coherence value, and (4) computation of the distribution of surrogate values. Our first statistical analysis of the coherence at the population level compared the distribution of coherence maximal values to the average of surrogate spectrum values measured at the same frequency (computed independently for each rat). The comparison across rats was then done using a linear mixed-effect model including also the animal state and the recorded structure as fixed effects, and all their interactions. To get a convergent model, only the intercept and the animal state were used as random effects but we checked that the full model (with all random effects) gave similar results. Besides, coherence values were log-transformed in order to insure homoscedasticity of residuals. Normality of residuals was checked after model fitting. ANOVA on fixed effects was obtained by computing degree of freedom with the Kenward-Roger approximation. Finally, post-hoc tests on fitted model used standard paired t-test (corrected for multiple comparisons with the false discovery rate method). Model fitting and post-hoc tests were done with software R 3.4.4 and libraries *afex* 0.25-1, *lme4* 1.1-21 and *emmeans* 1.4.2.

The same linear mixed model fitting approach and statistical analysis was used in a second statistical analysis in order to compare the distributions of coherence maximal values in air and CO<sub>2</sub> conditions.

**Covariation maps and coupling index.** To study frequency-frequency coupling between LFP signals and respiration, we designed a homemade method that allowed tracking instantaneous frequency synchrony<sup>42</sup>. To do so, for each detected respiratory cycle, the frequency was estimated as 1/cycle duration and the time course of the instantaneous respiratory frequency was extracted. In parallel, the continuous Morlet scalogram for the LFP signal was computed in our frequency band of interest (0.8–10 Hz). In each time bin (4 ms), we extracted the frequency of the point of maximum instantaneous power. Finally, this sequence of frequencies gave us the time course of the LFP predominant instantaneous frequency. From the two time series obtained (instantaneous respiration frequency and predominant instantaneous LFP frequency), a 2D matrix histogram was built, with the respiratory frequency represented on the x-axis and the LFP frequency on y-axis (2-dimensional distribution of joined LFP-respiration frequencies). This 2D histogram, called covariation map, was normalized so that the total sum equaled 1, and point density was represented on a color scale ranging from blue to yellow as the density of points increased. A coupling between respiration frequency and LFP frequency can be assumed when a high density (i.e., yellow color) was observed along the diagonal of the covariation map (see Fig. 5 for an illustration). Conversely, a non-correlated Gaussian shape indicated that the frequency of respiration and the main frequency of LFP varied independently. The two possibilities can co-occur on the same covariation map.

Based on this map, we were then able to introduce a new metric: the sum of density along the diagonal. To assess the density of the diagonal, we applied a smoothing Gaussian kernel ( $\sigma = 0.58$  Hz) to the covariation maps before summing the diagonal. This metric estimated the coupling strength between respiration and LFP with a factor in 0–1 range where 1 indicates that respiration frequency is always the dominant LFP frequency and 0 signals the two frequencies are never equal. We named “coupling index” this custom metric. To validate the accuracy of this metric, we constructed surrogates ( $n = 100$ ) by applying random time-shift (with the same method we used in “Coherence analysis”, see above) between the respiration time series and LFP time series. This procedure allows to remove the instantaneous coupling but maintains the global frequency distribution of both time series.

Statistical analysis of coupling index at the population level was performed using linear mixed models similarly as described for the coherence (see above). However to get homoscedasticity of residuals, the coupling index (CI), was transformed with  $\log(-\log(CI))$  when comparing air and shuffle data, and not transformed when comparing air and CO<sub>2</sub> data.

The two time-series (respiration frequency and LFP frequency) describing the covariation map could be segmented in short periods of variable duration before computing the covariation map. This segmentation allowed to group respiratory cycles with common characteristic, for instance iPF or iDur. For each of these groups of cycles, we could compute a covariation map and the corresponding coupling index. Ultimately, we were able to display a coupling index vs “inspiration peak flow rate” (or duration) plot across animal state and on an animal-by-animal basis. In some cases, a total duration of 60 s was not reached: the missing values were then not considered for the computation.

While looking at latter analyses, we often noticed the existence of a local maximum of coupling index for intermediate values of a given respiratory cycle characteristic. In order to statistically assess the existence of this intermediate maximum, we fitted our data with generalized linear mixed-effect models. Model fixed-effects included a first or second order polynomial of the respiratory cycle characteristic, while random effects always included a second order polynomial. Data were grouped per animal (distinct models have been done for each area). The link function was a logarithm and the variance described with a Gamma function (family function). We visually checked homoscedasticity and normality of the residuals after model fitting. Comparison between nested models was obtained with a Wald chi-square test. Mixed-model analysis was done with software R 3.4.4 and library lme4 1.1-21.

### Data availability

All data and scripts at any stage of analysis are available upon reasonable requests from Nathalie Buonviso (nathalie.buonviso@cns.fr).

Received: 31 July 2020; Accepted: 15 March 2021

Published online: 29 March 2021

### References

- Fries, P. A mechanism for cognitive dynamics: Neuronal communication through neuronal coherence. *Trends Cogn. Sci.* **9**, 474–480 (2005).
- Heck, D. H. *et al.* Breathing as a fundamental rhythm of brain function. *Front. Neural Circuits* **10**, 115 (2017).
- Tort, A. B. L., Brankač, J. & Draguhn, A. Respiration-entrained brain rhythms are global but often overlooked. *Trends Neurosci.* **41**, 186–197 (2018).
- Hegoburu, C. *et al.* The RUB cage: Respiration-ultrasonic vocalizations-behavior acquisition setup for assessing emotional memory in rats. *Front. Behav. Neurosci.* **5**, 25 (2011).
- Kurnikova, A., Moore, J. D., Liao, S.-M., Deschênes, M. & Kleinfeld, D. Coordination of orofacial motor actions into exploratory behavior by rat. *Curr. Biol.* **27**, 688–696 (2017).
- Arshamian, A., Iravani, B., Majid, A. & Lundström, J. N. Respiration modulates olfactory memory consolidation in humans. *J. Neurosci.* **38**, 10286–10294 (2018).
- Nakamura, N. H., Fukunaga, M. & Oku, Y. Respiratory modulation of cognitive performance during the retrieval process. *PLoS ONE* **13**, e0204021 (2018).
- Iwabe, T., Ozaki, I. & Hashizume, A. The respiratory cycle modulates brain potentials, sympathetic activity, and subjective pain sensation induced by noxious stimulation. *Neurosci. Res.* **84**, 47–59 (2014).
- Li, S. & Laskin, J. J. Influences of ventilation on maximal isometric force of the finger flexors. *Muscle Nerve* **34**, 651–655 (2006).
- Zelano, C. *et al.* Nasal respiration entrains human limbic oscillations and modulates cognitive function. *J. Neurosci.* **36**, 12448–12467 (2016).
- Perl, O. *et al.* Human non-olfactory cognition phase-locked with inhalation. *Nat. Hum. Behav.* **3**, 501–512 (2019).
- Ito, J. *et al.* Whisker barrel cortex delta oscillations and gamma power in the awake mouse are linked to respiration. *Nat. Commun.* **5**, 3572 (2014).
- Nguyen Chi, V. *et al.* Hippocampal respiration-driven rhythm distinct from theta oscillations in awake mice. *J. Neurosci.* **36**, 162–177 (2016).
- Biskamp, J., Bartos, M. & Sauer, J.-F. Organization of prefrontal network activity by respiration-related oscillations. *Sci. Rep.* **7**, 45508 (2017).
- Liu, Y., McAfee, S. S. & Heck, D. H. Hippocampal sharp-wave ripples in awake mice are entrained by respiration. *Sci. Rep.* **7**, 8950 (2017).
- Zhong, W. *et al.* Selective entrainment of gamma subbands by different slow network oscillations. *Proc. Natl. Acad. Sci.* **114**, 4519–4524 (2017).
- Tort, A. B. L. *et al.* Parallel detection of theta and respiration-coupled oscillations throughout the mouse brain. *Sci. Rep.* **8**, 6432 (2018).
- Herrero, J. L., Khuvis, S., Yeagle, E., Cerf, M. & Mehta, A. D. Breathing above the brain stem: Volitional control and attentional modulation in humans. *J. Neurophysiol.* **119**, 145–159 (2018).
- Yanovsky, Y., Ciatipis, M., Draguhn, A., Tort, A. B. L. & Brankač, J. Slow oscillations in the mouse hippocampus entrained by nasal respiration. *J. Neurosci.* **34**, 5949–5964 (2014).
- Lockmann, A. L. V., Laplagne, D. A., Leão, R. N. & Tort, A. B. L. A Respiration-coupled rhythm in the rat hippocampus independent of theta and slow oscillations. *J. Neurosci.* **36**, 5338–5352 (2016).
- Ravel, N. & Pager, J. Respiratory patterning of the rat olfactory bulb unit activity: Nasal versus tracheal breathing. *Neurosci. Lett.* **115**, 213–218 (1990).
- Grosmaître, X., Santarelli, L. C., Tan, J., Luo, M. & Ma, M. Dual functions of mammalian olfactory sensory neurons as odor detectors and mechanical sensors. *Nat. Neurosci.* **10**, 348–354 (2007).
- Cenier, T. *et al.* Odor vapor pressure and quality modulate local field potential oscillatory patterns in the olfactory bulb of the anesthetized rat. *Eur. J. Neurosci.* **27**, 1432–1440 (2008).
- Chaput, M. A., Buonviso, N. & Berthommier, F. Temporal patterns in spontaneous and odour-evoked mitral cell discharges recorded in anaesthetized freely breathing animals. *Eur. J. Neurosci.* **4**, 813–822 (1992).
- Buonviso, N. *et al.* Rhythm sequence through the olfactory bulb layers during the time window of a respiratory cycle. *Eur. J. Neurosci.* **17**, 1811–1819 (2003).
- Cenier, T. *et al.* Respiration-gated formation of gamma and beta neural assemblies in the mammalian olfactory bulb. *Eur. J. Neurosci.* **29**, 921–930 (2009).
- Briffaud, V., Fourcaud-Trocmé, N., Messaoudi, B., Buonviso, N. & Amat, C. The relationship between respiration-related membrane potential slow oscillations and discharge patterns in mitral/tufted cells: What are the rules? *PLoS ONE* **7**, e43964 (2012).
- Fourcaud-Trocmé, N., Briffaud, V., Thévenet, M., Buonviso, N. & Amat, C. In vivo beta and gamma subthreshold oscillations in rat mitral cells: Origin and gating by respiratory dynamics. *J. Neurophysiol.* **119**, 274–289 (2018).
- Oka, Y., Takai, Y. & Touhara, K. Nasal airflow rate affects the sensitivity and pattern of glomerular odorant responses in the mouse olfactory bulb. *J. Neurosci.* **29**, 12070–12078 (2009).
- Courtillot, E. *et al.* Individual and synergistic effects of sniffing frequency and flow rate on olfactory bulb activity. *J. Neurophysiol.* **106**, 2813–2824 (2011).
- Courtillot, E. *et al.* Reshaping of bulbar odor response by nasal flow rate in the rat. *PLoS ONE* **6**, e16445 (2011).

32. Esclassan, F. *et al.* Faster, deeper, better: The impact of sniffing modulation on bulbar olfactory processing. *PLoS ONE* **7**, e40927 (2012).
33. Rojas-Libano, D., Wimmer del Solar, J., Aguilar-Rivera, M., Montefusco-Siegmund, R. & Maldonado, P. E. Local cortical activity of distant brain areas can phase-lock to the olfactory bulb's respiratory rhythm in the freely behaving rat. *J. Neurophysiol.* **120**, 960–972 (2018).
34. Cavelli, M. *et al.* Nasal respiration entrains neocortical long-range gamma coherence during wakefulness. *Eur. J. Neurosci.* **51**, 1463–1477 (2020).
35. Burke, P. G. R. *et al.* Optogenetic stimulation of adrenergic C1 neurons causes sleep state-dependent cardiorespiratory stimulation and arousal with sighs in rats. *Am. J. Respir. Crit. Care Med.* **190**, 1301–1310 (2014).
36. Oyamada, Y., Ballantyne, D., Mückenhoff, K. & Scheid, P. Respiration-modulated membrane potential and chemosensitivity of locus coeruleus neurons in the in vitro brainstem-spinal cord of the neonatal rat. *J. Physiol.* **513**, 381–398 (1998).
37. Pineda, J. & Aghajanian, G. K. Carbon dioxide regulates the tonic activity of locus coeruleus neurons by modulating a proton- and polyamine-sensitive inward rectifier potassium current. *Neuroscience* **77**, 723–743 (1997).
38. Oikawa, S., Hirakawa, H., Kusakabe, T., Nakashima, Y. & Hayashida, Y. Autonomic cardiovascular responses to hypercapnia in conscious rats: the roles of the chemo- and baroreceptors. *Auton Neurosci.* **117**, 105–114 (2005).
39. Dejean, C. *et al.* Prefrontal neuronal assemblies temporally control fear behaviour. *Nature* **535**, 420–424 (2016).
40. Karalis, N. *et al.* 4-Hz oscillations synchronize prefrontal-amygdala circuits during fear behavior. *Nat. Neurosci.* **19**, 605–612 (2016).
41. Moberly, A. H. *et al.* Olfactory inputs modulate respiration-related rhythmic activity in the prefrontal cortex and freezing behavior. *Nat. Commun.* **9**, 1528 (2018).
42. Dupin, M., Garcia, S., Boulanger-Bertolus, J., Buonviso, N. & Mouly, A.-M. New insights from 22-kHz ultrasonic vocalizations to characterize fear responses: Relationship with respiration and brain oscillatory dynamics. *eNeuro* **6** (2019).
43. Jones, M. W. & Wilson, M. A. Theta rhythms coordinate hippocampal-prefrontal interactions in a spatial memory task. *PLoS Biol.* **3**, e402 (2005).
44. Siapas, A. G., Lubenov, E. V. & Wilson, M. A. Prefrontal phase locking to hippocampal theta oscillations. *Neuron* **46**, 141–151 (2005).
45. Colgin, L. L. Oscillations and hippocampal-prefrontal synchrony. *Curr. Opin. Neurobiol.* **21**, 467–474 (2011).
46. Heck, D. H., Kozma, R. & Kay, L. M. The rhythm of memory: How breathing shapes memory function. *J. Neurophysiol.* **122**, 563–571 (2019).
47. Zaccaro, A. *et al.* How breath-control can change your life: A systematic review on psycho-physiological correlates of slow breathing. *Front. Hum. Neurosci.* **12** (2018).
48. Kontaris, I., East, B. S. & Wilson, D. A. Behavioral and neurobiological convergence of odor, mood and emotion: A review. *Front. Behav. Neurosci.* **14**, 35 (2020).
49. Maric, V., Ramanathan, D. & Mishra, J. Respiratory regulation & interactions with neuro-cognitive circuitry. *Neurosci. Biobehav. Rev.* **112**, 95–106 (2020).
50. Fontanini, A. & Bower, J. M. Slow-waves in the olfactory system: An olfactory perspective on cortical rhythms. *Trends Neurosci.* **29**, 429–437 (2006).
51. Courtiol, E. *et al.* Sniff adjustment in an odor discrimination task in the rat: Analytical or synthetic strategy?. *Front. Behav. Neurosci.* **8**, 145 (2014).
52. Lefèvre, L. *et al.* Significance of sniffing pattern during the acquisition of an olfactory discrimination task. *Behav. Brain Res.* **312**, 341–354 (2016).
53. Ramanantsoa, N. *et al.* Breathing without CO<sub>2</sub> chemosensitivity in conditional Phox2b mutants. *J. Neurosci.* **31**, 12880–12888 (2011).
54. Winter, A., Ahlbrand, R., Naik, D. & Sah, R. Differential behavioral sensitivity to carbon dioxide (CO<sub>2</sub>) inhalation in rats. *Neuroscience* **346**, 423–433 (2017).
55. Reichart, E., Cogniel, O., Brothier, G., Marchand, M. & Colas, T. Blood acid-base status in the rat during 2 months of exposure to hypercapnia. *Pflügers Arch.* **334**, 253–263 (1972).
56. Roux, S. G. *et al.* Respiratory cycle as time basis: An improved method for averaging olfactory neural events. *J. Neurosci. Methods* **152**, 173–178 (2006).
57. Kronland-Martinet, R., Morlet, J. & Grossmann, A. Analysis of sound patterns through wavelet transforms. *Int. J. Pattern Recogn. Artif. Intell.* **01**, 273–302 (1987).

### Acknowledgements

This work was supported by the Centre National de la Recherche Scientifique and the LABEX CORTEX (ANR-11-LABX-0042) of Université de Lyon, within the program “Investissements d’Avenir” (ANR-11-IDEX-0007) operated by the French National Research Agency. We thank Emmanuelle Courtiol and Anne-Marie Mouly for careful reading of this manuscript.

### Author contributions

B.G. and N.B. designed the experiment, B.G. and L.L. performed the electrodes implantations surgery, B.G. performed recordings, S.G. designed most of the data analysis pipeline, B.G., M.J., N.F.-T. and S.G. analyzed the data, B.G., M.J., C.A., S.G. prepared the figures, N.F.-T. and N.B. wrote the manuscript main text, all the authors reviewed and edited the manuscript.

### Competing interests

The authors declare no competing interests.

### Additional information

**Supplementary Information** The online version contains supplementary material available at <https://doi.org/10.1038/s41598-021-86525-3>.

**Correspondence** and requests for materials should be addressed to N.B.

**Reprints and permissions information** is available at [www.nature.com/reprints](http://www.nature.com/reprints).

**Publisher's note** Springer Nature remains neutral with regard to jurisdictional claims in published maps and institutional affiliations.



**Open Access** This article is licensed under a Creative Commons Attribution 4.0 International License, which permits use, sharing, adaptation, distribution and reproduction in any medium or format, as long as you give appropriate credit to the original author(s) and the source, provide a link to the Creative Commons licence, and indicate if changes were made. The images or other third party material in this article are included in the article's Creative Commons licence, unless indicated otherwise in a credit line to the material. If material is not included in the article's Creative Commons licence and your intended use is not permitted by statutory regulation or exceeds the permitted use, you will need to obtain permission directly from the copyright holder. To view a copy of this licence, visit <http://creativecommons.org/licenses/by/4.0/>.

© The Author(s) 2021

## 6.2 Posters

NeuroFrance 2019 (Marseille)

The breath whispers in the membrane potential

**Juventin M**, Girin B, Fourcaud-Tocmé N, Garcia S, Buonviso N, Amat C

Complex behaviors implicate the collaboration of several brain areas, which could be distant from each other. This functioning assumes the temporal coordination of the involved areas activities. Brain activity displays rhythms ranging from 0.5 to 200Hz, in these, slow rhythms (<12Hz) are thought to enable long-range communication between brain areas by providing a common temporal reference to all areas. The respiration-related rhythm (from 1.5 to 12Hz in awake rodent) is an electrical brain rhythm which could act as a coordinator rhythm. This rhythm is found in the extracellular activity almost all over the rat brain, and in several human brain areas. However, this brain-wide presence is contested because extracellular signal can be contaminated by an artifactual diffusion of a distant-generated signal. Therefore, we chose to perform intracellular recordings to overcome this issue. We recorded neurons in different and distant areas to verify the widespread distribution of respiratory rhythm. We are the first to show that the intracellular activity of non-olfactory neurons can be modulated by the respiratory rhythm. Furthermore, we found that brain state (internal network signals) strongly influences this modulation. In addition, odor stimulation (external signals) can also modify the respiratory modulation even in non-olfactory structures. In summary, these findings support the fact that the respiratory rhythm, by directly modulating the neurons activity, could be a common clock for the brain.

# The breath whispers in the membrane potential

**Introduction**  
A single brain area displays numerous brain rhythms. Yet, some complex behaviors require the collaboration of several brain areas, which could be distant from each other. This functioning assumes the temporal coordination of neural activity between areas. Amongst them, the respiratory/ventral chrym (from 1 to 84 in awake rodent) recently emerged as a global coordinator since expressed in many brain areas. However, this hypothesis mainly relies on LFP recordings, which may be contaminated by volume conduction.

**Objectives**  
We performed an intracellular study to ensure the respiratory rhythm has a **direct impact** on the membrane potential evolution of a neuron. Also we recorded on a widespread population of neurons to approach a **brainwide** view of the respiratory modulation.

**Methods**  
Experiments were performed on freely breathing anesthetized rats. Intracellular activity (or Vm) was recorded with microelectrodes filled with a solution of 2M potassium acetate (resistance 45-120 Mohms). When a neuron was impaled, a negative current was injected to stabilize the cell. The current was held at -100 pA. All recordings were obtained in spontaneous conditions, without any kind of stimulations. Respiration was monitored using a pressure sensor placed before the right nostril.  
Four brain areas were monitored: the prefrontal, the somatosensory barrel, the primary visual cortex, and an subcortical structure the hippocampus (CA1).

**Analysis: How to observe and detect respiratory modulation?**

**Signal processing** -----> **Visualization** -----> **Measure**

- 1 - Raw Vm**: Membrane potential traces showing respiratory modulation.
- 2 - spike and cutting**: Traces with spikes removed and segments cut.
- 3 - Vm segmentation on respiratory cycles**: Vm segments aligned to respiratory cycles.
- 4a - overlaying**: Vm segments overlaid on top of each other.
- 4b - stacking**: Vm segments stacked vertically.
- 4c - overlaying**: Vm segments overlaid on a respiratory cycle.
- 4d - stacking**: Vm segments stacked vertically.

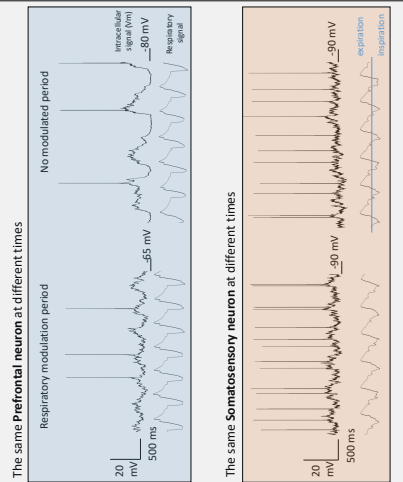
**Dynamic view: stacking (as 4b) Vm segments over time**  
Allow to see the evolution over time of respiration triggered Vm.

**Summarized view: overlaying (as 4a) Vm segments**  
Allow to precisely see the Vm waveform in relation with respiration, but the time dimension is lost.

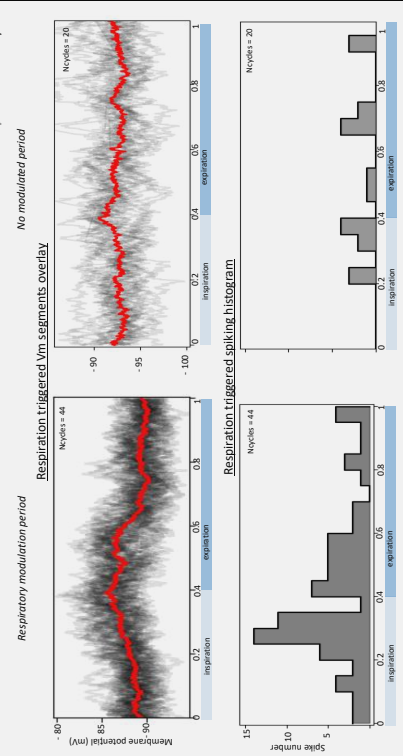
**Quantification of Vm respiratory modulation over time**  
The amplitude of each Vm segments ( $max - min$  of overlay) was compared to a surrogate noise (---). This allowed us to detect respiratory modulation individually, cycle by cycle, and to follow its temporal dynamics. The respiratory modulation power (---) was higher than the surrogate noise (confidence 95%).

**Respiratory modulation significance**  
Vm segment amplitude, Surrogate amplitude distribution, Vm amplitude/95% percentile surrogate amplitude = respiratory modulation power.

## Looking at raw signals: a respiratory modulation?



## Results 1

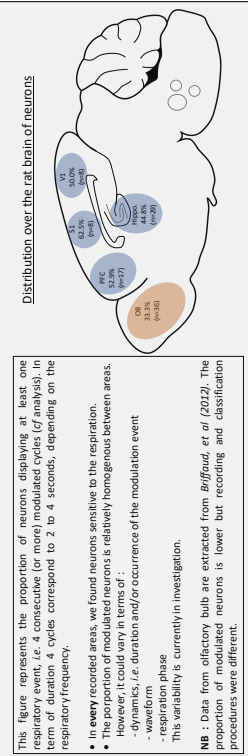


We focused our analysis on characterization of respiratory modulation events.

- Left panel:** Example of a modulation event. Top: The respiration triggered overlay shows the modulated Vm waveform, here a depolarization during the inspiration/expiration transition. Bottom: The respiration triggered spiking histogram highlights that this respiratory-related Vm oscillation modulates the spiking firing.
- Right panel:** Example of a no modulation event. No tendencies are observed neither in Vm nor in spike histogram.

These findings show respiratory modulation usually observed in LFP is not an epiphenomenon. The respiratory rhythm is really sensed by neurons.

## Results 2



## Conclusion

In all areas of interest we observed a significant respiratory modulation of the intracellular activity: both the membrane potential oscillations and the spiking discharge can be synchronized with respiration. Thus, the respiratory rhythm possesses the principle features of brain rhythm coordinator as it is global, and as it can modulates neural activity up to cellular level.

## Perspectives

During experiments, we co-recorded intracellular activity and LFP. So we will analyze the interaction between intra- and extracellular activity. It may reveal a different susceptibility to respiratory modulation according to the brain-state (since urethane anesthesia allows alternation of brain state-like activities).

Respiration-based synchronization in the brain: bottom-up and top-down influences

Girin B, **Juventin M**, Garcia S, Courtiol E, Buonviso N

Inter-area communication requires the different brain rhythms to be coordinated across areas. As others, we hypothesized respiratory rhythm could act as a central clock for cerebral rhythms coordination. If true, one can expect neuronal activity to be influenced by respiration in a large brain network. We tested that by recording respiration and neuronal activity in different brain areas (olfactory areas, V1, S1, CA1, DG, prefrontal) in the freely-moving rat during different vigilance states. In agreement with recent publications, we observed that all structures could be modulated by breathing. We provided the additional observation that such a modulation varies according to the vigilance state, each state being associated with a specific respiratory regime. Particularly, we observed a large-scale synchronization across areas on the breathing rhythm during quiet state, where animal's breath is around 2Hz. We then sought to decorrelate brain state from respiratory regime. Animals were thus recorded while breathing a CO<sub>2</sub>-enriched air, which changes the respiratory regimes. We observed the across-areas respiratory synchronization observed in quiet state can be extended, under CO<sub>2</sub> condition, to other vigilance states (REM and non-REM) and to higher respiratory frequencies (3-4 Hz). We thus evidenced that amplitude and spatial extent of breathing-related modulation correlate with air volume in the nasal cavity, suggesting that at least part of respiratory modulation in the brain is due to bottom-up influences. We concluded that large-scale synchronization of brain areas on respiration is mostly dependent on the respiratory regime (volume). However, we wanted to test to what extent a central respiratory influence could also exist. We collected data in urethane anesthetized tracheotomized rats and we showed that brain activity can be entrained to respiratory rhythm when 1) airflow is by-passed in the nasal cavity, 2) brain activity is in slow-wave regime so that nasal influence is shut down. We thus evidenced a top-down influence of respiration on the brain rhythms that has been underestimated until now. Data are still under process.

# Respiration-based synchronization in the brain : influence of air-flow features

## Introduction

Cerebral rhythms are known to be involved in numerous functions. Particularly, they could allow brain areas to communicate over long distances. To be efficient, inter-area communication requires the different brain rhythms to be synchronized.

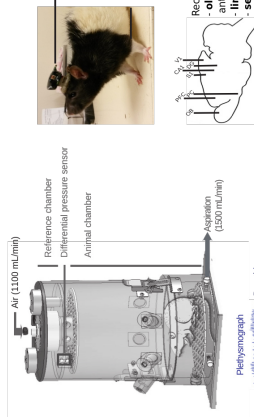
We hypothesize that respiratory rhythm could act as a central clock for synchronizing cerebral rhythms, by modulating their dynamics, thereby linking brain regions involved in the same functional network.

Since cerebral and breathing rhythms spontaneously vary during wake-sleep cycles, we used these natural changes to study how local field potentials (LFP) in different brain areas co-vary with respiratory rhythm. In agreement with recent publications, we observed that all structures could be modulated by breathing. This modulation is supposed to originate in the mechanosensitivity of olfactory receptor cells to respiration-related airflows into the nose. If this bottom-up influence is major in influencing respiration-related activity of the brains, then we should observe different patterns of respiration-synchronized activities according to the respiration parameters (frequency, amplitude, volume).

## Material & Methods

- Simultaneous recording of breaths and neuronal activities in freely moving rats

Whole-body plethysmograph: a non-invasive method to record breathing

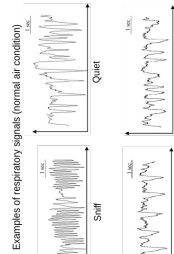
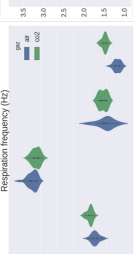


Telemetry recordings of LFP signals



## Results

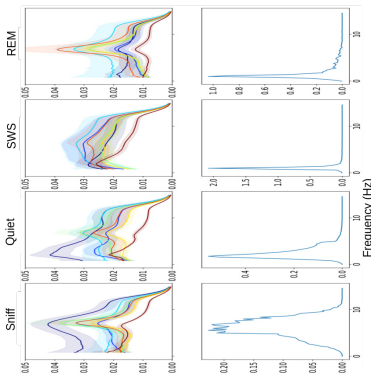
Respiration parameters analysis



3 main parameters were studied : frequency, volume and amplitude (inspiration and expiration). In order to decorrelate state and respiratory regime, we used 5%CO2 Air : respiratory parameters vary with the state. CO2 : Volumes and amplitudes are increased.

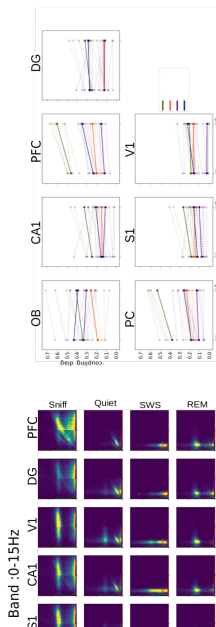
## Results

Spectral analysis of LFP and respiration signals



Spectral analysis shows a frequency overlap between LFP and respiration rhythms, particularly during Quiet Wakening

Correlation between brain rhythms and respiration frequency

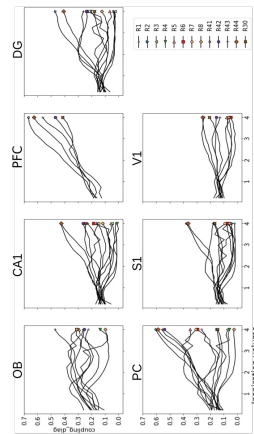


We looked for correlation between the respiratory rhythm and the LFP oscillation, in the theta band (0.8-15Hz), in the different brain areas during air and CO2 conditions

Air : Correlation exists in all areas during quiet waking state and only in olfactory areas during sleep.

CO2 : Correlation extends to all areas during sleep.

Correlation between LFP/respiration coordination and inspiration volume



We analyzed the correlation between LFP/Respiration coupling and the different respiration parameters.

We observed that the coupling increased with the inspiration volume in all structures. However the correlation level is different between structures

## Conclusion

We observed an inter-areas respiratory synchronization during quiet waking which can be extended to all sleep states under CO2 condition. This synchronization can be modulated by air flow characteristics particularly volume. We conclude that large-scale synchronization of brain areas on respiratory features is mostly dependent on the respiratory features (volume, duration and amplitude). This observation could help in understanding the effects of slow-breathing methods on well-being.

Neurons membrane potential beats to the rhythm of breath.

Juventin M, Girin B, Zbili M, Fourcaud-Tocmé N, Garcia S, Buonviso N, Amat C

Respiratory rhythm has recently emerged as a key element in the cortical dynamics, since an increasing number of studies have shown a global entrainment of LFP activities by the respiratory rhythm. This observation has been done in rodents as well in humans, and in a large set of brain areas (cortical and limbic areas). In olfactory areas, the respiratory rhythm has been shown to modulate the activity of both LFP oscillations and individual neurons discharge and membrane potential. Since this question has been tackled in non-olfactory structures almost exclusively through LFP analysis, the mechanisms underlying such respiratory modulation cannot be fully understood. To fill this gap, we performed intracellular and LFP co-recordings in four non-olfactory brain areas (CA1, barrel cortex, primary visual cortex, prelimbic cortex), in anesthetized rats. Similar to what observed in LFP, we observed moments where respiratory rhythm entrained membrane potential (Vm). Consequently, spiking discharge phase-locked to respiratory rhythm. Changing neuron excitability (by intracellular current injection) induced changes in the probability of Vm respiratory entrainment. Surprisingly, cell responses to injected current are highly variable, and no clear tendencies could be extracted. Regarding global brain state, periods of respiration-locked Vm not exclusively co-occurred with periods of respiration-locked LFP. We found then complex interactions between these parameters (neuron internal state and of global brain state) on membrane potential dynamics which have to be elucidated. As a conclusion, these findings reinforce the idea that the respiratory rhythm is a fundamental component of the neuronal network dynamics, and should not be underestimated.



# Neurons membrane potential beats to the rhythm of breath.

Juventin M., Girin B., Zbili M., Fourcaud-Trocmé N., Garcia S., Buonviso N., and Amat C.

Lyon Neuroscience Research Center, team : Olfaction : from Coding to Memory, CNRS UMR5292 – INSERM U1028 – University Lyon 1

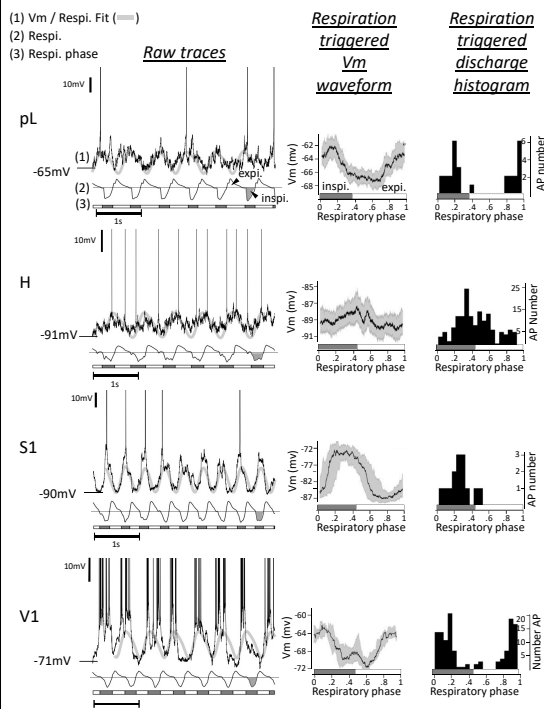
## Introduction

Respiratory rhythm has recently emerged as a key element in the cortical dynamics, since an increasing number of studies have shown a global entrainment of LFP activities by the respiratory rhythm. This observation has been done in rodents as well in humans, and in a large set of brain areas (cortical and limbic areas). Since this question has been tackled in non-olfactory structures almost exclusively through LFP analysis, the mechanisms underlying such respiratory modulation cannot be fully understood. To carry on understanding, we performed intracellular and LFP co-recordings in four non-olfactory brain areas : Hippocampus (H), and the somatosensory (S1), primary visual (V1) and prefrontal cortices (pL), in anesthetized rats.

## Methods

Experiments were performed on freely breathing anesthetized rats. Intracellular activity (or Vm) and LFP were co-recorded. For Vm, sharp electrodes filled with a solution of 2M potassium acetate (Resistance 45-120 Mohms) were used. Respiration was monitored using a pressure sensor placed before the right nostril.

## Result 1 : Respiratory-rhythm (RR) can entrain neuron activity in widespread brain areas



➔ We observed that both Vm and spiking discharge could be RR-entrained in all recorded areas. To what extent brain areas are sensitive to RR ?

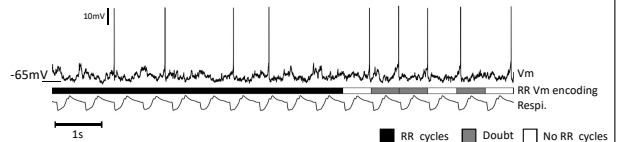
## Conclusions

Our results suggest that a respiratory drive of cellular membrane potential exists in a large brain network, influencing temporal discharge pattern. This drive is not unique but varies according to the brain area, LFP dynamics and probably other parameters that remain to be explored.

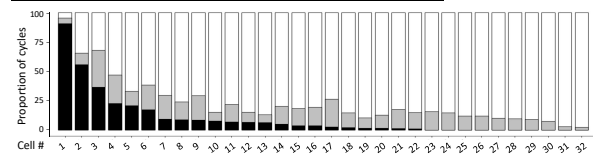
## Result 2 : Brain-wide quantification of Vm RR oscillations

To precisely quantify RR entrainment of Vm oscillations, we developed a detection method using respiration triggered waveform Vm (4 respi. cycles sliding windows), and compared to surrogates. This algorithm finally led to a RR encoding of Vm for each respiratory cycles.

### Cell-wide : time dynamics of RR Vm encoding (pl ex.)

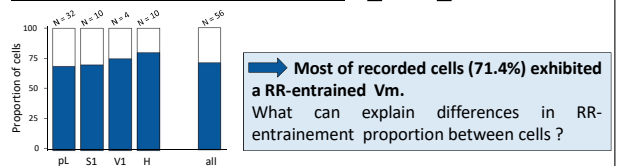


### Structure-wide : proportion of RR entrained cycles (pl ex.)



➔ From cell to cell we observed a variable proportion of cycles RR-entrained.

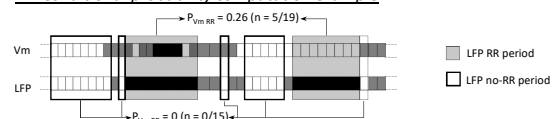
### Brain-wide : proportion of RR entrained cells



## Result 3 : Vm and LFP entrainment are partly coordinated

We encoded with the same detection method both Vm and LFP. Then we computed the probability for Vm to be RR-entrained as a function of LFP dynamics.

### Vm conditional probability computation example



### Vm conditional probability by structures

